INFORMATION TO USERS

This manuscript has been reproduced from the microfilm master. UMI films the text directly from the original or copy submitted. Thus, some thesis and dissertation copies are in typewriter face, while others may be from any type of computer printer.

The quality of this reproduction is dependent upon the quality of the copy submitted. Broken or indistinct print, colored or poor quality illustrations and photographs, print bleedthrough, substandard margins, and improper alignment can adversely affect reproduction.

In the unlikely event that the author did not send UMI a complete manuscript and there are missing pages, these will be noted. Also, if unauthorized copyright material had to be removed, a note will indicate the deletion.

Oversize materials (e.g., maps, drawings, charts) are reproduced by sectioning the original, beginning at the upper left-hand corner and continuing from left to right in equal sections with small overlaps.

ProQuest Information and Learning
300 North Zeeb Road, Ann Arbor, MI 48106-1346 USA
800-521-0600

UMI®

Reduction of Air Intake Contamination in High-Rise Residential Buildings in an Urban Environment

Hongwei Yan

A Thesis

in

Department

of

Building, Civil, and Environmental Engineering

Presented in Partial Fulfillment of the Requirements

for the Degree of Master of Applied Science at

Concordia University

Montreal, Quebec, Canada

August 2002

© Hongwei Yan, 2002

National Library of Canada
Acquisitions and Bibliographic Services
395 Wellington Street
Ottawa ON K1A 0N4
Canada

Bibliothèque nationale du Canada
Acquisitions et services bibliographiques
395, rue Wellington
Ottawa ON K1A 0N4
Canada

Your file Votre référence

Our file Notre référence

The author has granted a non-exclusive licence allowing the National Library of Canada to reproduce, loan, distribute or sell copies of this thesis in microform, paper or electronic formats.

The author retains ownership of the copyright in this thesis. Neither the thesis nor substantial extracts from it may be printed or otherwise reproduced without the author's permission.

L'auteur a accordé une licence non exclusive permettant à la Bibliothèque nationale du Canada de reproduire, prêter, distribuer ou vendre des copies de cette thèse sous la forme de microfiche/film, de reproduction sur papier ou sur format électronique.

L'auteur conserve la propriété du droit d'auteur qui protège cette thèse. Ni la thèse ni des extraits substantiels de celle-ci ne doivent être imprimés ou autrement reproduits sans son autorisation.

0-612-72902-8

Canada

ABSTRACT

Reduction of Air Intake Contamination in High-Rise Residential Buildings in an Urban Environment

Hongwei Yan

The re-ingestion of toxic or odorous gases exhausted from rooftop stacks of a building may be a cause of indoor air quality problems of the same or an adjacent building. Although many experimental studies have been carried out to investigate the dispersion of exhaust from low-rise buildings, relatively little work has been conducted for high-rise buildings.

The present study examines the dispersion of pollutants from rooftop stacks on high-rise buildings and their effect on adjacent buildings. The water flume of the Building Aerodynamics Laboratory (BAL) has been used to carry out flow visualization experiments to identify building configurations that may produce exhaust re-ingestion. Results from the water flume were verified in the boundary layer wind tunnel of the BAL using the tracer gas technique. General flow patterns are discussed in terms of dilution contours. Thirteen empirical equations of the minimum dilution variation with different building configurations have been derived based on a significant amount of experimental data. The effects of various factors are investigated. The dilution measurement results are compared with prediction from ASHRAE dilution model and those from other recent similar studies.

It was found that the distance of stack to wall inlet and the exhaust momentum ratio affect the exhaust dilution dramatically. However, the stack location does not make any significant difference on dilution within the wake cavity zone with the same stack distance. Higher stack provides higher wall dilution. The gap between emitting and adjacent buildings affects the distribution of dilution, but it does not affect the value of the minimum dilution.

ACKNOWLEDGEMENT

I would like to express my profound gratitude to **Dr. Theodore Stathopoulos** for his thorough and patient guidance and his constant support and encouragement in the course of this work, his valuable advice and his provision of financial support throughout the research period.

A special note of appreciation and thanks are due to **Dr. Pat Saathoff** for his valuable help during the whole period of this study, including his very useful suggestions about the model design.

The technical craftsmanship of Joseph Zilka and Joe Hrib in the fabrication of experimental models is deeply appreciated. Many thanks are also due to Mrs. Hongyu Huang, Mr. Girma Tsegaye, and Mr. Kai Wang, for their helpful advice during the study period.

A very special thanks is given to my parents and my brother and sister, whose unselfish love has been without boundary, and for their moral guidance of life.

Finally, I would like to give my deepest thanks to my wife, **Xiaofang Liao**, for her love, patience, encouragement, understanding and supporting; and to my son, **Han**, for showing me the way how to look at the world around me with the wonder of a child.

TABLE OF CONTENTS

LIST OF FIGURES

CHAPTER 1

CHAPTER 2

CHAPTER 3

CHAPTER 4

CHAPTER 5

APPENDIX B

APPENDIX C

LIST OF TABLES

CHAPTER 3

CHAPTER 4

CHAPTER 5

APPENDIX B

LIST OF SYMBOLS

English letters

A_e	exhaust effective area
A_y	empirical constants for σ_y (standard deviation of the concentration distribution in the crosswind direction)
A_z	empirical constants for σ_z (standard deviation of the concentration distribution in the vertical)
B_5, B_6, B_8	empirical constants for Wilson model
B_o	empirical constant for initial dilution in Wilson-Chui model
C	contaminant mass concentration at receptor
C_e	exhaust volume concentration
C_{max}	maximum contaminant concentration at a receptor
C_o	contaminant mass concentration at ground level
C_r	roof centerline concentration
D	i) dilution factor
	ii) dimension of the upwind face
D_{adj}	dilution at the adjacent building roof height
$D_{crit,o}$	critical dilution at roof level for uncapped vertical exhaust with zero stack height at critical wind speed $U_{crit,o}$ for given distance S
D_d	distance dilution factor

D_{emit}	dilution at the emitting building roof height
D_{large}	largest dimension of the upwind face of the building
D_{min}	minimum dilution factor D at given wind speed for all exhaust locations at same distance S from intake
D_o	initial dilution factor
D_{small}	smallest dimension of the upwind face
Fr	Froude number
g	the gravitational acceleration constant
H	i) emitting building height ii) exhaust effective height
H_a	height of adjacent building model
H_c	maximum recirculation cavity height of the ASHRAE
H_{cavity}	recirculation cavity height of Wilson model
h	undisturbed effective plume rise height
h_s	stack height above the reflecting surface z = 0
h_{total}	effective plume height
K	constant of Barry's (1964) mean concentrations equation
k	turbulent kinetic energy
L	along wind length of the building
L_c	length of the separated flow region on the roof at the leading edge of the building

L_{cavity}	recirculation cavity length of Wilson model
l	distance from the source
M	exhaust momentum ratio
Q	contaminate volumetric release rate
Q_e	exhaust volume flow rate
Q_o	initial entrainment at the source
R	i) recirculation length scale
	ii) radius of exhaust plume with uniform concentration profile
Re	Reynolds number
Re_b	building Reynolds number
Re_s	stack Reynolds number
Ri	Richardson number
R_s	radius of the exhaust stack
S	distance between the emitting and adjacent buildings
s	exhaust-to-intake stretched-string distance
T	temperature in °K
U	mean wind velocity
U_c	effective plume convection wind speed at release point
$U_{crit,o}$	critical wind speed that produces the smallest minimum dilution factor $D_{crit,o}$ at a particular location for flush vent

U_g	gradient wind speed
U_H	i) wind speed at building roof height
	ii) wind speed at exhaust height
U_{ref}	mean velocity at reference height
U_s	wind speed at the top of the stack $z = h_s$
u_x	wall shear velocity
U(z)	mean velocity at height z
W	width of emitting building model
W_a	width of adjacent building model
w	turbulence velocity components in the vertical (z) direction
w_e	exhaust velocity
x, y, z	location within the Cartesian coordinate system, x is the downwind distance, y is the crosswind position and z is the vertical position above the mass-reflecting surface
x_a	distance from the stack to the wall of the adjacent building
$x_{m,f}$	plume final rise distance,
Y	crosswind width of the upwind wall of the building where the roof edge cavity forms
z	receptor height
z_g	gradient height
z_{impact}	height difference between the adjacent building top and the plume

	trajectory
z_o	roughness length

Greek Letters

α	exponent of the power law wind speed profile
β	internal self-generated turbulent entrainment constant
β_{eff}	effective entrainment constant
ΔH	height difference of the roof level at the upwind edge where the cavity forms
Δh	plume rise by jet momentum or exhaust gas buoyancy above the top of the stack
Δh_b	plume buoyancy rise
Δh_d	stack tip downwash
Δh_f	plume final rise height of the fully bent-over plume
Δh_m	jet momentum rise
$\Delta h_{m,f}$	final momentum rise height
ΔT	temperature difference
$\Delta \sigma_o$	extra initial spread caused by plume trapping
$\Delta \sigma_{z,\ wake,}$	extra vertical spread in the wake
Δz_{wake}	plume trajectory correction caused by building downwash

ε	turbulent energy dissipation rate
θ	wind direction
ν	kinematic viscosity
ρ_a	ambient air density
ρ_e	exhaust gas density
σ	i) standard deviation
	ii) Gaussian parameters for square root of variance
σ_o	effective initial spread at x = 0
$\Delta\sigma_{o,\,wake}$	effective initial spread in the wake region
σ_x	standard deviation of the concentration distribution in the horizontal direction
σ_y	standard deviation of the concentration distribution in the crosswind direction
σ_z	standard deviation of the concentration distribution in the vertical direction
$\sigma_{z,wake}$	total vertical spread in the wake region
σ_θ	standard deviations of the horizontal wind direction

Acronyms

AC	air-conditioned
ASHRAE	American Society of Heating, Refrigerating and Air-Conditioning

	Engineers
BAL	Building Aerodynamics Laboratory
CBS	Centre for Building Studies
CFD	Computational Fluid Dynamics
GC	Varian Gas Chromatograph
HVAC	heating, ventilation, and air conditioning
LDA	Laser Doppler Anemometer
NO_2	nitrogen dioxide
PWA	pulsed-wire anemometer
SF_6	Sulfur hexafluoride
SHR	Stack Height Reduction factor
VIPS	Video Image Processing System

CHAPTER 1

INTRODUCTION

1.1 General

Wind engineering has been an interdisciplinary research area dealing with the study of wind effects on buildings and other structures. Basically, there are three kinds of such effects: structural, environmental and energy-related. The environmental aspects of wind engineering research include but are not limited to air pollution and pedestrian level wind comfort around buildings.

Airborne pollutants, besides other drawbacks, constitute a very serious health hazard. Under the influence of the wind, pollutants from the building emission sources can contaminate the area around the buildings, as shown in Figure 1.1. If the pollutants are reingested either via the open windows or through the intakes of the ventilation system, the health and welfare of people living or working in the building may be severely influenced. Sometimes, this may require the evacuation of the building. Pollutants around a building can also influence the people passing or working nearby. Often the source of the contaminants is an adjacent building, which may or may not be a residential structure. In order to avoid such problems, certain precautions should be taken during the design period.

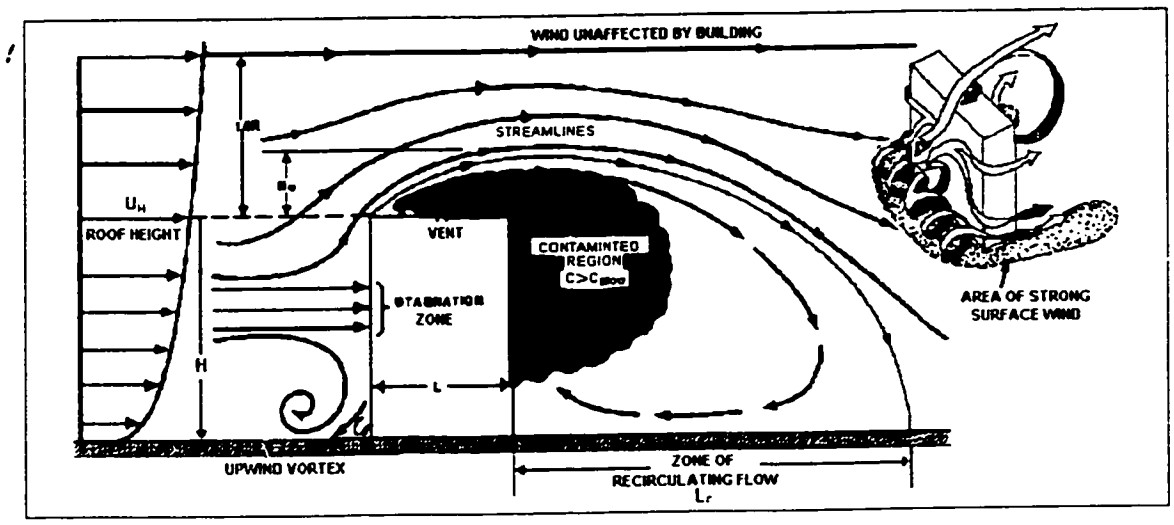

Figure 1.1 Flow around a rectangular building [after ASHRAE (2001)]

The entrainment of plumes emitted from short stacks into the building wakes can result in maximum ground-level concentrations that are significantly greater than those found for similar sources in the absence of buildings [Wilson et al. (1998)]. This is often potentially hazardous. Dilution of these emissions with surrounding air along with the application of control devices is necessary in order to meet ambient air quality standards. The effectiveness of such a control device depends upon the designer's estimate of the probable external dilution. Thus it is important to evaluate the ground level concentration in the building wake.

As has been proved by previous studies, a high stack can significantly reduce pollutant concentrations at roof and ground level. Due to aesthetic considerations, however, mini-chimneys and flush outlets are still widely used by designers, especially in an urban environment. As a consequence, a large number of problems may be brought out, such as the re-entry of odorous or hazardous pollutants and the blackening or deterioration of

building facades. Some effort has been made by many researchers to cope with such problems. The dilution of building exhaust from rooftop stacks has been studied extensively for more than 30 years. In general, four methods are considered feasible for estimating the concentration at roof level and in the near wake region from a rooftop stack.

The first method is using the maximum concentration value, which can be acquired using semi-empirical diffusion equations recommended by American Society of Heating, Refrigerating and Air-Conditioning Engineers [ASHRAE Fundamentals (2001)]. These models estimate the minimum dilution, D_{min}, (i.e., the ratio of the emission concentration to the maximum concentration at a receptor) as a function of the shortest distance from a stack or outlet, taking into account the parameter of wind velocity, exhaust velocity, exhaust face area, and building generated turbulence. For general dilution estimation, ASHRAE models can be considered as the most economical and simplest approach. However, for buildings with complex upstream geometry, the equations may not produce accurate estimates of D_{min}. The ASHRAE formulas are presented in detail in section 2.4 and application results are discussed in Chapter 5.

The second alternative for investigating building exhaust dispersion is the wind tunnel or water flume study. Generally, if most of the modeling criteria are satisfied, this method is expected to give relatively accurate predictions of exhaust dilutions around the building. This approach is especially preferred when the upstream topography may have a significant influence on the flow patterns around the building of interest. The advantages of a wind tunnel or water flume study can be summarized as follows:

1) The study is not affected by exterior weather conditions;

2) the same experiment can be repeated easily; and

3) it is convenient to test and compare several design alternatives.

It should be noted, however, that the validity of wind tunnel results, in terms of dispersion of exhaust from buildings, has not been thoroughly proved with full-scale data yet.

The third method for evaluating the dispersion of building exhaust is the full-scale investigation, which can be carried out to obtain accurate dilution data at specific locations. In general, this method reveals the actual dispersion processes best but it has many serious difficulties, such as varying wind conditions and high cost due to the use of significant amount of labor, material and time. This explains why relatively few field studies have been performed. Previous full-scale tests are reviewed in Section 2.6.

The fourth method is the numerical computation of the building exhaust diffusion using Computational Fluid Dynamics (CFD) methods. A reliable computer simulation of wind flow around buildings can make a contribution to this problem by facilitating a less time-consuming exploration of the model space. In principle, a computer wind-flow simulation can make wind-related design information accessible to an architect or engineer at every stage of the design process. This alternative should become more and more cost effective considering that the relative cost of computation for a given algorithm and flow

stage of the design process. This alternative should become more and more cost effective considering that the relative cost of computation for a given algorithm and flow decreased. The progress in the computational technology makes the possibility to use a mathematical analysis based on numerical simulation really attractive for this kind of project. Computational Wind Engineering can be applied to all classical wind engineering problems such as wind-induced pressures on buildings, dispersion of pollutants around buildings, etc. Many research works have been done to establish and improve the models used in the CFD methods. Presently, CFD methods based on a k-ε turbulence model are widely accepted except for the separated flow regions [Selvam and Huber (1995) and Kot (1989)]. The stochastic models can manipulate inhomogeneous turbulence and unsteadiness, but more powerful computers and extra statistical information are necessary. No matter what model is used in the numerical simulation, the results still need to be validated by comparing with either wind tunnel or field data.

1.2 Present study

A research project was carried out in order to evaluate the dispersion of pollutants from rooftop sources on high-rise buildings. The re-ingestion of building exhaust into fresh air intakes has been shown to adversely affect indoor air quality.

A water flume was used to carry out the task of visualization experiments to identify building configurations that may produce exhaust re-ingestion. The results were verified in a boundary layer wind tunnel by using tracer gas experiments.

1.3 Purpose of the study

Although a number of experimental studies have investigated the dispersion of exhaust from low-rise buildings, relatively little work has been conducted concerning high-rise buildings. The purpose of this study is to provide some guidelines concerning the placement of fresh-air intakes on such buildings.

The current study has five objectives:

1. conduct a literature review concerning dispersion around high-rise buildings;

2. carry out flow visualization experiments in a water flume to identify building configurations that may produce exhaust re-ingestion;

3. find the critical distances, for which the adjacent building will not be affected by the plume, of different configurations consisting of a higher adjacent building upwind;

4. carry out tracer gas experiments in a wind tunnel to verify the results found in the water flume, and

5. compare the results with ASHRAE minimum dilution model, ASHRAE critical dilution model and Wilson dispersion model in near wake region.

1.4 Thesis organization

This thesis consists of the collection of quantitative data for the critical building configurations identified in the water flume study and the analysis of results to examine the effect of a stack - placed flush with the roof surface - location on the dispersion of exhaust from rooftop stacks. These critical configurations were subsequently tested in a boundary layer wind tunnel that has been used extensively for the measurements required in the study.

The thesis is organized as follows:

Chapter 2 reviews the basic theories, ASHRAE models and previous research associated with the current study.

Chapter 3 introduces the experimental methodology used in the water flume and the wind tunnel tests.

Chapter 4 presents the water flume experimental results.

Chapter 5 presents and discusses the wind tunnel experimental results and compares with ASHRAE minimum models and Wilson dispersion model in near wake region.

Chapter 6 summarizes the findings of the study and makes suggestions for future work.

CHAPTER 2

LITERATURE REVIEW

2.1 General

This chapter presents a review of the literature pertaining to the flow about structures and on the diffusion of contaminants on or near buildings.

Wind-induced dispersion of building exhaust has been studied extensively for over 30 years. Although several mathematical formulas exist for estimating the diffusion downstream the source, the complexity of real airflow around buildings brings out new questions constantly concerning the results provided by those formulas. A number of full-scale tests as well as wind tunnel studies were carried out for the purpose of establishing or improving the atmospheric dispersion models. Based on the experimental results, a few dispersion models have been developed. One of the widely used models in today's engineering practice, Wilson-Lamb model, and one new developed model, Wilson model, will be discussed in detail hereafter and related experimental works will be reviewed as well.

Very high concentrations of some fumes, like the sulfur compounds, can cause rapid deterioration of the building and air-conditioning equipment. So there are additional cost considerations that should be added to the toxic problems. Re-entry from cooling towers

can also be a problem. Thus air pollution around buildings is of great concern for architects, HVAC engineers and health physicists.

Unfortunately, pollutant dispersion is a very complex phenomenon, which includes oncoming atmospheric boundary layer flow, stagnation zone and upwind vortex in front of the building and building wake-recirculating zone. On the roof, the flow can be divided into the roof recirculation region, high turbulence region and roof wake region as shown in Figure 2.3 [Wilson (1979)].

The location and height of the exhaust stack can also play an important role for the pollutants around the building. The problem becomes much more difficult when the complex geometry of the building is considered since more separation and recirculation areas may appear.

Several other parameters can also influence the dispersion of pollutants around a building. These include wind directionality, wind turbulence intensity, exhaust momentum, surface roughness of the ground, intake location, building configuration, buoyant effect of the pollutants and the character of the atmosphere (neutral, super-adiabatic or sub-adiabatic).

Contamination of fresh air entering high-rise residential buildings can occur if the exhaust plume of the building or a nearby building comes in contact with the air intake. There have been numerous incidents of air intake contamination, although such incidents have not been publicized broadly. The cost of poor placement of an exhaust vent or air

intake can be significant [Bahnfleth and Govan (1987)].

The ingestion of pollutants cannot be completely eliminated. However, the risk of significant intake contamination can be minimized by placing the air intake in the optimum location. Little information is currently available to assist the building designer with the placement of fresh air intakes. Much of the previous research on dispersion of plumes near buildings is based on wind tunnel studies performed with isolated buildings. A need exists to develop simple guidelines for predicting the influence of nearby buildings on the behavior of plumes emitted from rooftop stacks. As noted in ASHRAE (1999), *"large buildings, structures and terrain close to the emitting building can have adverse effects on dilution of stack exhaust because the emitting building can be within the recirculation flow zones downwind of these nearby flow obstacles."*

Kukadia and Palmer (1996) compared concentrations of various external pollutants in an air-conditioned (AC) building with those measured in an adjacent building that was naturally ventilated. The buildings were located in a large urban centre in the U.K. The study found that contaminant levels were generally similar in the two buildings. The air-conditioned building usually had slightly lower pollutant concentrations than the naturally ventilated building. However, boiler emissions from the AC building were occasionally entrained into the fresh air intake. Figure 2.1 shows a one-week record of nitrogen dioxide (NO_2) concentration measured in the two buildings. Also shown is the concentration of NO_2 measured outside the buildings. Although the records are limited in duration, they clearly show that the indoor concentration correlates well with the exterior concentration. However, the buildings tend to filter out short duration peak values present

in the external time series. It is also apparent that the air-conditioned building is subject to occasional very high concentrations due to reingestion at its fresh air intake. In this case, very high NO_2 concentration was recorded for several hours when the plume from a rooftop boiler made contact with the air intake.

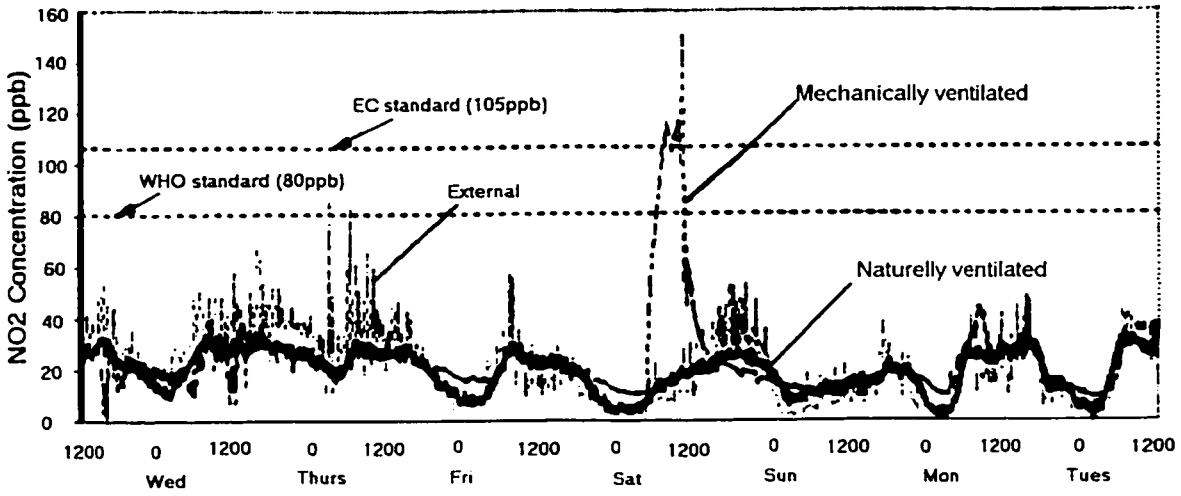

Figure 2.1 Time series of nitrogen dioxide concentration in two buildings in Birmingham, U.K. for the week of Feb. 13-20, 1996 [after Kukadia and Palmer (1996)]

The placement of fresh air intakes has recently been investigated by Rock and Moylan (1999). They noted that "*more research is needed on ventilation intake placement for common commercial HVAC systems with rooftop, through-the-wall and at-grade louvers. Most existing knowledge is derived from the many studies on industrial stack exhaust gas reentrainment and not common HVAC geometries.*" Rock and Moylan (1999) concluded that the current ASHRAE Standard for ventilation [ANSI/ASHRAE

62-1989] needs to provide better design guidelines concerning the placement of fresh air intakes.

Current design standards recommend that stacks have high exit velocities to alleviate the problem of exhaust reingestion at fresh air intakes of buildings. They also refer to the ASHRAE minimum dilution formulas [ASHRAE (2001)]. However, case studies performed by a number of researchers have shown that, even with high exit velocities, pollutant concentrations may be unacceptably high at particular locations [Stathopoulos et al. (1999), Georgakis et al. (1995), Wilson and Lamb (1994)]. Several factors may account for the occasional poor performance of such stacks. These factors include the location of the stack relative to regions of flow separation and flow re-attachment, the height of the stack (h_s), and the occurrence of high upstream turbulence.

Wilson (1976) measured concentration distributions on the roof and walls of building models in a wind tunnel. The results show that vent location and building shape can have a significant influence on maximum concentration. However, the results are of limited use to building designers because M (i.e., the exhaust momentum ratio, which is given by $M = (\rho_e/\rho_a)^{0.5} W_e/U_H$, where ρ_a is ambient air density, ρ_e is exhaust gas density, W_e is exhaust velocity, U_H is wind speed at exhaust height) values were quite low (<1). Furthermore, the experiments were performed with isolated buildings with flush vents.

In an earlier water flume study, Wilson (1979) evaluated the size of the recirculation zone that forms on the roof of the buildings. This is important for the design of building exhaust systems since stacks should be located outside this zone.

2.2 The nature of the flow

2.2.1 Flow patterns around isolated buildings

The flow around cubical buildings has been extensively studied in a number of wind tunnel and field studies, such as Halitsky (1961, 1963), Hunt (1970, 1971), Cermak (1976), Castro and Robins (1977), Hunt et al. (1978), Wilson (1979), Hosker (1980), Ogawa et al. (1983), Slawson (1987), Stathopoulos et al. (1999), and others. All these studies give excellent descriptions of the nature of the flow around buildings.

The flow around even the simplest building shape tends to be 3-dimensional in nature and consequently very complex. Further complications arise due to the presence of other structures. Although most buildings are located near other buildings, most of the fundamental knowledge about building aerodynamics has been obtained with isolated buildings.

As drawn schematically in Figure 2.2 [Hosker (1980)], the approaching wind profile represents shear flow. There is a stagnation zone at about two thirds of the building height above ground. As the wind hits the windward face, part of the flow goes over the downwind surfaces (i.e. both sides and roof surface) while part of the flow moves downward and generates a vortex at the lower part of the windward face. If the along wind length L of the building is long enough, the flow may re-attach on the roof and sides. Re-circulating streamlines can be found in separation zones, as shown in Figure 2.3 [Wilson (1979)]. Behind the building is a cavity zone of negative pressure, where the

separation streamline reattaches to the ground surface.

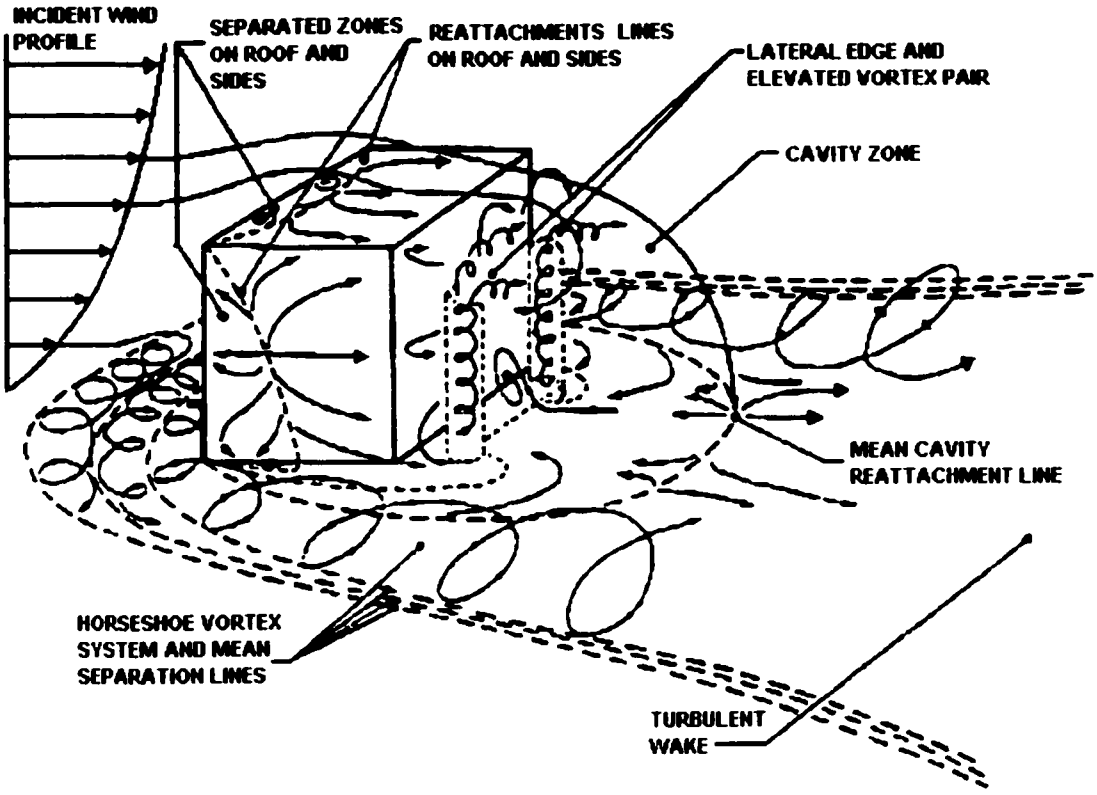

Figure 2.2 Three-dimensional flow past a cubic structure in a turbulent shear flow [after Hosker (1980)]

2.2.2 Estimation of recirculation zone dimensions

As introduced previously, dilution models are very useful in predicting the critical dilution values likely to occur at a particular location. However, detailed information regarding the wind climate, the exhaust gas composition and flow rate is necessary when applying these methods for design purposes. As an alternative approach, particularly

when the wind data and exhaust specifications are difficult to obtain, Wilson (1979) proposed a relatively simple method to estimate the dimensions of the high turbulence regions above a building roof. With this method, stacks and intakes can be located at appropriate places to avoid the effect of high atmospheric turbulence.

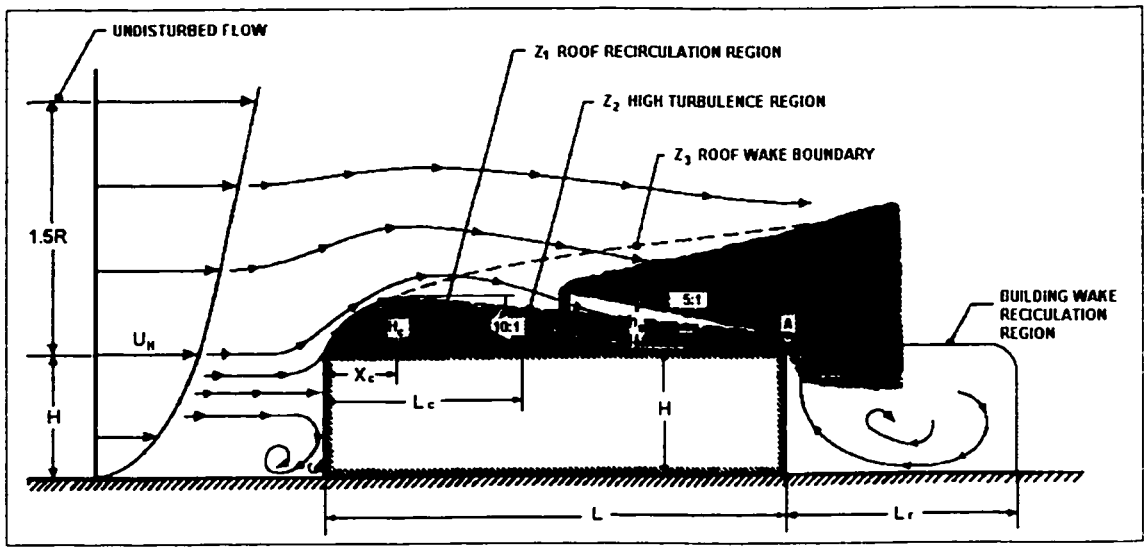

Figure 2.3 Flow regions over a building roof for wind normal to upwind face [after Wilson (1979)]

Figure 2.3 illustrates the cross-section of different flow zones with the wind normal to the upwind surface. Due to the separation of the approaching wind at the upwind edge, a cavity is created and a reverse flow can be found in this region. If the downwind roof dimension is long enough, the separation flow reattaches the roof surface and generates a closed region called re-circulation zone. The turbulence level in this region is very high and if the exhaust gas is emitted within the re-circulation zone, a uniform high concentration will be detected. The boundaries of zone Z_2 and zone Z_3 are somewhat

subjective. Generally, the turbulence levels decrease and downwash flows become insignificant as the measurement location moves towards outside zones.

Based on experiments with a large number of building shapes, the following expression for the recirculation length scale, R, was obtained:

$$R = \left(D_{small}^{0.67}\right)\left(D_{large}^{0.33}\right) \tag{2.1}$$

where D_{large} is the largest dimension of the upwind face of the building and D_{small} is the smallest dimension of the upwind face.

Consequently, the length of the separated flow region on the roof at the leading edge of the building, L_c, the length from the leading edge of the building to the maximum cavity height, X_c, and the maximum cavity height, H_c, can be expressed as a function of R such that:

$$L_c = 0.9\ R \tag{2.2}$$

$$X_c = 0.5R \tag{2.3}$$

$$H_c = 0.22R \tag{2.4}$$

It should be noted that these formulas only apply for the case of a wind that is approximately normal to a building wall, which is considered to be the critical case.

However, for wind directions of 30° - 60°, delta-wing type conical vortices form along the leading edges of the roof.

2.2.3 Flow fields in the vicinity of buildings

Snyder W.H. and Lawson R. E. (1994) developed a physically realistic model that predicts the behavior of pollutants released in the vicinity of buildings using a pulsed-wire anemometer (PWA). Based on their wind tunnel experiments using rectangular-shaped blocks with a power-law exponent $\alpha = 0.16$, they investigated the flow patterns with different building dimensions. For example, the crosswind dimensions of the building were W, 2W, 4W and 10W with L = W = H, the along-wind dimensions were 0.015L, 0.5L, L, 2L and 4L, the height of the building were H, 2H, and 3H, and finally, the cube was rotated 45°.

As shown in Figure 2.4, the cavity size obviously increases as the crosswind width of the building increases, as well as other aspects of the flow field change markedly. The stagnation point located on the upwind face of the building appears to move only slightly upwards from of approximately 2H/3, but the far upstream elevation of the stagnation streamline changes continuously from about 2H/3 to essentially ground level for the building with crosswind width of 10H.

As shown in Figure 2.5, the cavity height decreases with along-wind dimension, L, with a maximum (of about 1.4H) when L = 0.015H (square flat plate). When L = H/2, the cavity height is about 1.15H; for L ≥H, the cavity height is constrained to be the same as the

building height since reattachment occurs on the roof, horizontal separation follows at the downwind roof edge. Correspondingly, the cavity length decreases from 2.3H for the flat plate to 1.5H when L = H/2. For L ≥H, the cavity length is nearly constant with a value near 1.3H.

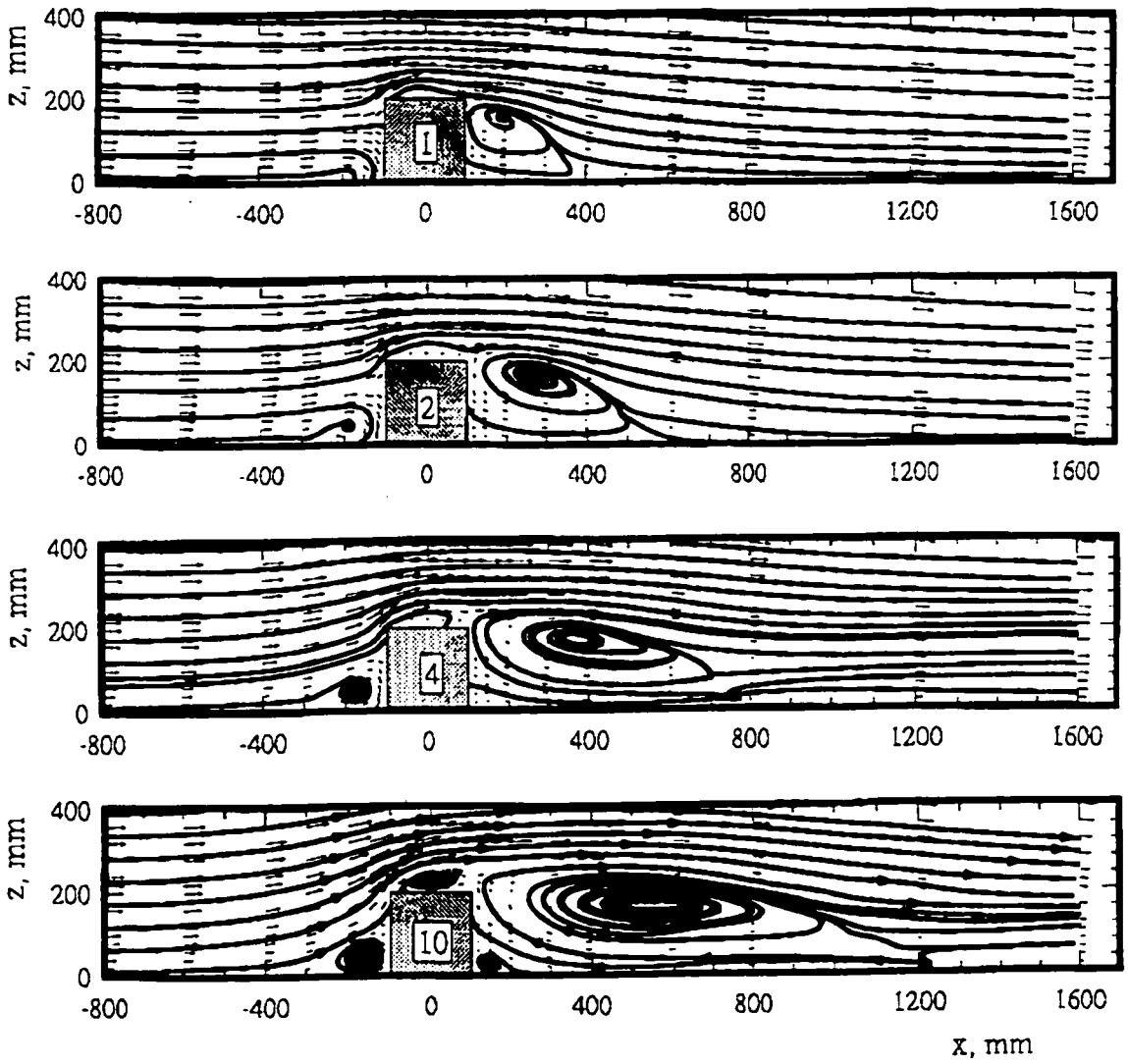

Figure 2.4 Streamline patterns around buildings (L=H) of various of crosswind widths. Number on building is W/H. [after Snyder and Lawson (1994)]

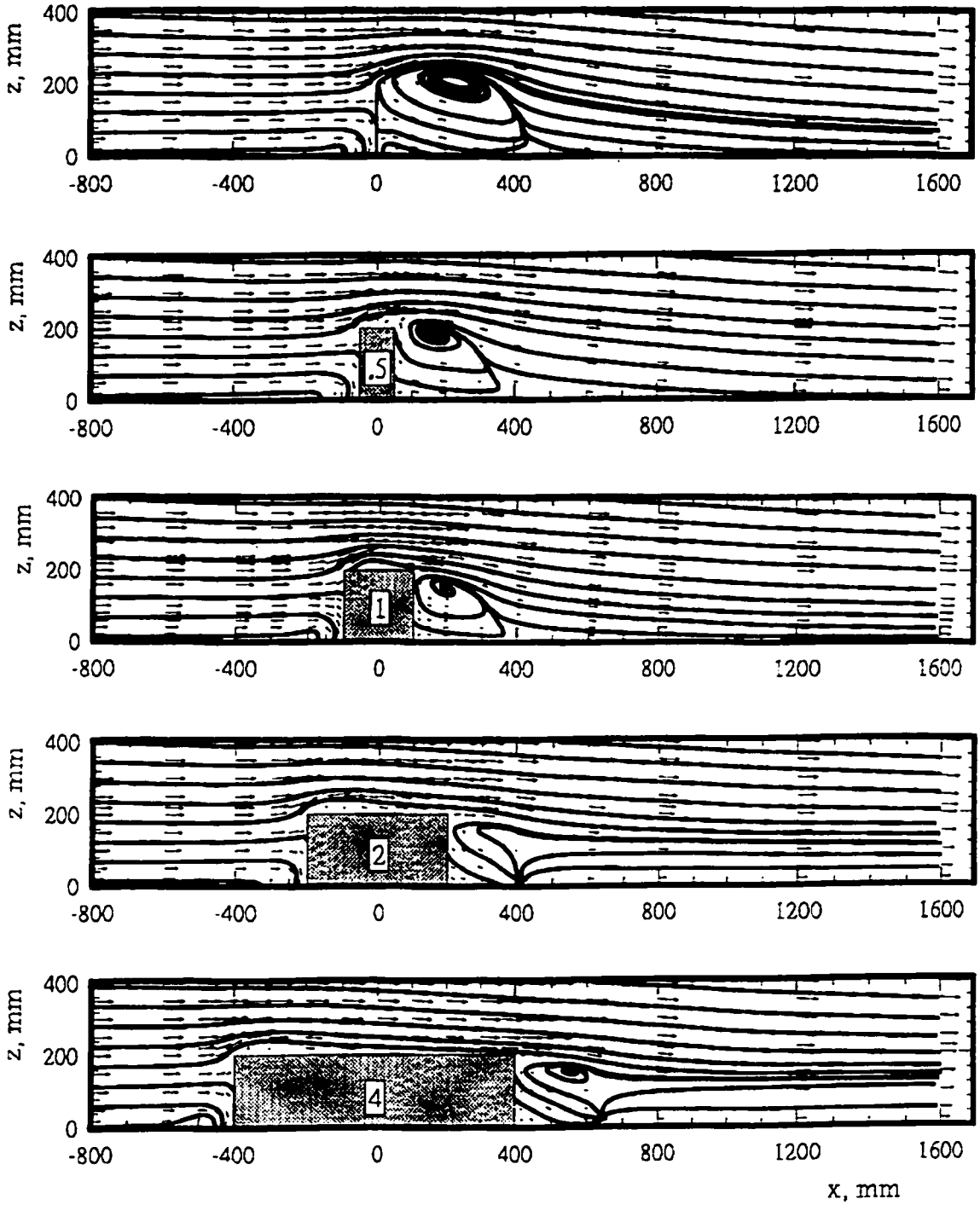

Figure 2.5 Streamline patterns around buildings (W=H) of various along-wind lengths. Number on building is L/H. [after Snyder and Lawson (1994)]

As shown in Figure 2.6, the elevation of the stagnation point on the upwind face of the building remains at approximately 2H/3, and the streamlines upstream of about 1.5W are essentially horizontal.

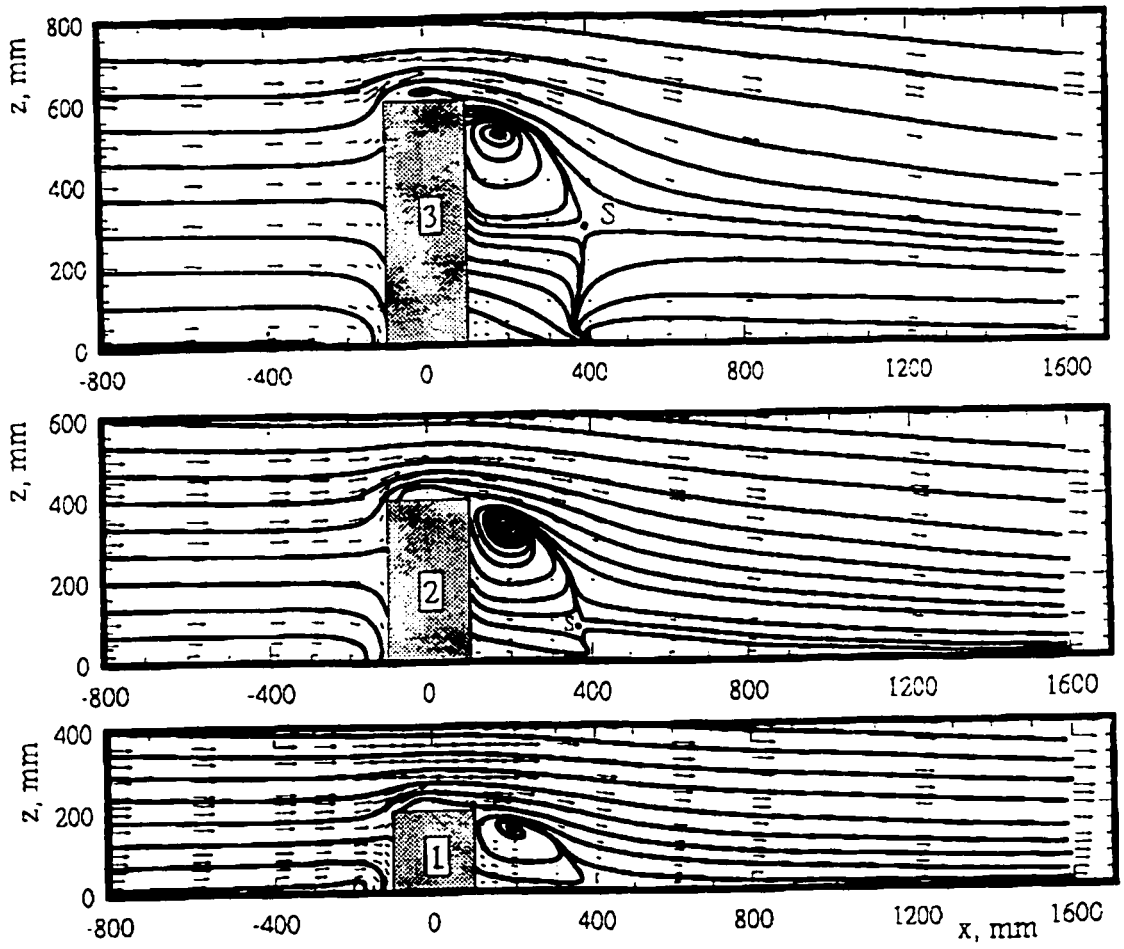

Figure 2.6 Streamline patterns around buildings (L = W) of various heights. Number on building is H/W. [after Snyder and Lawson (1994)]

2.2.4 Flow patterns with a taller adjacent building upwind

Based on their water flume experimental results, Wilson et al. (1998) postulated a flow

pattern model for the case of a plume formed in the wake of a building with a lower emitting building downwind. Figure 2.7 illustrates their finding.

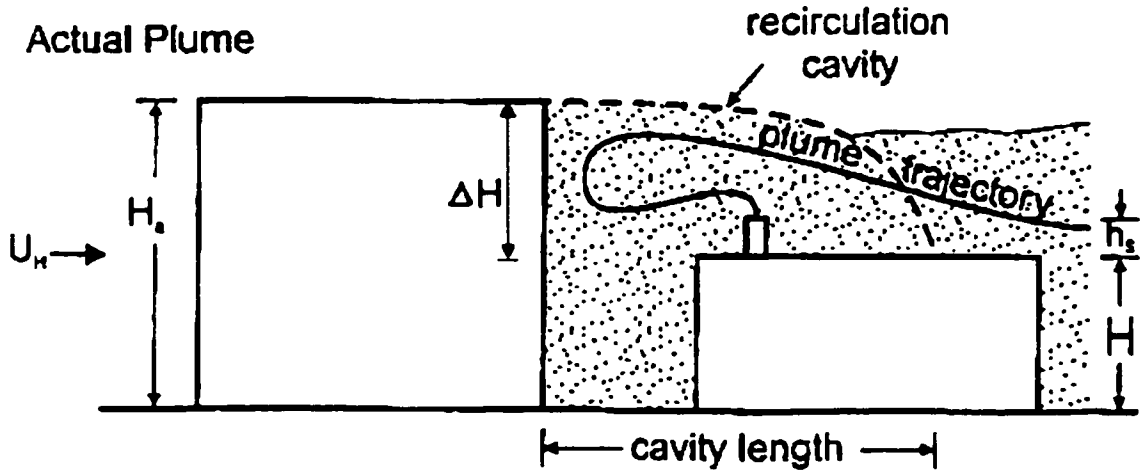

Figure 2.7 Effect of plume trapping in the recirculation cavity for an upwind adjacent building [after Wilson et al. (1998)]

In this particular case, the height-difference scaling length R based on increase or decrease in height ΔH of the roof level at the upwind edge where the cavity forms. In this case, Equation (2.1) becomes

$$R = \Delta H^{2/3} Y^{1/3} \qquad \text{for } \Delta H \leq Y \qquad (2.5)$$

$$R = \Delta H^{1/3} Y^{2/3} \qquad \text{for } \Delta H > Y \qquad (2.6)$$

where Y is the crosswind width of the upwind wall of the building where the roof edge cavity forms. The height change ΔH for the upwind building is just H_a, i.e., its roof height

above ground. For a downwind building, the roof height increase ΔH is the absolute value of the difference in heights,

$$\Delta H = | H_a - H | \tag{2.7}$$

If the initial location of the plume is within the cavity trapping zone shown in Figure 2.4 then the origin is shifted to the downwind wall of the upwind adjacent building. The dimensions of this recirculation cavity trapping zone were determined empirically by examining roof level dilution to see if exhaust had been carried upwind. The cavity length L_{cavity} and height H_{cavity} are roughly given by,

$$L_{cavity} = 2.0\ R \tag{2.8}$$

$$H_{cavity} = 1.5\ R \tag{2.9}$$

2.3 Gas diffusion theory

Atmospheric diffusion is caused by turbulence. Pasquill (1962) defined turbulence as *"that quality which is manifested in the random character of the velocity of a fluid (say at a fixed point as a function of time), in contrast to the constancy of such a velocity in steady stream-lined flow, or to the recognizable periodicity of a wave motion"*.

2.3.1 Methods of turbulence analysis

The turbulent diffusion can be described in two basic ways: Eulerian approach and

Lagrangian approach. In an Eulerian system, the velocities at all locations within a fixed coordinate system at a given instant are taken into account. The mass conservation is the basis on which the Gaussian is derived using Eulerian approach. In a Lagrangian system, the motion of a specific particle or element is considered as the basis for the concentration equation. The mean concentration at a certain position is given by the sum of a group of particles' probability densities. Nevertheless, the exact solution for concentration calculation in turbulent flow is not available by using either of the above approaches. Thus, more effort on other theoretical or empirical methods is needed in order to solve the diffusion problem.

2.3.2 Gaussian model for dispersion estimation on a flat-roof building

The Gaussian plume model, which is based on the Eulerian approach, is one of the most commonly-used methods for estimating the plume dispersion downstream a continuous source. The major reasons for using the Gaussian model are that it well represents the random nature of the turbulence and the solution can be acquired easily by mathematical operations.

Considering a continuous source with exhaust volume concentration C_e and exhaust volume flow rate Q_e at effective height h, as shown in Figure 2.8, the concentration C at a certain location (x, y, z) within the coordinate system is given by

$$C(x,y,z;h) = \frac{C_e Q_e}{2\pi U_c \sigma_y \sigma_z} \exp\left[-\frac{y^2}{2\sigma_y^2}\right]\left\{\exp\left[-\frac{(h-z)^2}{2\sigma_z^2}\right] + \exp\left[-\frac{(h+z)^2}{2\sigma_z^2}\right]\right\} \qquad (2.10)$$

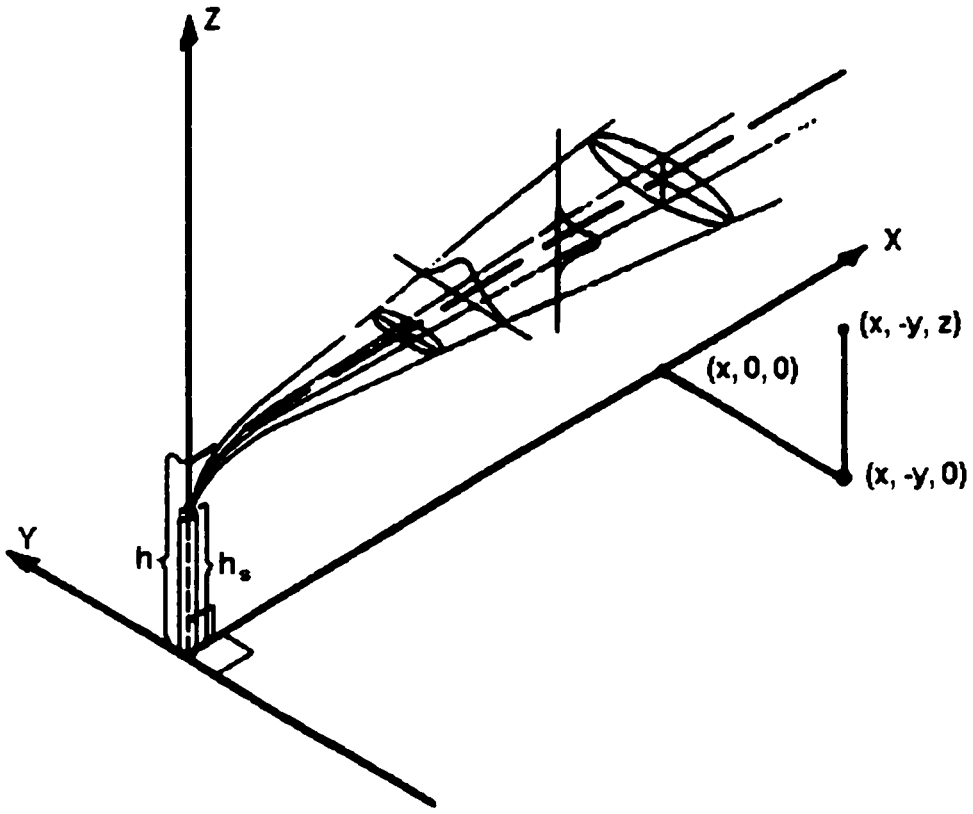

Figure 2.8 Coordinate system showing Gaussian distributions in the horizontal and vertical direction [after Turner (1994)]

where U_c is the effective plume convection wind speed at release point, x is the downwind distance, y is the crosswind position and z is the vertical position above the mass-reflecting surface (either the roof or ground level), measured from the base of the stack. The second exponential term with (z + h) is the contribution from mass reflection from the solid surface. The variation of C with downwind distance x from the stack appears implicitly in the standard deviation of the concentration distribution in the crosswind direction σ_y and vertical direction σ_z at the downwind distance x. The undisturbed effective plume rise height h above the reflecting surface (z = 0) is

$$h = h_s + \Delta h \tag{2.11}$$

where h_s is the stack height above the reflecting surface ($z = 0$), and Δh is the plume rise above the top of the stack produced by jet momentum or exhaust gas buoyancy.

Several constraints should be satisfied when using the Gaussian model [Turner (1994)]:

- Wind conditions must be stationary (i.e. mean wind speed and mean wind direction are constant);
- The turbulence must be isotropic and homogeneous;
- The mass is conserved within the plume;
- The concentration profiles in both crosswind and vertical directions are well described by the Gaussian distribution.

Huber and Snyder (1982) suggested that the Gaussian model is generally appropriate for dispersion estimation around buildings based on the wind tunnel results. However, the real airflow around buildings is so complicated that most of the above assumptions are violated.

2.3.3 Dispersion model for the wall dilutions with lower emitting building downwind

Based on their water flume experimental results, Wilson et al. (1998) developed a new

back wall pollutant dilution dispersion model with lower emitting building down wind using Gaussian model. The average of the concentration at emitting and adjacent building roof levels predicted by the Gaussian model is assumed to be uniform at all heights on the down wind wall of the adjacent building.

The main adjustments of the model is shifting the virtual origin of the plume trajectory back to the wall location of the upwind adjacent building if the plume lies inside the wake cavity trapping zone, as shown in Figure 2.9. Otherwise the plume trajectory origin remains above the stack, as shown in Figure 2.10.

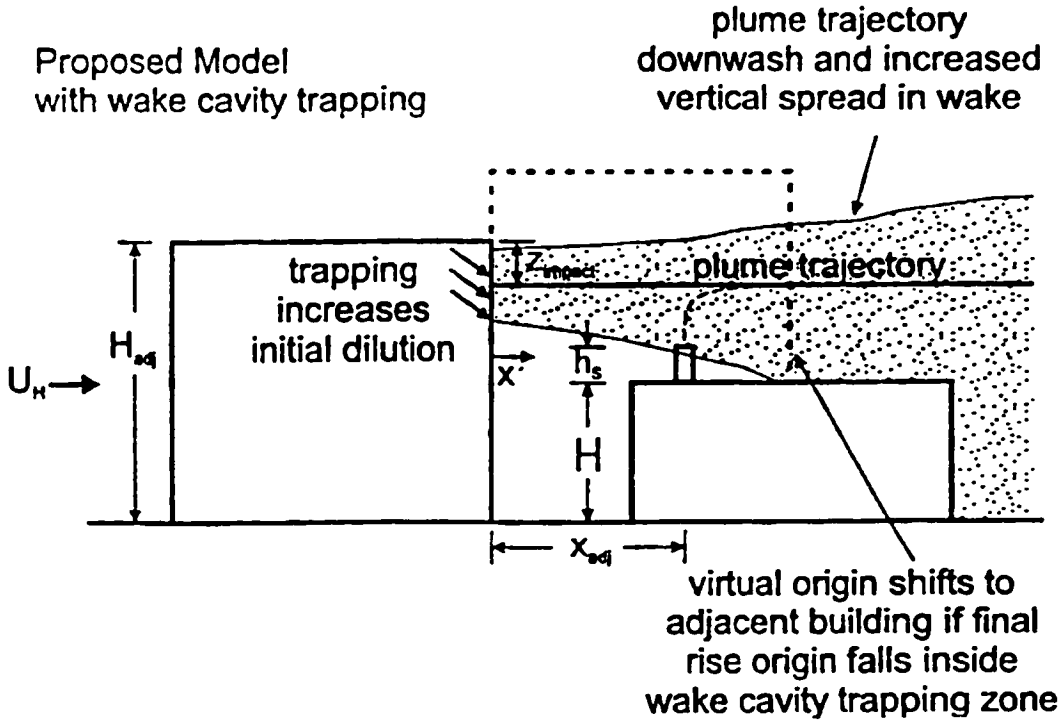

Figure 2.9 Proposed dispersion model with virtual origin shift plus added initial dilution caused by plume trapping, along with building wake downwash and increased vertical spread [after Wilson et al. (1998)]

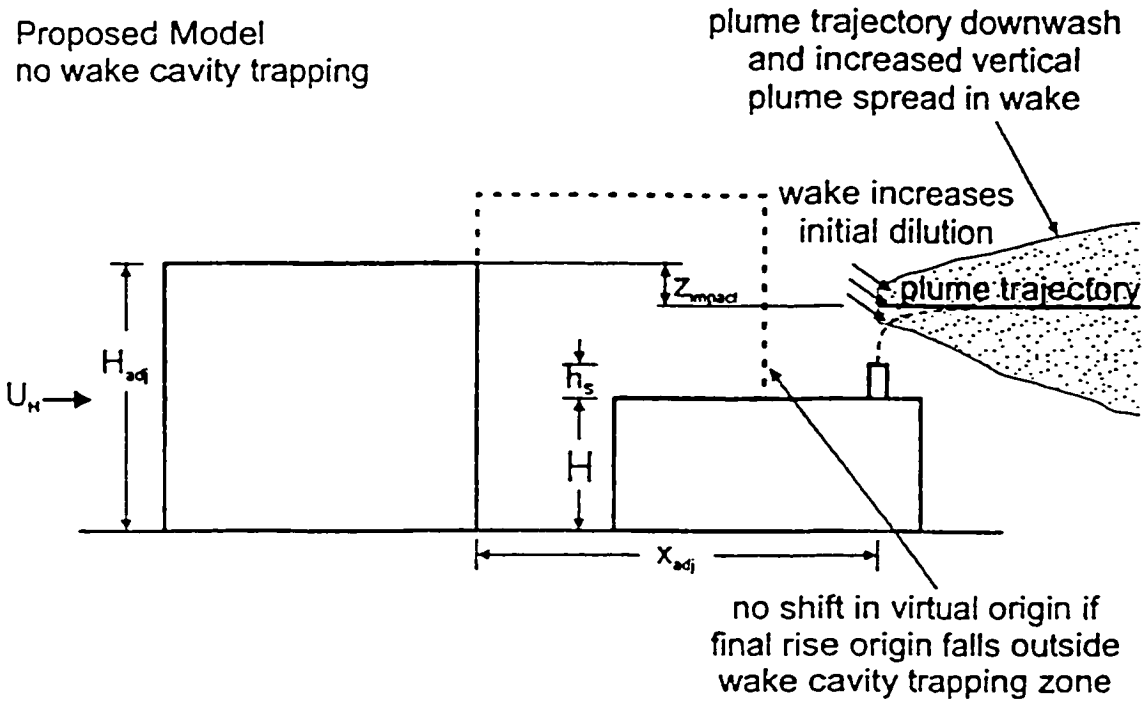

Figure 2.10 Proposed dispersion model with only building wake downwash and added vertical spread for stacks located to avoid plume trapping in recirculation cavity [after Wilson et al. (1998)]

The dilution at any distance z on the taller adjacent building back wall above the emitting building roof is given by

$$\frac{DQ_e}{U_H H^2} = 2\pi\left(\frac{\sigma_y}{H}\right)\left(\frac{\sigma_{z,wake}}{H}\right)\left[\exp\left(-\frac{(z-h_{total})^2}{2\sigma_{z,wake}^2}\right)+\exp\left(-\frac{(z+h_{total})^2}{2\sigma_{z,wake}^2}\right)\right]^{-1} \quad (2.12)$$

where Q_e is exhaust volume flow rate, U_H is wind speed at the emitting building height H, σ_y is crosswind plume spread, $\sigma_{z,wake}$ is the total vertical spread, h_{total} is the effective plume height.

The model assumes constant dilution with height, so the minimum dilution over the entire wall is,

$$D_{\min} = \frac{2D_{emit}D_{adj}}{D_{emit} + D_{adj}} \tag{2.13}$$

where D_{emit} and D_{adj} are the dilutions obtained at the emitting and adjacent building roofs, which can be calculated using Equation (2.12). See Appendix A for more details.

The authors concluded that the increased stack height would have allowed more exhaust to escape from the building wake cavity; dilution obtained by a larger M-value is higher than that by a low M-value, where M is the exhaust momentum ratio, defined as the ratio of the exhaust velocity to the wind speed at emitting roof height, $M = w_e/U_H$.

It should be noted that this model only shows the correct relative effects of changing stack height h_s, exhaust momentum ratio M, and adjacent building height H_a. Therefore, it should only be used as an approximation since it does not fully simulate the complex dispersion effects caused by the building wake cavity.

Tests performed by Wilson et al. (1998) with a higher adjacent building downwind of the emitting building showed that concentrations measured on the windward wall of the tall building did not vary significantly with height. The study concluded that it is difficult to develop design guidelines for the case of an emitting building lower than an adjacent building. Increasing the height of the stack or the exhaust velocity usually does not

significantly improve dilution levels at nearby receptors for this building configuration due to the fact that the exhaust always make contact with the adjacent building wall.

2.3.4 Wilson's flow patterns of tall buildings

The ASHRAE minimum dilution model developed by Wilson's group is based mainly on data obtained with low-rise buildings. However, Wilson (1979) also investigated the flow around high-rise structures. He found that when the angle between the upwind face of a building and the wind direction is less than about 70° the recirculation cavity becomes very small and intense vortex patterns develop along the upwind edges of the roof, as shown in Figure 2.11 (b).

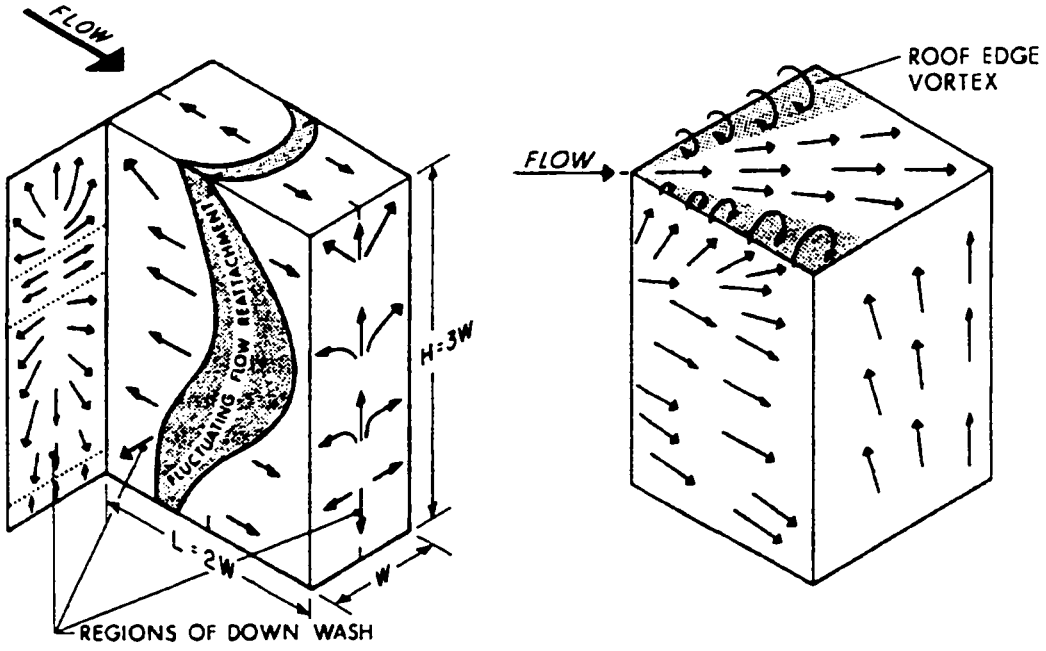

(a) (b)

Figure 2.11 Flow patterns around a tall building [after Wilson (1977)]

2.4 Dilution estimation models

2.4.1 General

Due to the complicated nature of flow around buildings, scale model studies in wind tunnels and water flumes have proved invaluable in the understanding and prediction of these flows. Model tests provide the data to formulate the empirical relations used to estimate concentration levels of contaminants near structures. These estimates may be required to satisfy government regulatory bodies.

Halitsky (1961) and Wilson (1979) described wind tunnel studies investigating the dilution of vented gases in and around buildings. In these papers the authors presented models for the estimate on of pollution concentrations downwind of a structure.

Hosker (1979) reported on wind tunnel experiments used to verify a model to predict the size of the wake cavity.

A comprehensive data set of concentration measurements downstream of a model cube was presented by Meroney and Yang (1982). The cube was located in a sheared, turbulent free stream, with both neutral, and inversion stratification reported. Meroney and Yang reported that, for this flow, the mean velocity profiles have fully recovered to their free stream values by x/h = 20, for both a 90° and a 45° orientation to the flow.

In Robins and Castro (1977) and Castro and Robins (1977) details were presented of

experiments to study the flow around a cube located in both a uniform free stream [Castro (1973)], and in a thick turbulent boundary layer [Castro and Robins (1975)]. Measurements of surface pressure coefficients and extensive turbulent velocity data in the wake of a cube were also presented.

In Ogawa et al. (1983) the authors described a wind tunnel study set up to verify their own full-scale experiments [Ogawa et al. (1983)]. The authors concluded that in order to adequately model the ratio of wake cavity length L_c, to building dimension H, it is necessary to match the longitudinal and lateral intensities of atmospheric turbulence, as well as the ratio of wall shear velocity to free stream velocity, u_x/U.

Huber and Snyder (1982), and Huber (1989) described several wind tunnel simulations while studying the dispersion of contaminants near structures. Huber (1989) made the interesting observation that incident wind at oblique angles to the structure results in increased downwind concentrations of 2 to 3 times at x/h = 3, and 1.5 times at x/h = 10. In addition, he noted that wider buildings have the effect of decreasing concentrations downwind for a given source strength.

Huber et al. (1991) described a different method for determining special concentration details and temporal concentration fluctuations in the wake of a long low building, with possible benefits over more traditional point sampling techniques. The method involves emitting oil-fog smoke from a ground level point source midway along the leeward face of the model, and using imagery to determine concentrations downstream.

2.4.2 Minimum dilution model (Wilson-Lamb model)

Several semi-empirical models have been developed to estimate the minimum dilution in a plume as a function of downwind distance and the exhaust parameter. The minimum dilution factor D_{min} has been employed as the quantity that shows the reduction in concentration between exhaust source and any receptor or given point around the building. It is defined as:

$$D_{min} = C_e / C_{max} \tag{2.14}$$

where C_e is the contaminant concentration in the exhaust and C_{max} is the maximum contaminant concentration at a receptor.

Two important factors should be taken into account when determining the minimum dilution: exhaust-to-intake stretched-string distance s and effective stack height h_s, as shown in Figure 2.12. The stretched string distance is defined as the shortest distance between building exhaust and intake location. The effective stack height is referred to as the stack height above any large roof barrier, such as a penthouse.

Wilson and Lamb (1994) developed a dilution dispersion model for short stacks and flush vents with zero stack height using field data of Lamb and Cronn (1986). The basic formulation of the model is,

$$D_{min} = (D_o^{0.5} + D_d^{0.5})^2 \tag{2.15}$$

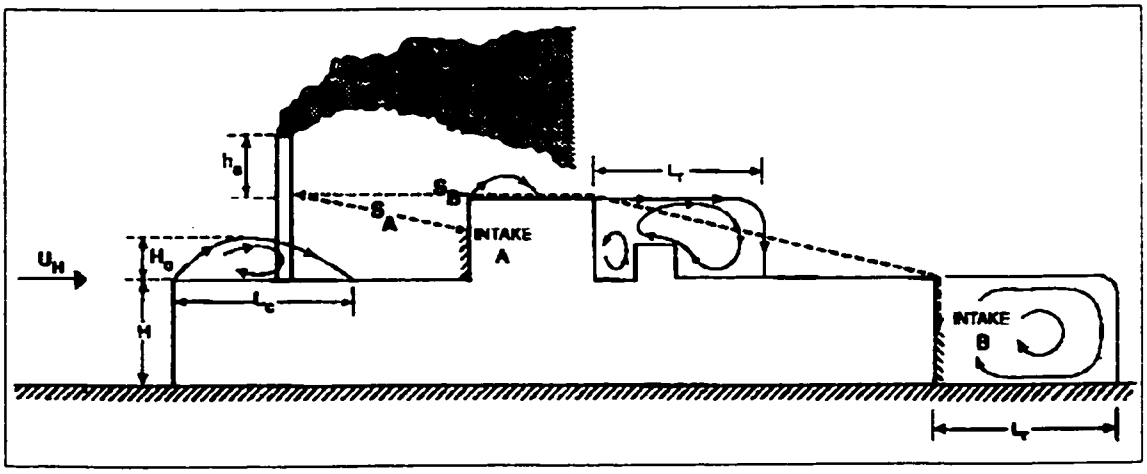

Figure 2.12 Flow recirculation regions and exhaust-to-intake stretched-string distances [after Wilson (1982)]

where initial dilution D_o and distance dilution D_d can be obtained by

$$D_o = 1 + \frac{Q_o}{Q_e} \tag{2.16}$$

and

$$D_d = B_1 \frac{U_H s^2}{Q_e} \tag{2.17}$$

where Q_o is the initial entrainment at the source, Q_e is the exhaust volume flow rate, U_H is the wind speed at emitting building roof height.

It should be noted that Equation (2.15) is applicable for a flush vent (i.e. $h_s = 0$), although

ASHRAE (2001) also provided formulas for estimating the influence of stack height on dilution values. These formulas have recently been revised [ASHRAE (1999)].

Wilson and Lamb (1994) proposed two major modifications for the minimum dilution model. First, a revised equation for initial dilution is suggested:

$$D_o = 1 + 13\ M \tag{2.18}$$

By using the standard entrainment assumption that $v_a = \beta \frac{d_s(\Delta h)}{dz}$, where β is the internal self-generated turbulent entrainment constant and Δh is the height of the plume rise (see Appendix A for Δh and Δh_f), the volume flow of a fully bent-over plume at its final rise height Δh_f is $Q_o = \pi U_H(\beta \Delta h_f)^2$. As the exhaust volume flux is $Q_e = \pi w_e R_s^2$, where R_s is the radius of the exhaust stack, the original initial dilution equation can be written as,

$$D_o = 1 + \frac{U_H}{w_e}\left(\frac{\beta \Delta h_f}{R_s}\right)^2 \tag{2.19}$$

with $\beta = 0.6$ and $\beta \Delta h_f = 6.0 R_e w_e / U_H$ from Briggs (1975), Equation (2.18) is obtained.

Wind tunnel results obtained by Wilson and Chui (1987) show that B_1 may be affected by a number of factors, including building shape, wind direction and atmospheric turbulence. The ASHRAE (2001) model takes into account the effect of upstream turbulence using the following formula for B_1:

$$B_l = 0.027 + 0.0021\sigma_\theta \tag{2.20}$$

where σ_θ is the standard deviation of wind direction fluctuations in degrees and varies between 0° and 30°.

The Wilson-Lamb model does not consider the influence of building geometry, although ASHRAE (2001) recommended that B_l should be small for isolated high-rise structures due to low turbulence levels at roof level. For building heights greater than 90m, it is recommended that $\sigma_\theta = 0$, giving $B_l = 0.027$. This value of B_l may reduce predicted dilution (increase predicted concentration) by 30% or more, compared to that for a low-rise building in an urban environment. Note that this recommendation only applies for an isolated high-rise building. If surrounding buildings are similar in height or higher than the building of interest, turbulence will be high at roof level and consequently, dilution values are expected to be higher than those for an isolated building are.

The ASHRAE (2001) model was derived from wind tunnel experiments for which the emission source and the receptors were on the roof. Li and Meroney (1983) found that minimum dilution measured at wall receptors is significantly larger than at a rooftop receptor that is located the same distance away from the source. Thus, it is generally preferable to locate fresh air intakes on the upper walls of a building when emission sources are on the roof. ASHRAE (2001) recommends that the first term of Equation (2.19) should be increased from 0.027 to 0.10 for wall receptors, to account for the absence of direct contact of the plume at these locations. This increase in B_l will result in an increase of 30% to 50% in predicted minimum dilution, depending on the distance

from the stack to the receptor.

Saathoff and Stathopoulos (1997) have questioned the methodology of the Wilson-Lamb study. They contend that the influence of atmospheric turbulence on dilution cannot be determined accurately using the Lamb and Cronn field data because of the significant influence of other factors, such as stack height and momentum ratio.

Nevertheless, Wilson and Lamb (1994) and Wilson (1997) showed that the Wilson-Lamb model predictions of D_{min} compare reasonably well with the field data of Lamb and Cronn (1986). Likewise, Ramsdell and Fosmire (1997) found that the Wilson-Lamb model provided an acceptable lower bound to field dilution measurements obtained at a number of nuclear reactor facilities.

2.4.3 Critical dilution estimation with zero stack height

Building exhaust dispersion is critically affected by the wind. If the wind speed is very low and the exhaust speed is high, the plume rise will be large, causing a high dilution at roof level, especially near the stack. Likewise, if the wind speed is very high, the exhaust plume will be stretched longitudinally, resulting in relatively high dilution at roof level. Between these two extremes exists a critical wind speed, U_{crit} that produces the minimum dilution at a particular location. Note that U_{crit} will vary with distance from the stack. By finding the absolute minimum dilution in Equations (2.14) to (2.18), the critical wind speed for a flush vent can be given by:

$$U_{crit,o} = \frac{3.6 w_e}{s}\left(\frac{A_e}{B_1}\right)^{0.5} \tag{2.21}$$

The critical dilution at this wind speed and distance, s, is given by: [ASHRAE (2001)]

$$D_{crit,o} = \frac{\left(1 + \frac{26 w_e}{U_{crit,o}}\right)^2}{1 + \frac{13 w_e}{U_{crit,o}}} \tag{2.22}$$

Note that the subscript o of $D_{crit,o}$ and $U_{crit,o}$ denotes a flush vent.

2.5 Full-scale studies on pollutant dispersion

A number of field experiments and wind tunnel studies have been performed to evaluate the empirical dispersion models as well as wind tunnel modeling techniques.

2.5.1 Previous field studies

Lam and Kot (1993) carried out a field test to evaluate the effect of wind speed on dilution for a single source and receptor pair. Besides the influence of short sample duration, wind direction fluctuation may have affected the validation of experimental data because only one intake location was considered.

Georgakis et al. (1995) carried out 72 full-scale tracer gas tests with stacks of different

height and diameter at two buildings at the University of Toronto. The data were used to evaluate eleven minimum dilution models. The Wilson-Chui and Wilson-Lamb models were not included, however. One drawback of the study is that the source and receptor pairs were not always on the same line as the wind direction. Therefore, some of the test data may not be appropriate for model evaluation.

Lamb and Cronn (1986) performed a field study by using a chemistry building at Washington State University. A group of stacks with varied heights and flow rates and an array of rooftop and ground-level receptors were used in the experiment. Results of this study have been analyzed by Wilson and Lamb (1994) as previously discussed. It should be noted that the sampling duration was one hour in this study. As a result, an averaging time correction is required in order to evaluate the minimum dilution models. Other possible problems with the data set include the lack of wind stationarity and the influence of stack height.

2.5.2 Wind tunnel and field comparison studies

Although a number of researchers have investigated the accuracy of wind tunnel modeling of atmospheric dispersion, few studies have considered the particular case of near-field dispersion of pollutants from rooftop stacks.

The results of several ground-level source wind tunnel simulations have been found to compare well with field data [Martin (1965), Petersen and Ratcliff (1991), Petersen (1986) and Bachlin et al. (1991), Stathopoulos et al. (1999)]. Allwine et al. (1980) carried

out several wind tunnel simulations of field studies, which were conducted at the Rancho Seco Nuclear Power Station by Start et al. (1977). It was concluded that the wind tunnel results over-estimated ground-level concentrations by a factor of 1.7 on average.

Higson et al (1994) compared wind tunnel data with the full-scale measurements obtained with a small-scale building. It was found that the highest mean concentrations measured in the field test tend to be overestimated in the wind tunnel experiment. On the other hand, the minimum concentrations were more likely to be underestimated. The possible explanation was proposed as the differences in turbulence scales corresponding to the dimension of the model building.

Saathoff et al. (1996) performed wind tunnel simulations of the field test conducted at Washington State University by Lamb and Cronn (1986). The wind tunnel results were generally within a factor of two of the field data.

Stathopoulos et al. (1999) carried out a full scale and wind tunnel experiment to evaluate minimum dilution models and provides guidelines for reducing the risk of reingestion of stack emissions. Detailed measurements have been carried out in seven field tests using roofs of two buildings on the downtown campus of Concordia University in Montreal. During the tests, a tracer gas was emitted from a short stack and air samples were obtained at up to fifteen locations on the roofs using radio-controlled samplers. A sampling period of 15 minutes was used for the field tests and, usually, ten samples were obtained at each location. The field dilution data were then compared with minimum dilution estimates obtained with three design formulas, the Halitsky model, the Wilson-

Chui model, and the Wilson-Lamb model; as well as with the wind tunnel study respective data. Results of both the field study and wind tunnel study indicate that the behavior of the plume may be dramatically affected by the momentum ratio of the exhaust flow in the vicinity of a critical value.

2.6 Previous flow visualization and digital image processing studies

In wind engineering field, flow visualization has been widely used to study the flow patterns, complement the quantitative estimations and provide guidance for wind tunnel experiments. With the development of computer techniques, digital image analysis is becoming an effective tool in pollutant dispersion studies.

Vincent (1978, 1977) described various flow visualization experiments conducted to better quantify the growth of the wake and the effects of inlet velocity profiles on the dispersion of contaminants within the wakes.

Lee et al. (1988) developed a video image analysis system to investigate the vertically integrated concentrations downwind of the building. Smoke was used to visualize the flow and is photographed from above. Image processing provided color-contoured descriptions of the plume, which revealed the vertically integrated concentrations. The image analysis system was calibrated by comparison with concentration measurements. Due to the existence of particular complications, for example the nonlinear relation between smoke intensity and vertically integrated concentration at high smoke intensity levels [Lee et al. (1988)], the final image may not be regarded as the true vertically

integrated concentration measurements. However, the application of video image analysis is demonstrated to be very useful in the study of building exhaust diffusion.

Olivari and Babuska (1990) conducted a study of pollutant dispersion in the near wake of a cube using the digital image processing method. The flow was recorded using a high frequency black and white video camera. Similar with Lee's method, the video images were quantified by referencing them with surface concentration measurements. Therefore, both qualitative and quantitative results were obtained. Moreover, the digital image analysis method again was proved applicable in pollutant dispersion studies.

Wu, Higuchi and Meroney (1991) reviewed the application of digital image analysis in wind engineering studies. Samples were given to illustrate how to use video image processing system (VIPS) to measure the flow velocity and plume dispersion. It was also suggested that an interpretive connection between wind tunnel studies and numerical models might be established using the digital image processing approach.

Apparently much more work is required in order to investigate the dispersion mechanism of the building exhaust in its near-wake area.

CHAPTER 3

EXPERIMENTAL METHODOLGY

3.1 General

As discussed in Chapter 2, boundary layer wind tunnel or water flume experiments have been widely used in atmospheric dispersion studies. Water flume is used to conduct visualization experiments because water has low viscosity and the velocity obtained by water can be lower compared with air. One of the most often used experimental techniques is the measurement of tracer gas concentration in a boundary layer wind tunnel. The basic procedure of tracer gas test is composed of three parts: the emission of tracer gas, the collection of air samples at receptors and the analysis of air samples. This method was also employed in the current study.

3.2 Wind tunnel and water flume modeling criteria

The boundary layer wind tunnel or water flume is ideal for evaluating near-field dilution of building exhaust. In order to obtain an accurate wind tunnel or water flume simulation, various physical modeling criteria need to be satisfied. ASHRAE (1997) recommends the following criteria based on the research work of Cermak (1976), Snyder (1981) and Petersen (1986):

- Equivalent exhaust velocity to wind speed ratio, w_e/U_H;

- Equivalent exhaust to ambient air density ratio, ρ_e/ρ_a;

- Similar emission Froude number $Fr^2 = \rho_a w_e^2/[(\rho_e - \rho_a)gd_s]$;

- Similar building Reynolds number $Re_b = U_H D/v$ or ensure that it is higher than 11,000;

- Stack Reynolds number $Re_s = w_e d_s/v$ should be higher than 2000 to ensure turbulent exhaust;

- Similar atmospheric stability, as indicated by Richardson number $Ri = gz\Delta T/(TU^2)$;

- Similar vertical profiles of mean wind speed and turbulence intensity;

- Identical scale applied to all model dimensions; and

- Blockage of the wind tunnel cross section caused by the simulated model less than 5%

where w_e is exhaust velocity, U_H is wind speed at building height, ρ_a and ρ_e are the density of air and exhaust gas, respectively, g is the gravitational acceleration constant, d_s

is the effective exhaust stack diameter, v is the kinematic viscosity of outdoor air, D is the nominal dimension, T is the temperature in °K at height z, U is the wind speed at height z and ΔT is the temperature difference between that at height z and at a lower height.

It is generally not possible to satisfy all of these criteria. Fortunately, some criteria may be relaxed, depending on the type of study. In the present wind tunnel study, the building exhaust is non-buoyant. Therefore, it is not necessary to match the Froude number. Moreover, since the study was limited to neutral atmospheric stability, Richardson number matching became unnecessary.

In the wind tunnel study, the stack Reynolds number criterion was not satisfied for most tests. Because of the small diameter of the stack, the stack Reynolds number satisfied the above criterion only when the exhaust momentum ratio was higher than 3. For $0.5 \leq M \leq 3$, values of Re_s range between 400 and 2000. However, since the exhaust dispersion is dominated by building generated turbulence [Wilson and Lamb (1994)], it is expected that the relaxation of the stack Reynolds number criterion has little influence on wind tunnel results, especially when the stack is in wake of upstream building. Note that a laminar exhaust flow has been used in previous studies [Wilson and Chui (1995), Wilson et al. (1998)].

3.3 Experimental procedure

Flow visualization experiments in the water flume at CBS were carried out to identify the building configurations, for which the exhausted plume would affect the adjacent

building. The results were verified in the boundary layer wind tunnel at CBS using tracer gas technique. The experiment procedure is shown in Figure 3.1 diagrammatically.

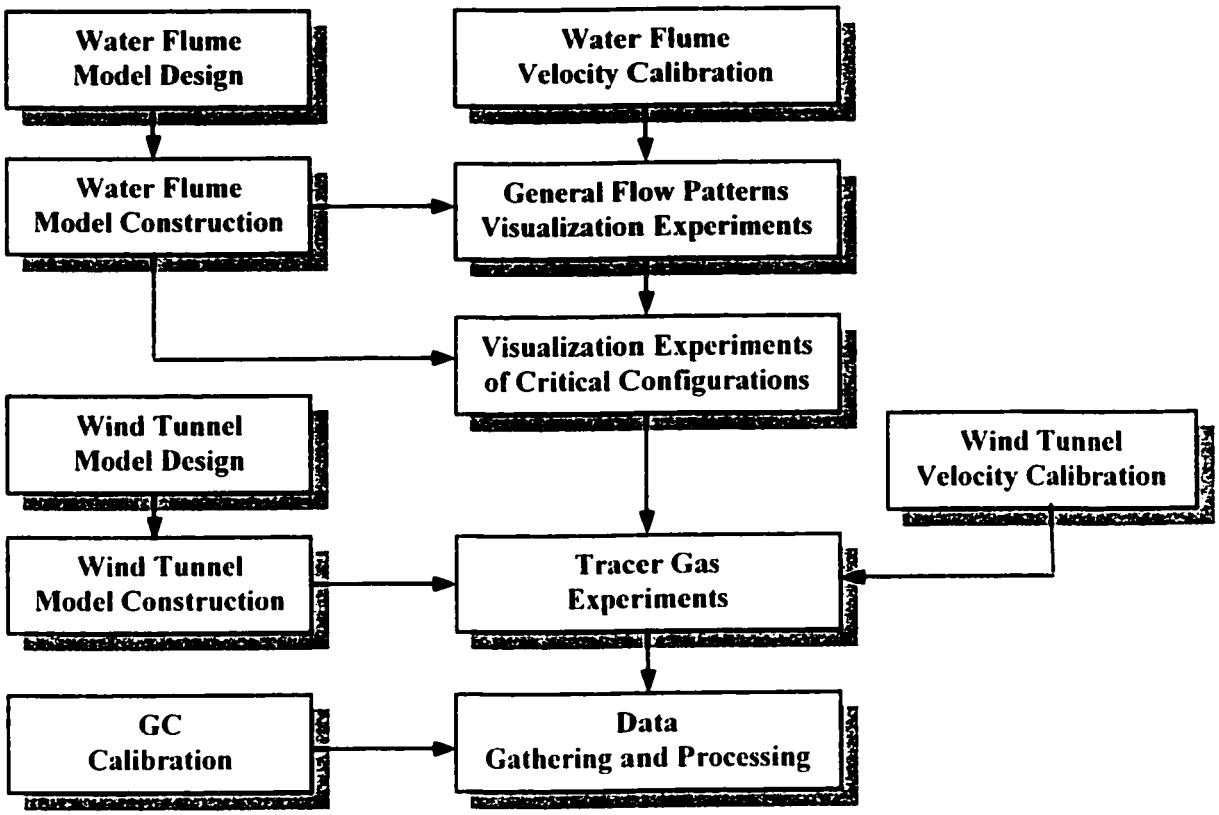

Figure 3.1 Experimental procedure

3.4 Flow visualization study

A flow visualization study was carried out in a water flume to assess the dispersion of effluent from a rooftop source on a typical multi-unit residential building. The main purpose of the study was to identify building configurations that may cause reingestion of exhaust at fresh air intakes. In particular, the study focused on the effect on the near wall of a taller adjacent building, which is upwind or downwind of an emitting building.

3.4.1 Water flume at CBS

The flow visualization experiments were carried out in the water flume of the Building Aerodynamics Laboratory (BAL) at the Center for Building Studies (CBS), Concordia University. The flume has a length of 4.0m, width of 1.8m, and depth of 0.6m, respectively. The flume width at the test section is 0.75m; the water depth was approximately 0.22m. Figure 3.2 shows a plan view and cross-sectional view of the flume.

3.4.2 Water flume experimental procedure

In order to get the range of critical configurations of the emitting building and the taller upwind adjacent building, a series of visualization experiments were carried out in the water flume.

A suburban atmospheric boundary layer was simulated in the tests. The boundary layer was created using a roughness fetch consisting of plastic blocks (Lego). In addition, triangular spires and a fence were placed at the entrance of the channel (as shown in Figure 3.2).

The water flume velocity was controlled by adjusting the input voltage of the pump. The dependence of flow mean velocity at the emitting building height on voltage of the pump for different depths of water is shown in Figure 3.3.

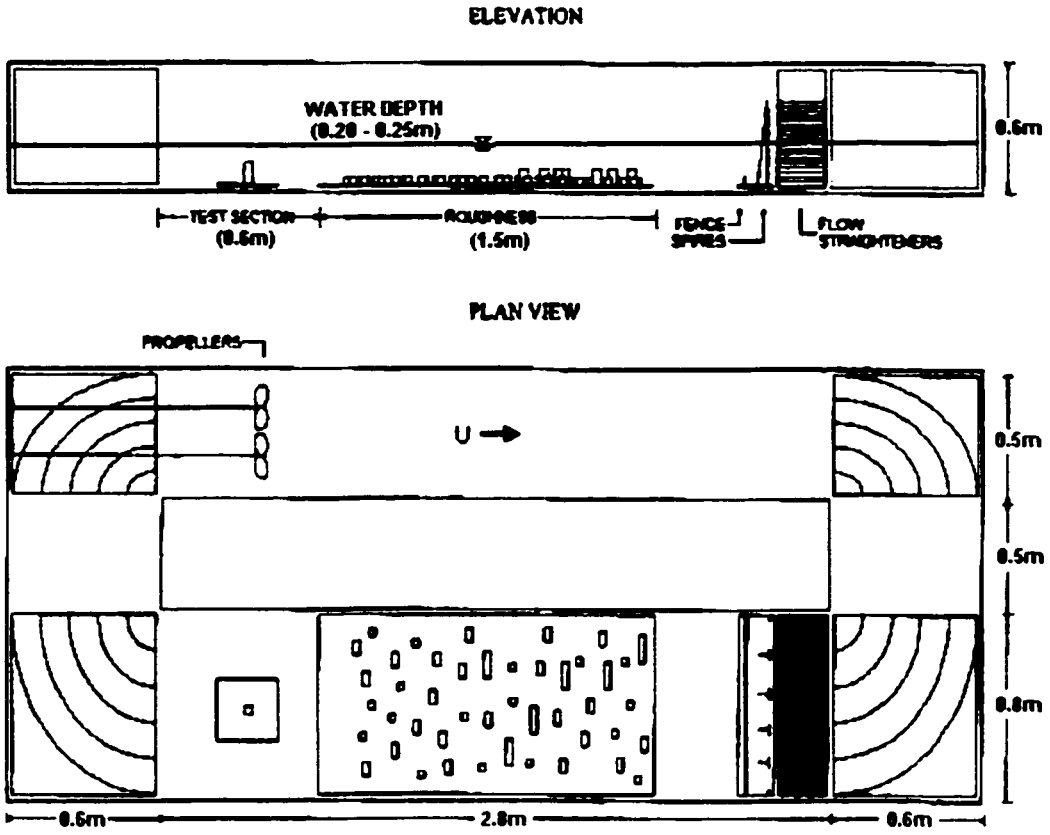

Figure 3.2 Plan and elevation views of the water flume at BAL at CBS, Concordia University

Vertical profiles of mean velocity and turbulence intensity were measured with a TSI hot film anemometer. The data were analyzed by a Universal Waveform Analyzer (Model 6100), made by ANALOGIC, is shown in Figure 3.4. The velocity profile can be approximated by the formula:

$$U_z = U_g\left(\frac{z}{z_g}\right)^{\alpha} \tag{3.1}$$

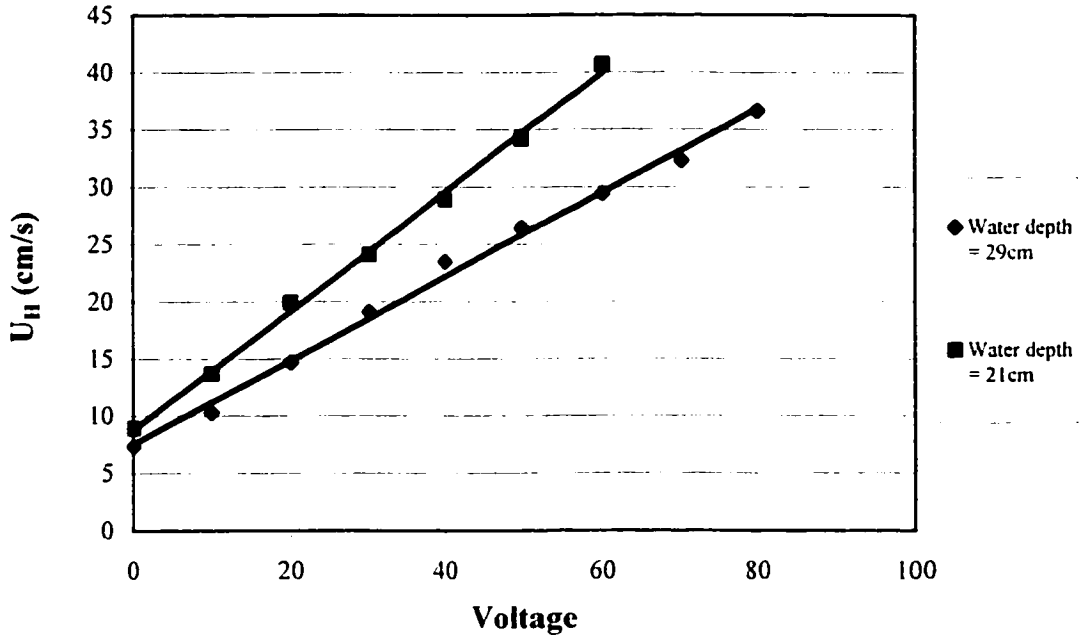

Figure 3.3 Flow mean velocity at building height varies with the voltage of the pump

where U_z is mean velocity at height z and z_g is the reference height. U_g is mean velocity at gradient height. The power law exponent, α, was approximately 0.24.

Two emitting building models were constructed using plastic blocks. Model A was a square-shaped building with side dimensions of W * L = 31mm*31mm. Rectangular-shaped Model B had side dimensions of W * L = 62mm *31mm. The heights of both emitting building models (H) were 57mm. Assuming a model scale of 1:1000, the models simulate full-scale buildings 31m*31m wide 57m high, and 62m*31m wide 57m high, respectively. The models represent buildings with approximately 15 stories. However, the results may be assumed to be relatively insensitive to model scale, following Wilson and Chui (1994). Figures 3.5 and 3.6 show the dimensions of Model A and Model B,

respectively.

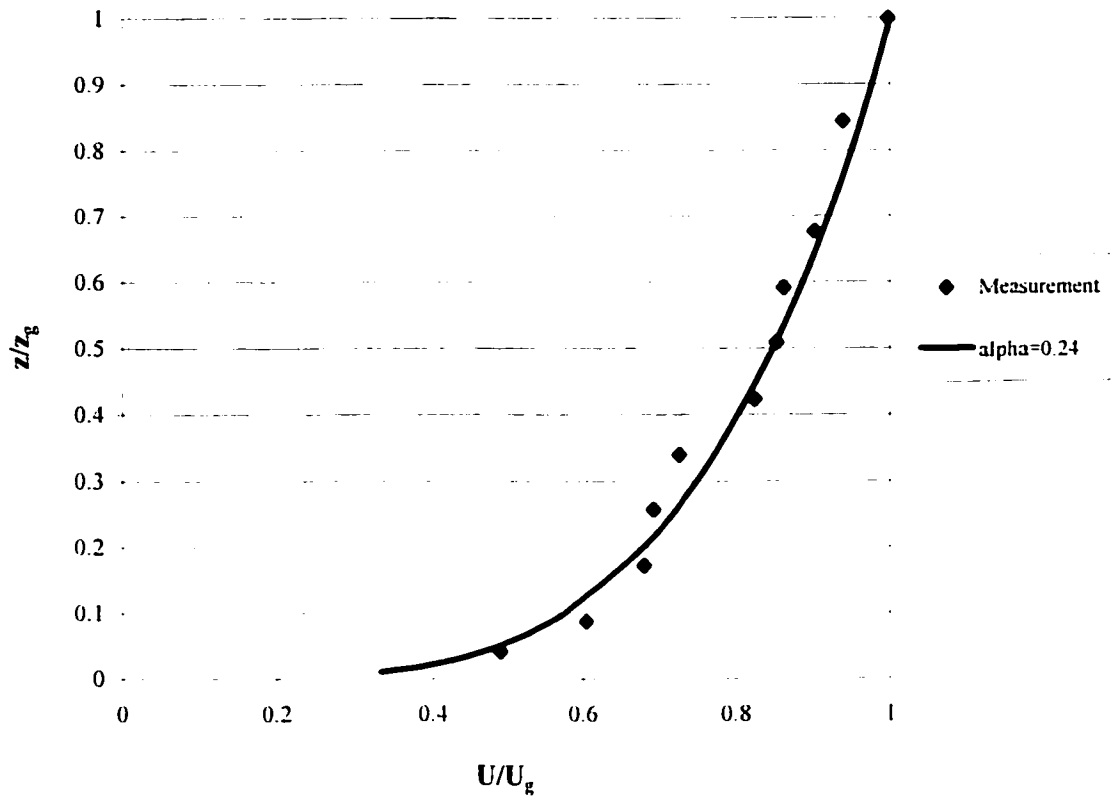

Figure 3.4 Mean velocity profile in the water flume at the model location

In the water flume study, either Model A or Model B had a single, centrally-located exhaust outlet, which was flush with the roof surface. The outlet diameter was 1.6mm. The plume was visualized using colored water. Most of the tests were carried out with exhaust momentum ratio, M = 2; thus, the exhaust speed, w_e, was approximately 2 times the velocity of the channel flow measured at the building height (U_H). Three other M values (0.5, 1 and 3) were also used to compare the results by changing the exhaust velocity. For typical stacks, M-values will vary between 1 and 6, depending on the wind

speed. The test M values represent moderate to strong wind conditions, which tend to produce the most critical situation for design.

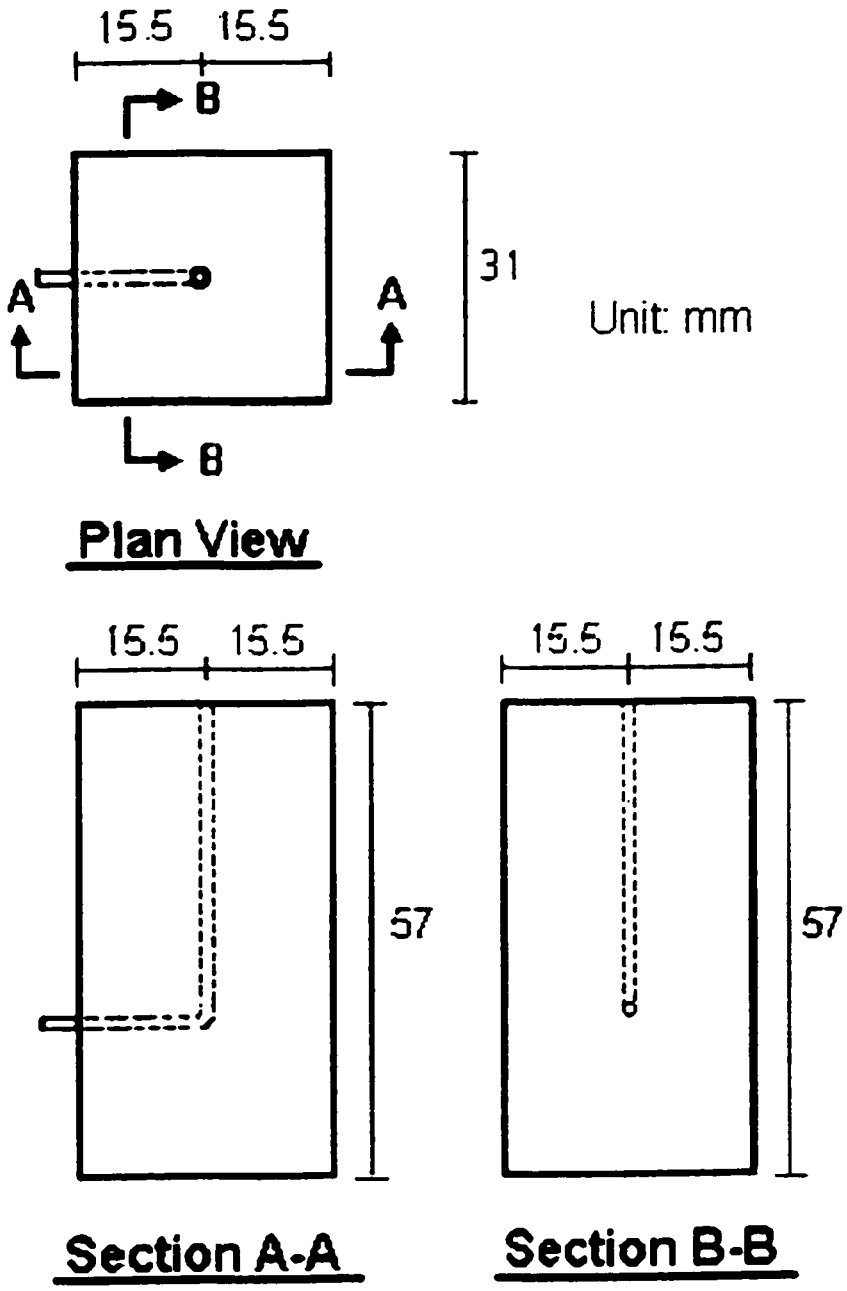

Figure 3.5 Dimensions of emitting Model A (Water flume experiment)

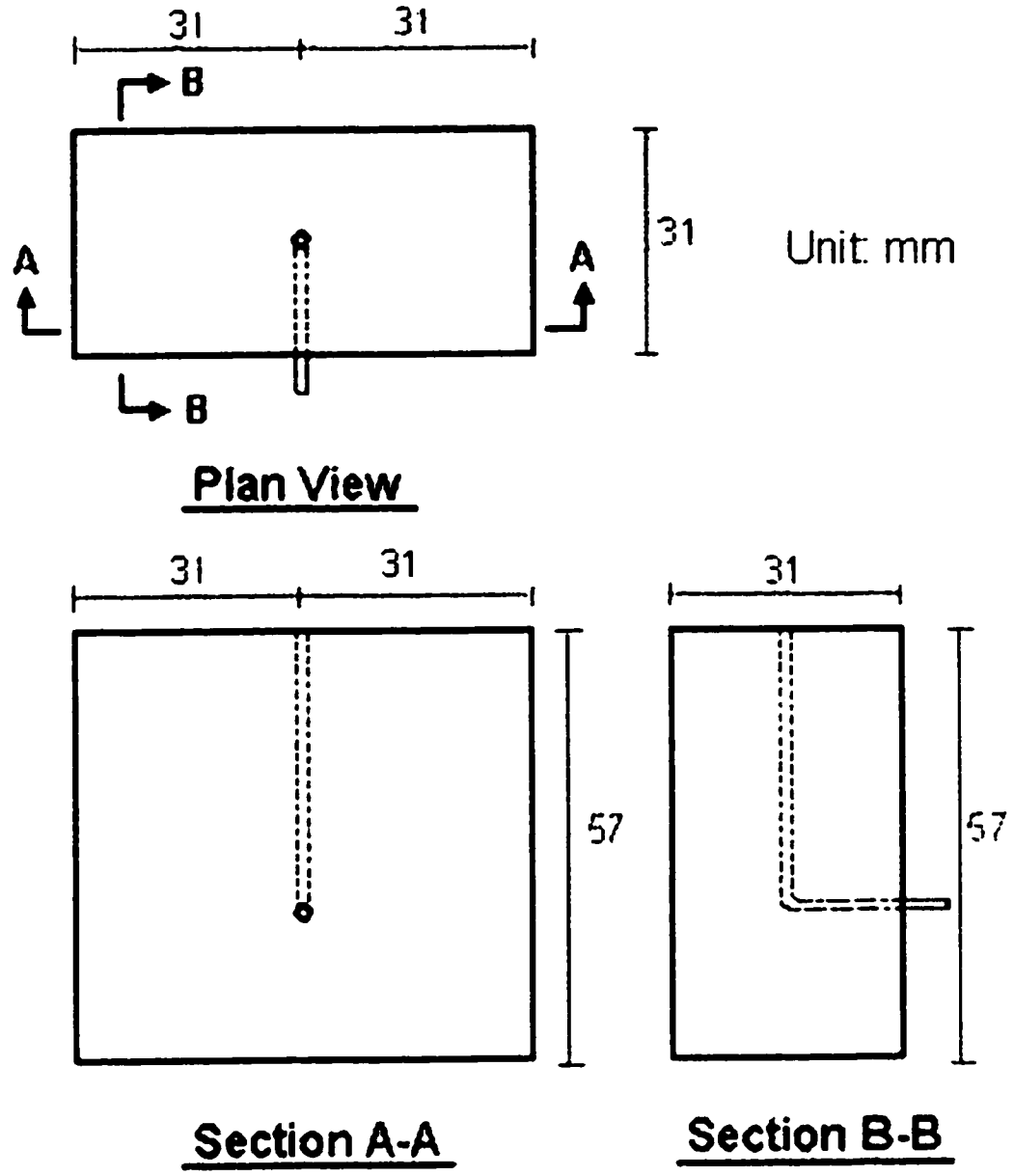

Figure 3.6 Dimensions of emitting Model B (Water flume experiment)

The flow speed at the building height was 0.26m/s. This value of U_H gave a building Reynolds number ($Re_b = U_H W/\nu$) of approximately 8000, where ν is the kinematic viscosity of water (0.01cm^2/sec at 20°). This value does not meet the strict criterion for

Reynolds number independence, Re_b = 11,000, specified in ASHRAE (2001). However, Castro and Robins (1977) have shown that in a turbulent boundary layer, the flow around a sharp-edged building is insensitive to Reynolds number for $Re_b > 4000$.

Another parameter that may influence the results is the stack Reynolds number ($Re_s = w_e d_s/v$), where d_s is the outlet diameter. The value of Re_s in the present study, assuming an M-value of 2, was approximately 800, which is significantly below the critical value to provide turbulent exhaust flow (Re_s = 2000). The lack of turbulent exhaust flow may have influenced the plume behavior to some extent. However, the effect of non-turbulent exhaust flow should be most significant near the stack. It is expected that at the location of interest (the adjacent building wall), the lack of turbulent exhaust does not affect plume behavior appreciably, especially when the emitting building is in the wake of the taller upwind building.

The exhaust momentum ratio, M, is an important parameter for plume modeling. The exhaust flow, which was simulated by colored water, was controlled by adjusting the speed of a syringe pump. The syringe draining speed was controlled by using 74900-Series Multichannel Syringe Pumps made by Cole-Parmer Instrument Company.

Different configurations of the emitting and adjacent buildings were tested in the initial visualization experiment phase. Figures 3.7 and 3.8 show the various configurations that were tested.

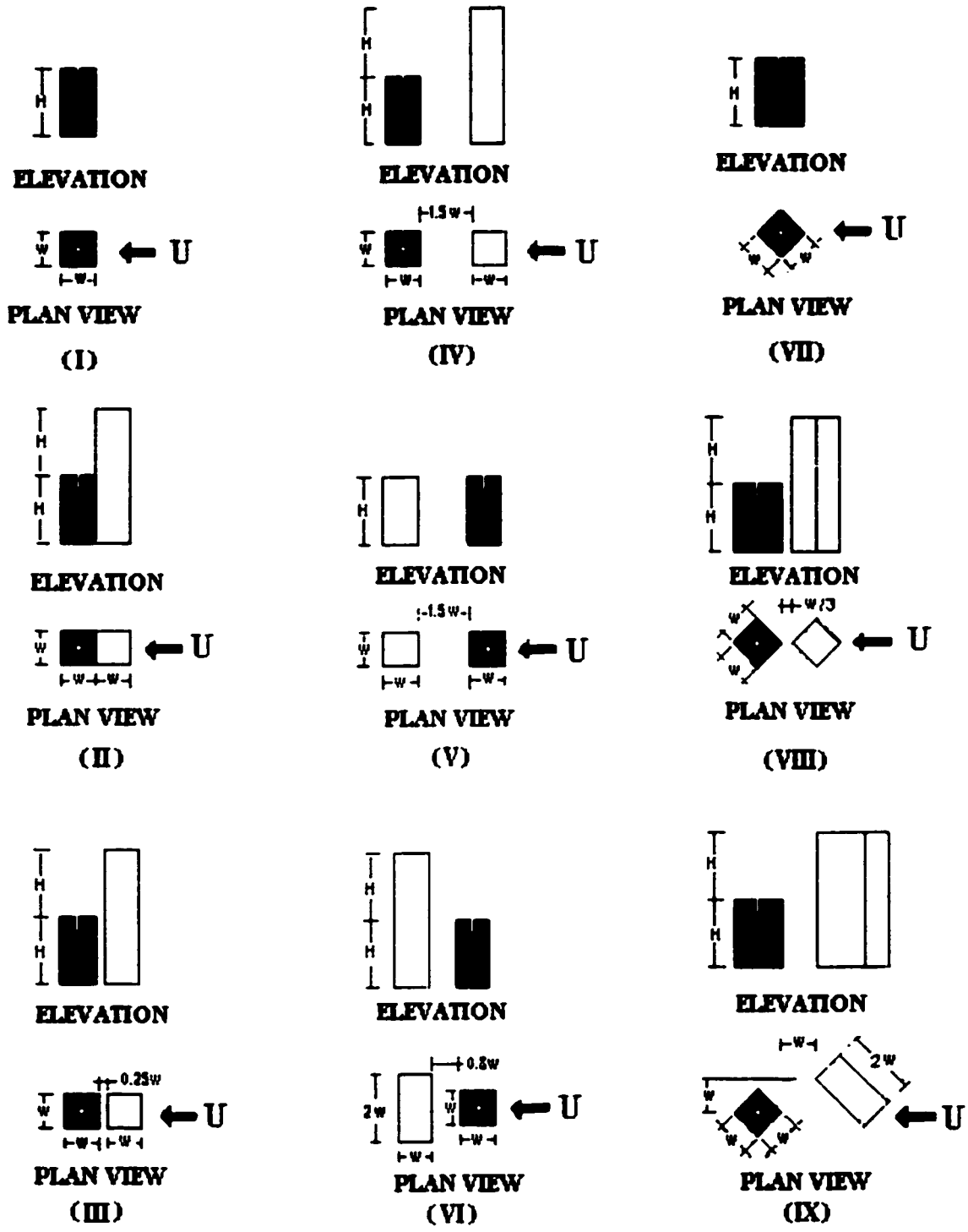

Figure 3.7 Configurations with Model A (square emitting building)

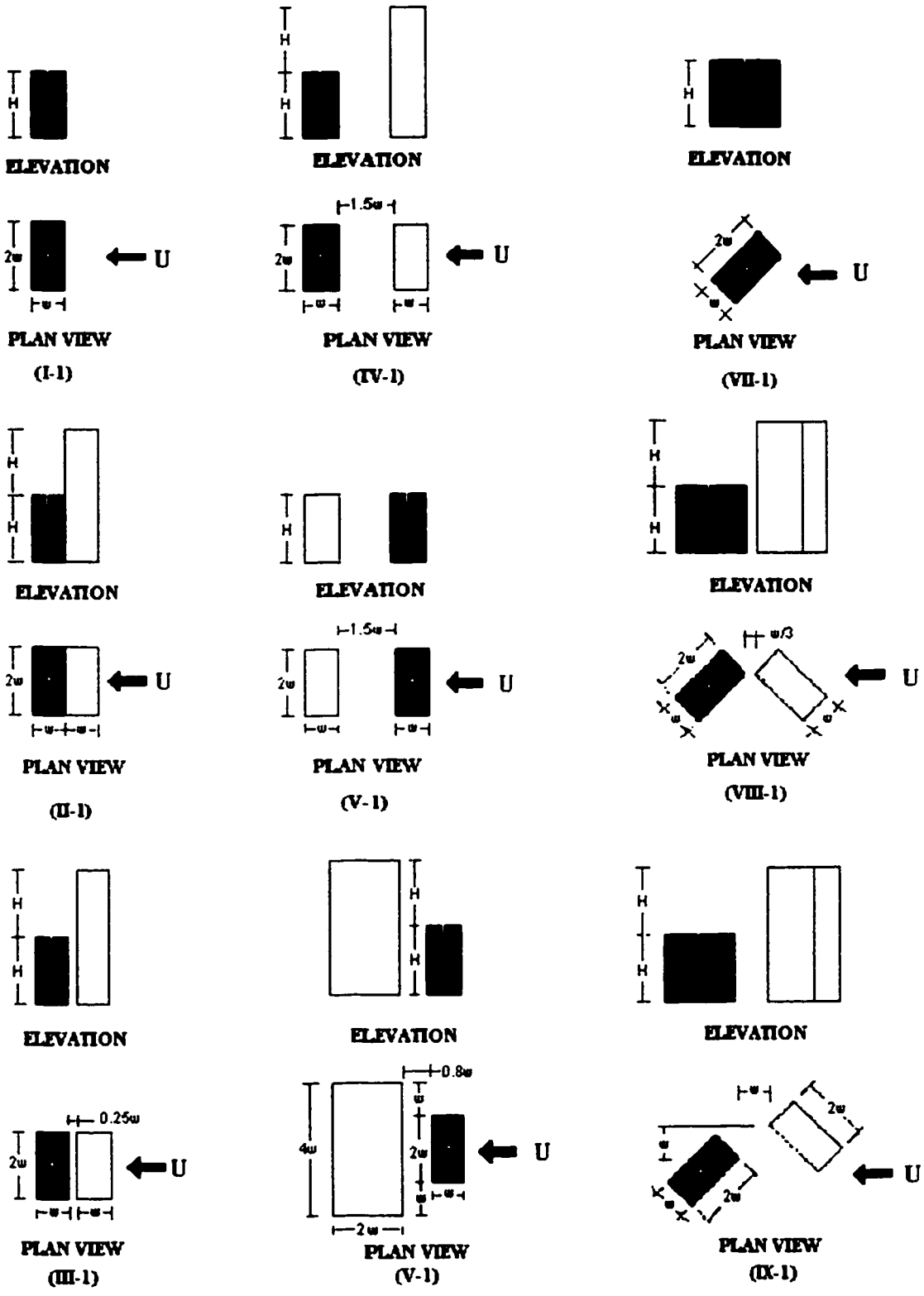

Figure 3.8 Configurations with Model B (rectangular emitting building)

Totally about 150 configurations were tested to verify the critical configurations. Different critical configurations of the emitting building and adjacent building, i.e., the plume from the emitting building roof-top will or will not affect the back wall of the adjacent building, were examined after the first phase (initial visualization experiments). Details of the critical configurations will be presented in Chapter 4.

3.4.3 Plume visualization system

A Sony DCR-TRV11 NTSC digital handy camera was used to record the visualization results. The camera was placed at the location of the emitting building models and perpendicular to the flow. The center of the lens was set up at the same level as the emitting building so that the magnitude of the plume rise could be captured. The test section was covered with black plastic to exclude ambient light and eliminate reflection from flume side-wall. The flow visualization system is shown in Figure 3.9 diagrammatically.

3.5 Wind tunnel study

After the completion of the flow visualization study in the water flume, a series of wind tunnel tests were conducted in the boundary layer wind tunnel of the Building Aerodynamics Laboratory (BAL). In these tests, the influence of various parameters was investigated. Of particular interest were the distance between the emitting building and the upwind tall building, stack location, wind direction, and exhaust momentum ratio.

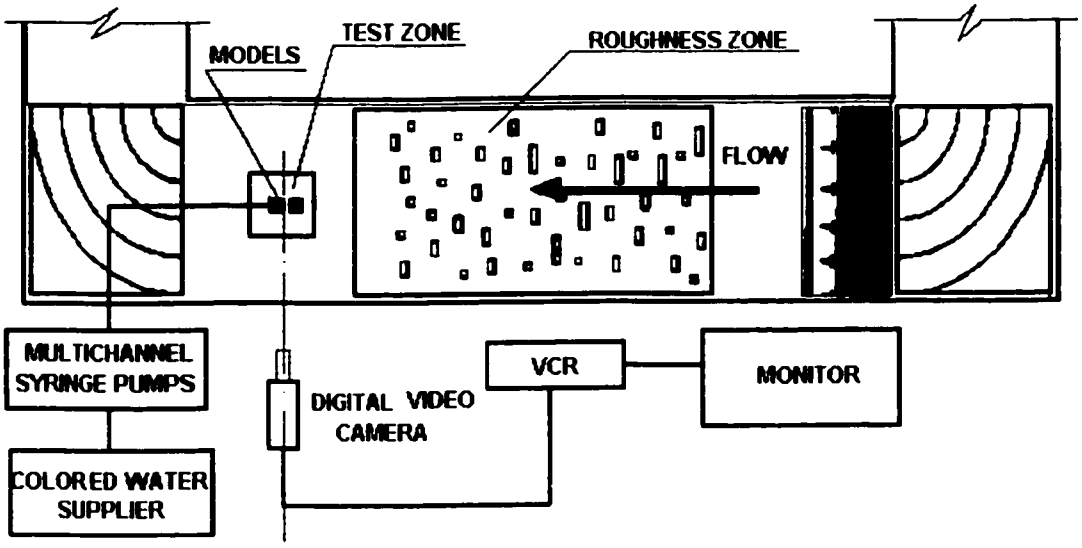

Figure 3.9 Plan view of water flume showing the flow visualization system

3.5.1 The boundary layer wind tunnel at BAL

The boundary layer wind tunnel used in the current study is an open return type with a rectangular cross-section. It is 1.8m wide and 12.2m long. The height can be raised from 1.4m to 1.8m by adjusting the suspended roof. A turntable with a diameter of 1.21m is placed at the downstream end of the facility. Figure 3.10 shows the plan view, the elevation and the section view from downstream end of the tunnel.

The wind is generated by a double inlet centrifugal blower, which is driven by a 50HP motor through a constant pitch V-belt drive. A wind speed range from 3 m/s to 14 m/s can be obtained at the test section by adjusting the flow controller of the blower outlet. By changing the floor roughness, atmospheric boundary layers for three different standard terrain exposures (opening country, suburban, urban) can be simulated. Egg-boxes were used in the present study to simulate the suburban exposure.

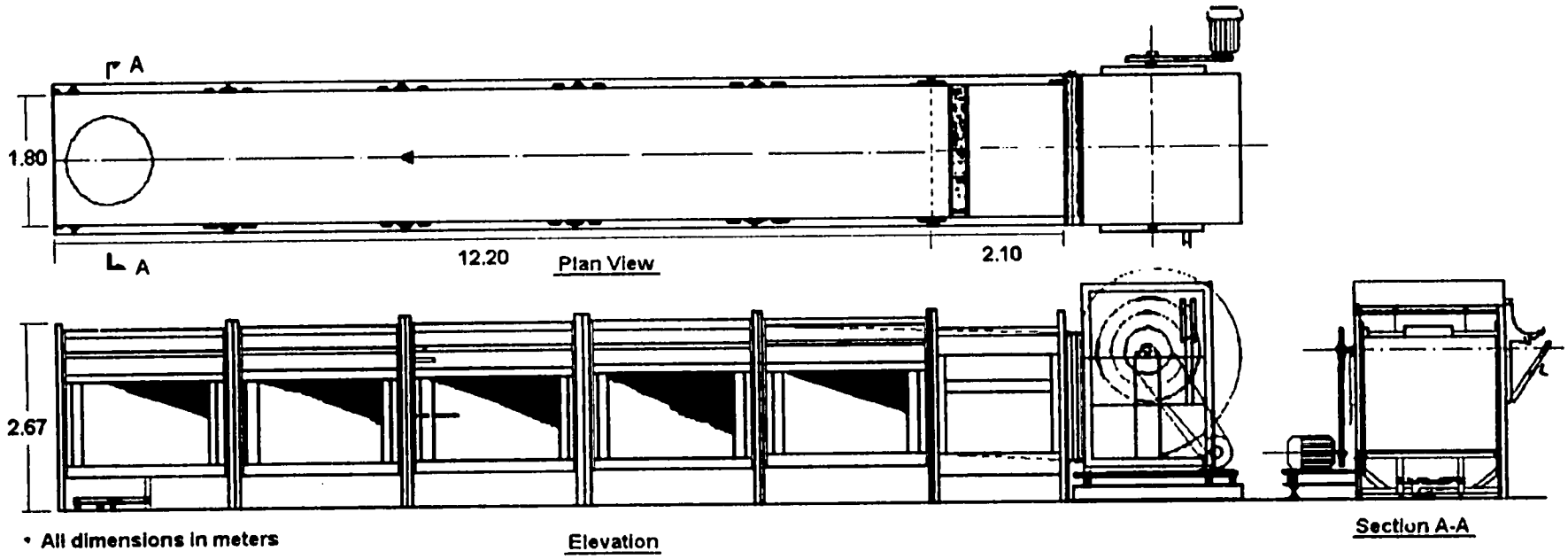

Figure 3.10 Plan view, elevation and section view of the boundary layer wind tunnel at BAL

3.5.2 Wind tunnel experimental procedure

3.5.2.1 Model design

The emitting building was constructed using square-shaped wood blocks with a side dimension (W) of 75 mm and a height (H) of 135 mm. Assuming a model scale of 1:400, the model represents a building 30 m wide 54 m high, i.e., almost the same dimensions as the building used in the water flume.

The model had four different exhaust outlets, which were flush with the roof surface. By changing the building orientation by 180°, seven different outlet locations (A, B, C, D, E, F, and G) were obtained as shown in Figure 3.11. Two adjacent building models, namely Model A and Model B, were constructed. Model A had side dimensions of 75mm*75mm (i.e., W_a = W); Model B had side dimensions of 75mm*150mm (i.e., W_a = 2W). Three different heights, 180mm (H_a = 1.33H), 225mm (H_a = 1.67H), 270mm (H_a = 2H), were obtained by adjusting the attached wood blocks for either Model A or Model B. Figures 3.11 to 3.13 show the measurement wall (leeward wall) for both Model A and Model B.

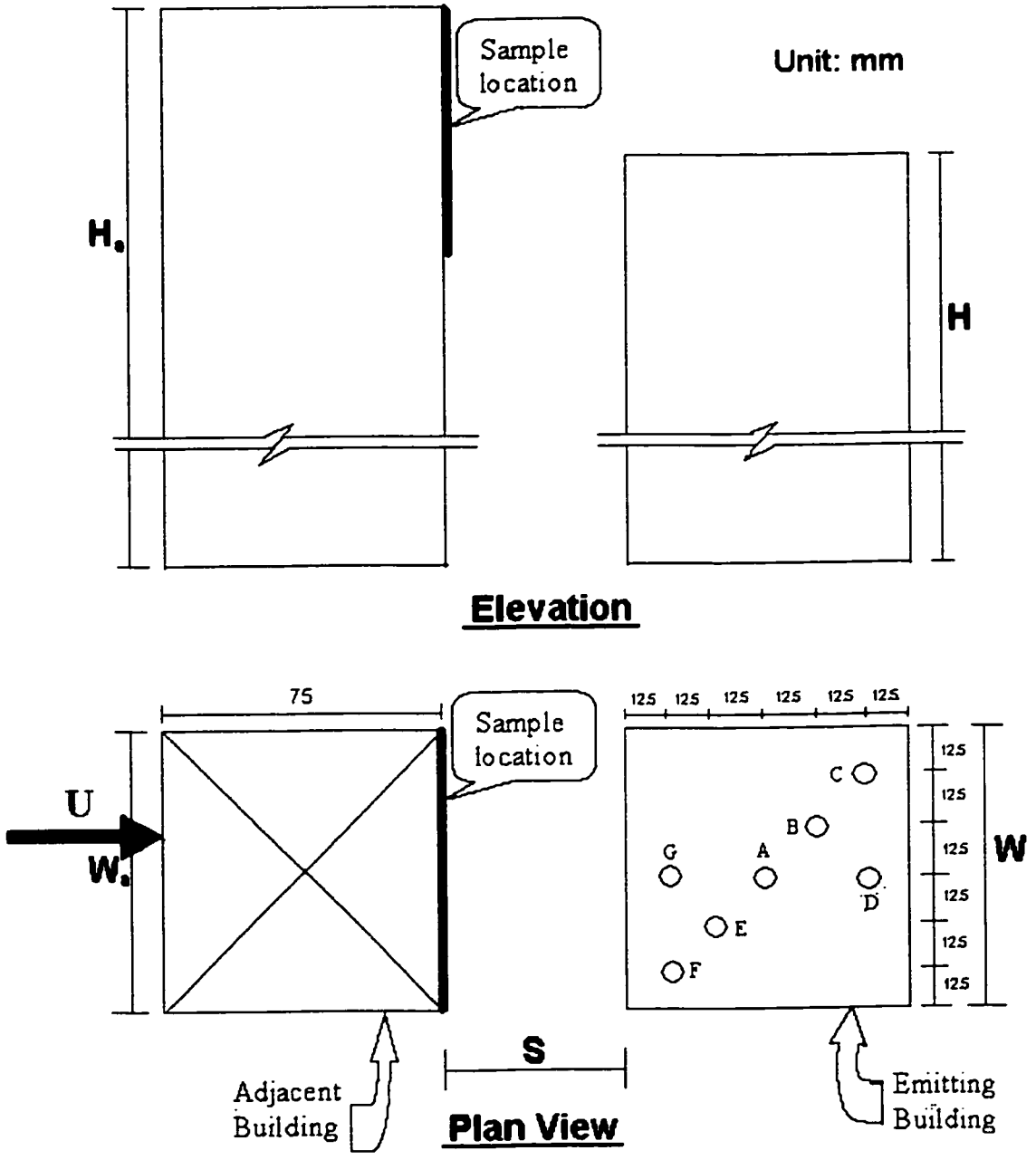

Figure 3.11 Locations of the outlets (Model A, W_a = W, θ = 0°) (wind tunnel experiment)

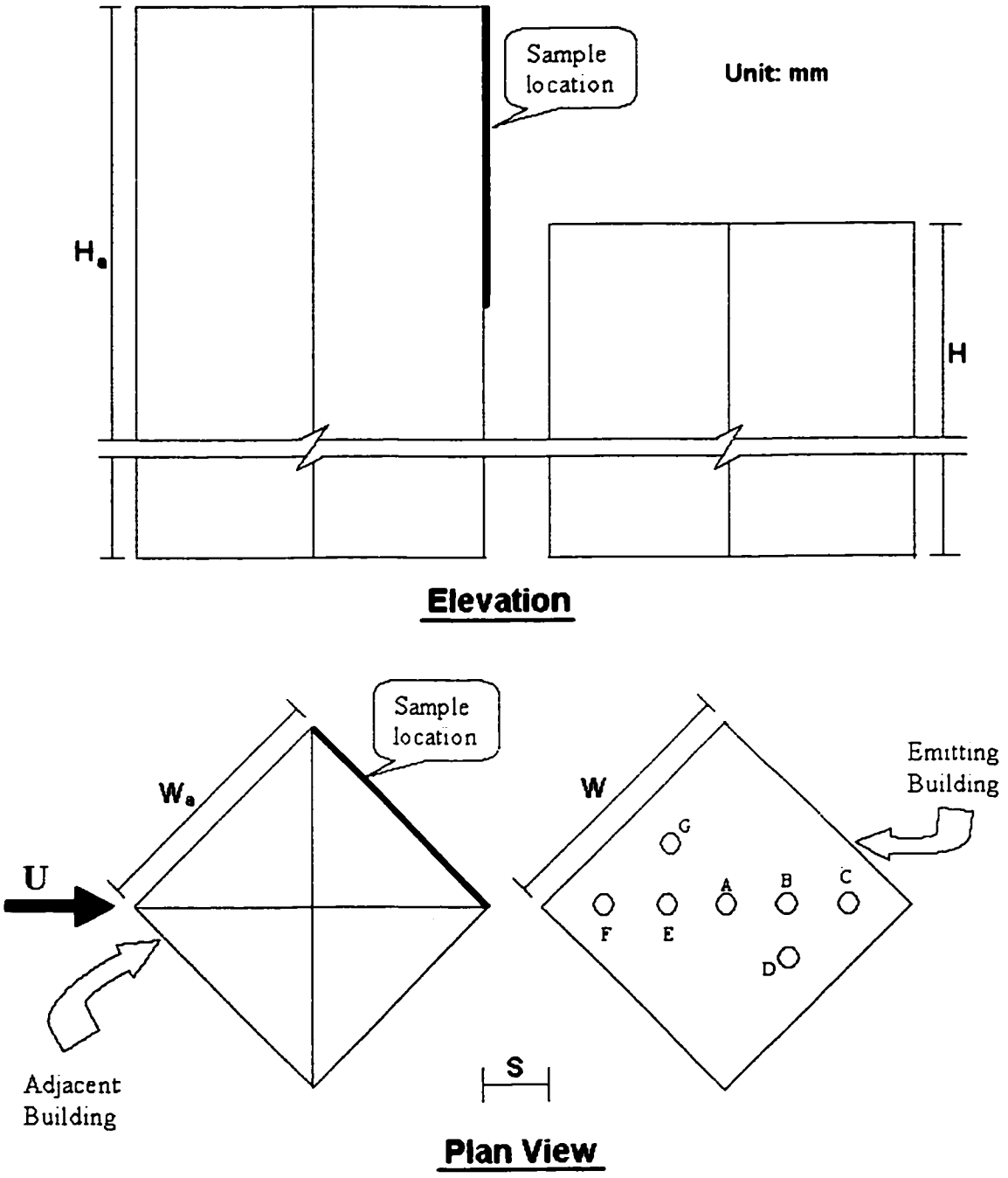

Figure 3.12 Locations of the outlets (W_a = W, θ = 45°) (wind tunnel experiment)

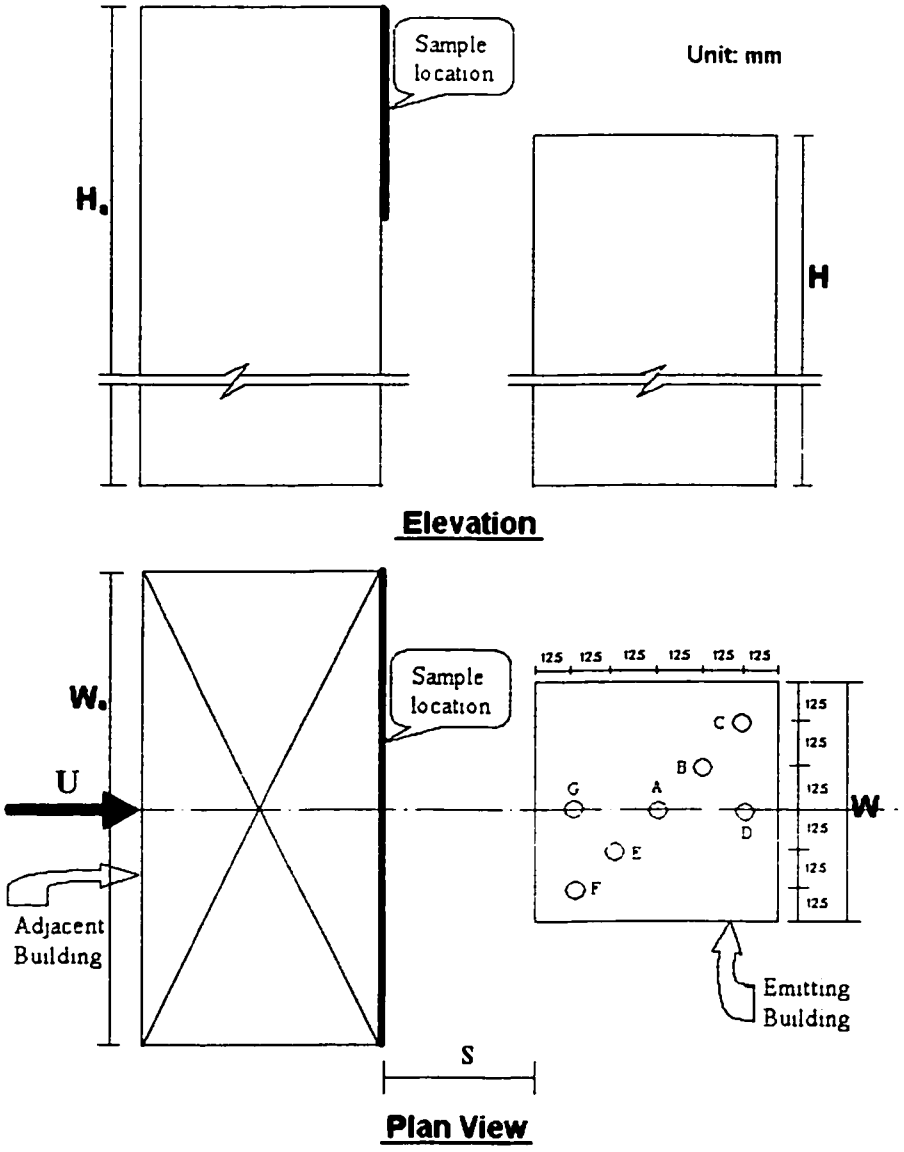

Figure 3.13 Locations of the outlets (Model B, W_a = 2W, 0 = 0°) (wind tunnel experiment)

Figures 3.14 and 3.15 present the sampling locations of the two adjacent building models. The 4mm outlet diameter represents a 1.6m full-scale diameter outlet. Most of the tests are carried out with exhaust momentum ratio, M = 2. A limited number of tests were performed at other M-values (0.5, 1, 3 and 4) for comparison.

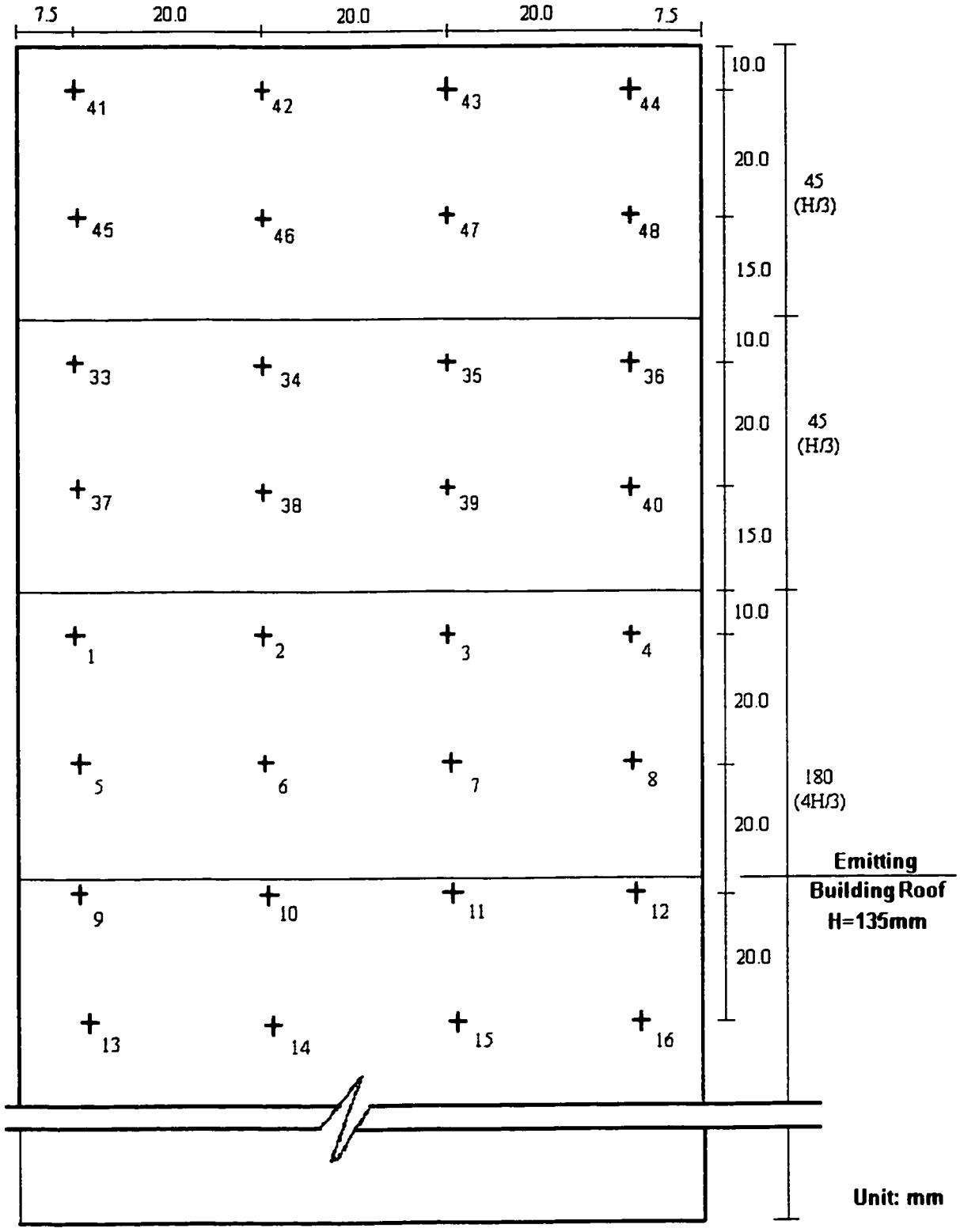

Figure 3.14 Locations of receptors on wind tunnel model (Model A, $W_a = W$)

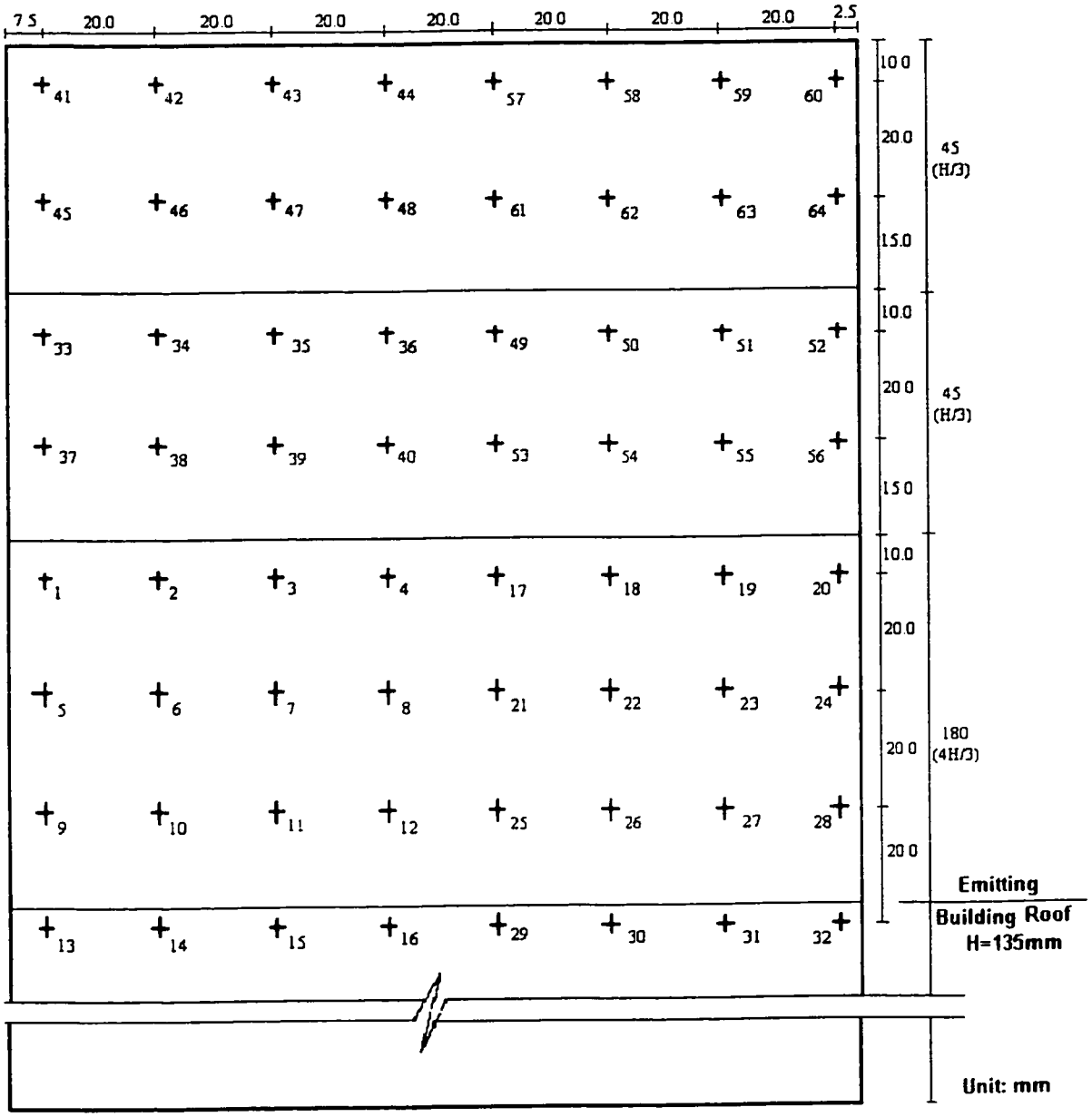

Figure 3.15 Locations of receptors on wind tunnel model (Model B, $W_a = 2W$)

Figures 3.16 and 3.17 show the pictures taken from the case of $H_a = 2H$, $W_a = W$, $S = 0$, and $\theta = 0°$. Figure 3.16 shows the crosswind direction photo as well as Figure 3.17 the along-wind direction.

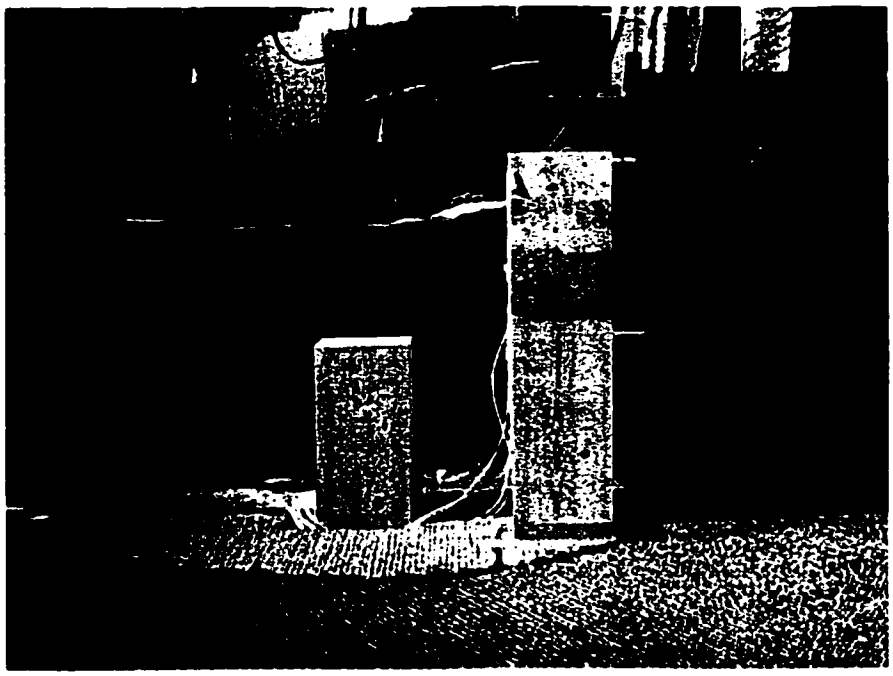

Figure 3.16 Photo of wind tunnel models (crosswind direction)

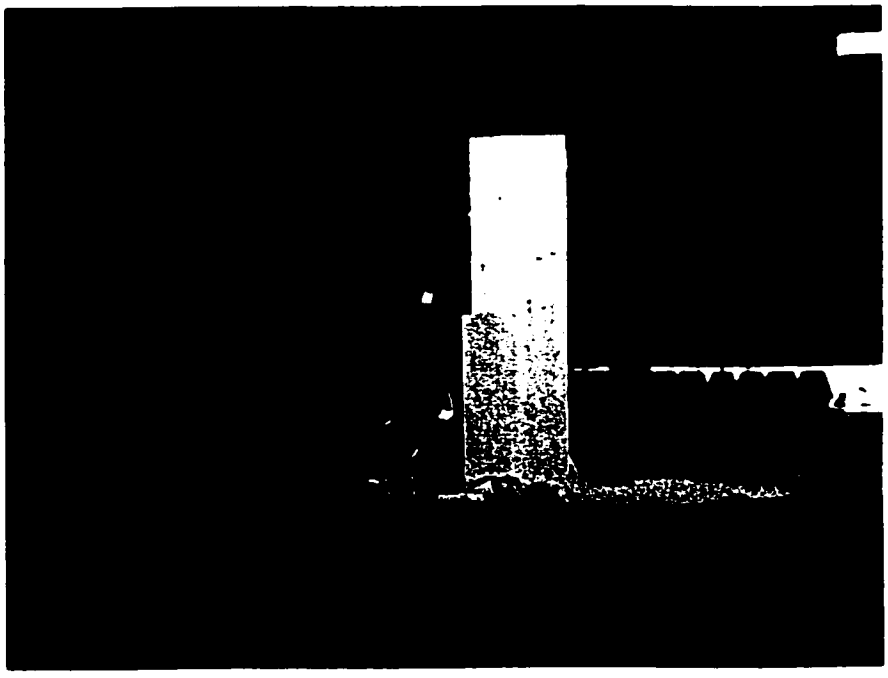

Figure 3.17 Photo of wind tunnel models (along-wind direction)

3.5.2.2 Wind tunnel velocity calibration

Before each test, mean wind speed and turbulence intensity were measured. The reference wind velocity, U_g, was measured with a Pitot tube located 600 mm above the floor of the tunnel. In a 1:400 scale, it represented a reference height of 240m. A second reference wind speed, U_H, was measured using a TSI hot film anemometer at the height of the emitting building model roof. The data were obtained with an ANALOGIC Universal Waveform Analyzer (Model 6100).

The wind speed at the building height was 4.6m/s. This value of U_H gave a building Reynolds number ($Re_b = U_H W/\nu$) of approximately 23000, which met the strict criterion for Reynolds number independence, $Re_b = 11000$, specified in ASHRAE (2001), where ν is the kinematic viscosity of the air, 0.15cm^2/sec at 20°.

The value of Re_s ($Re_s = w_e d_s/ \nu$) in the present study, assuming M = 2 (i.e., $w_e = 9.2$m/s), was approximately 2500, which met the strict criterion for Reynolds number independence, $Re_s = 2000$, specified in ASHRAE (2001).

A suburban exposure, with a power law exponent of 0.24, was used to simulate the atmospheric boundary layer that exists far upwind of the test section. Vertical profiles of mean velocity and turbulence intensity are shown in Figures 3.18 and 3.19.

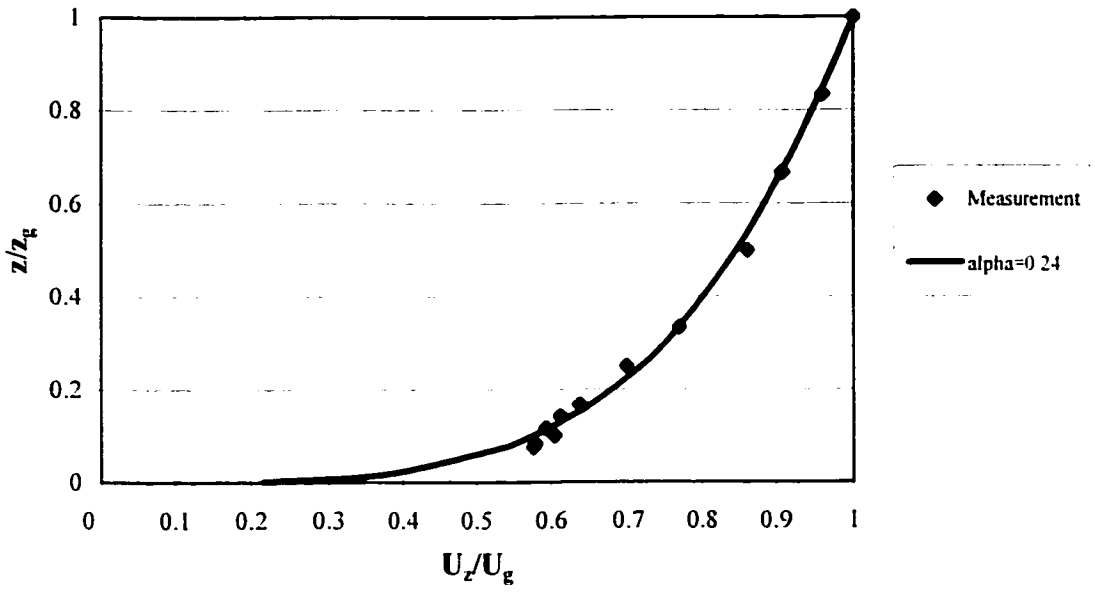

Figure 3.18 Vertical profiles of mean velocity at model location

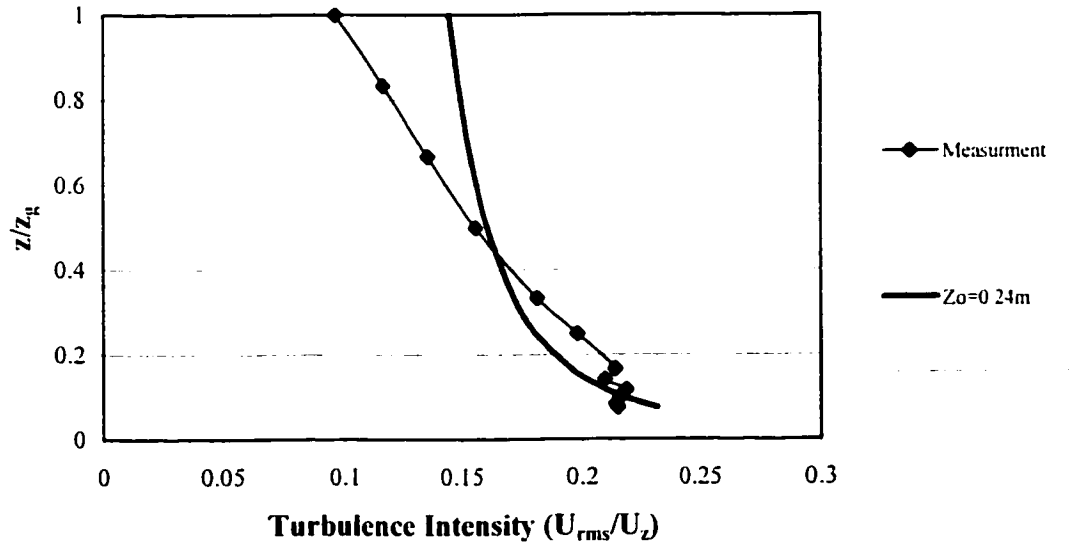

Figure 3.19 Vertical profiles of turbulence intensity at model location

The reference wind speed height, z_g = 600mm, represents 240-meter in a 1:400 scale. As shown in Figure 3.19, turbulence intensity is about 20% at emitting building model roof (H = 135mm, which represents a 54m high building in full-scale). The solid line represents the turbulence intensity in terms of $I_u \approx \frac{1}{\ln \frac{z}{z_o}}$ for roughness length z_o = 0.24m, which is derived from the measured mean velocity data. Generally, in a suburban to urban environment, z_o varies from 0.8m to 3m (Biétry et al. [1983]). However, the flow structure is very difficult to simulate. The low z_o value may be due to the fact that mean wind velocity and turbulence intensity were measured without any very near surrounding buildings.

3.5.2.3 Concentration measurement procedure

As discussed in Chapter 2, the exhaust momentum ratio, which is given by $M = (\rho_e/\rho_a)^{0.5} w_e/U_H$, is a key parameter for modeling plume rise. If it is assumed that the densities of exhaust and ambient air are the same, this parameter can be simplified as $M = w_e/U_H$. Once the wind speed at roof height is obtained, the exhaust mass flow rate (MFR) can be varied to provide specific values of the momentum ratio. For example, to obtain M = 1, the exhaust MFR is adjusted so that $w_e = U_H$.

The experiments were carried out by adjusting the exhaust flow rate and wind speed to match the desired M-value.

Sulfur hexafluoride (SF_6) was used as tracer gas for the wind tunnel experiments because

it is inert and easily detectable. A certified mixture of SF_6 and nitrogen was emitted from a model outlet and the mean concentrations of SF_6 at the wall of the adjacent building were measured by using a Varian Gas Chromatograph (GC). Calibration curves for the Varian GC are provided in Appendix B.

The tracer gas experiment method is presented schematically in Figure 3.20. The outlet concentration (C_e) was varied depending on dilution measured at the receptors, so that the concentrations remained within the optimum measurement range of the GC - refer to the calibration curves provided in Appendix B. A Matheson flow meter was employed to obtain the precise exhaust mass flow rate. The flow control meter was calibrated periodically during the study.

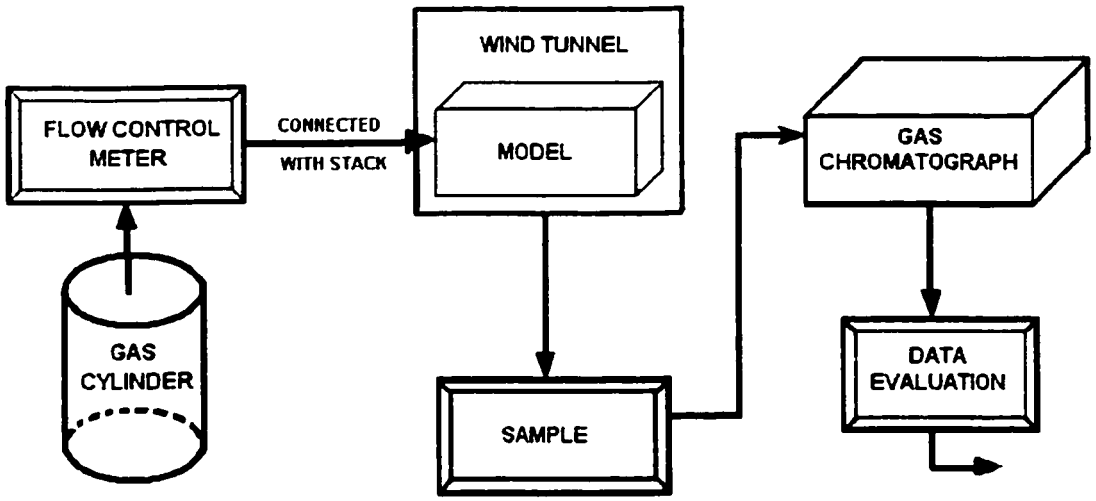

Figure 3.20 Tracer gas experiment system

Samples of air were collected via plastic tubes and syringes from each sample location

shown in Figures 3.14 and 3.15 by using a Multichannel Syringe Pump made by Cole-Parmer Instrument Company. Figure 3.21 shows the syringe pump and the models.

Figure 3.21 Photo of syringe pump and models

3.5.2.4 Critical configurations

The water flume visualization study identified the most critical building configurations with respect to the potential for reingestion at fresh air intakes. Wind tunnel experiments were carried out to obtain quantitative data for these configurations.

Table 3.1 presents the study configurations that were used in the wind tunnel study. Figures 3.22 to 3.24 illustrate all the configurations listed in Table 3.1. In the figures, emitting buildings are marked with black.

Table 3.1 Configurations used in the wind tunnel study

Case No.	Wind Direction	M-Value	Adjacent Building Width (W_a)(mm)	Adjacent Building Height (H_a)(mm)	Separation Distance (S)(mm)
1	0°	2	W(75)	1.33H(180)	0
2	0°	0.5	W(75)	1.33H(180)	0
3	0°	1	W(75)	1.33H(180)	0
4	0°	3	W(75)	1.33H(180)	0
5	0°	4	W(75)	1.33H(180)	0
6	0°	2	W(75)	1.33H(180)	0.25W(18.8)
7	0°	2	W(75)	1.67H(225)	0.75W(56.3)
8	0°	2	W(75)	1.67H(225)	W(75)
9	0°	2	W(75)	2H(270)	0.75W(56.3)
10	0°	2	W(75)	2H(270)	W(75)
11	0°	2	2W(150)	1.33H(180)	0.75W(56.3)
12	0°	2	2W(150)	1.33H(180)	W(75)
13	0°	2	2W(150)	1.67H(225)	1.75W(131.3)
14	0°	2	2W(150)	1.67H(225)	2W(150)
15	0°	2	2W(150)	2H(270)	2W(150)
16	0°	0.5	2W(150)	2H(270)	2W(150)
17	0°	1	W(75)	2H(270)	2W(150)
18	0°	3	W(75)	2H(270)	2W(150)

Table 3.1 Configurations used in the wind tunnel study (Continued)

Case No.	Wind Direction	M-Value	Adjacent Building Width (W_a)(mm)	Adjacent Building Height (H_a)(mm)	Separation Distance (S)(mm)
19	0°	4	W(75)	2H(270)	2W(150)
20	0°	2	W(75)	2H(270)	2.25W(168.8)
21	45°	2	W(75)	1.33H(180)	0
22	45°	2	W(75)	1.33H(180)	0.71W(53)
23	45°	2	W(75)	1.67H(225)	0.71W(53)
24	45°	2	W(75)	1.67H(225)	1.06W(79.5)
25	45°	0.5	W(75)	1.67H(225)	1.06W(79.5)
26	45°	1	W(75)	1.67H(225)	1.06W(79.5)
27	45°	3	W(75)	1.67H(225)	1.06W(79.5)
28	45°	4	W(75)	1.67H(225)	1.06W(79.5)
29	45°	2	W(75)	2H(270)	1.41W(106.1)
30	45°	2	W(75)	2H(270)	1.77W(132.6)
31	0°	2	2W(150)	1.33H(180)	2W(150)
32	0°	1	W(75)	2H(270)	0
33	0°	2	W(75)	2H(270)	0
34	0°	3	W(75)	2H(270)	0
35	0°	1	W(75)	2H(270)	W/3(25)
36	0°	2	W(75)	2H(270)	W/3(25)
37	0°	3	W(75)	2H(270)	W/3(25)

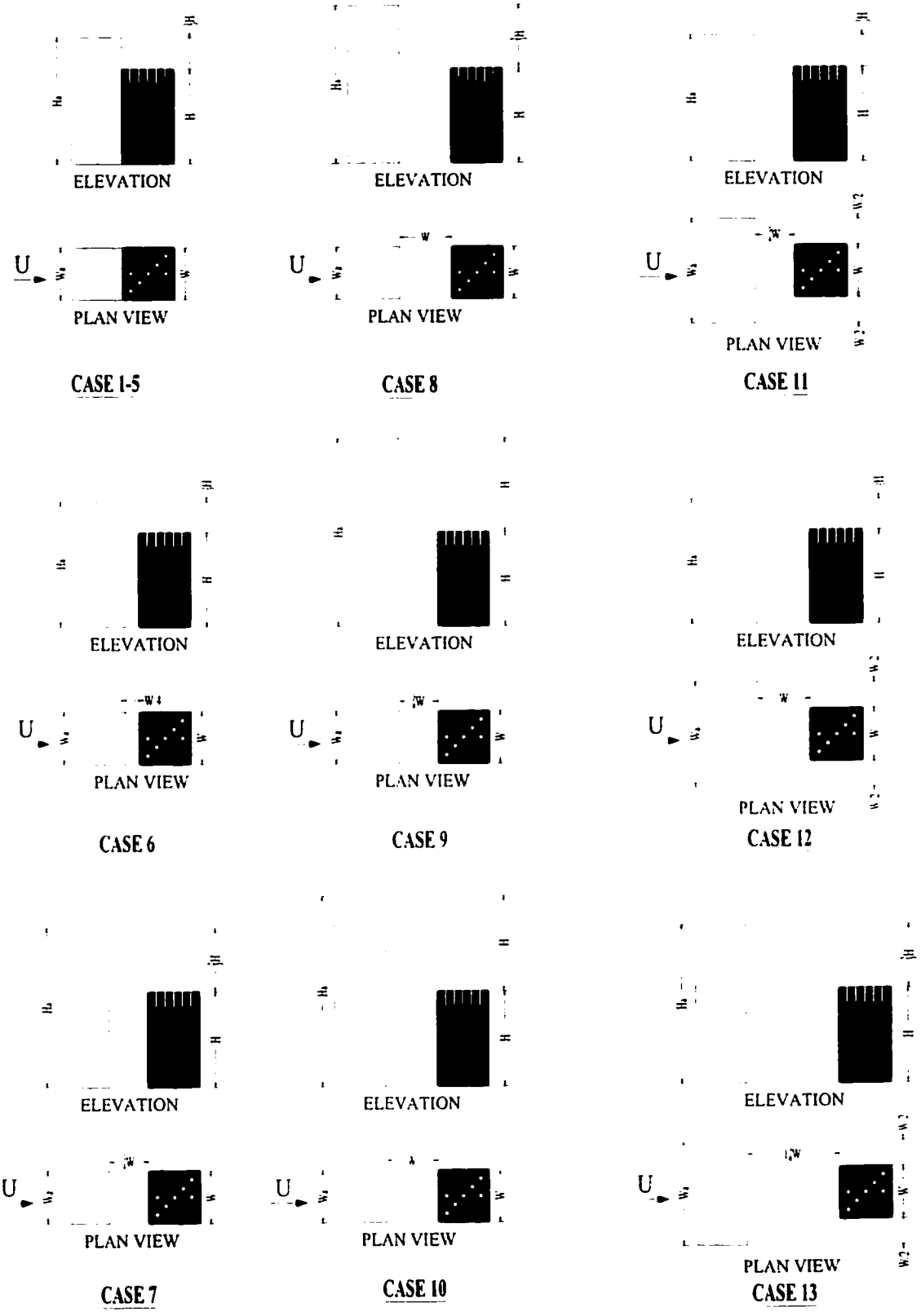

Figure 3.22 Configurations tested in the wind tunnel study (I)

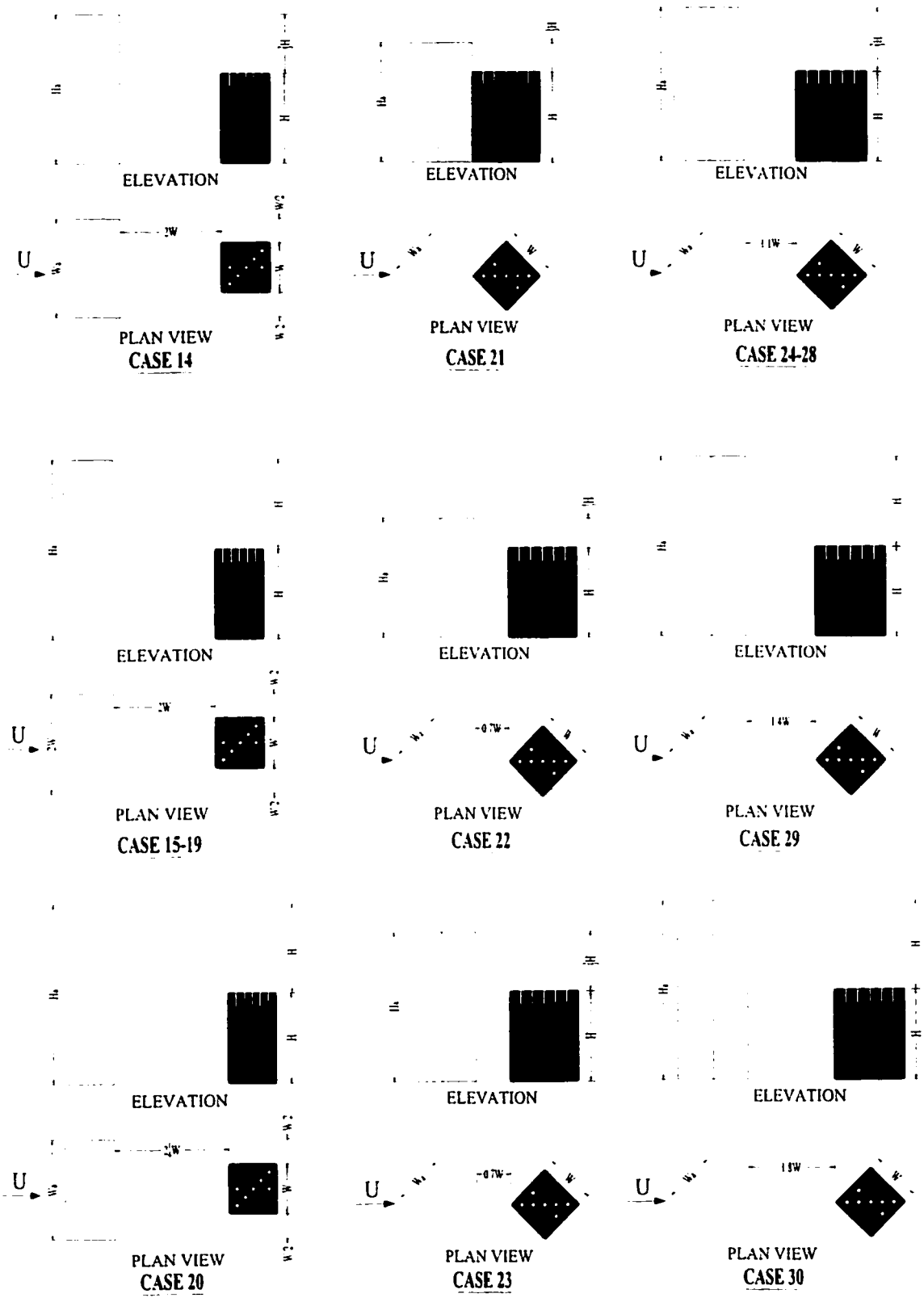

Figure 3.23 Configurations tested in the wind tunnel study (II)

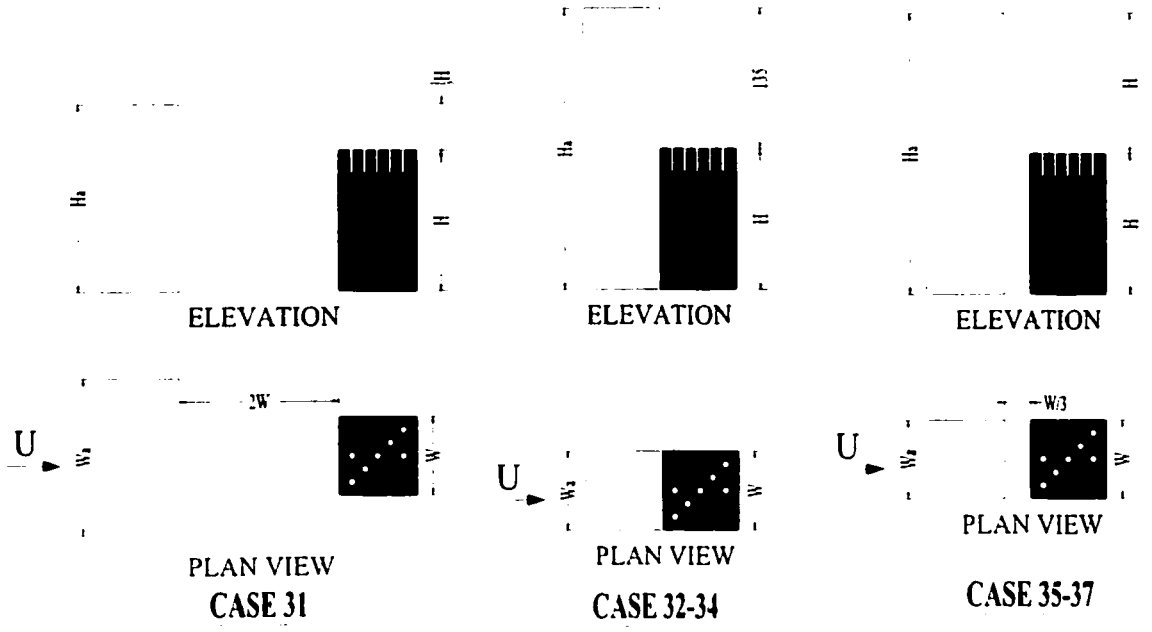

Figure 3.24 Configurations tested in the wind tunnel study (III)

3.5.2.5 Repeatability experiments

Repeatability experiments were conducted by repeating the same test on different days. During the present study period, the injection valve of the GC was changed because of technical problems. Typical repeatability test results are shown in Figure 3.25 for the central stack. Some tests were performed using different exhaust concentration. Since the exhaust concentration has an uncertainty of only 1%, the use of different tracer gas mixtures should not contribute significantly to measurement error except due to different GC range. Other sources of discrepancies in repeated tests are expected to be associated with slight changes in model orientation. The variances between dilution values measured on three different days were usually lower than 15%, although in some cases variances of

up to 40% were obtained. The reason for the high variation in certain samplers maybe due to the fact that their locations were lower than the emitting building rooftop (i.e., z/H < 1, where z is sampler height and H is emitting building height), and the dilution values obtained were higher than those obtained on the other locations.

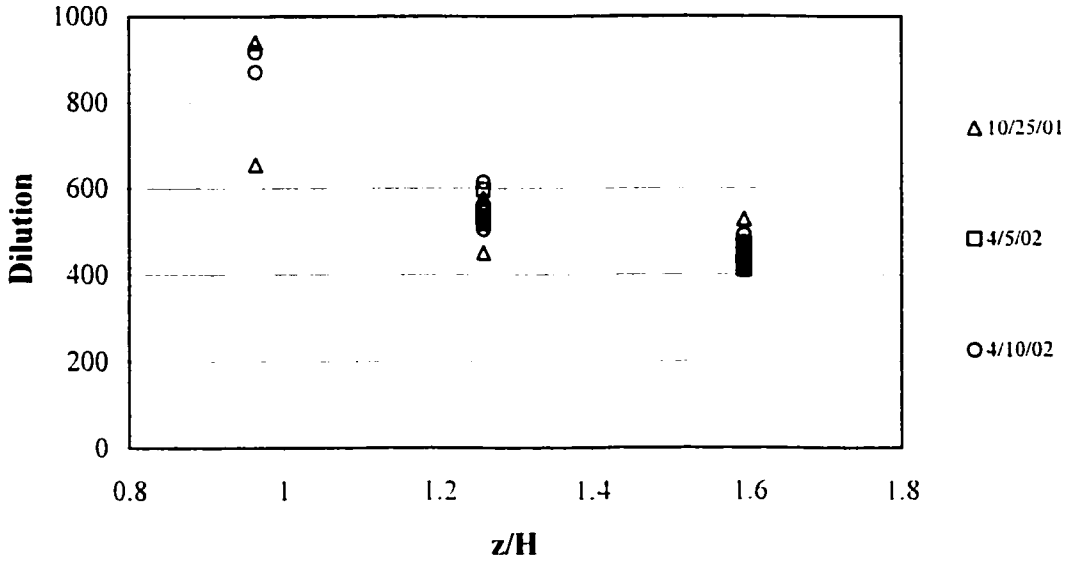

Figure 3.25 Repeatability of dilution measurements

3.5.2.6 Effect of stack height

A common method for increasing dilution is to increase the stack height. Concentrations with three different stack heights, h_{s1} = 2.5mm, h_{s2} = 12.5mm, and h_{s3} = 25mm were measured and compared with results obtained with the flush outlets. At a scale of 1:400, these stacks represent full-scale stack heights of 1m, 5m, and 10m, respectively.

CHAPTER 4

RESULTS AND DISCUSSION OF WATER FLUME STUDY

4.1 Introduction

Water flume experiments were carried out to identify the critical building configurations with respect to re-ingestion of exhaust gases at fresh air intakes. The study focussed on plumes emitted from a lower downwind building which might affect the adjacent building. The water flume study investigated the significance of various parameters. These include:

- M-value (M = 0.5, 1, 2, and 3);
- Wind direction ($\theta = 0°$ and 45°);
- Adjacent building height (H_a = 1.33H, 1.67H, and 2H);
- Adjacent building width (W_a = W and 2W);

During the study, two emitting building widths, Model A (squared-shaped W * L = 31mm * 31mm), and Model B (rectangular-shaped W * L = 62mm * 31mm) were used in some cases for comparison purposes.

This chapter provides qualitative results obtained in visualization study. Based on the video images, critical cases are identified for more detail study in the boundary layer wind tunnel.

4.2 General flow patterns

As described in Chapter 3, eighteen (18) configurations were examined in the first phase (initial visualization experiments) to verify the general flow patterns — see Figures 3.7 and 3.8.

The visualization results of the general flow patterns for all the eighteen configurations are presented in detail in Appendix C.

The plume did not make contact with the isolated building for M = 2 and wind direction θ = 0° and θ = 45°, a typical video image for θ = 0° is shown in Figure 4.1. Note that building shape is a key factor for an isolated building. If streamwise depth is small relative to height (i.e., H/D > 2), the plume will not make direct contact with roof receptors. On the other hand, if the streamwise depth is large, the plume may make contact with the roof.

Significant changes to the plume behavior were evident when a tall building was located either upwind or downwind of the emitting building. Figures 4.2 to 4.4 show that plume rise is significantly reduced when a building with height H_a = 2H and width W_a = W or W_a =2W is located near the emitting building for M = 2 and wind direction is either θ =

0° or θ = 45°.

Figure 4.1 Visualization of plume from isolated building (θ = 0°) (Configuration I)

Figure 4.2 shows that the flow field around the tall building significantly affects the plume. Flow bifurcates on the windward face. At $z \approx 2/3H$, plume travels downward but also toward edges due to low pressure, as shown in Figure 4.2 (a). However, Figure 4.2 (b) shows that if upstream building is wide, plume cannot travel around it, but instead is brought down toward the ground and re-circulates. This phenomenon is known as Street

Canyon Effect, — see Figure 1.1.

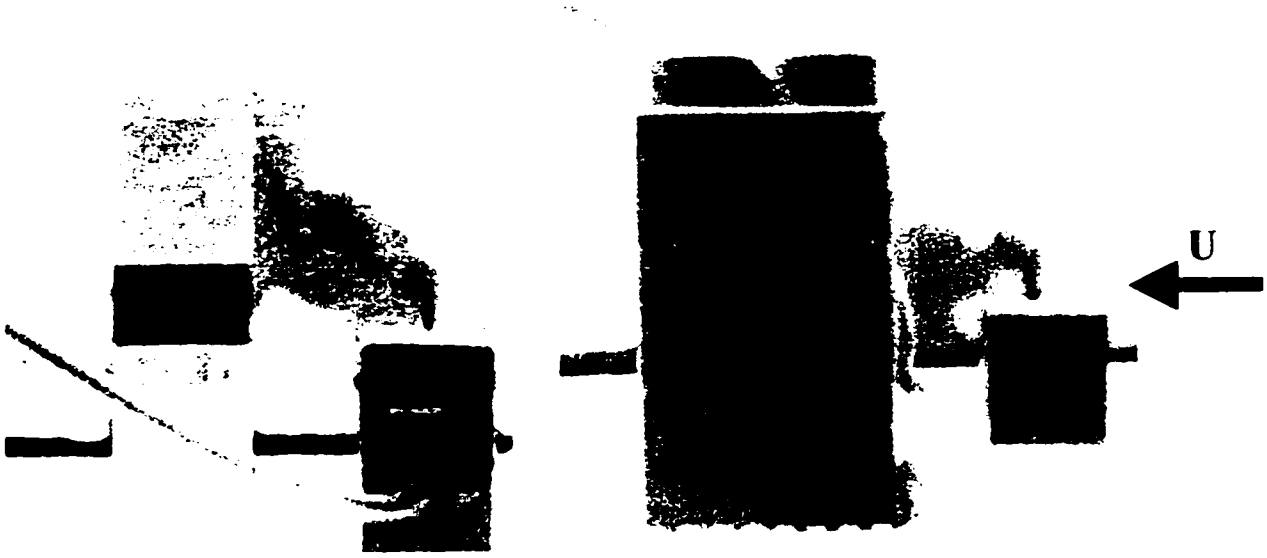

(a) Model A **(b) Model B**

Figure 4.2 Visualization of plume with tall building downwind of emitting building ($\theta = 0°$) (Configuration VI)

Figure 4.3 shows the flow patterns when a tall adjacent building was located upwind for wind direction $\theta = 0°$. Plume was dragged back to the adjacent building due to the wake formed by the adjacent building. The plumes travel upward till the edge of the rooftop. Similar results can be found for $\theta = 45°$, as shown in Figure 4.4.

As shown in Figure 4.5, M-value is not a very important factor in this context within a certain range (from 0.5 to 3).

(a) Model A (b) Model B

Figure 4.3 Visualization of plume with tall building upwind of emitting building ($\theta = 0^{\circ}$) (Configuration III)

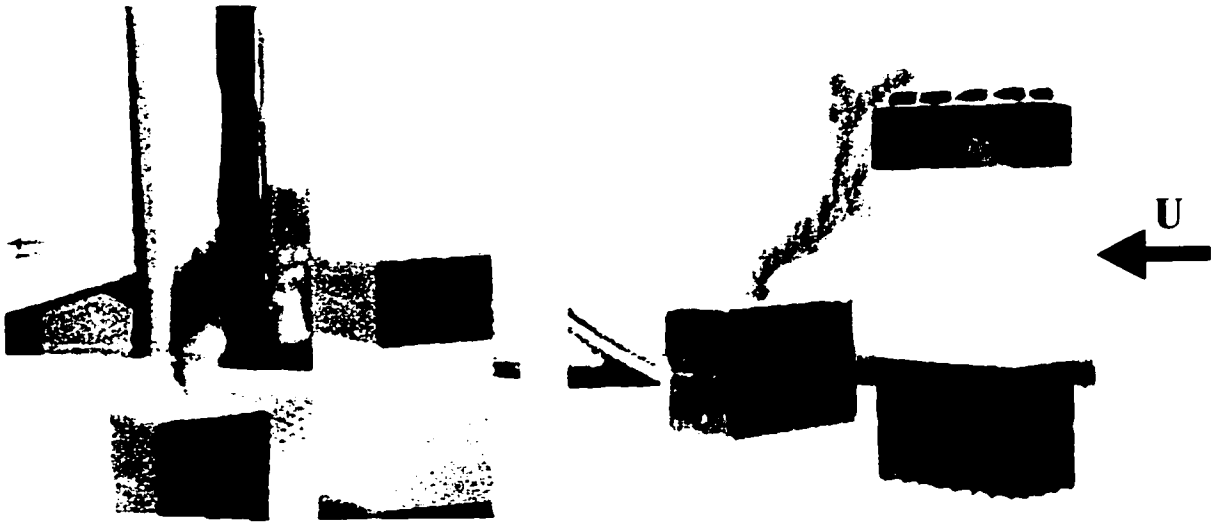

(a) Model A (b) Model B

Figure 4.4 Visualization of plume with tall building upwind of emitting building ($\theta = 45^{\circ}$) (Configuration VIII)

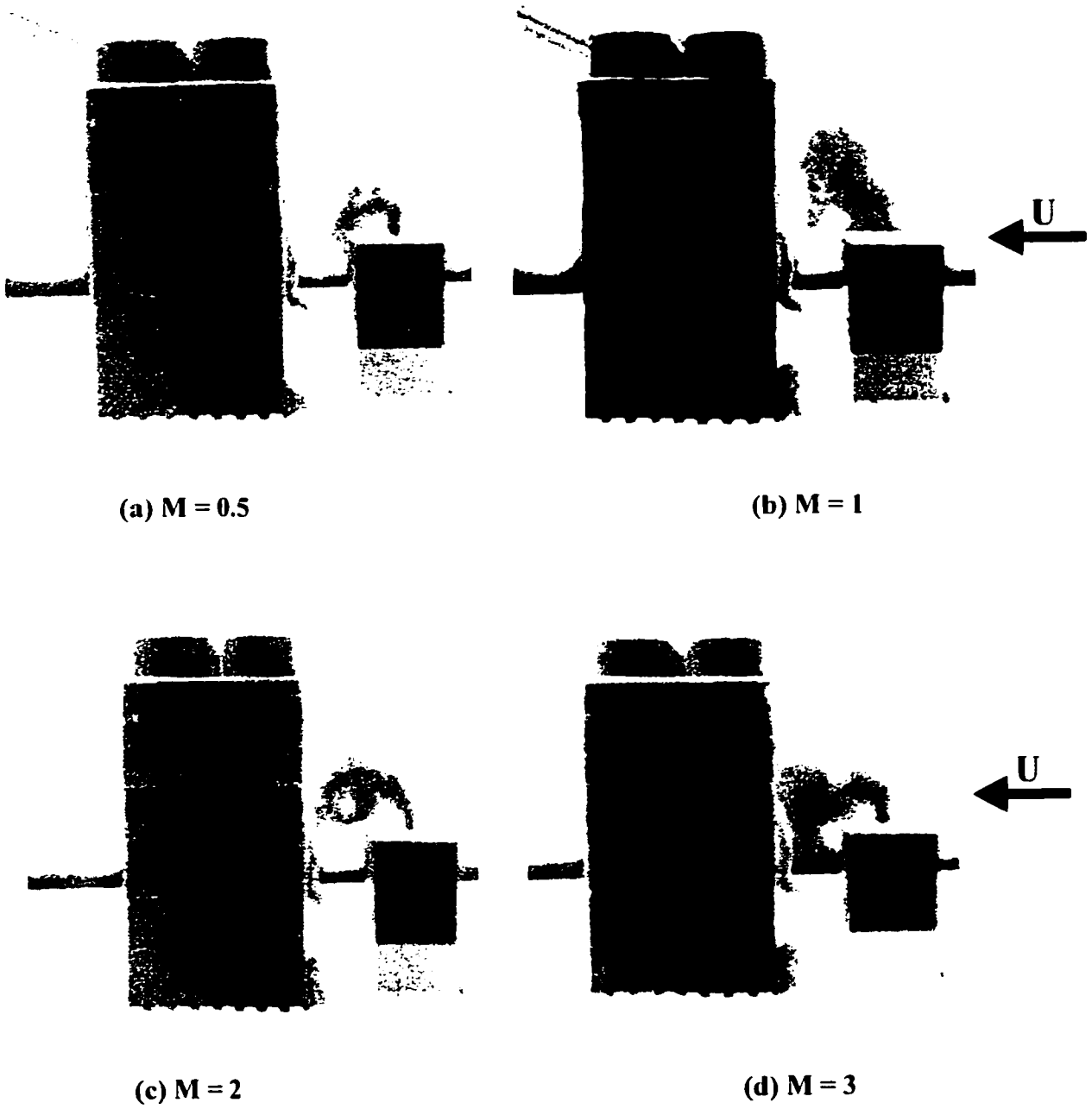

(a) M = 0.5

(b) M = 1

(c) M = 2

(d) M = 3

Figure 4.5 Visualization of plume with tall building downwind of emitting building ($\theta = 0^{\circ}$, M = 0.5, 1, 2 and 3) (Configuration VI-1)

From the study, the zone of influence of a building on the exhaust emitted by an adjacent building can be summarized as follows:

- The plume always makes contact with an adjacent building downwind of emitting building. For some separations, the "street canyon" effect may occur, causing contamination of the leeward wall of the emitting building and the windward wall of the adjacent building; this configuration should be avoided by the designer.

- The wake of upwind adjacent building may cause the plume from the emitting downwind building to travel upwind. The zone of influence will depend on separation distance of buildings, width of the adjacent building, wind direction, and relative heights of buildings. This situation will be discussed in detail in next section.

4.3 Critical configurations for a taller adjacent building upwind

Based on the general flow pattern study, the critical distance between the emitting building and the upwind adjacent building was investigated. In total about 150 building configurations were examined to verify the critical distance. Table 4.1 presents the critical and non-critical distances for which the exhaust will or will not affect the adjacent building. Figures 4.6 to 4.10 show the different cases listed in Table 4.1. Emitting building in all these figures is marked with black.

Table 4.1 The effective distances between two buildings

Configurations	Wind Direction (θ°)	Adjacent Building Width (W_a)	Adjacent Building Height (H_a)	Critical Distance	Non-critical Distance	Figure
A	0	W	1.33H	0.25W	0.5W	4.6
			1.67H	0.75W	W	
			2H	W	1.25W	
B	0	2W	1.33H	0.5W	0.75W	4.7
			1.67H	2W	2.25W	
			2H	2.25W	2.5W	
C	0	2W	1.33H	0.5W	0.75W	4.8
			1.67H	2W	2.25W	
			2H	2.25W	2.5W	
D	45	W	1.33H	N/A	N/A	4.9
			1.67H	0.71W	1.06W	
			2H	1.41W	1.77W	
E	45	W	1.33H	N/A	0	4.10
			1.67H	0	0.25W	
			2H	0	0.25W	

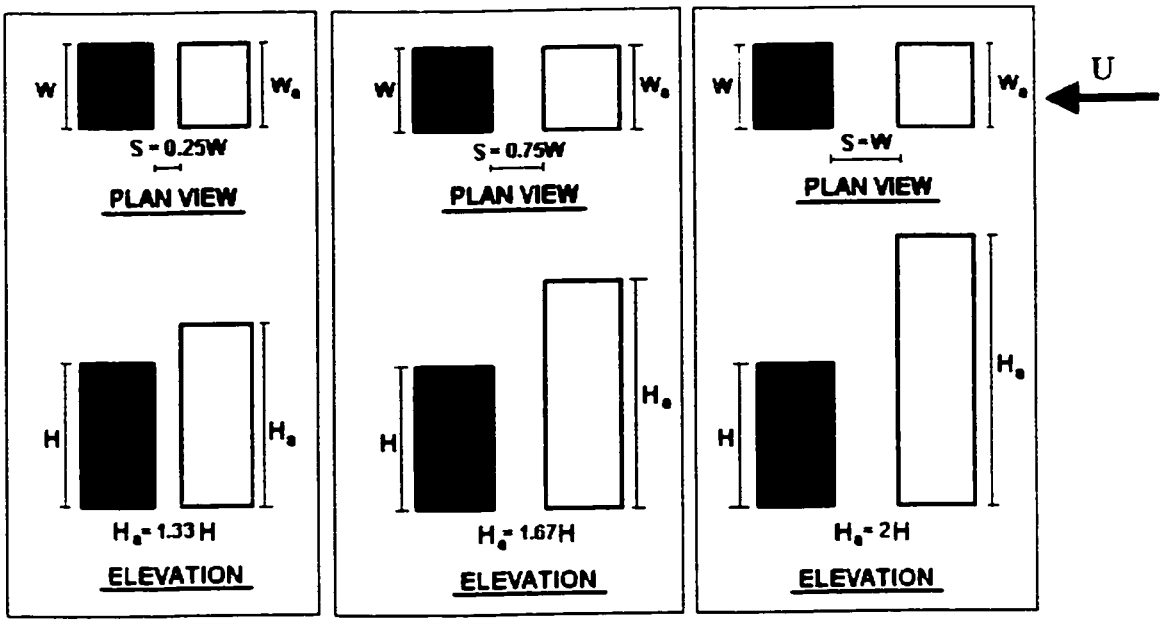

Figure 4.6 Critical building separations (Case A)

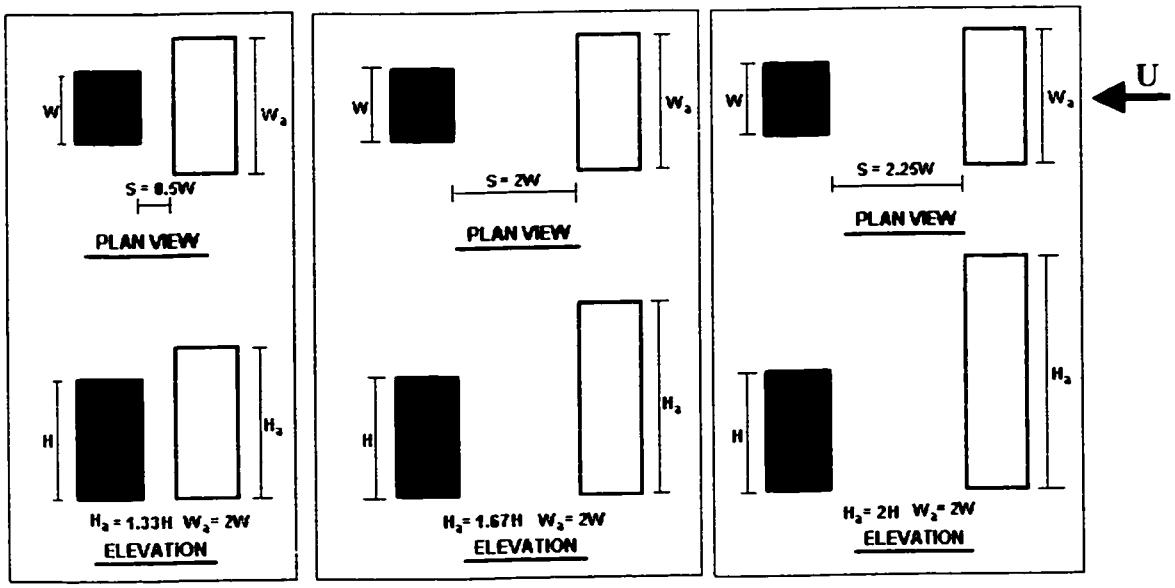

Figure 4.7 Critical building separations (Case B)

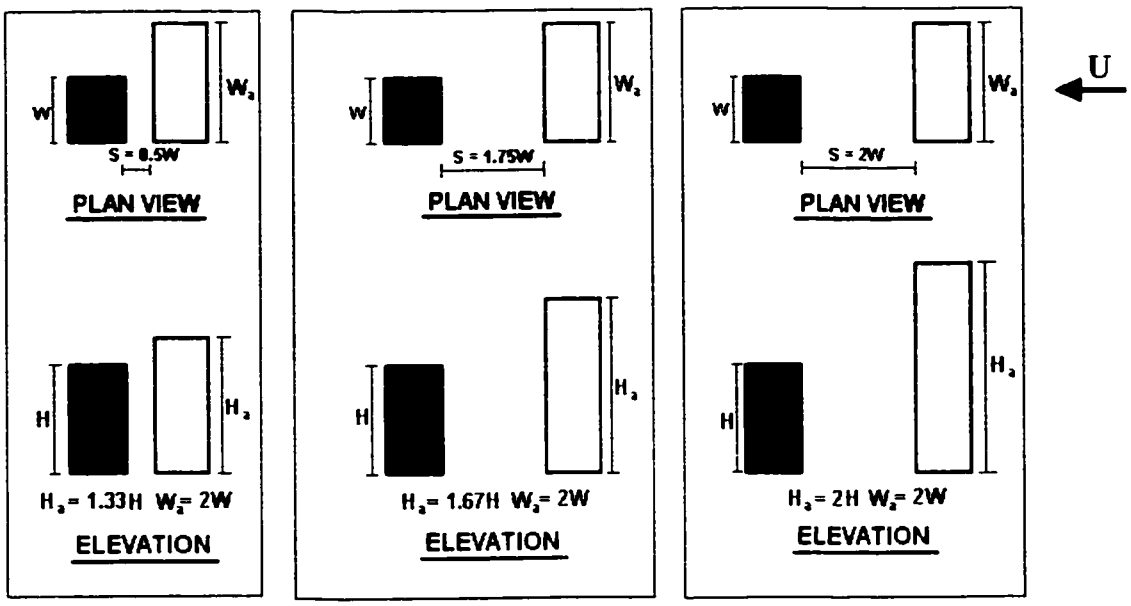

Figure 4.8 Critical building separations (Case C)

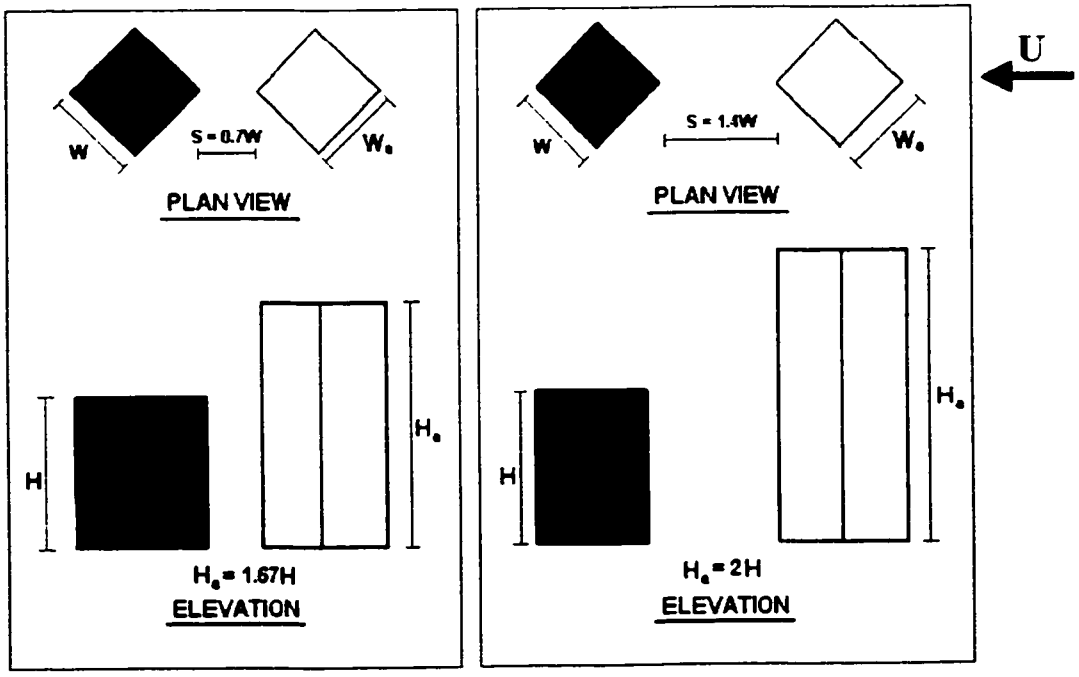

Figure 4.9 Critical building separations (Case D)

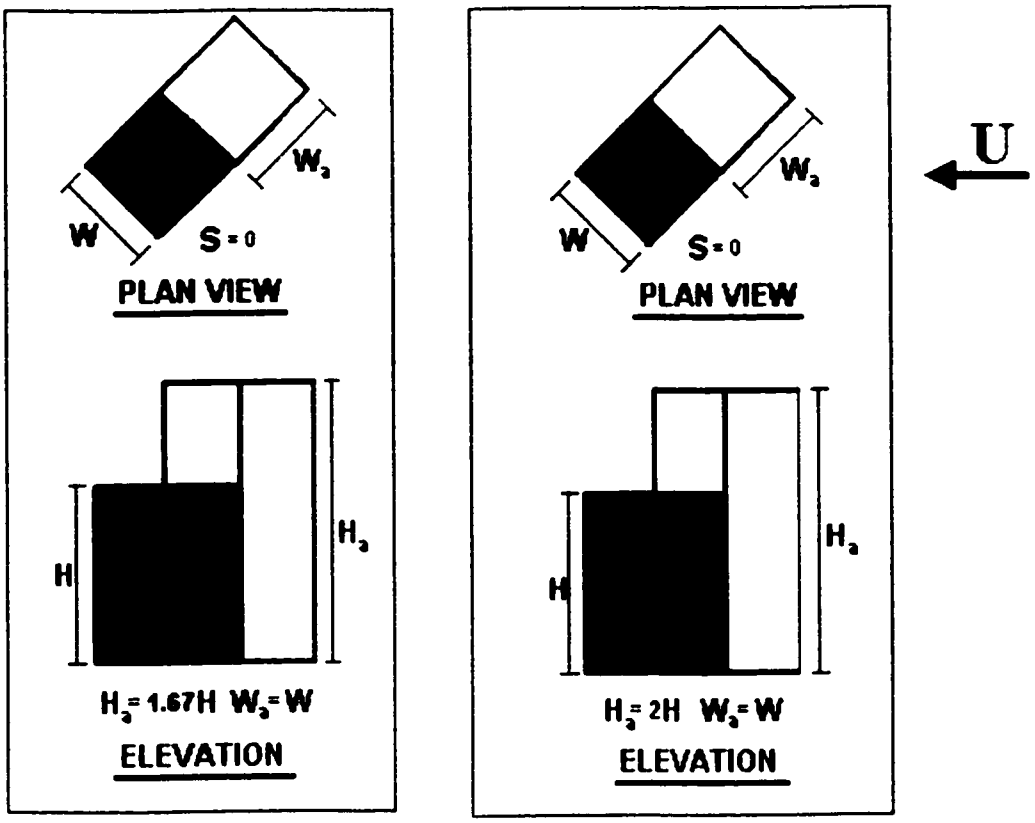

Figure 4.10 Critical building separations (Case E)

As shown in Figure 4.11, the critical distance depends on relative height and width. As height of upwind adjacent building increases, the critical distance will increase; likewise as the width of upwind building increases, the critical distance will increase.

The full-scale equivalent width of emitting building is W = 31m. Therefore, the critical separation of the buildings (S_c) is 0.75W = 23m for the case of W_a = W and H_a/H less than 1.67. If adjacent building height increases to 2H, the separation should be increased to 31m for θ = 0° and 44m for θ = 45°. On the other hand, for a wide upwind adjacent building (W_a =2W), separations should become much larger than those of W_a = W.

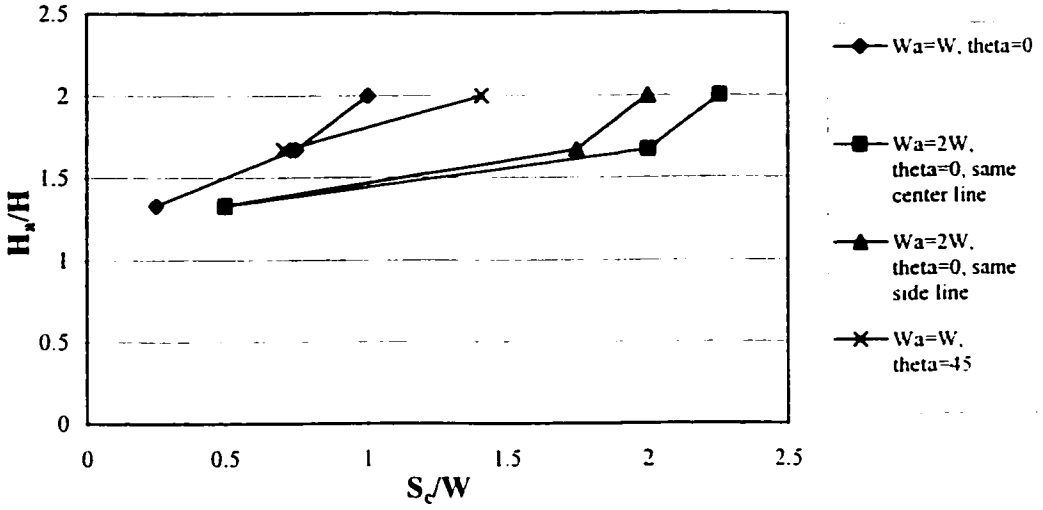

Figure 4.11 Relationship between height ratio and critical separation for M = 2

Figures 4.6, 4.9, and 4.11 indicate that when the wind direction is changed from $\theta = 0°$ to $\theta = 45°$, the critical distance will change from W to 1.41W at a ratio of $H_a/H = 2$ (Case A and Case D). Wind direction plays an important role in the pollutant dispersion. Significant change in dilution will occur if the wind direction changes.

4.4 Closure

Totally about 170 building configurations were investigated in the water flume study. Critical configurations with respect to the potential for reingestion at fresh air intake for several building combinations were found from the tests. These configurations have been examined in the boundary layer wind tunnel to obtain more reliable quantitative data. The results from the wind tunnel study will be discussed in detail in Chapter 5.

CHAPTER 5

RESULTS AND DISCUSSION OF WIND TUNNEL STUDY

5.1 General

Wind tunnel experiments were carried out to provide quantitative results corresponding to the building configurations investigated in the water flume. In the present study, thirty-seven (37) tests were performed using the boundary layer wind tunnel, as mentioned in Chapter 3. All tests were performed with the emitting building downwind and obtained data on the wall of upstream building. The wind tunnel study investigated the influence of various parameters. These include:

- Stack distances (x_a);
- exhaust momentum ratio M values (M = 0.5, 1, 2, 3, 4);
- Adjacent building heights (H_a);
- Adjacent building widths (W_a);
- Wind directions ($\theta = 0°$ and 45°)
- Stack locations; and

- Stack heights (h_s)

The wind tunnel experimental methods have been described in Chapter 3. This chapter includes flow pattern analysis, and the evaluation of the all parameters listed on minimum dilution. Three (3) comparisons were made between the experimental results and the Wilson-Lamb model, ASHRAE critical dilution estimation model, and the Wilson adjacent building back wall model.

5.2 Flow pattern analysis

A plume emitted in the wake of a structure may be trapped in there or may escape into the free-stream depending on stack height and plume rise. In the present study, comparison with two wake size models, namely the Wilson model and the Snyder-Lawson model, was conducted. Details are as follows:

5.2.1 Comparison with Wilson wake size model

The likelihood of plume entrapment can be evaluated using formulas developed by Wilson [Wilson et al. (1998)].

As previously discussed in Chapter 2, the height-difference scaling length R, cavity length L_{cavity}, and cavity height H_{cavity}, as shown in Figure 2.7, can be estimated using Equations (2.6), (2.8), and (2.9). Table 5.1 shows cavity wake dimensions for the configurations used in the present study.

Table 5.1 Dimensions of wake cavity calculated by Wilson model

Model Type	Adjacent Building Relative Height (H_a/H) (m)	Wind Direction (θ°)	R (m)	L_{cavity} (m)	H_{cavity} (m)
Model A (W_a = W 0.075m)	1.33 (0.18)	0	0.10	0.20	0.15
		45	0.13	0.25	0.19
	1.67 (0.225)	0	0.11	0.22	0.16
		45	0.14	0.27	0.20
	2 (0.27)	0	0.12	0.23	0.17
		45	0.15	0.29	0.22
Model B (W_a = W 0.075m)	1.33 (0.18)	0	0.16	0.32	0.24
	1.67 (0.225)	0	0.17	0.34	0.26
	2 (0.27)	0	0.18	0.37	0.27

Figure 5.1 sketches the building wake recirculation cavity for the case of adjacent building height H_a = 1.67H (225mm), adjacent building width W_a = W (75mm) (where W is the emitting building width), wind direction $\theta = 0^\circ$, exhaust momentum ratio M = 2. For a separation distance S = 2W, distance between stack and upstream adjacent building leeward wall x_a = 2.5W = 0.188m < 0.216m for center stack, and $h = H + h_s + \Delta h$, where

H = 0.135m is the emitting building height, $h_s = 0$ is the stack height, and $\Delta h = B_3 M d_s$ = 3*2*0.004 = 0.024m ($B_3 = 3$ was suggested by Briggs (1975)) is the plume rise by jet momentum above the top of the stack, see Appendix A for details. Since h and H_{cavity} are almost the same ($\approx$ 0.16m), the plume can be treated as inside the recirculation cavity, as shown in Figure 5.1. Similar results can be found for the case H_a = 1.33H (180mm), W_a = W, S = W (75mm), $\theta = 0°$, M = 2. However, in the present study, there is no concentration on the upstream adjacent building wall for these cases. Therefore, it appears that Wilson's building wake recirculation cavity dimension estimation model overestimates the cavity dimension and cannot apply for this particular building configuration.

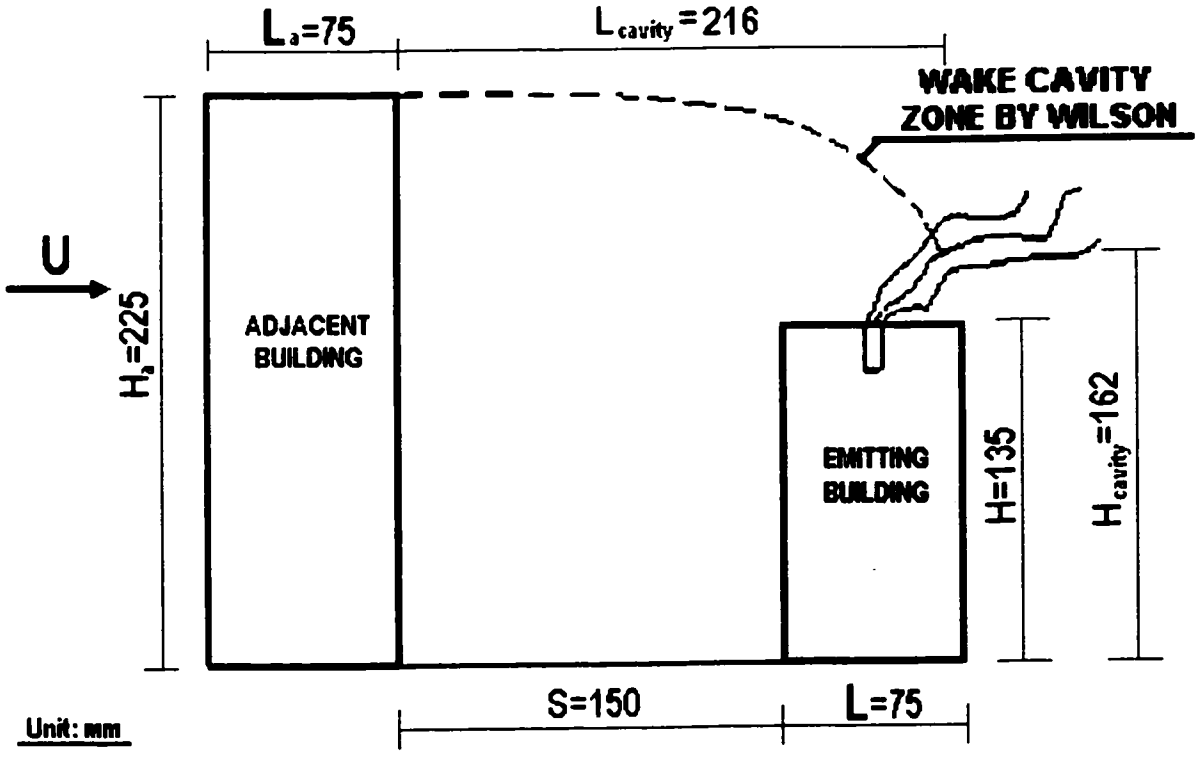

Figure 5.1 Adjacent buildings and recirculation cavity — Wilson model

5.2.2 Comparison with the Snyder-Lawson wake size model

Case 8 (H_a = 1.67H, W_a = W, S = W, θ = 0°) was chosen to compare with the Snyder-Lawson wake size model. In the present study, W = 75mm, H = 135mm = 1.8W, this makes H_a = 3W and the cross-wind width W equal to along-wind length L. This configuration can be deemed similar with the Snyder and Lawson's case [Snyder and Lawson (1994)] shown in Figure 2.6.

As shown in Figure 5.2, three stack locations, G, D, and A, were located at inside, outside, and the edge of the recirculation cavity zone, respectively. In the present study, the minimum dilution measured on the adjacent building leeward wall obtained by these three stack locations were about 400, 15000, and 1900, respectively. Due to the low wall dilution obtained from the adjacent building, it appears that Stack G is located within the wake cavity zone. Stack D, which is farther, can be deemed as being out of the recirculation cavity since the measured dilution value was extremely high. The plume emitted from Stack A (center stack) seems to have partly escaped from the wake cavity since the measured dilution value was in between the values measured for the other stacks. Therefore, it can be concluded that Stack A was located at the edge of the recirculation cavity and the model provides a good prediction for this particular building configuration.

5.2.3 General dilution dispersion

All the results obtained from wind tunnel tracer gas experiments, described in the form of

contour plots of dilution ($D = C_e/C$, where C_e is the contaminant concentration in the exhaust and C is the contaminate concentration at receptor), are presented in Appendix D.

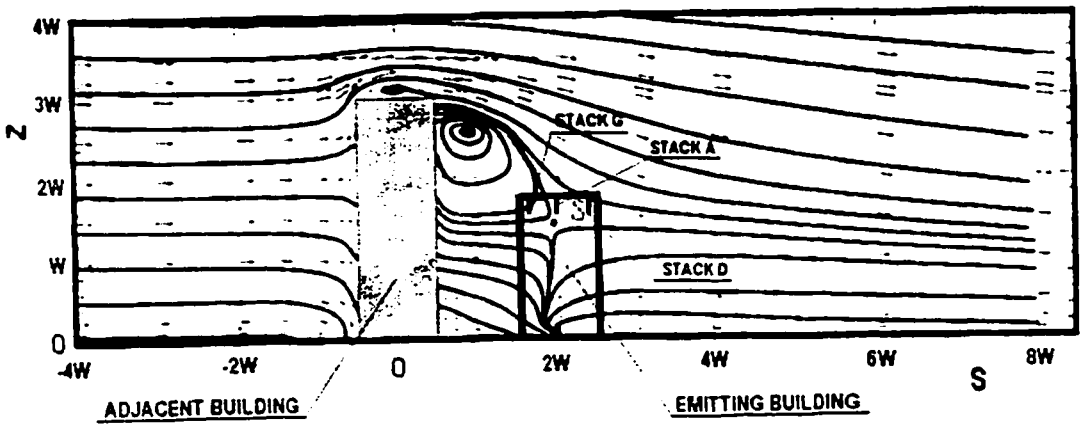

Figure 5.2 Comparison with Snyder and Lawson model

The adjacent building wall dimensions were normalized as y/W and z/H, as shown in Figure 5.3.

For the wind direction $\theta = 0°$, most of the dilution profiles were basically inverse bell-shaped curves, decreased with the height increase, following the Gaussian concentration profile. A typical example is shown in Figure 5.4. Figures 5.5 and 5.6 show two other examples for different adjacent building heights and widths, separation distances, stack locations, and momentum ratios. For the case of wind direction $\theta = 45°$, the minimum dilution normally occurred near the roof edge of the upwind adjacent building for the cases of H_a = 1.33H and 1.67H, as shown in Figure 5.7. For the case of H_a = 2H, the minimum dilution occurred near the downstream edge of the wall at a height about 1.5H, as shown in Figure 5.8.

In the contour plots, regions with dilution less than 500 have been shaded. This limit was chosen rather arbitrarily to indicate potential areas of concern. In reality the critical dilution will depend on the pollutant.

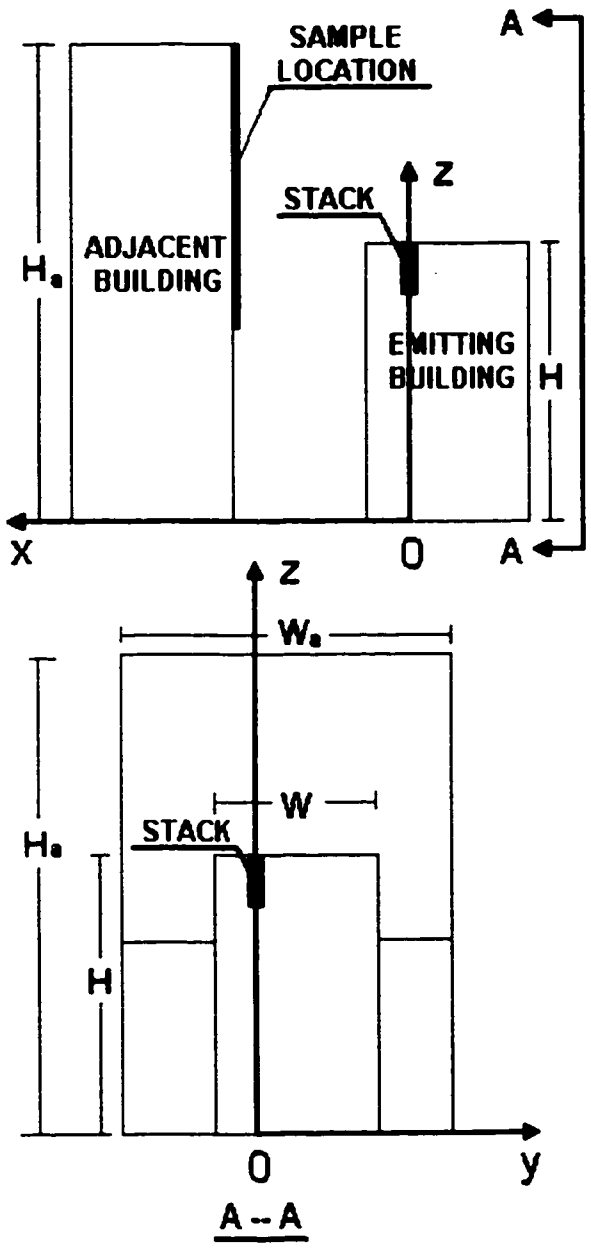

Figure 5.3 Coordinate system of dilution contours on adjacent building wall

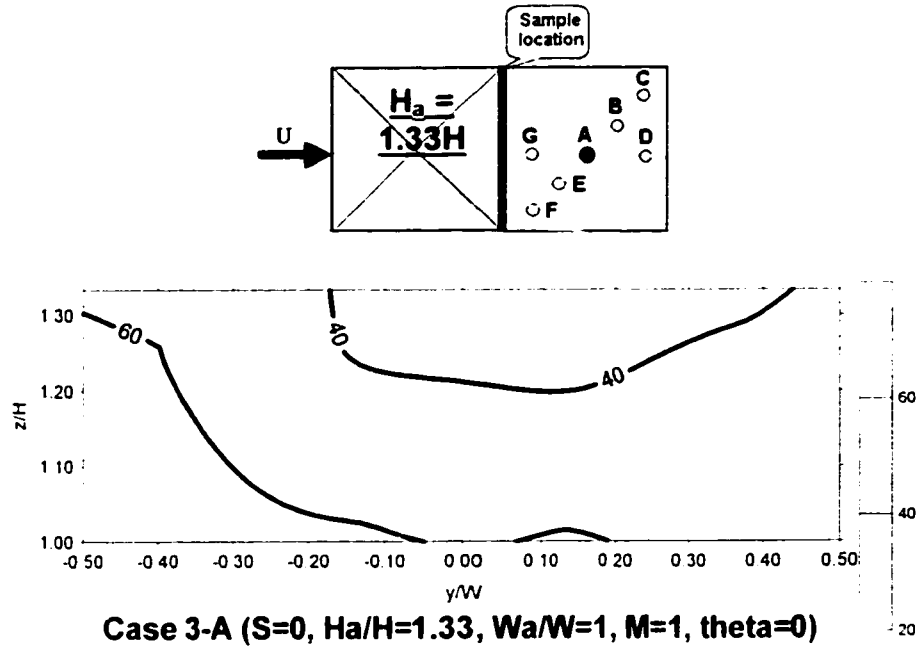

Figure 5.4 Dilution contours obtained in Case 3 (Stack location A)

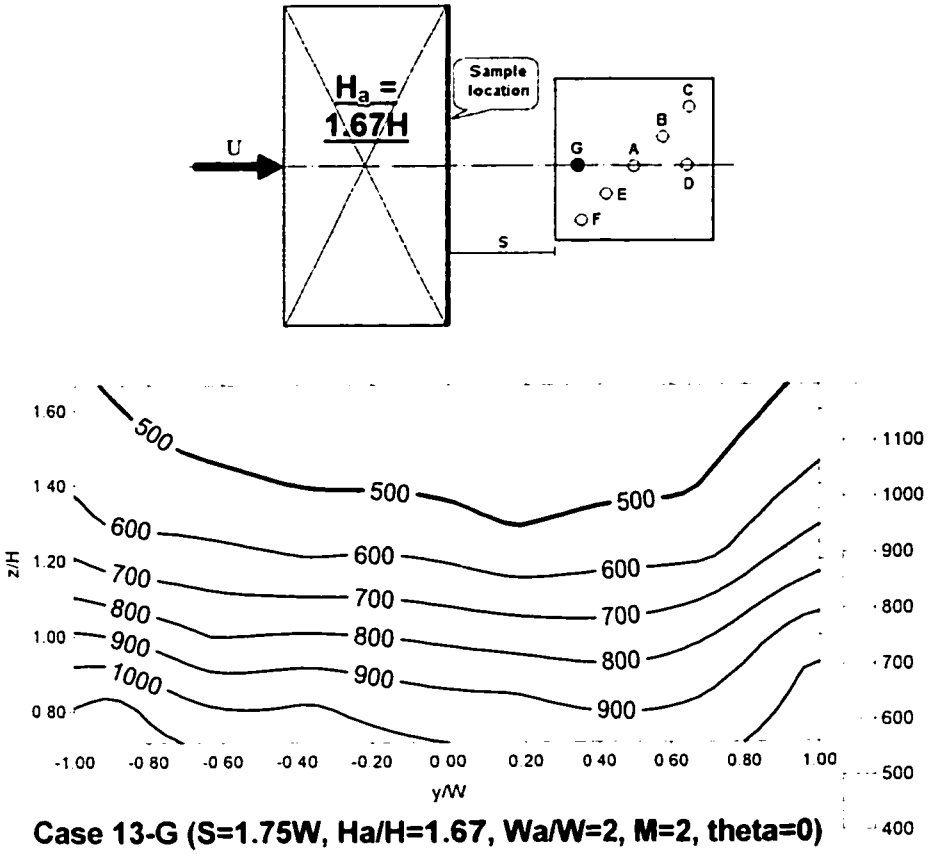

Figure 5.5 Dilution contours obtained in Case 13 (Stack location G)

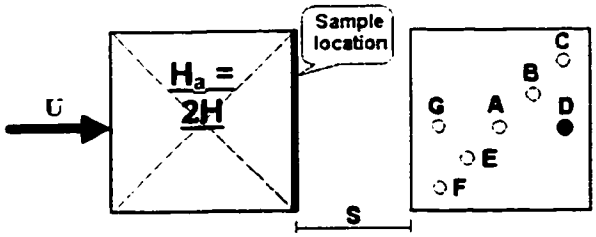

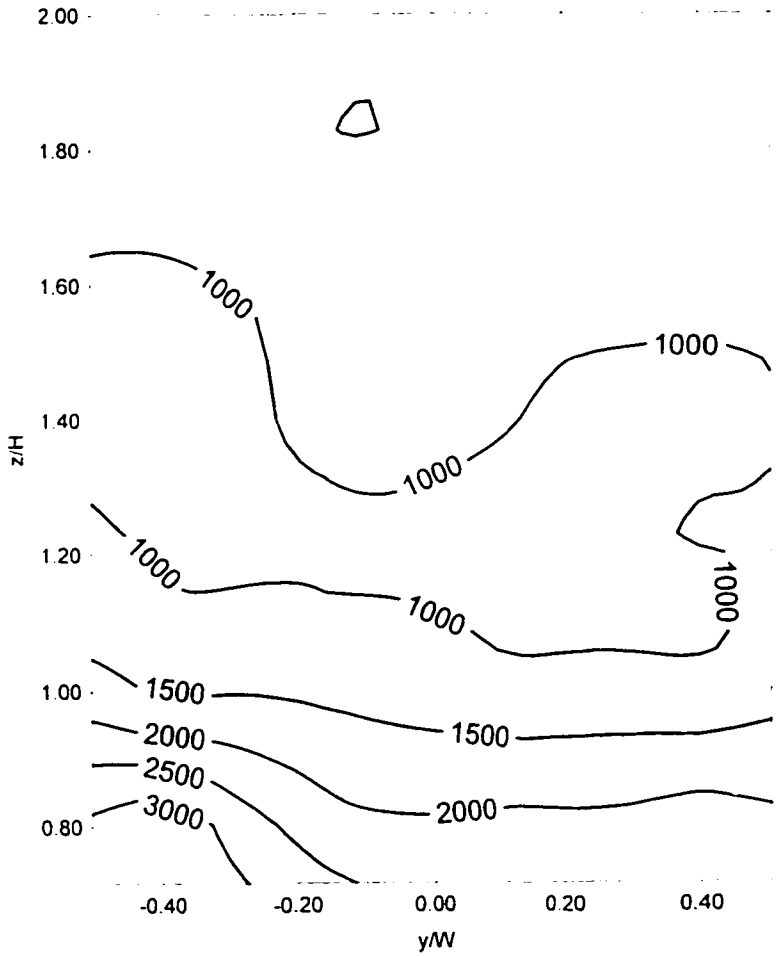

Case 9-D (S=0.75W, Ha/H=2, Wa/W=1, M=2, theta=0)

Figure 5.6 Dilution contours obtained in Case 9 (Stack location D)

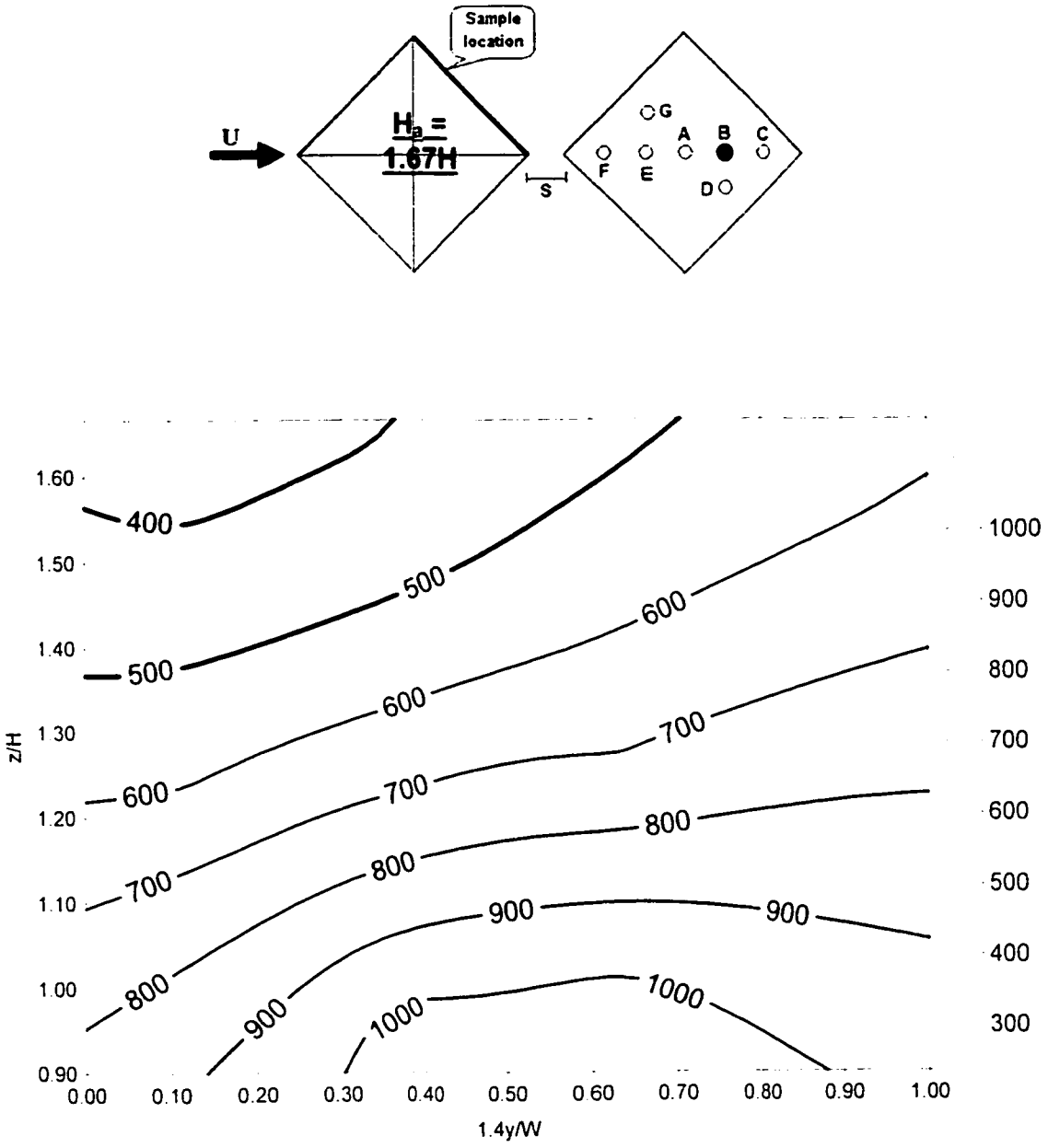

Case 28-B (S=1.1W, Ha/H=1.67, Wa/W=1, M=4, theta=45)

Figure 5.7 Dilution contours obtained in Case 28 (Stack location B)

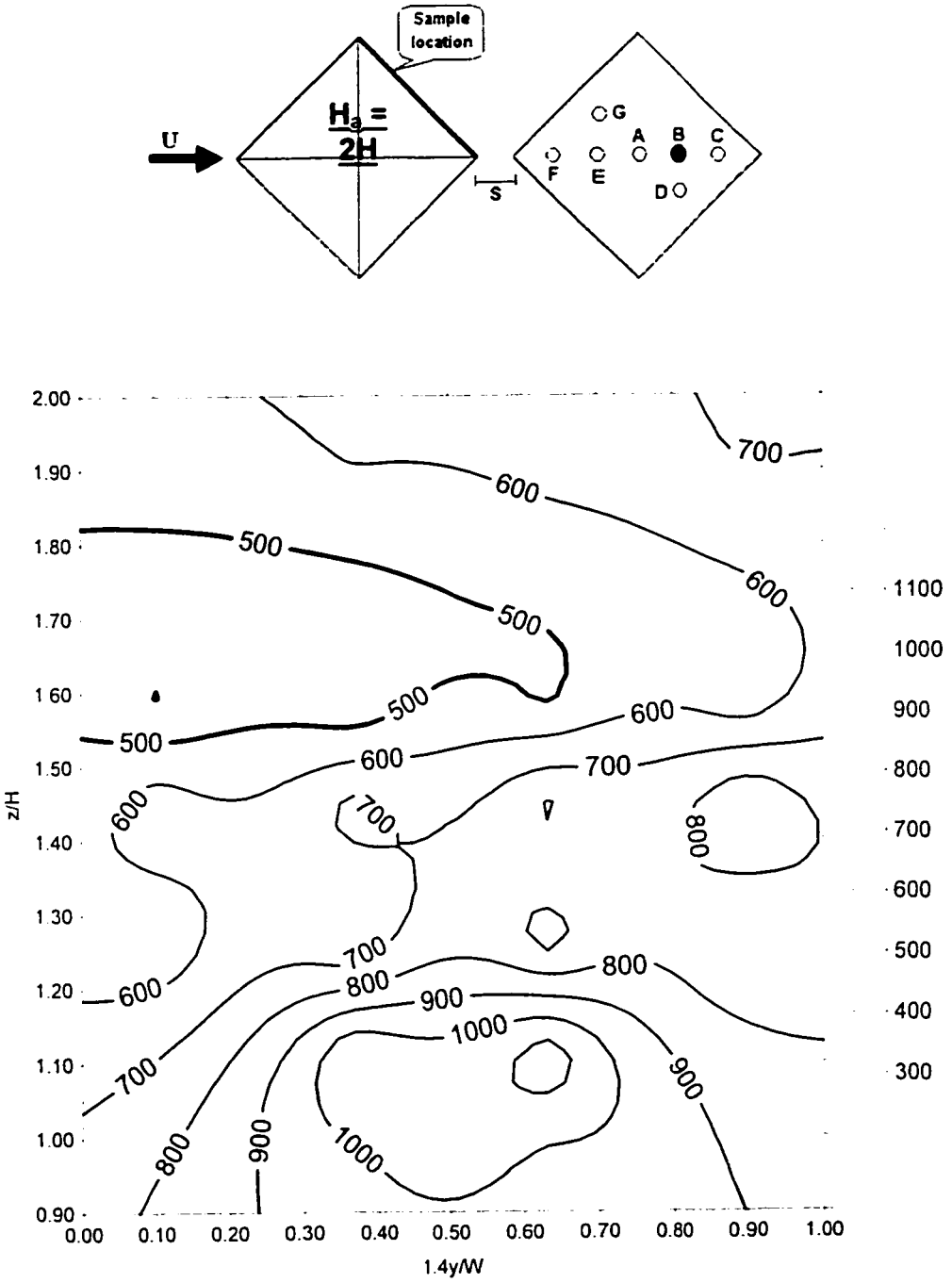

Figure 5.8 Dilution contours obtained in Case 29 (Stack location B)

5.2.4 Closure

Two recirculation-cavity size estimation models, namely the Wilson model and the Snyder-Lawson model, were compared. Generally, it can be concluded that:

- Wilson model does not give a representative wake cavity size for some particular building configurations;

- Snyder and Lawson model provides a good estimation of wake cavity size in some particular cases;

- Generally, dilution distribution obtained in the case of $\theta = 0°$ exhibits a U-shape; the minimum dilution occurred at the middle of the wall near the roof;

- For the case of $\theta = 45°$, the minimum dilution occurred near the roof edge of the upwind adjacent building for the cases of $H_a = 1.33H$ and $1.67H$; For the case of $H_a = 2H$, the minimum dilution occurred near the downstream edge of the wall at a height about $1.5H$.

5.3 Effect of stack distance on minimum dilution

The influence of building separation distance S (varied from 0 to 2.25W) on dilution was investigated. As shown in Figure 5.9, since the distances are different in the case of $\theta = 0°$

and θ = 45°, and variant with the different stack locations, the normalized distance between the stack and the upwind adjacent building (x_a/W) was used. A typical value of the exhaust momentum ratio M = 2 has been considered in this section. The influence of M on the results is discussed in Section 5.4.

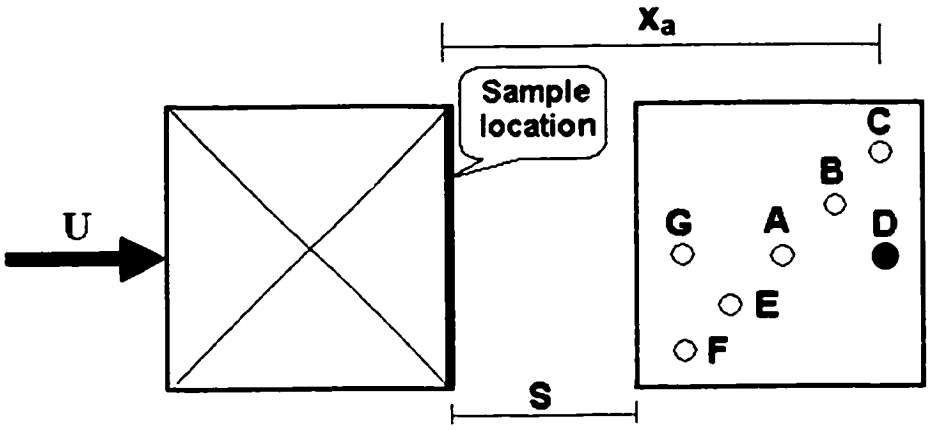

Figure 5.9 Distance between stack and sample locations

Several empirical equations are derived in this section. Generally, the equations give a good prediction of the minimum dilution except for the case of H_a = 1.33H, W_a = W, which forms a small recirculation cavity zone.

5.3.1 Case of W_a = W, 0 = 0°

Figure 5.10 shows the variation of the minimum dilution measured on the upstream building wall with the separation distance for the case of W_a = W, θ = 0° for centerline stacks. The minimum dilution of H_a = 2H, x_a/W = 1.17 ($D_{min} \approx 320$) is only about 18%

lower than that of H_a = 1.67H, x_a/W = 1.42 ($D_{min} \approx 390$) due to the stacks of both configurations were within the wake cavity zone. Nevertheless, $D_{min\text{-}Ha=2H}$ (560) is about 36% lower than $D_{min\text{-}Ha=1.67H}$ (1900) for the case of x_a/W = 1.5 and $D_{min\text{-}Ha=2H}$ (2350) is about 84% lower than $D_{min\text{-}Ha=1.67H}$ (15000) for the case of x_a/W = 1.83. This may be because in the latter case the plume has partly escaped the cavity. Similar results can be found for the side stack locations (C and D).

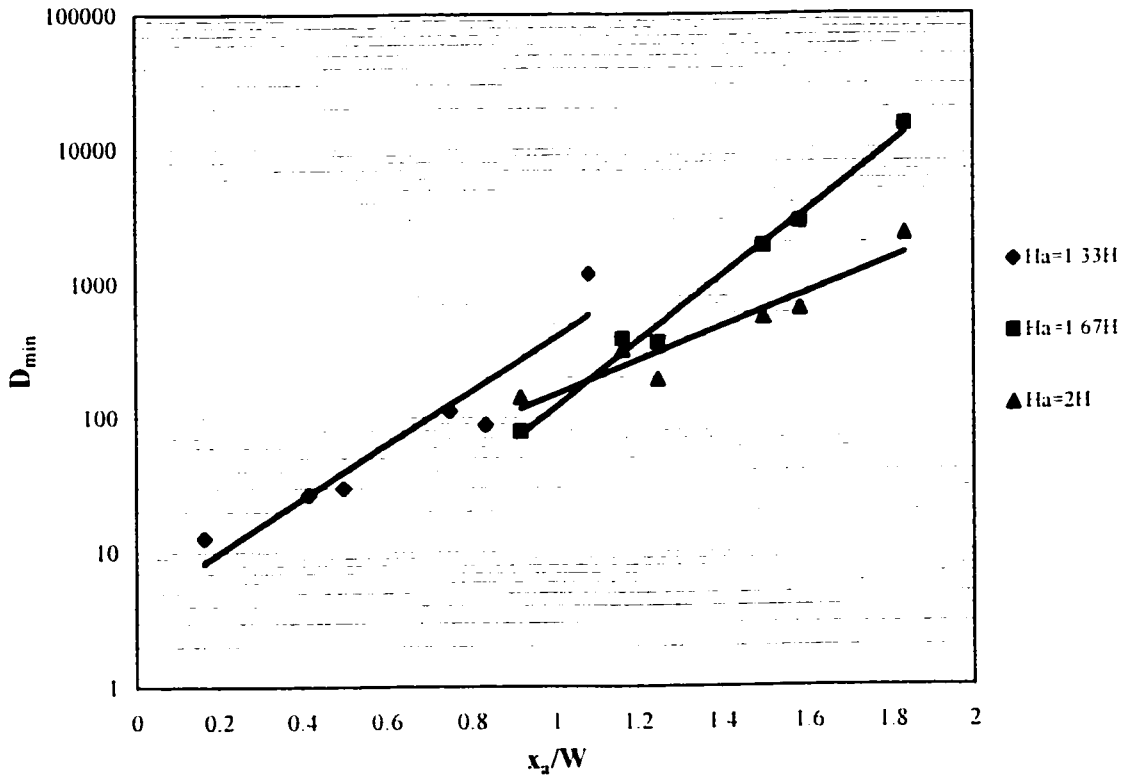

Figure 5.10 Minimum dilution variation with stack distance for the case of M = 2, W_a = W, θ = 0° (centerline stacks)

It is interesting to find from Figure 5.10 that the minimum dilution curves exhibit linear

variation with the stack distance in a semi-logarithmic scale. The logarithmic of the minimum dilution appears inversely proportional to the distance from stack.

Since the wake cavity zone of the case of H_a = 1.33H, W_a = W, θ = 0°, M = 2 is much smaller than that of the other two relative building heights (H_a = 1.67H and H_a = 2H), the magnitude predicted by the regression line of the minimum dilution is larger.

From Figure 5.10, three (3) empirical equations were derived for three different adjacent building relative heights, as shown in Table 5.2.

Table 5.2 Empirical equations for the case of W_a = W, θ = 0°, M = 2

Relative Adjacent Building Height	Empirical Equation	Standard Deviation σ (%)	Equation
H_a = 1.33H	D_{min} = 3.89exp[4.62(x_a/W)]	56.1	(5.1)
H_a = 1.67H	D_{min} = 0.43exp[5.63(x_a/W)]	18.6	(5.2)
H_a = 2H	D_{min} = 8.15exp[2.90(x_a/W)]	31.6	(5.3)

The standard deviations (or average discrepancies) for the cases of H_a = 1.67H and H_a = 2H are 18.6%, 31.6%, respectively. However, for the case of H_a = 1.33H, σ = 56.1% due to the small wake cavity size. It can be deemed that the equations give a reasonable prediction, considering the complexity of this phenomenon and the limitation of the samplers.

5.3.2 Case of $W_a = 2W$, $\theta = 0°$

Figure 5.11 shows results for the wide adjacent building ($W_a = 2W$). The dependence of D_{min} on distance is similar to that for the single-width building. However, since the wake size is larger than that of the case of single-width adjacent building, the trends of the minimum dilution for the three relative adjacent building heights are almost the same.

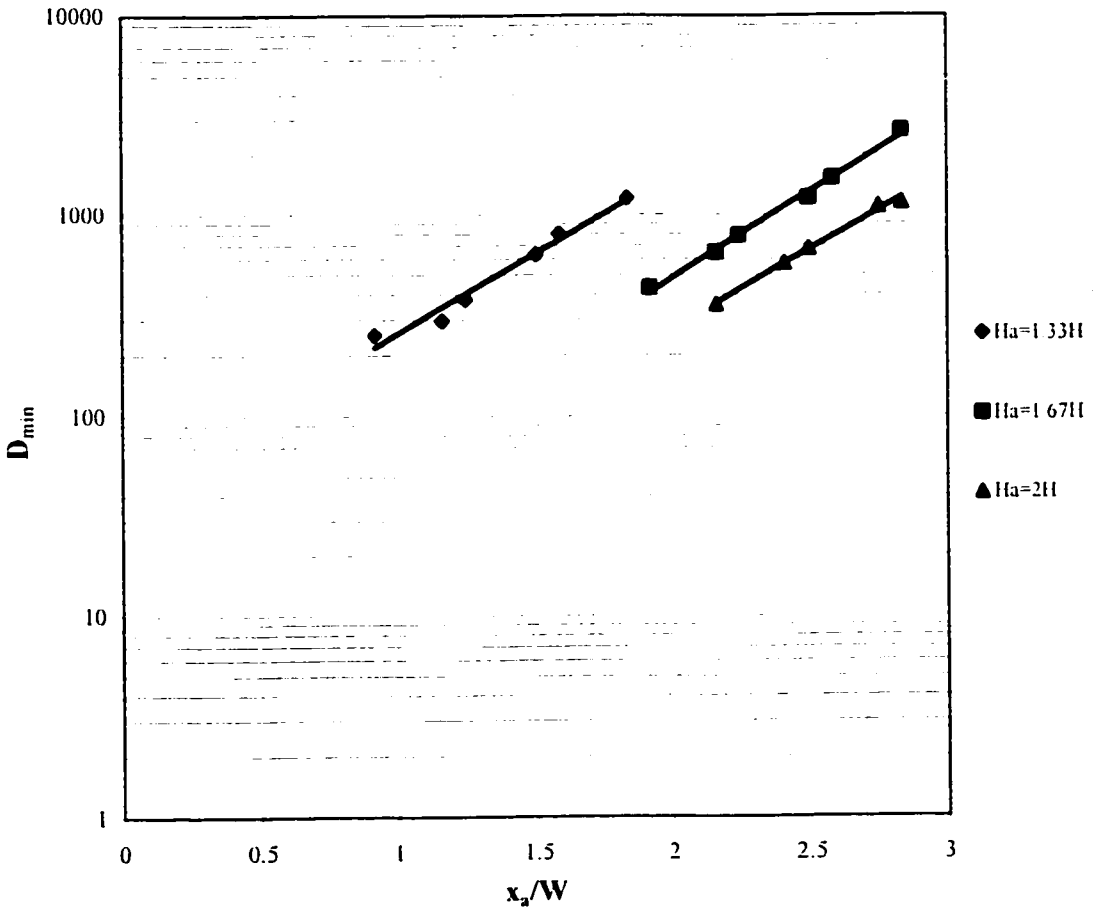

Figure 5.11 Minimum dilution variation with stack distance for the case of M = 2, $W_a = 2W$, $\theta = 0°$ (centerline stacks)

Table 5.3 presents the empirical equations for the case of $W_a = 2W$, $\theta = 0°$. In a semi-logarithmic graph, Equations (5.4) to (5.6) represent three almost parallel straight lines due to large wake cavity zone formed by wide adjacent buildings.

Table 5.3 Empirical equations for the case of $W_a = 2W$, $\theta = 0°$, $M = 2$

Relative Adjacent Building Height	Empirical Equation	Standard Deviation σ (%)	Equation
$H_a = 1.33H$	$D_{min} = 40.58\exp[1.84(x_a/W)]$	10.4	(5.4)
$H_a = 1.67H$	$D_{min} = 9.30\exp[1.97(x_a/W)]$	4.9	(5.5)
$H_a = 2H$	$D_{min} = 7.16\exp[1.81(x_a/W)]$	4.1	(5.6)

The differences between dilution values measured and Equations (5.4) to (5.6) were usually lower than 6%. The standard deviations are only 10.4 %, 4.9% and 4.1% for the three equations, respectively. It can be deemed that the equations give a very good predicted value.

5.3.3 Case of $W_a = W$, $\theta = 45°$

Figure 5.12 shows the results of the case of $M = 2$, $W_a = W$ and $\theta = 45°$. D_{min} is roughly proportional to the separation distance in a semi-logarithmic scale.

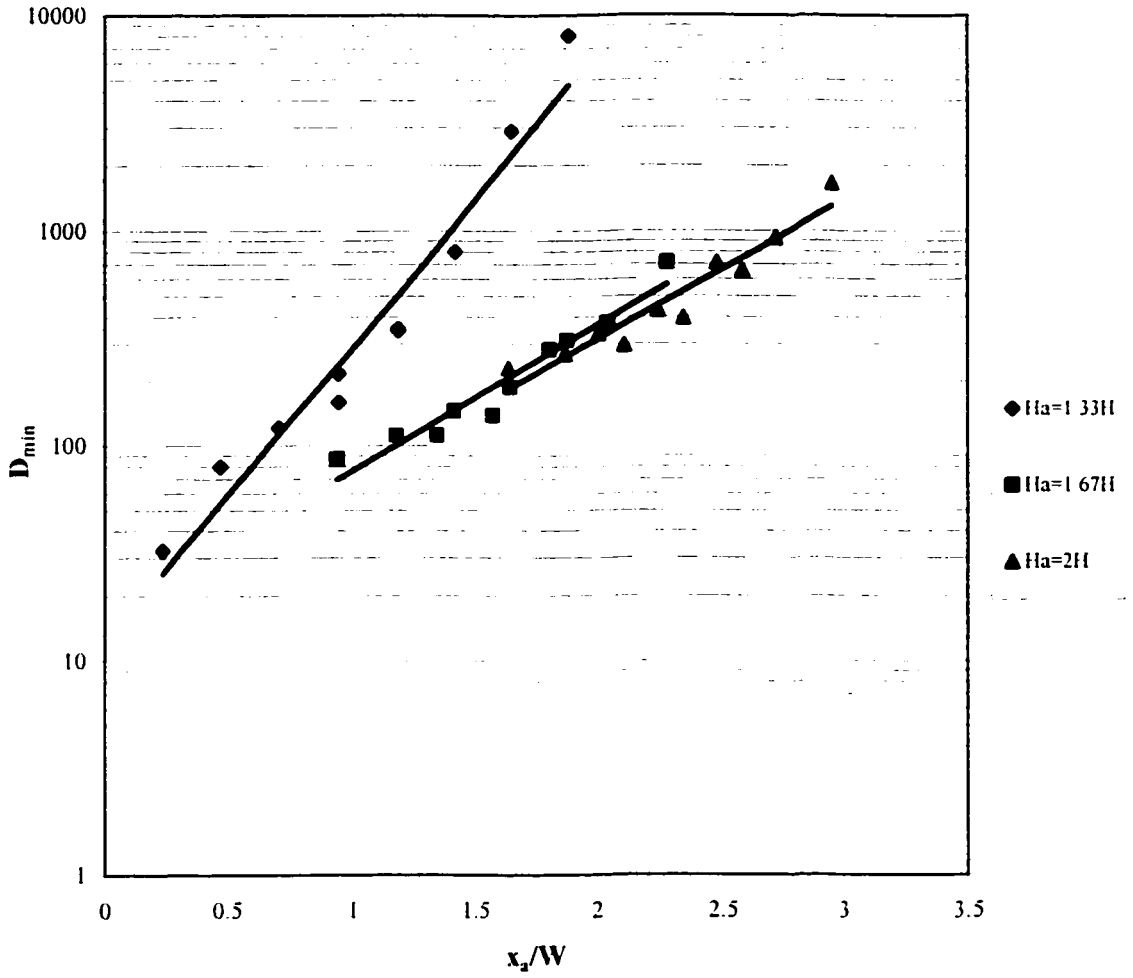

Figure 5.12 Minimum dilution variation with stack distance for the case of M = 2, W_a = W, θ = 45° (centerline stacks)

Table 5.4 presents the empirical equations for the case of W_a = W, θ = 45°, M = 2. It is interesting that for these configurations, the minimum dilution obtained by H_a = 1.67H and H_a = 2H is almost the same. However, the minimum dilution regression line for the case of H_a = 1.33H exhibited different behavior due to a smaller wake cavity.

Table 5.4 Empirical equations for the case of $W_a = W$, $\theta = 45°$, $M = 2$

Relative Adjacent Building Height	Empirical Equation	Standard Deviation σ (%)	Equation
$H_a = 1.33H$	$D_{min} = 12.01\exp[3.17(x_a/W)]$	37.0	(5.7)
$H_a = 1.67H$	$D_{min} = 15.85\exp[1.50(x_a/W)]$	19.0	(5.8)
$H_a = 2H$	$D_{min} = 16.12\exp[1.56(x_a/W)]$	15.0	(5.9)

For the cases of $H_a = 1.67H$ and $H_a = 2H$, the differences between dilution values measured and Equations (5.8) and (5.9) were generally lower than 20% and the standard deviation is 19% for $H_a = 1.67H$ and 15% for $H_a = 2H$. However, for the case of $H_a = 1.33H$, the differences were usually lower than 30%, although in some cases differences of up to 70% were obtained; the standard deviation for this case is $\sigma = 37\%$. It can be deemed that the equations give a reasonable prediction.

5.3.4 Closure

Generally, within the recirculation cavity, the minimum dilution increases with stack distance for all configurations, independent of the adjacent building width, height, and wind direction. It has been found that the distance between stack and receptor is one of the most important factors in reducing exhaust concentration for a flush outlet design. Nine (9) empirical equations between the minimum dilution and stack distance were derived for different building configurations.

5.4 Effect of momentum ratio on dilution

In the present study, the effect of M-value on dilution was investigated in detail by using five different M values, namely 0.5, 1, 2, 3 and 4, in three different building configurations for seven stack locations. The three configurations are:

(1) Adjacent building height $H_a = 1.33H$, width $W_a = W$, building separation distance $S = 0$ (i.e., no gap), and wind direction $\theta = 0°$;

(2) $H_a = 2H$, $W_a = 2W$, $S = 2W$, $\theta = 0°$, and

(3) $H_a = 1.67H$, $W_a = W$, $S = 1.1W$, $\theta = 45°$.

These configurations represent most of the cases examined in the present study.

5.4.1 Case of buildings with no separation

Figure 5.13 shows the variation of dilution with M-value for the case of $H_a = 1.33H$, $W_a = W$, $S = 0$, and $\theta = 0°$ for stack location A (center stack). In general, dilution values decrease by factors of 1.5 to 2 as M increases from 0.5 to 2. A significant change occurs when M-value reaches 2, whereby dilution values increase with M-value from 2 to 4 by a factor of 2. Similar results could be found for the other 6 stack locations.

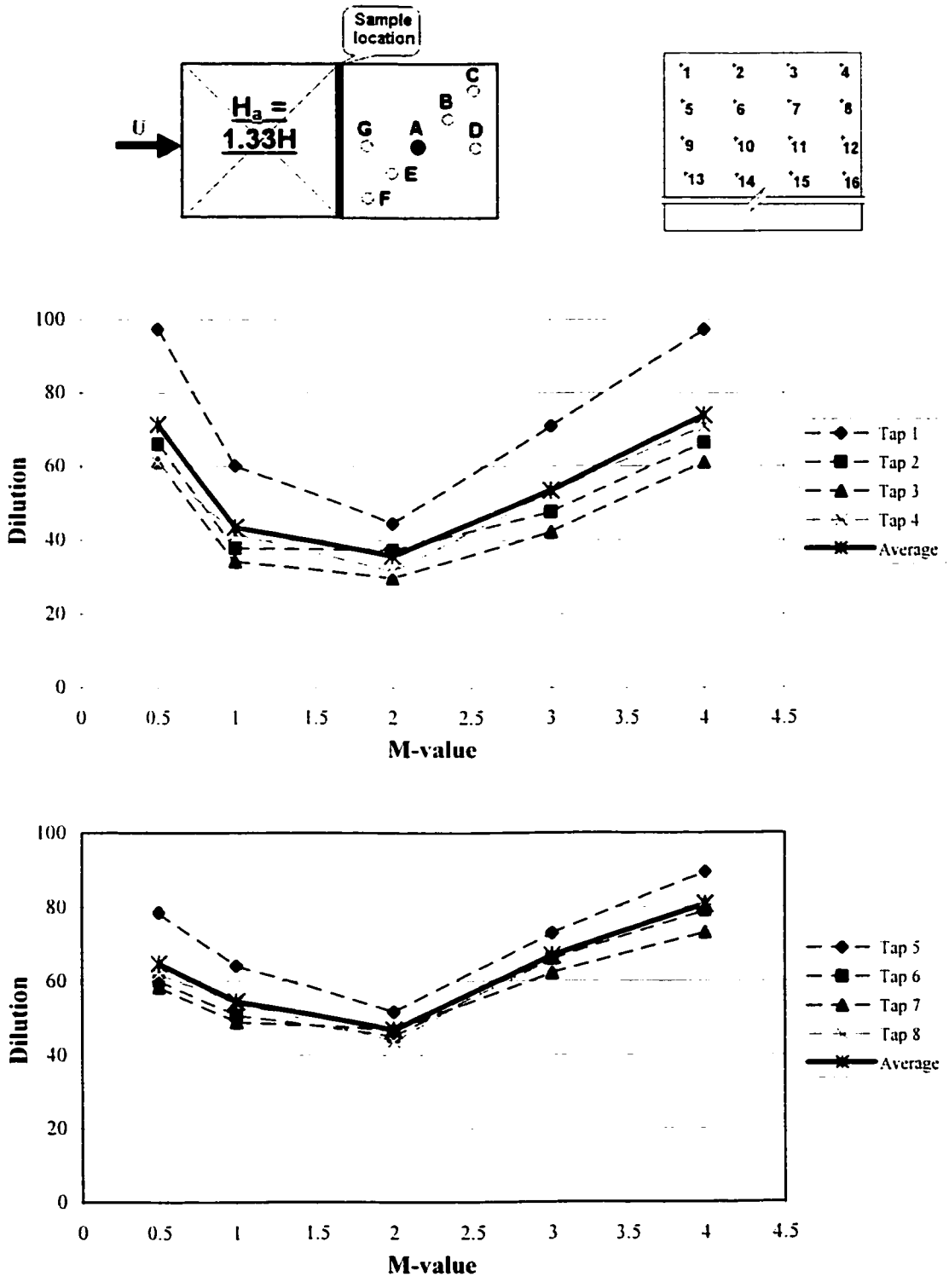

Figure 5.13 Dilution variations with M-value (Stack A, S=0, H_a=1.33H, W_a=W, 0 = 0°)

5.4.2 Case of buildings with separation

Figures 5.14 and 5.15 show results for case of H_a = 2H, W_a = 2W, S = 2W, θ = 0° for stack C. It is interesting that with this building configuration, dilution factors for all taps decrease sharply as M-value increases from 0.5 to 2, but decrease only slightly with increasing M for M > 2. Similar results were found for the other six stack locations.

Figure 5.16 shows the case of H_a = 1.67H, W_a = W, S = 1.1W, for stack location G, but θ = 45°. Similar results are shown in this case. Dilution factors decreased as M-value increased from 0.5 to 3. For M > 3, dilution was relatively constant at all taps. Results obtained with the other stacks for θ = 45° exhibited similar behavior.

A previous study carried out in a water flume for a low-rise building has found that dilution obtained on the leeward wall of a taller upwind adjacent building increased with M-value [Wilson et al. (1998)]. This is completely different compared with the present study. Comparison between the present study and the previous study will be discussed in detail in Section 5.11.

For a simple flat roof building with a flush stack, dilution on the roof has a U-shaped variation with M. At very low M, wind speed is relatively high and consequently, entrainment of ambient air causes high dilution. At high M, plume rise is large and thus the apparent dilution for rooftop receptors is large [ASHRAE (2001), Stathopoulos et al. (1999)].

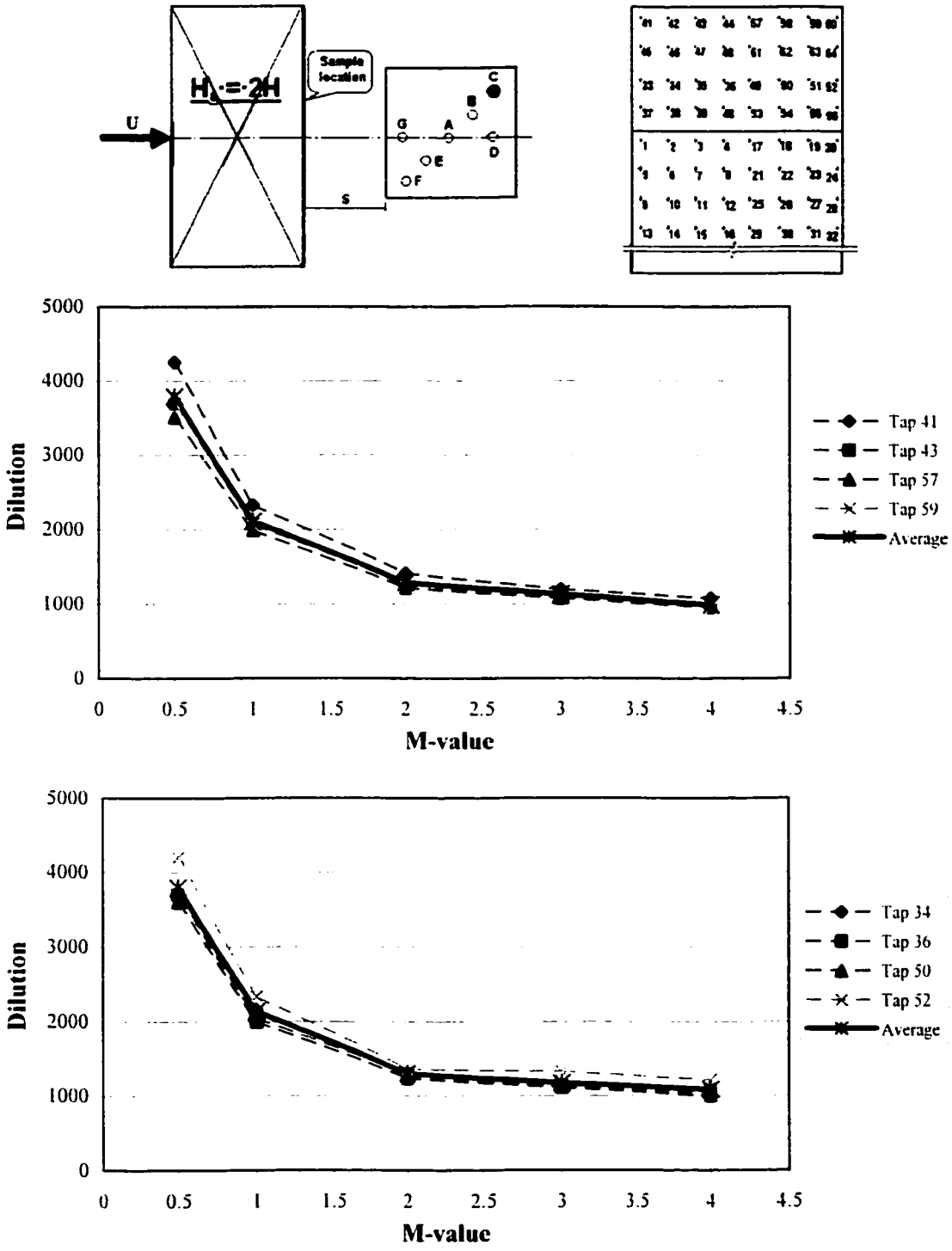

Figure 5.14 Dilution variations with M-value on upper wall surface (Stack C, S=2W, H_a=2H, W_a=2W, θ = 0°)

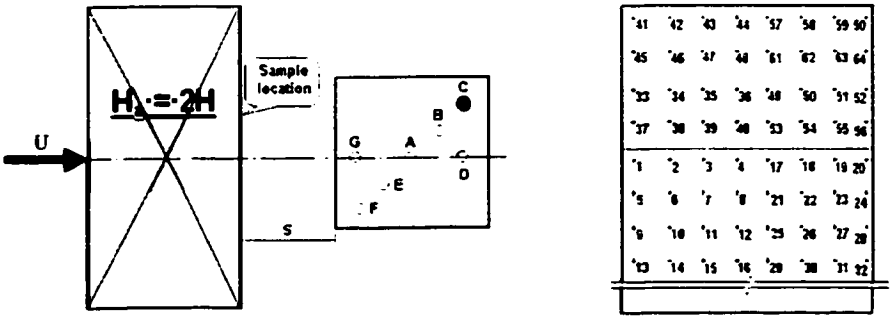

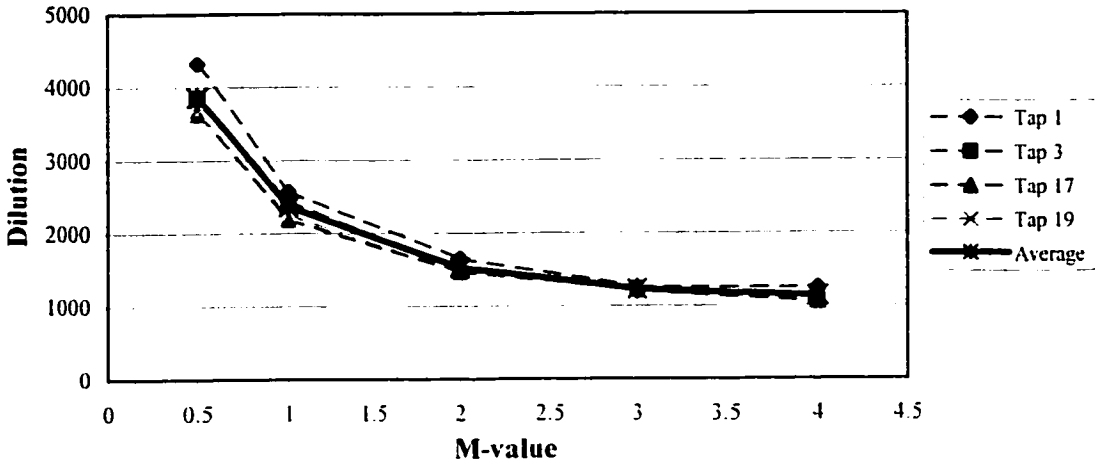

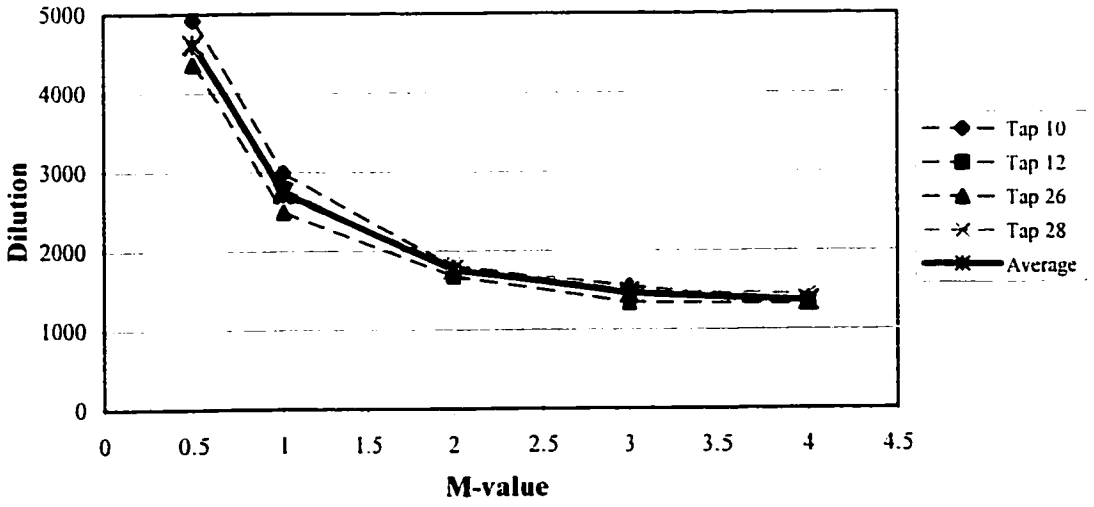

Figure 5.15 Dilution variations with M-value on lower wall surface (Stack C, S=2W, H_a=2H, W_a=2W, θ = 0°)

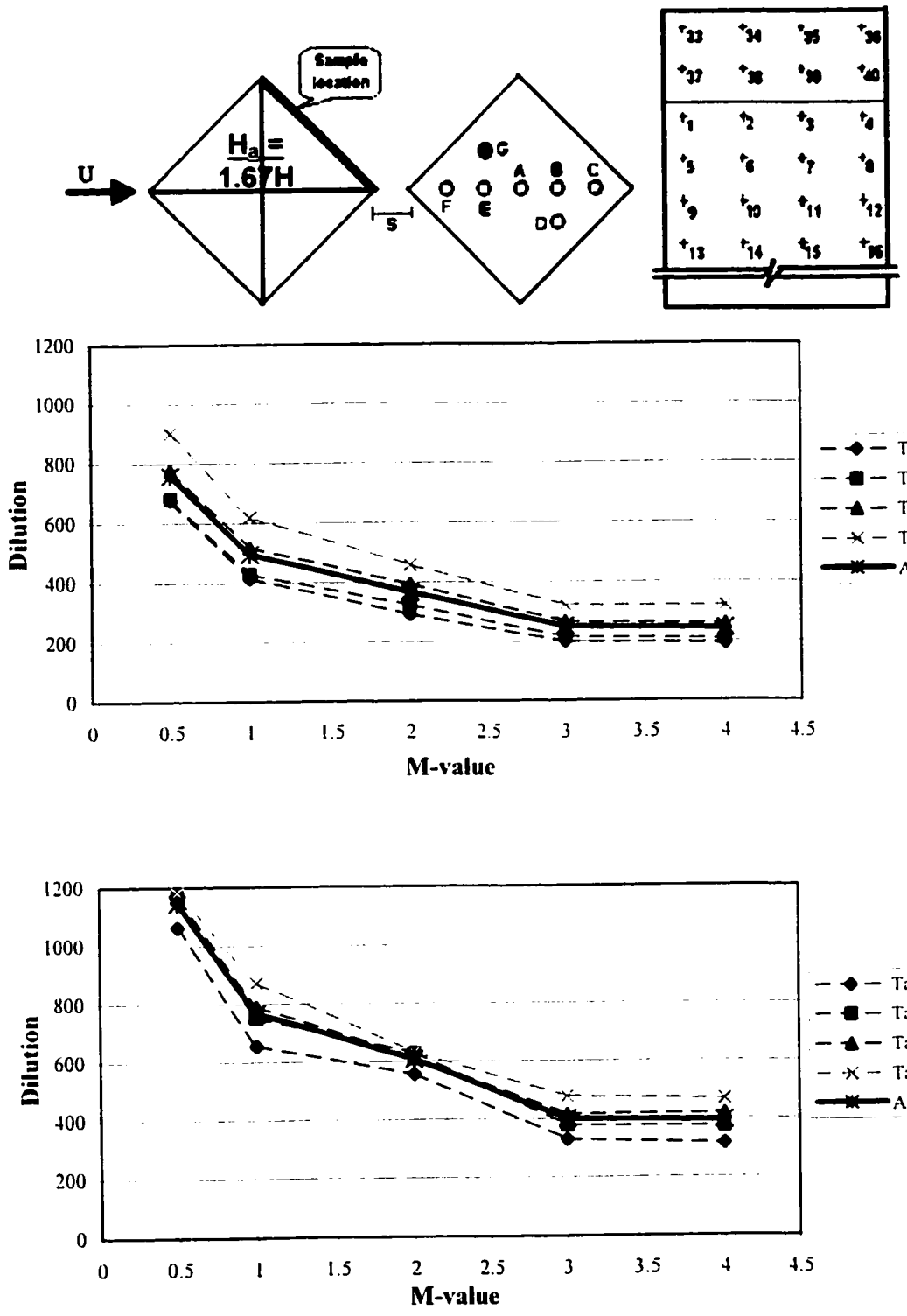

Figure 5.16 Dilution variations with M-value (Stack G, S=1.1W, H_a=1.67H, W_a=W, θ = 45°)

Theoretically, dilution dispersion also follows a "U-shape" for the wall receptors due to the same reason. It is still not clear why dilution dispersion in the present study in most cases does not follow a "U-shape", but the distance between the stack and the sample points on the wall seems to play an important role.

All detailed results are presented in Appendix E.

5.4.3 Closure

There are two different kinds of curves for dilution distribution variation with M-value: a reversed-bell shape behavior (U-shape) for the case of H_a = 1.33H, W_a = W, S = 0, and θ = 0°; and a decreasing with increasing M-value shape for the other cases with separation. These two types of curves were obtained regardless of relative adjacent building height and width, stack location and wind direction.

It seems that the building separation is an important factor for dilution variation with M-value. For the cases with separation, within the wake cavity zone, the plume will be dragged into the gap formed between the two buildings. Therefore, the exhaust emitted from the downwind lower building cannot escape easily from the wake zone even for a high M-value (i.e., M = 4).

A more detailed study should be conducted in the future to further investigate this phenomenon.

5.5 Effect of adjacent building height on minimum dilution

In the present study, two different adjacent building heights, Ha = 1.67H and 2H, were chosen to check the effect of height on minimum dilution.

Figure 5.17 shows the case of W_a = W, S = W, M=2, θ = 0° and the case of W_a = 2W, S = 2W, M=2, θ = 0°. As expected, minimum dilution increases with the distance between the stack and the adjacent building. This will be the case if the emitting building is located within the recirculation cavity formed by the taller upwind adjacent building.

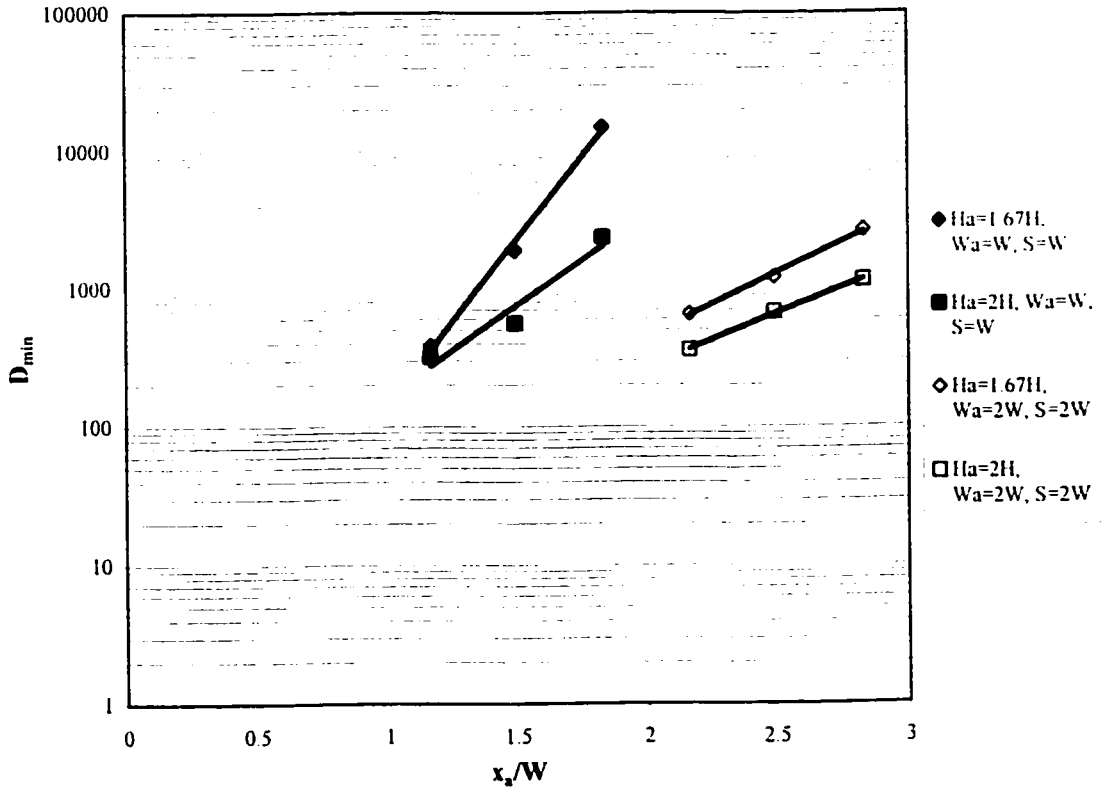

Figure 5.17 Effect of adjacent building height on the minimum dilution

Generally, it can be found from Figure 5.17 that

- A taller upstream adjacent building gives lower minimum dilution due to larger wake region which causes the plume to be trapped in the recirculation area;

- For the single width upstream adjacent building, a large range of minimum dilution has been observed, since the plume escapes the wake region for some stacks.

- The large wake region of double width upstream adjacent building traps the plume. Minimum dilution values are similar to those for single width even though S = 2W. There is a change by a factor about 2 in the minimum dilution regardless of x_a/W ranging from 2.17 to 2.83.

Four empirical equations have been derived from the data of Figure 5.17, as shown in Tables 5.5 and 5.6.

Table 5.5 Empirical equations for the case of $W_a = W$, $S = W$, $\theta = 0°$, $M = 2$

Relative Adjacent Building Height	Empirical Equation	Standard Deviation σ (%)	Equation
$H_a = 1.67H$	$D_{min} = 0.59\exp[5.49(x_a/W)]$	13.0	(5.10)
$H_a = 2H$	$D_{min} = 8.32\exp[3.00(x_a/W)]$	23.6	(5.11)

Table 5.6 Empirical equations for the case of Wa = 2W, S = 2W, θ = 0°, M = 2

Relative Adjacent Building Height	Empirical Equation	Standard Deviation σ (%)	Equation
$H_a = 1.67H$	$D_{min} = 6.85\exp[2.09(x_a/W)]$	13.0	(5.12)
$H_a = 2H$	$D_{min} = 8.20\exp[1.75(x_a/W)]$	23.6	(5.13)

Comparing Equations (5.2) and (5.10), (5.3) and (5.11), (5.5) and (5.12), (5.6) and (5.13), it can be found that there is very small difference between these four pairs of equations, as shown in Figure 5.18. It is believed that Equations (5.1) to (5.9) can predict the minimum dilution on the leeward wall of the tall upstream building.

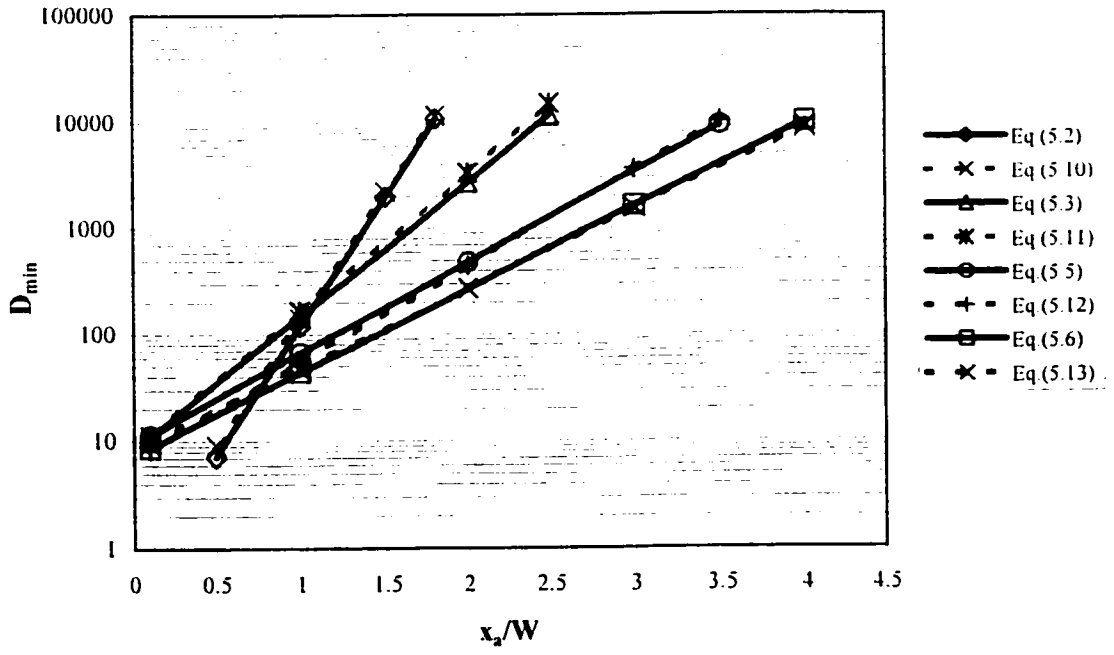

Figure 5.18 Comparison between empirical equations for various cases

5.6 Effect of adjacent building width on dilutions

Two adjacent building widths, W_a = W and W_a = 2W, were investigated in the present study. The effect of adjacent building width on dilution of contaminants and the minimum dilution are discussed in this section. The adjacent building height was H_a = 1.67H, building separation distance S = 0, the momentum ratio M = 2, and wind direction $\theta = 0°$ for both cases.

5.6.1 Effect of adjacent building width on dilution distribution

Figure 5.19 shows the dilutions obtained from the case of H_a = 1.67H, S = W, M = 2, θ = 0°, W_a = W (Case 8) and W_a = 2W (Case 31) from Stack A. It can be found that for the center stack, dilutions obtained for W_a = W are roughly 8 to 9 times as those for W_a = 2W. For farther stack locations, this factor becomes larger, i.e., 20-40 for Stack B, 50-70 for Stack C and Stack D.

5.6.2 Effect of adjacent building width on the minimum dilution

Figure 5.20 shows the minimum dilution variation with adjacent building width for the case of H_a = 1.67H, M = 2, S = W, and $\theta = 0°$. Results show that for the double width building, the minimum dilution does not vary significantly with stack location. On the other hand, for the single width upstream building, D_{min} increases significantly as the stack moves away from upwind building. D_{min} increases by a factor of 37, from approximately 400 at x_a/W = 1.16 to about 15,000 at x_a/W = 1.83. For the double width

upstream building, D_{min} increases by only a factor of 1.8 over this distance. The farther stacks for the case of W_a = W were partly or completely out of the recirculation cavity and the plume could actually escape.

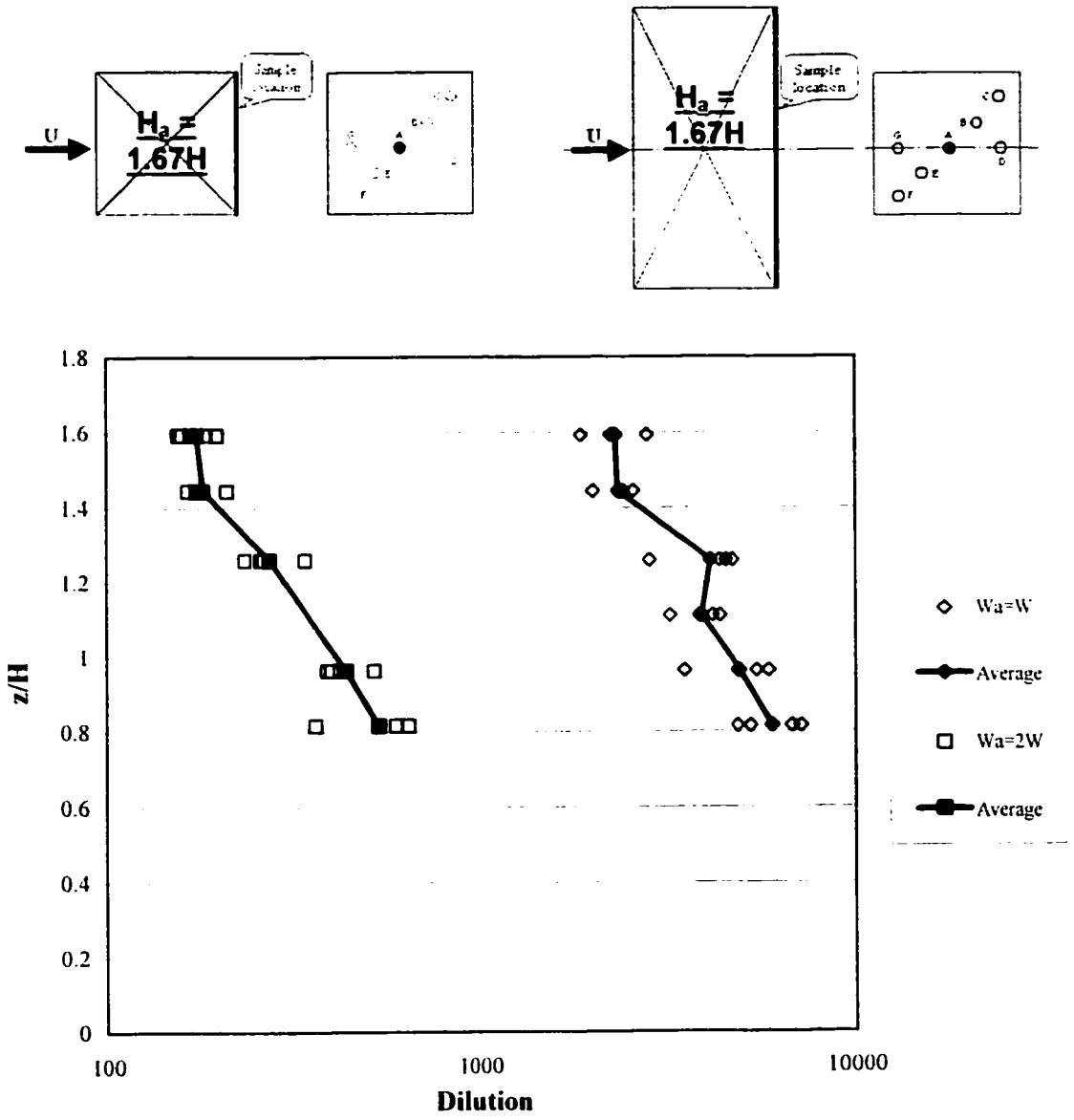

Figure 5.19 Effect of adjacent building width on dilution distribution for case of H_a = 1.67H, S= W, M = 2, 0 = 0° (Stack A)

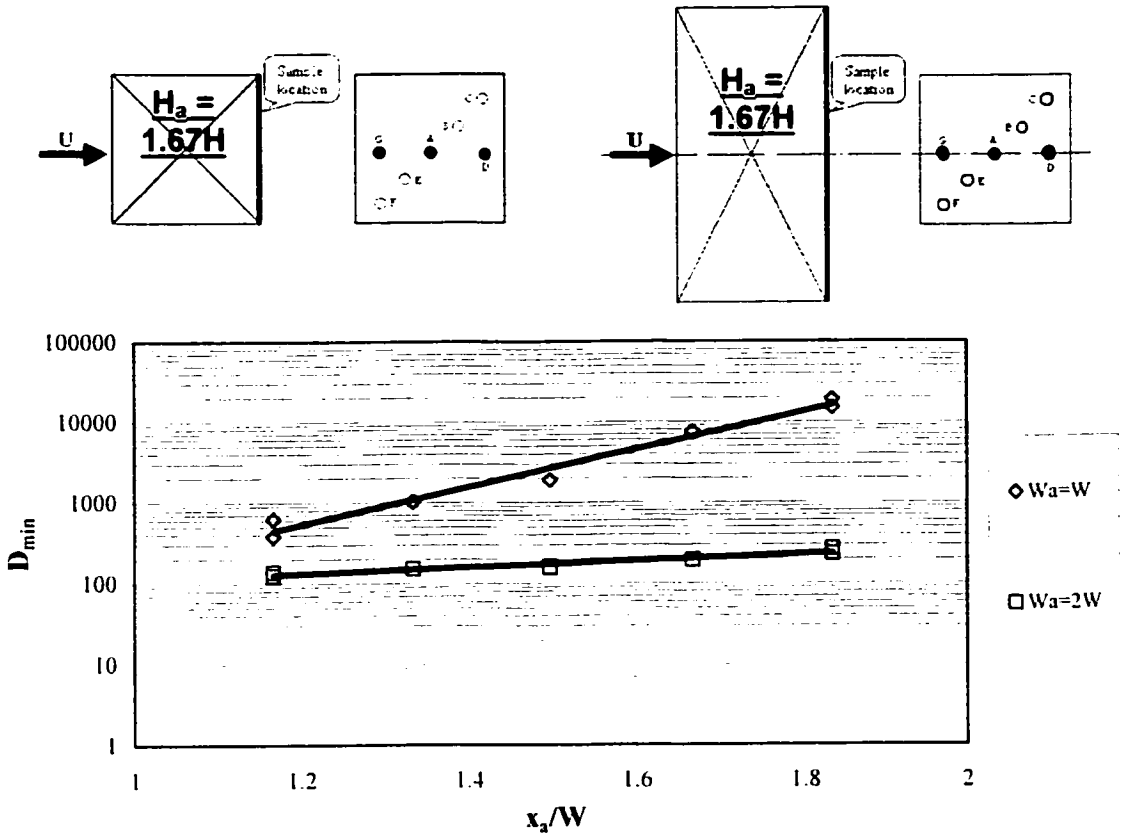

Figure 5.20 Effect of adjacent building width on the minimum dilution for the case of H_a = 1.67H, S = W, M = 2, θ = 0°

It can be found that adjacent building width has a significant effect on the minimum dilution. Wide buildings produce less dilution at a given exhaust velocity than do narrow buildings. The change in the minimum dilution can be a factor of 3 (for x_a/W = 1.18) to about 70 (for x_a/W = 1.83) when the adjacent building width changes from W to 2W.

5.7 Effect of wind direction on the minimum dilution

Two wind directions, namely θ = 0° and θ = 45° were tested to verify the building

orientation effect on the dilution of contaminants. Both, dilution distribution and the minimum dilution will be discussed in detail in this section. Both emitting and adjacent building had the same width (w_a = W) and the momentum ratio M was equal to 2 for all cases investigated.

5.7.1 Case of H_a = 1.33H

Figure 5.21 shows the dilution contours on upstream building wall obtained for $\theta = 0°$ and $\theta = 45°$ for H_a = 1.33H. Note that the separation distance is not the same due to orientation. This figure shows the general shape of dilution distribution. Dilution obtained on the upwind building wall decreases with increasing height for both cases.

For buildings with no separation, the minimum dilution of $\theta = 45°$ is roughly 3 times as that of $\theta = 0°$ (for $x_a \approx 0.5W$), as shown in Figure 5.22. Similar results were obtained for other stack locations. For both cases of $\theta = 0°$ and $\theta = 45°$, the minimum dilution increases with stack distance, and the regression lines are very close to each other in a semi-logarithmic scale.

It is interesting that $D_{min\text{-}45°}$ is larger than $D_{min\text{-}0°}$ for small stack distances (i.e., $x_a/W <$ 0.75). Theoretically, $D_{min\text{-}45°}$ should be smaller than $D_{min\text{-}0°}$ since the crosswind width of adjacent building for $\theta = 45°$ is 1.41 times large as that of $\theta = 0°$. However, the magnitudes of the minimum dilution are lower than 100 for this case, which means the concentrations are relatively high and the measurement error may be high compared to the magnitude of D_{min}. On the other hand, the flow structure is very different for the two

wind directions.

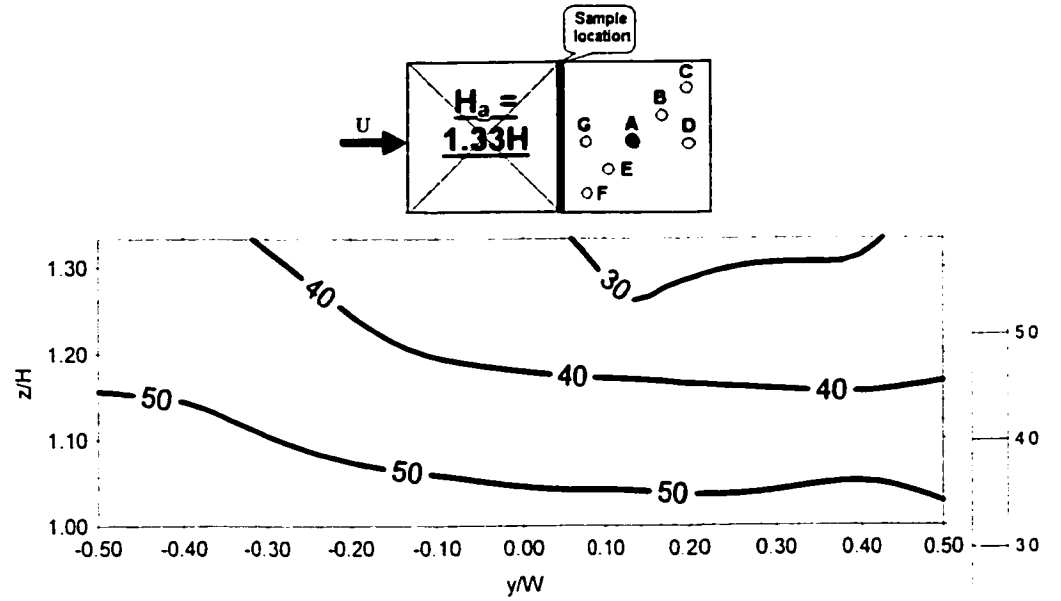

Case 1-A (S=0, Ha/H=1.33, Wa/W=1, M=2, theta=0)

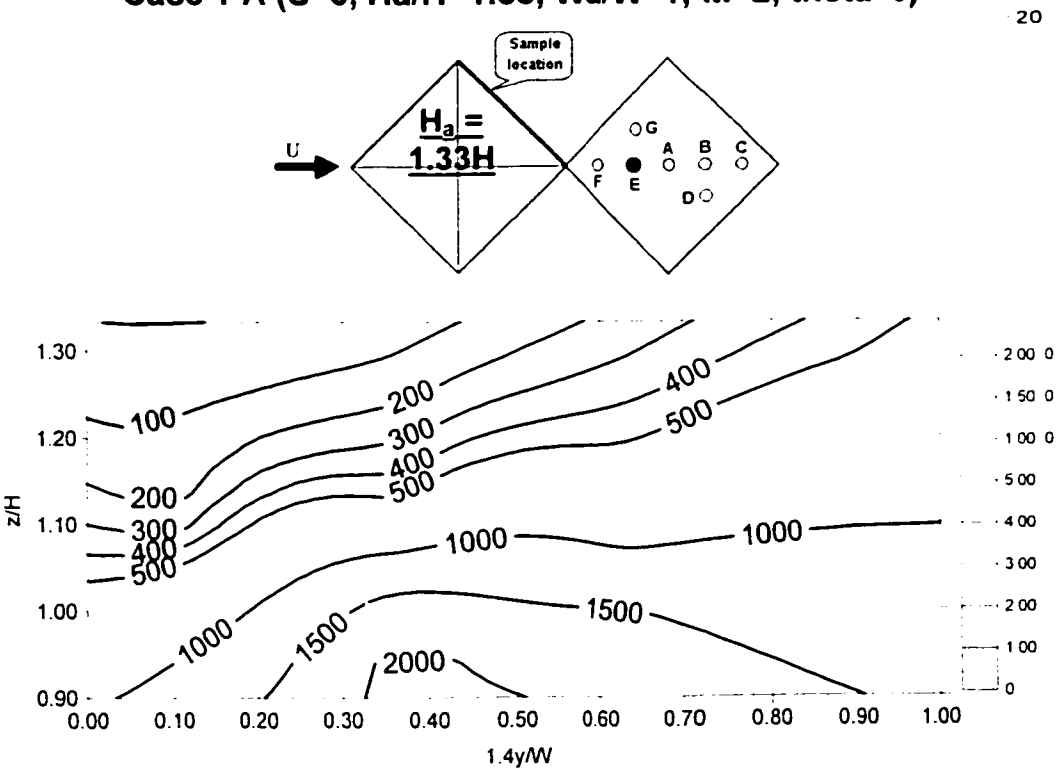

Case 21-E (S=0, Ha/H=1.33, Wa/W=1, M=2, theta=45)

Figure 5.21 Dilution contours obtained in cases 1 and 21 (centerline stack)

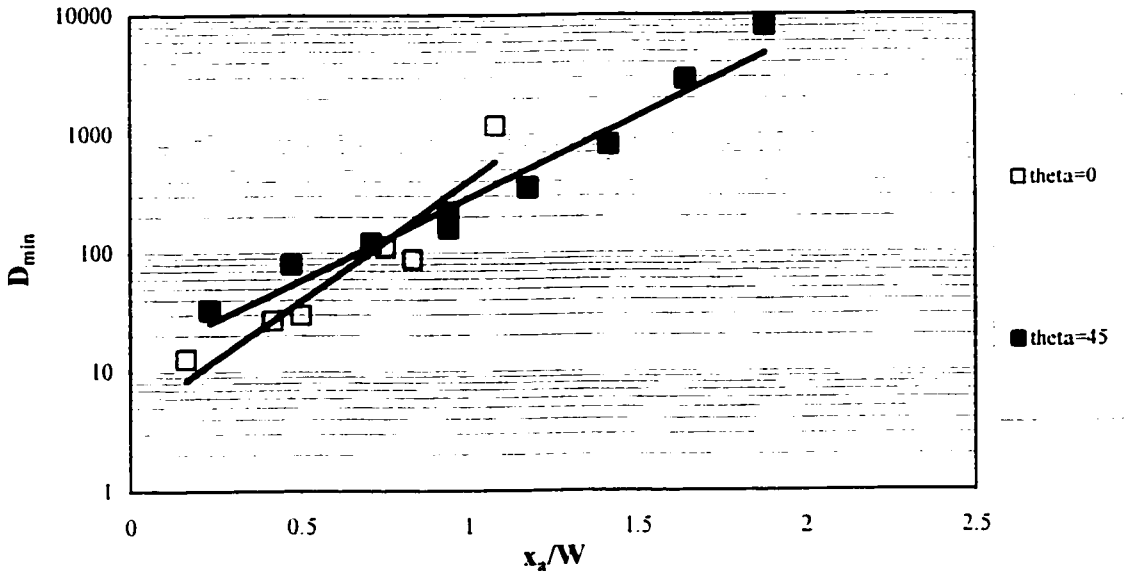

Figure 5.22 Effect of wind direction on the minimum dilutions for the cases of H_a = 1.33H, W_a = W, M = 2 (centerline stacks)

5.7.2 Case of H_a = 1.67H

Figure 5.23 shows that θ = 45° may be the critical direction for some wall locations. For both wind directions, dilution decreases with height. $D_{min\text{-}45°}$ (≈ 90) for $x_a/W \approx 0.94$, which occurred in a small region in the top corner of the wall, was almost the same as $D_{min\text{-}0°}$ (≈ 80) for $x_a/W = 0.92$, which occurred at the top center of the wall.

For the case of H_a = 1.67H, the minimum dilution increases with stack distance for both wind directions, but much more rapidly at θ = 0° than at θ = 45°, as shown in Figure 5.24. This is not surprising since the wake region formed by θ = 0° is smaller than that of θ = 45°. Two regression lines intersect at about $x_a \approx W$ in a semi-logarithmic scale, where $D_{min} \approx 80$. The difference between the slopes of the two regression lines may be

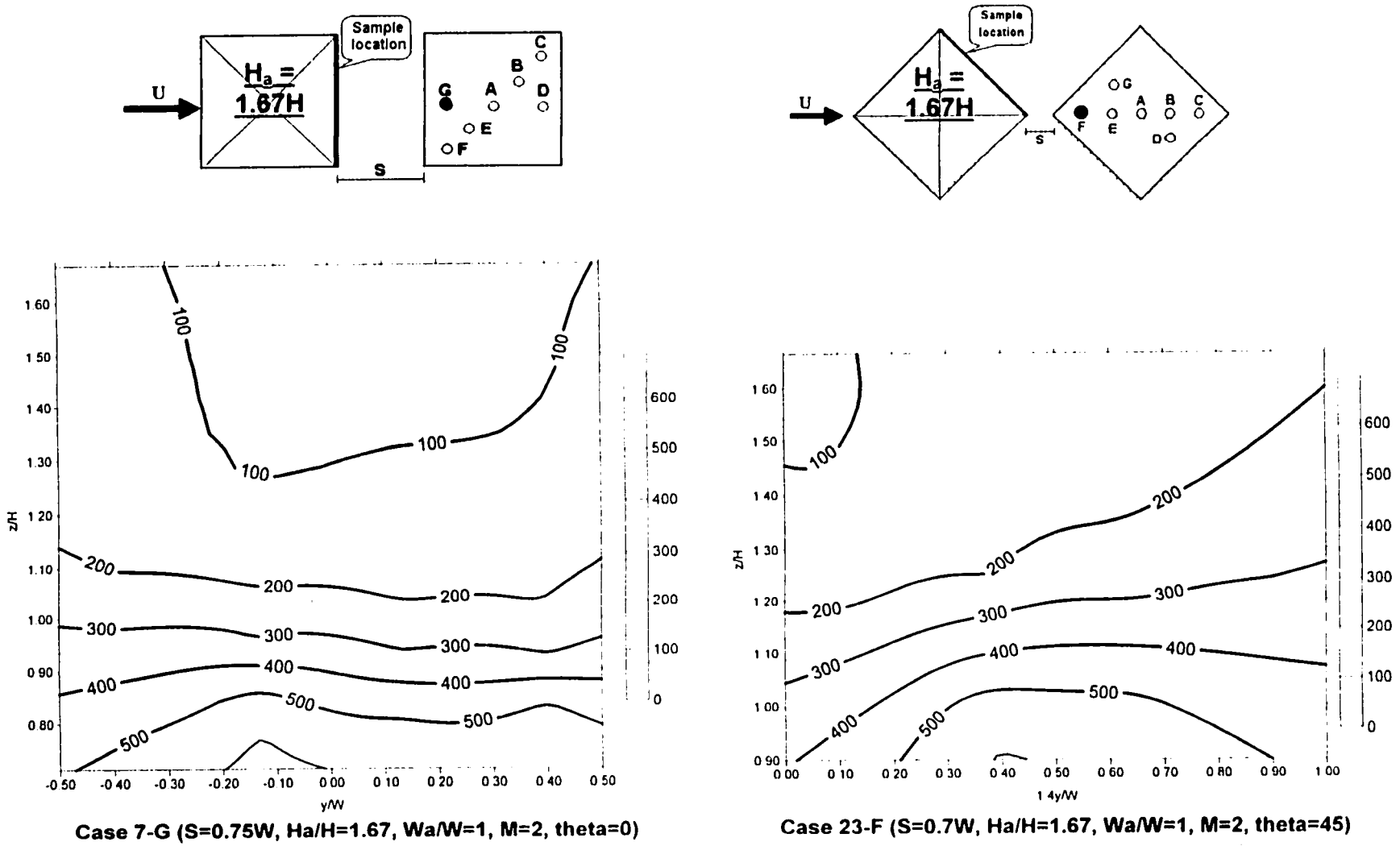

Figure 5.23 Dilution contours obtained for case 7(Stack G) and case 23 (stack F)

due to the fact the flow patterns are very different in the cases of θ = 0° and θ = 45°, leading to different dispersion distributions in the wake.

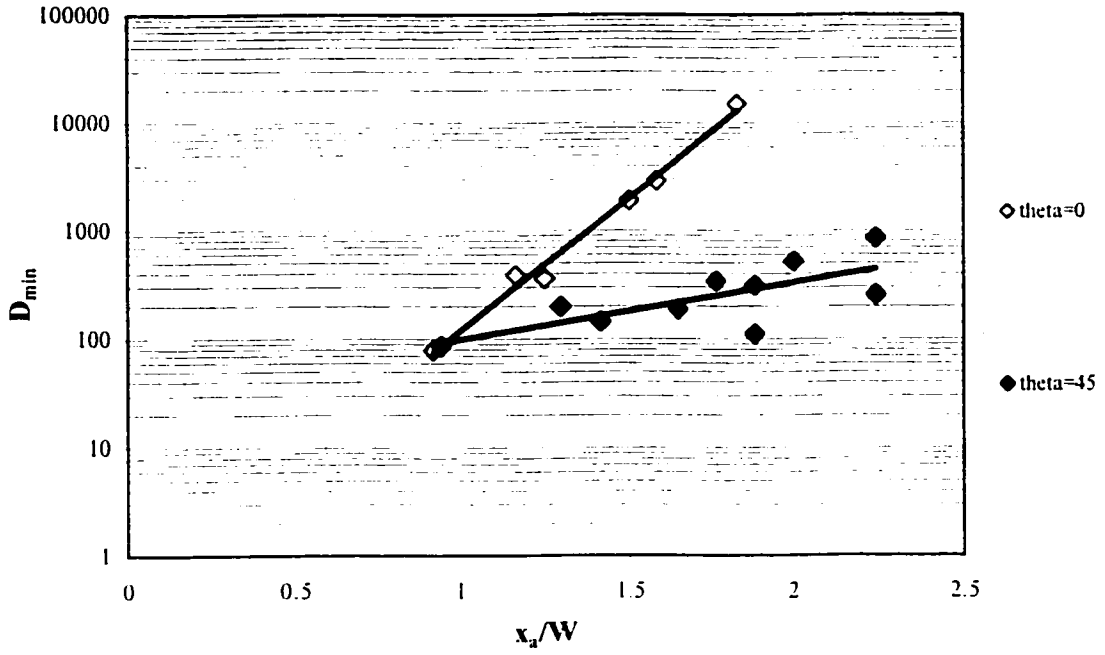

Figure 5.24 Effect of wind direction on the minimum dilution for the case of H_a = 1.67H, W_a = W, M = 2 (centerline stacks)

5.7.3 Case of H_a = 2H

For the case of H_a = 2H, as shown in Figure 5.25, $D_{min\text{-}45°}$ occurred at the downstream side of the adjacent wall at a height about 1.6H, as well as $D_{min\text{-}0°}$ occurred at the middle of the wall at almost same height. Note that the separation distance is not the same in the two cases.

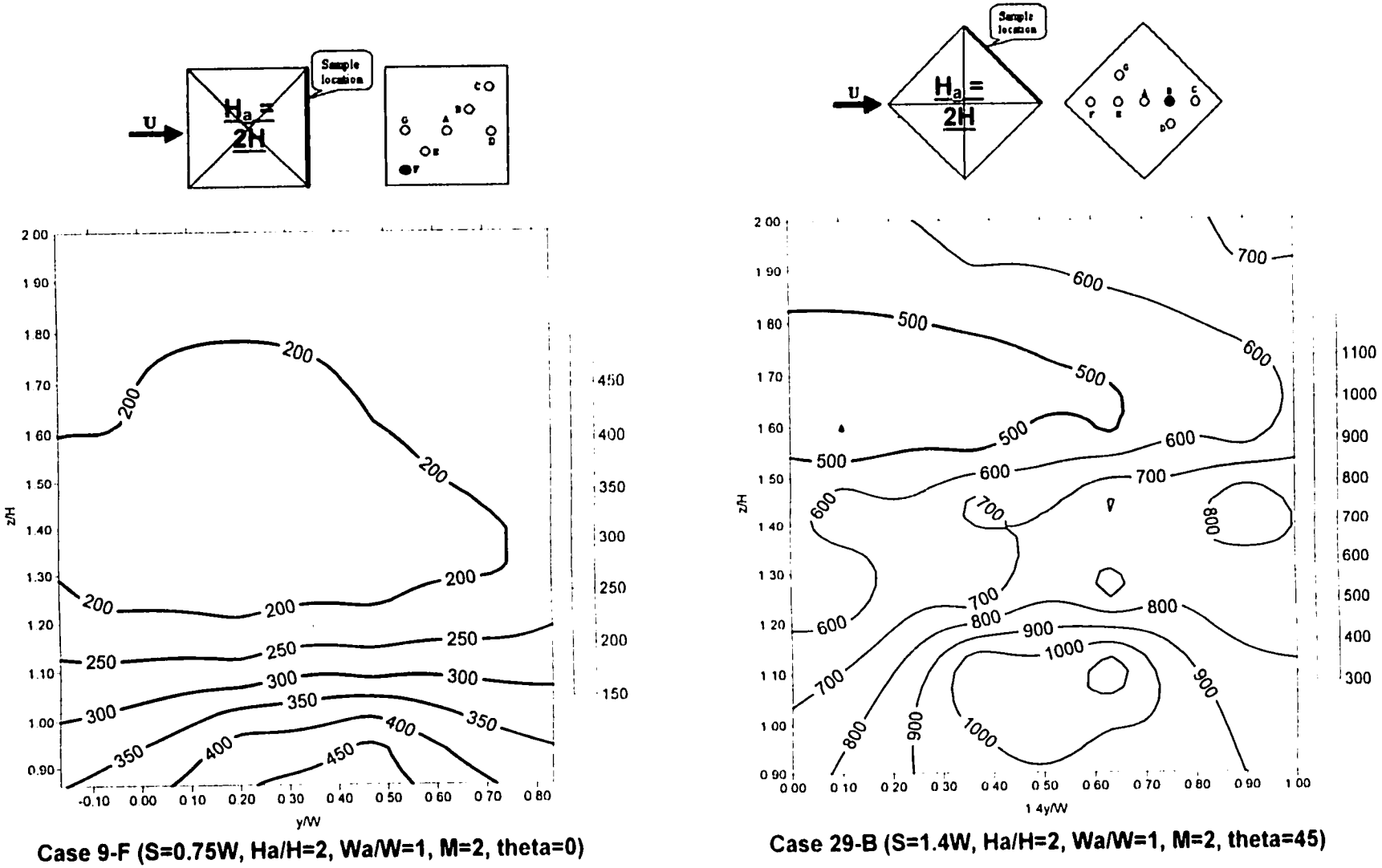

Figure 5.25 Dilution contours obtained for case 9 (Stack F) and case 29 (stack B)

Minimum dilution variation with the wind direction for the case of $H_a = 2H$ is shown in Figure 5.26. Since the adjacent building is taller than in the previous two cases, the wake region is larger, especially when $\theta = 45°$. The slope of the regression line of $D_{min\text{-}45°}$ is much flatter than that of $D_{min\text{-}0°}$.

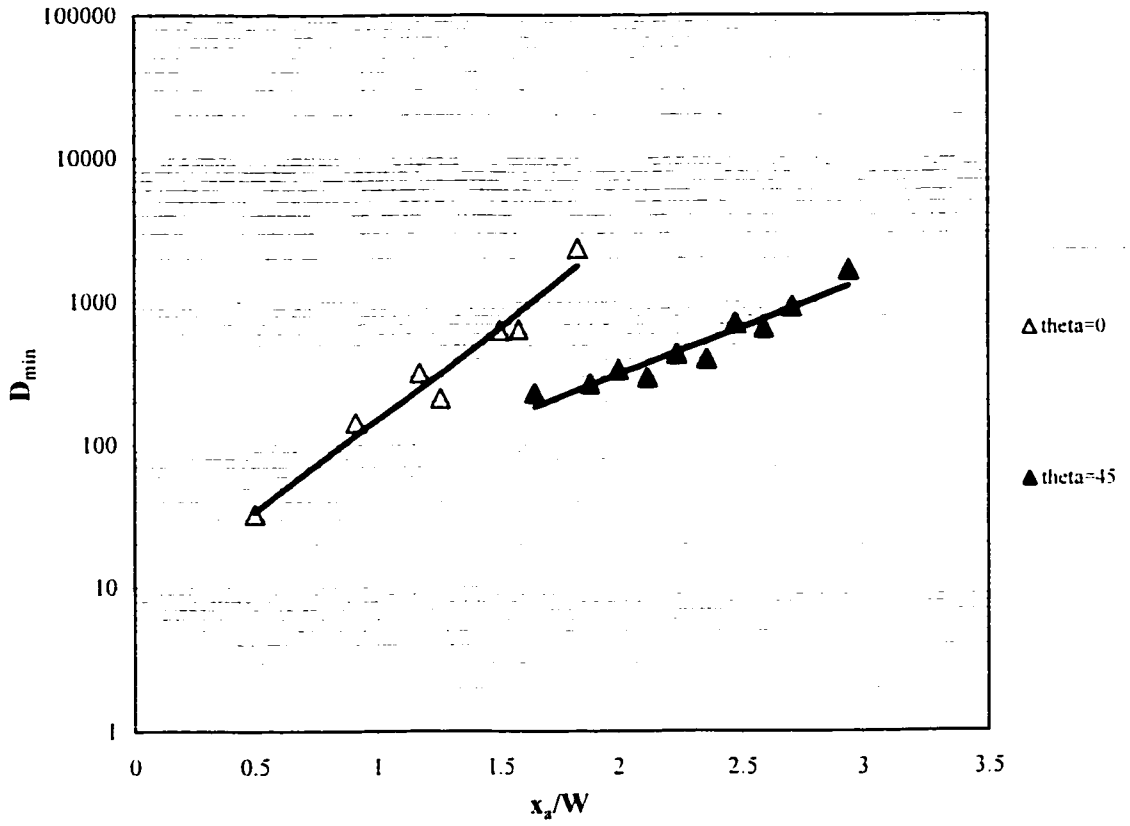

Figure 5.26 Effect of wind direction on the minimum dilution for the case of $H_a = 2H$, $W_a = W$, $M = 2$ (centerline stacks)

5.7.4 Closure

Generally, it can be found from this section that:

- Wind direction affects wake dispersion significantly;
- The minimum dilution obtained from $\theta = 45°$ is smaller than that from $\theta = 0°$, except for the case of building separation distance S = 0, which yields very low dilution;
- The minimum dilution increases with stack distance for both wind directions.

5.8 Effect of stack location on dilution

Seven different stack locations, namely A, B, C, D, E, F, and G, were investigated for all cases in the present study.

Theoretically, the farther the stack, the higher the minimum dilution, since the plume emitting from a farther stack maybe out or partly out of the recirculation cavity zone, also, simply due to distance dilution effect. It is interesting that for the farthest two stacks, C (located at corner) and D (located at the center line), although the straight distance between them and the adjacent building is the same, minimum dilutions obtained for Stack C are slightly higher than those for Stack D by a factor of about 1.2~1.8, since

stack C is nearer the edge of the cavity than Stack D. The same was found for Stack F (located at corner) and G (located at the centerline), the closest stacks to the adjacent building, for the case of $\theta = 0°$. This trend was inversed for the case of $\theta = 45°$, because stack D was on the other side of measuring wall.

Figure 5.27 shows minimum dilution obtained for the case of $H_a = 2H$, $W_a = W$, and $\theta = 0°$. Comparing with stacks F and G, which are the closest to the upstream building, it can be found that either center or corner stack did not affect D_{min} much. On the other hand, for the farthest stacks, C and D, minimum dilutions obtained from corner stacks were about 2 times as those from center stacks. Similar results were found for the other adjacent building heights, $H_a = 1.33H$ and $1.67H$.

Figure 5.28 shows the case for $H_a = 1.33H$, $W_a = 2W$, $\theta = 0°$. The main difference between Figures 5.27 and 5.28 is that even for the farthest stacks, there is no significant difference on D_{min} between center and corner stacks. As previously discussed, wider upstream buildings form larger wake zones and the plume cannot escape in the free stream.

For the case of $\theta = 45°$, since the crosswind width of upstream adjacent building is 1.41 times as that of $\theta = 0°$, the wake zone in this case is larger than that of $\theta = 0°$. D_{min} obtained from either center or corner stack did not show any significant difference within a certain separation distance, as shown in Figure 5.29.

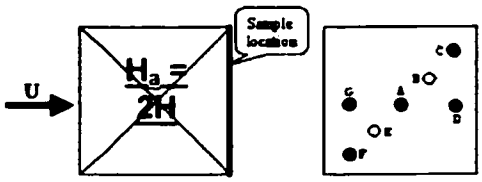

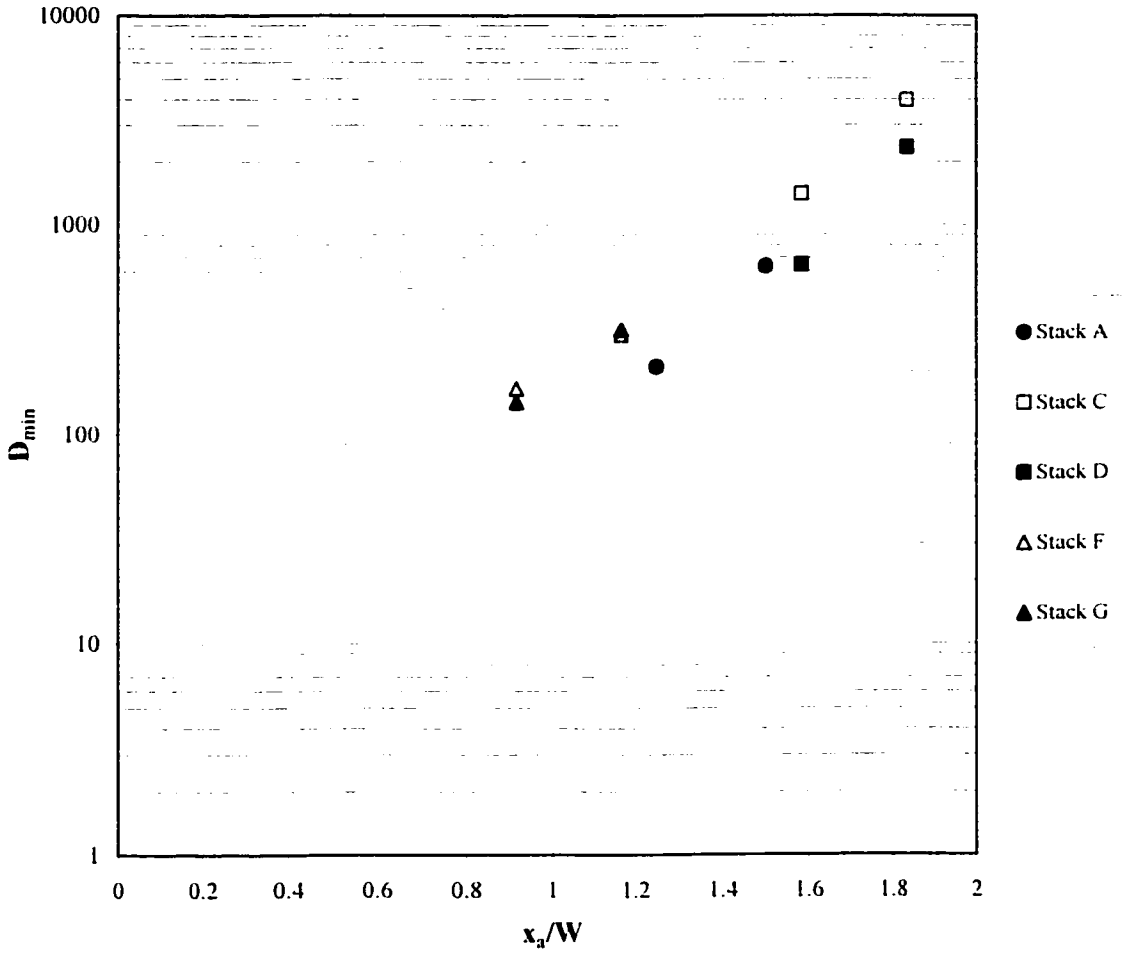

Figure 5.27 Effect of stack location on the minimum dilution for the case of H_a = 2H, W_a = W, θ = 0°

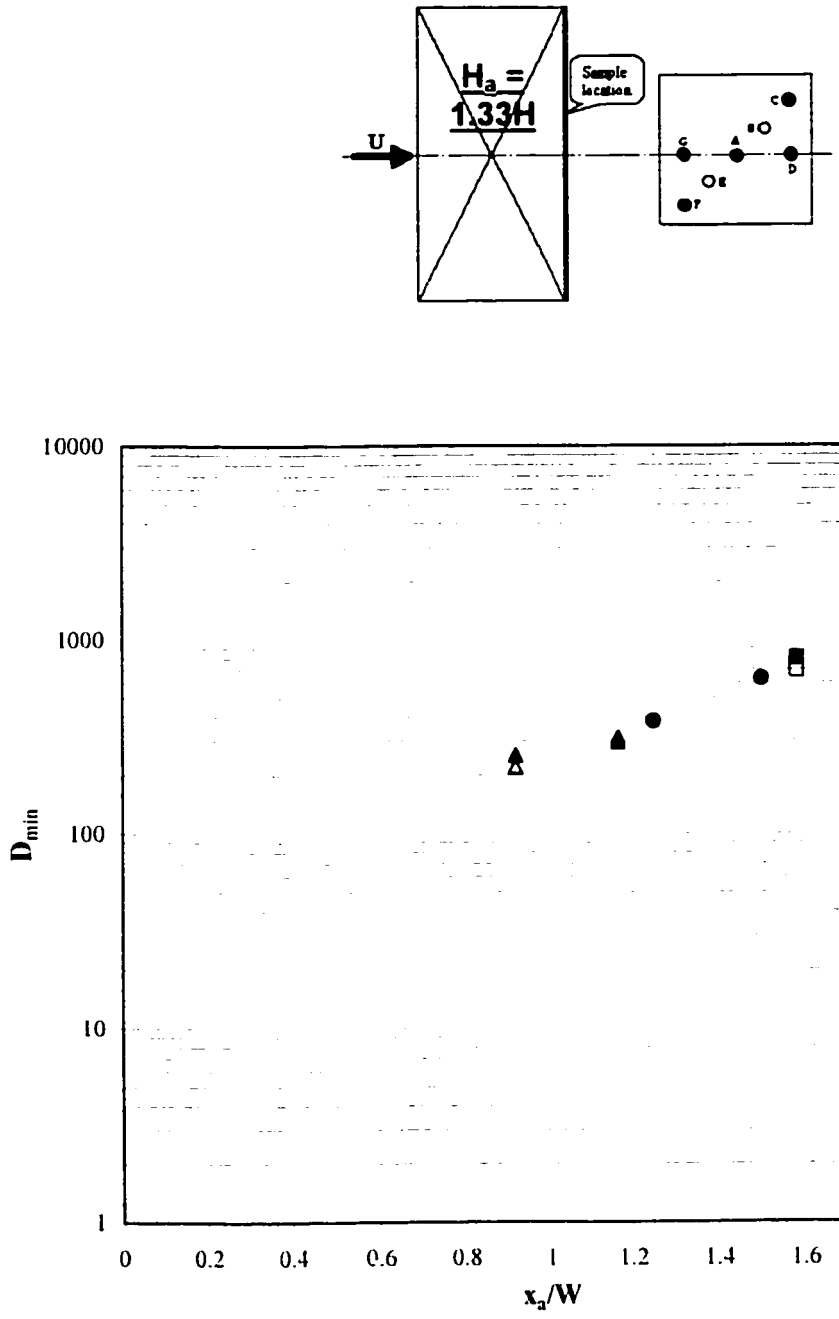

Figure 5.28 Effect of stack location on the minimum dilution for the case of $H_a = 1.33H$, $W_a = 2W$, $0 = 0°$

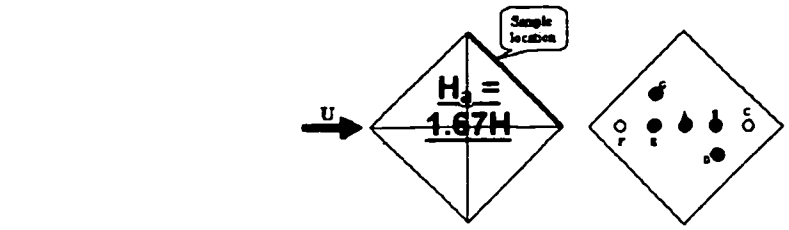

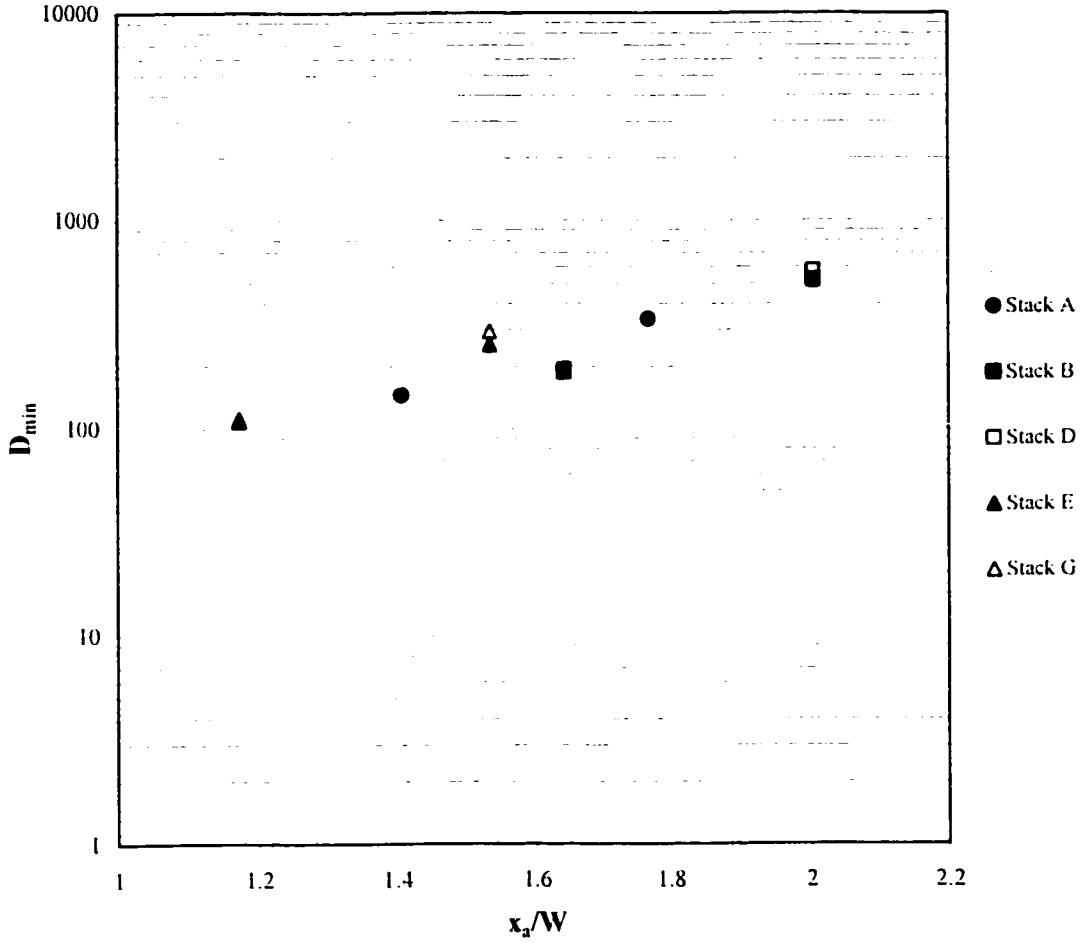

Figure 5.29 Effect of stack location on the minimum dilution for the case of $H_a = 1.67H$, $W_a = W$, $0 = 45^o$

Three cases are chosen to represent the effect of stack location on dilution distribution in detail: case 1 (H_a = 1.33H, W_a = W, S = 0, θ = 0°), case 11 (H_a = 1.33H, W_a = 2W, S = 0.75W, θ = 0°), and case 24 (H_a = 1.67H, W_a = 1.1W, S = 0, θ = 45°). These cases are expected to be representative of all various configurations tested.

Figure 5.30 represents the dilution obtained from two farther stacks, C (corner stack) and D (centerline stack) of Case 1 (H_a = 1.33H, W_a = W, S = 0, M = 2, and θ = 0°) for the same distance between stack and adjacent building, i.e., x_a = 0.83W. It can be found that for the center stack, dilution dispersion is more uniform than that for the corner stack, especially near the adjacent building top. The minimum dilution obtained from the corner stack is about 2.8 times higher than that from the center stack.

For the closer stacks, F (corner stack) and G (center stack) of Case 1, with x_a = 0.17W, similar results are evident, as shown in Figure 5.31. However, the difference in dilution for corner and center stacks is much less in this case. Thus, the influence of stack location in the cross-wind direction (as opposed to the along-wind direction) cannot be estimated without a detailed knowledge of the flow field (wake) of the upstream building. Considering that flow field depends on building height, shape, width, wind direction and upstream roughness, it is not feasible to develop a design method that accounts for lateral stack position. The best that can be done is to provide estimates of minimum dilution for the worst-case stack position.

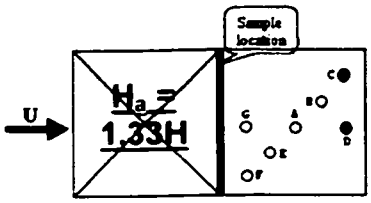

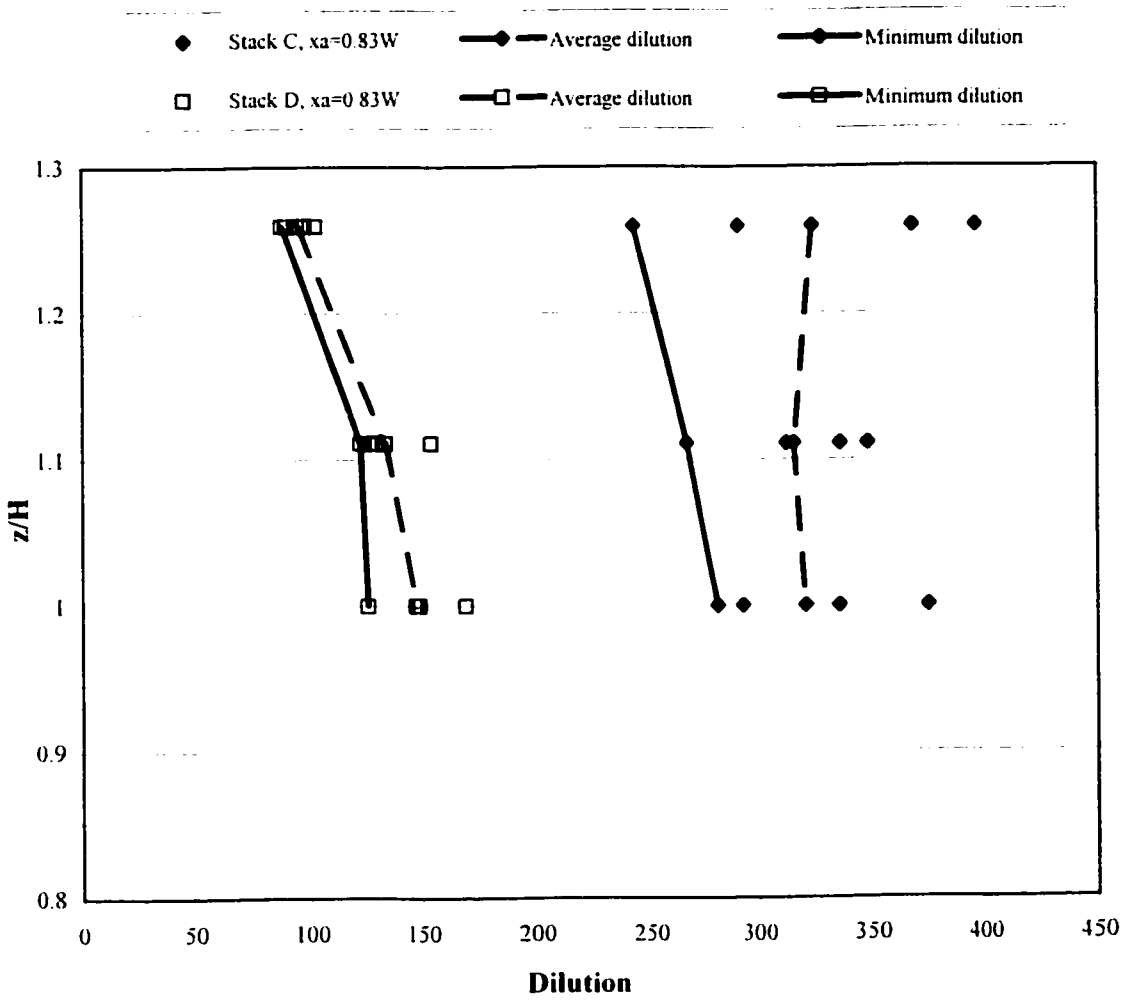

Figure 5.30 Effect of stack location on dilution for the case of H_a = 1.33H, W_a = W, S = 0, M = 2, 0 = 0° (farther stacks)

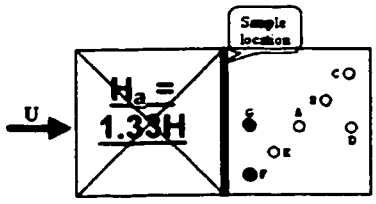

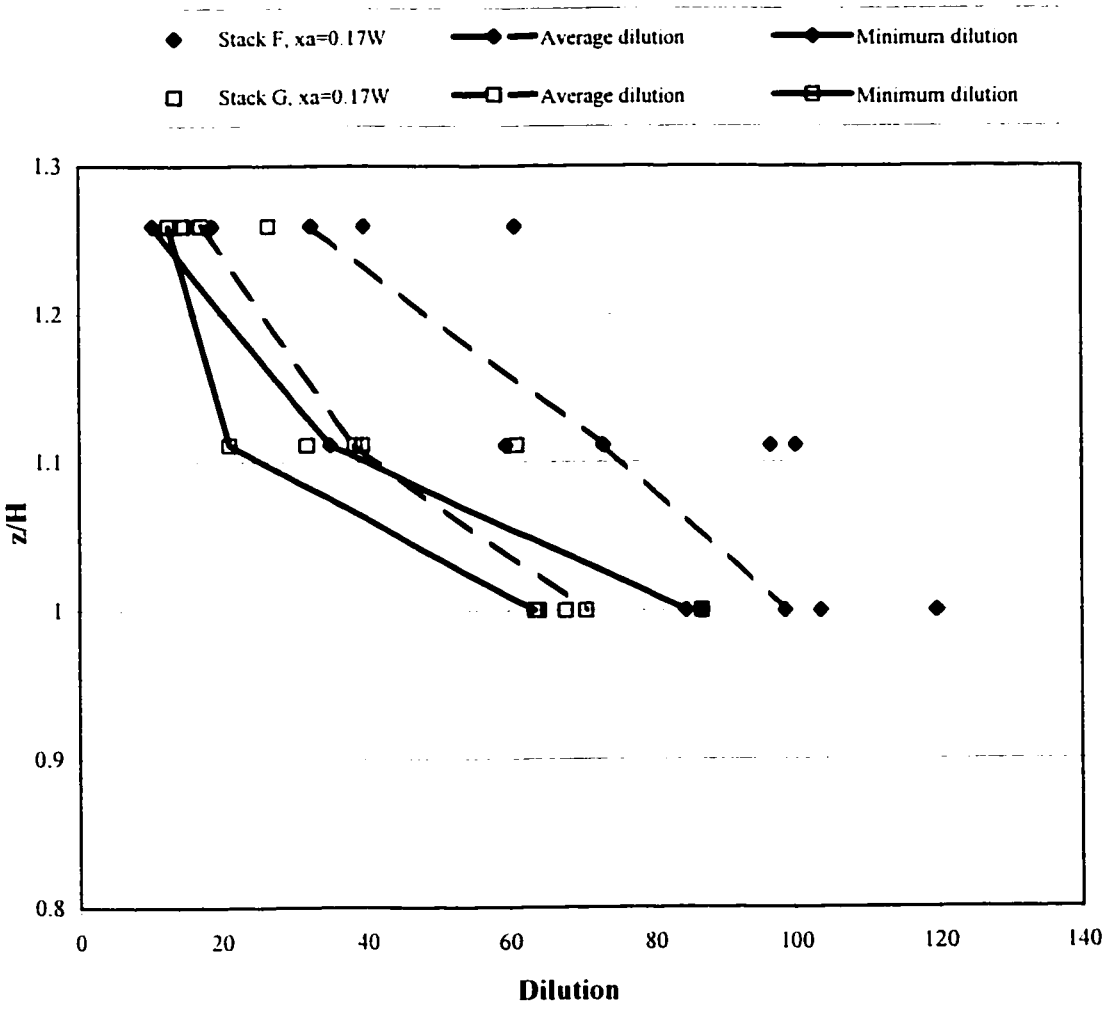

Figure 5.31 Effect of stack location on dilution for the case of H_a = 1.33H, W_a = W, S = 0, M = 2, 0 = 0° (closer stacks)

When the adjacent building height and the separation distance increased, dilution exhibited quite large variations. Figure 5.32 shows the dilutions obtained from the two farther stacks, C (corner stack) and D (center stack), with x_a = 1.58W of the case H_a = 1.67H, W_a = W, S = 0.75W, M = 2, and θ = 0°. Since most dilution factors are higher than 3000, the stacks can be treated as out of the wake region and the extensive variation of dilutions is not surprising. The minimum dilution obtained from the corner stack was 2.6 times that from the center stack. On the other hand, for the closer stacks, F (corner stack) and G (centerline stack), with x_a = 0.92W, the variation became smaller. As shown in Figure 5.33, the variation becomes more uniform with height increase, especially for the top of the adjacent building. The minimum dilution obtained from the corner stack (F) is only 1.3 times that from the center stack (G).

Note that the minimum dilution obtained by x_a/W = 1.58 is 35 times higher than that by x_a/W = 0.92 for centerline stack and more than 75 times for corner stack. In this configuration the stacks were out of the wake zone formed by the upstream building ($D_{min\text{-}center\text{-}xa=1.58w} \approx 2900$ and $D_{min\text{-}corner\text{-}xa=1.58w} \approx 7300$). The effect of exhaust emitting from lower downstream building rooftop can be neglected here.

When the adjacent building width was changed from W to 2W, dilutions obtained with the leeward stacks varied from 700 to 1500, the plumes were partly within the recirculation cavity, as shown in Figures 5.34 and 5.35 for case 11 (H_a = 1.33H, W_a = 2W, S = 0.75W, M = 2, θ = 0°). The minimum dilution obtained from the center stacks (D or G) is almost the same as that from the corner stacks (C or F). This is due to the fact that the wake is much wider than the case of W_a = W.

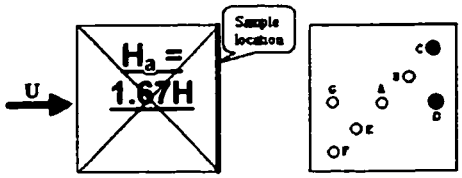

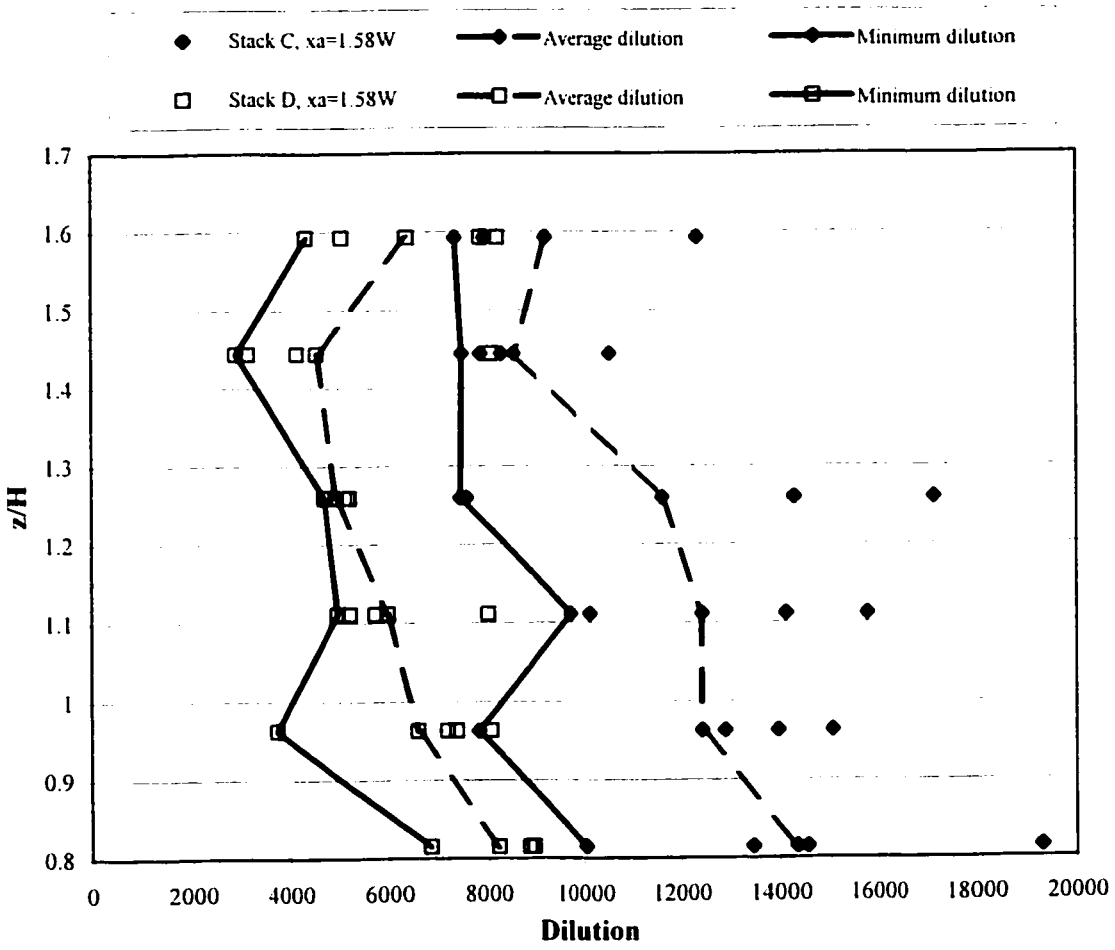

Figure 5.32 Effect of stack location on dilution for the case of H_a = 1.67H, W_a = W, S = 0.75W, M = 2, θ = 0° (farther stacks)

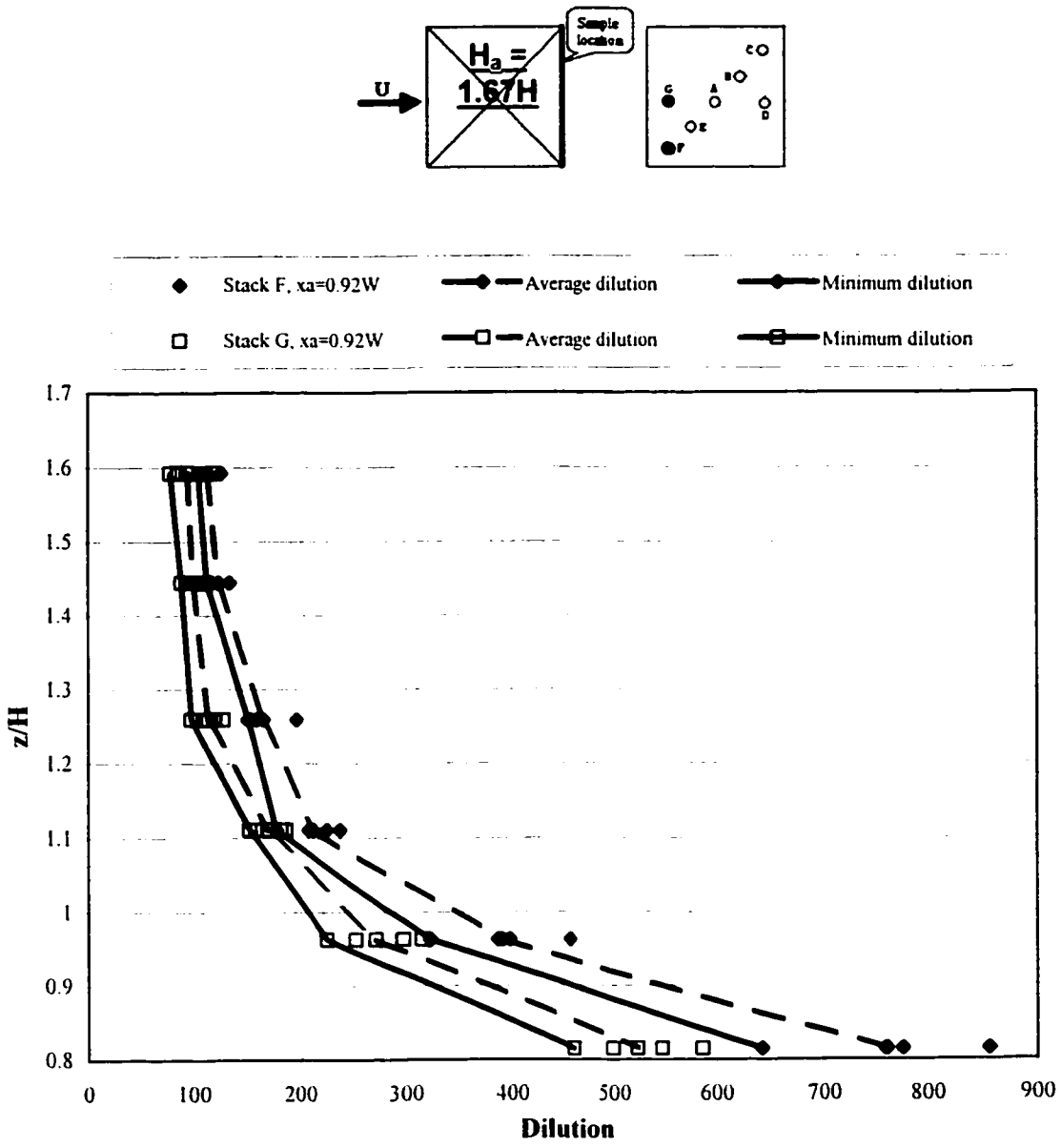

Figure 5.33 Effect of stack location on dilution for the case of H_a = 1.67H, W_a = W, S = 0.75W, M = 2, 0 = 0° (closer stacks)

As shown in Figure 5.35, dilution data obtained with stacks near the windward wall, F (corner stack) and G (centerline stack x_a = 0.92W) are similar, but the dilutions were

more uniform, as described in Case 1 and Case 7.

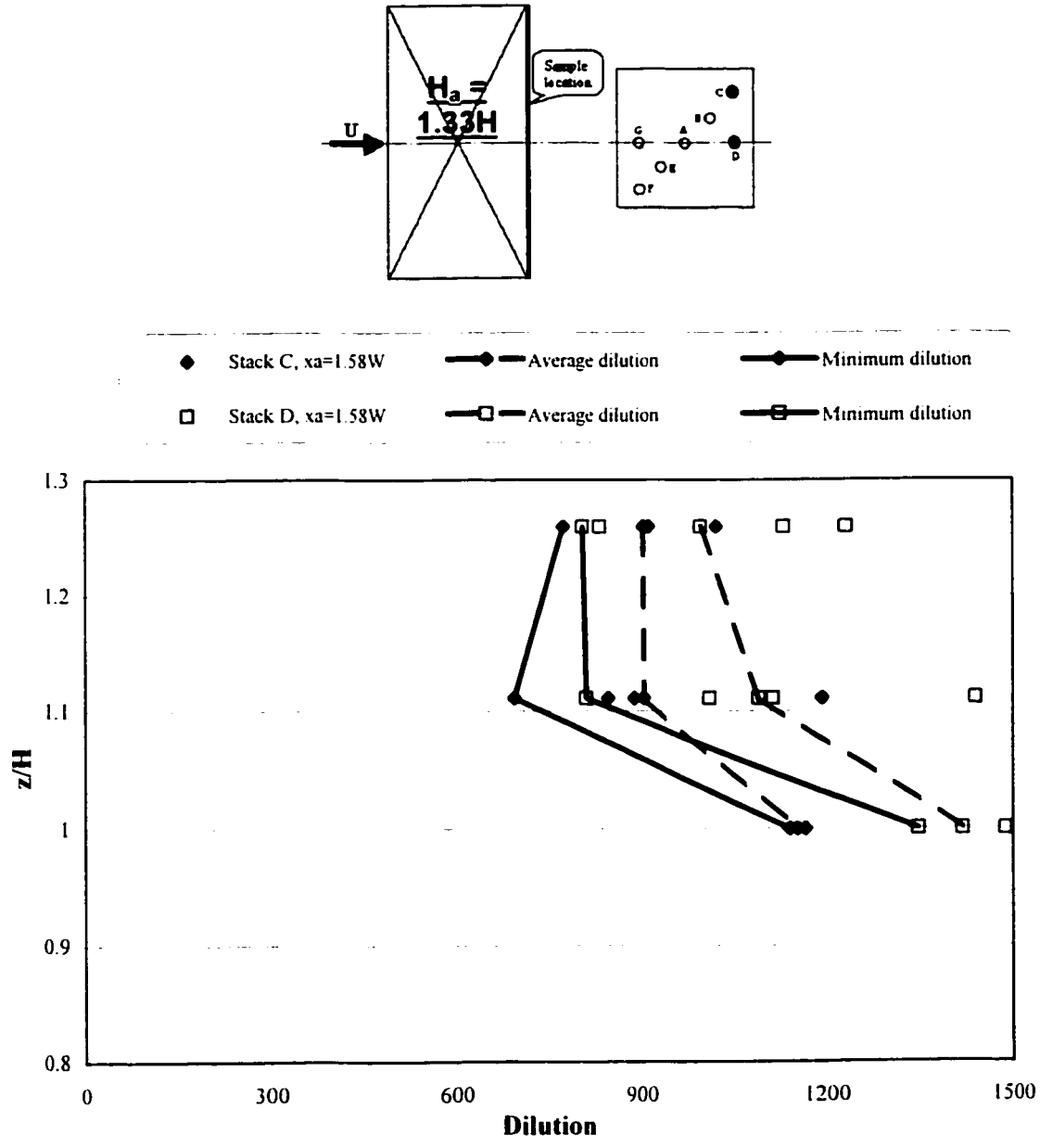

Figure 5.34 Effect of stack location on dilution for the case of H_a = 2H, W_a = 2W, S = 0.75W, M = 2, θ = 0° (farther stacks)

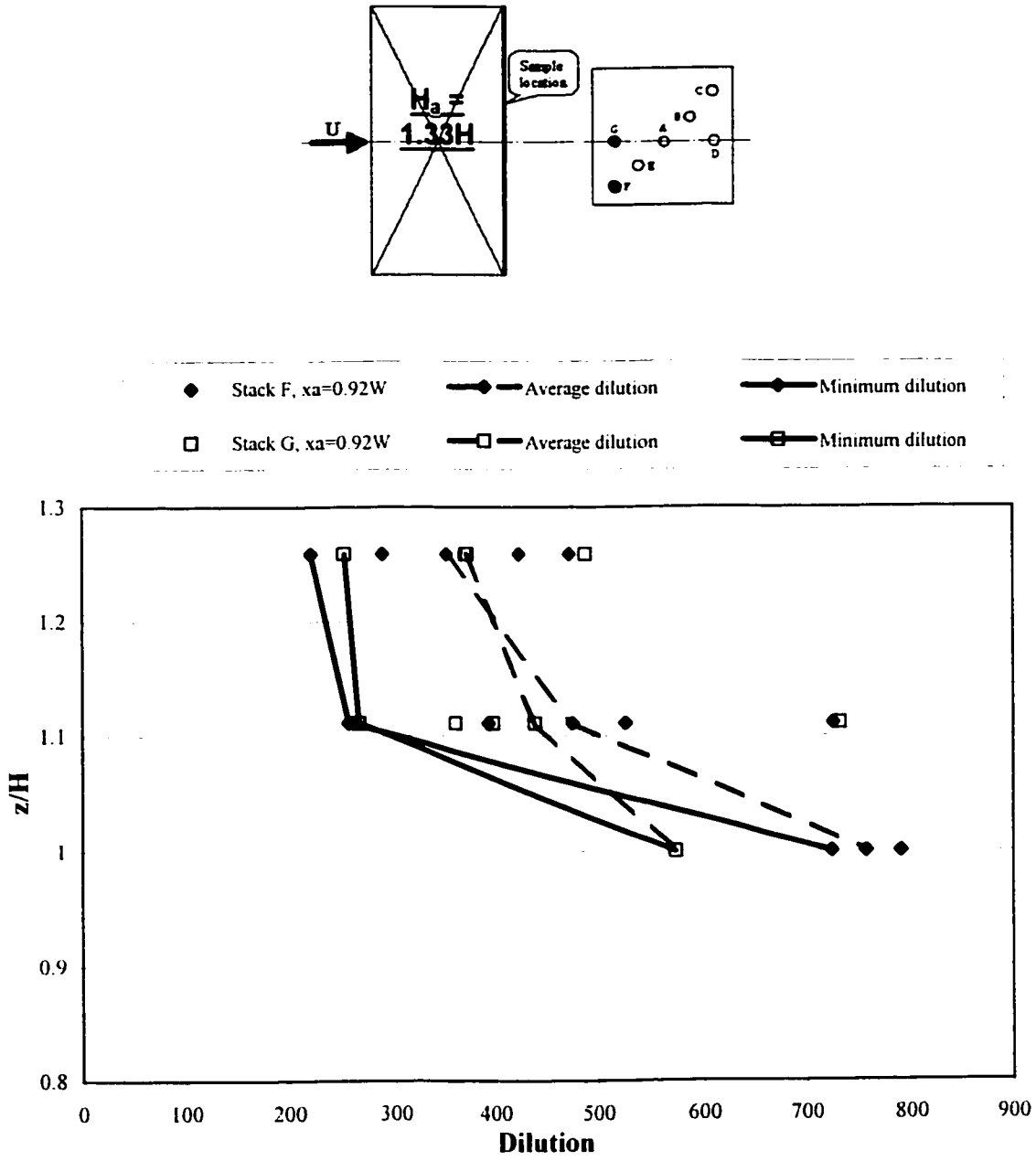

Figure 5.35 Effect of stack location on dilution for case of H_a = 2H, W_a = 2W, S = 0.75W, M = 2, 0 = 0° (closer stacks)

Similar results were found when the wind direction changed from 0° to 45°.

5.9 Effect of stack height on dilution

Dilution data were obtained with four different stack heights, h_s = 0, 2.5mm, 7.5mm, 12.5mm, and 25mm, for two stack locations, center stack (A) and corner stack (F), for the case H_a = 1.67 H, W_a = W, S=0.75W, θ = 0°. At a scale of 1:400, they represented full-scale stack heights of 1m, 3m, 5m, and 10m, respectively. The ratio of stack height to building height had a range of $0 < \frac{h_s}{H} < 0.19$. The results are plotted in Figures 5.36 to 5.39.

Generally, as a consequence of increasing the stack height, higher dilution will be obtained at all locations on the leeward wall of the upstream building. However, for the center stack, as shown in Figures 5.36 and 5.38, when stack height increases from 1m to 3m, not only minimum dilution but also all the dilutions obtained from every tap decreased by approx 10%. For stack height greater than 3m, dilutions increase with stack height.

It is interesting to note that for this building configuration and wind direction, increasing stack height provides relatively little benefit. D_{min} increases by a factor of 2.1 when stack height increases from 0 to 10m. However, this 10m height of stack will not be likely to be accepted by architects in most cases.

Figures 5.37 and 5.39 show the influence of stack height on dilution and the minimum dilution for corner stack (F). Unlike results obtained with center stack, data for $0 < h_s <$

3m show a general increase with stack height. Note the magnitude of $D_{min\text{-}0\text{-}F}$ is only about 25% of $D_{min\text{-}0\text{-}A}$, the benefit of increasing stack height is less than that of Stack A. The increase in D_{min} is only 1.5 times for a 10-meter stack.

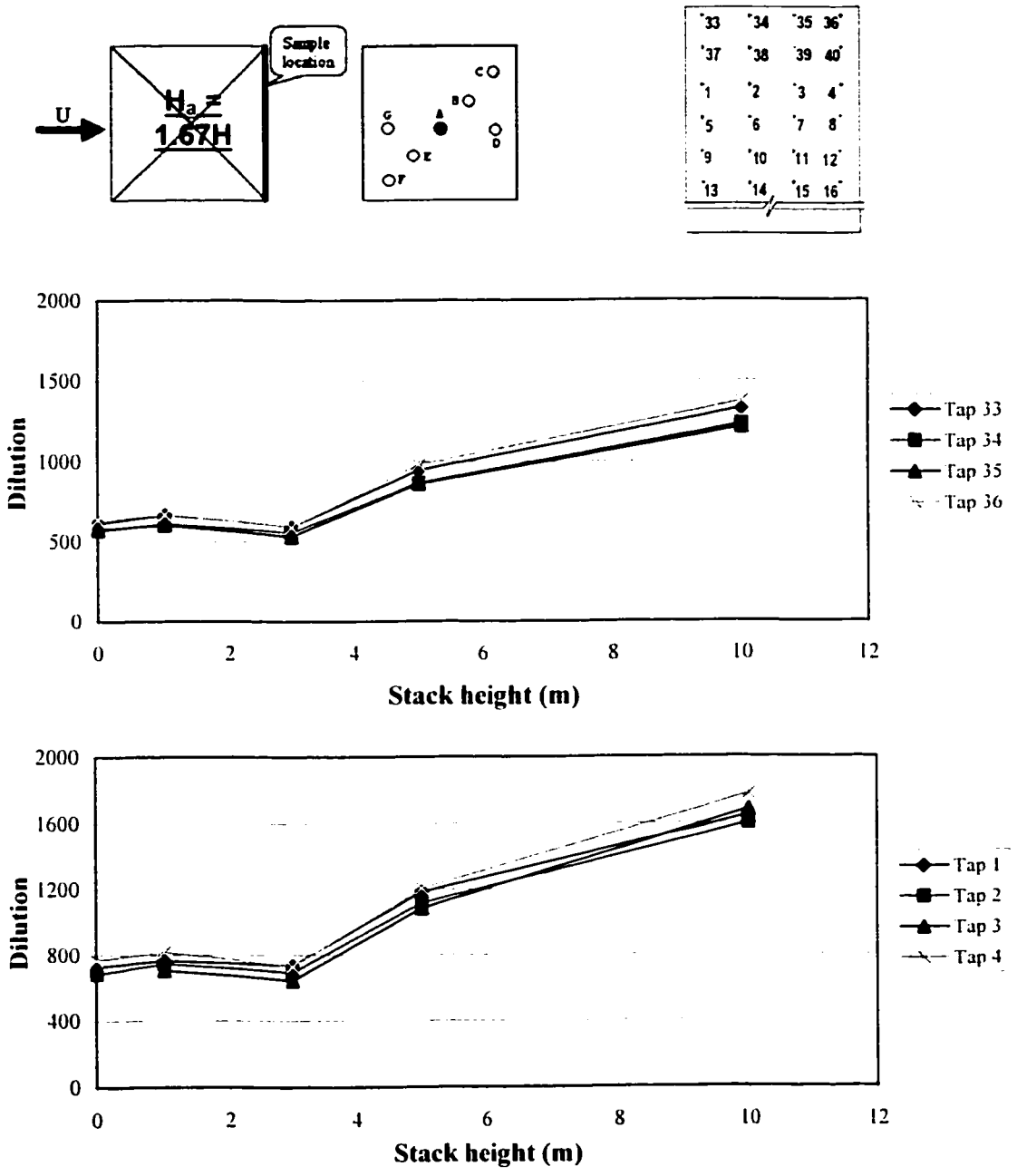

Figure 5.36 Dilution variation with stack height for the case of H_a = 1.67H, W_a = W, S=0.75W, 0 = 0° (Stack A)

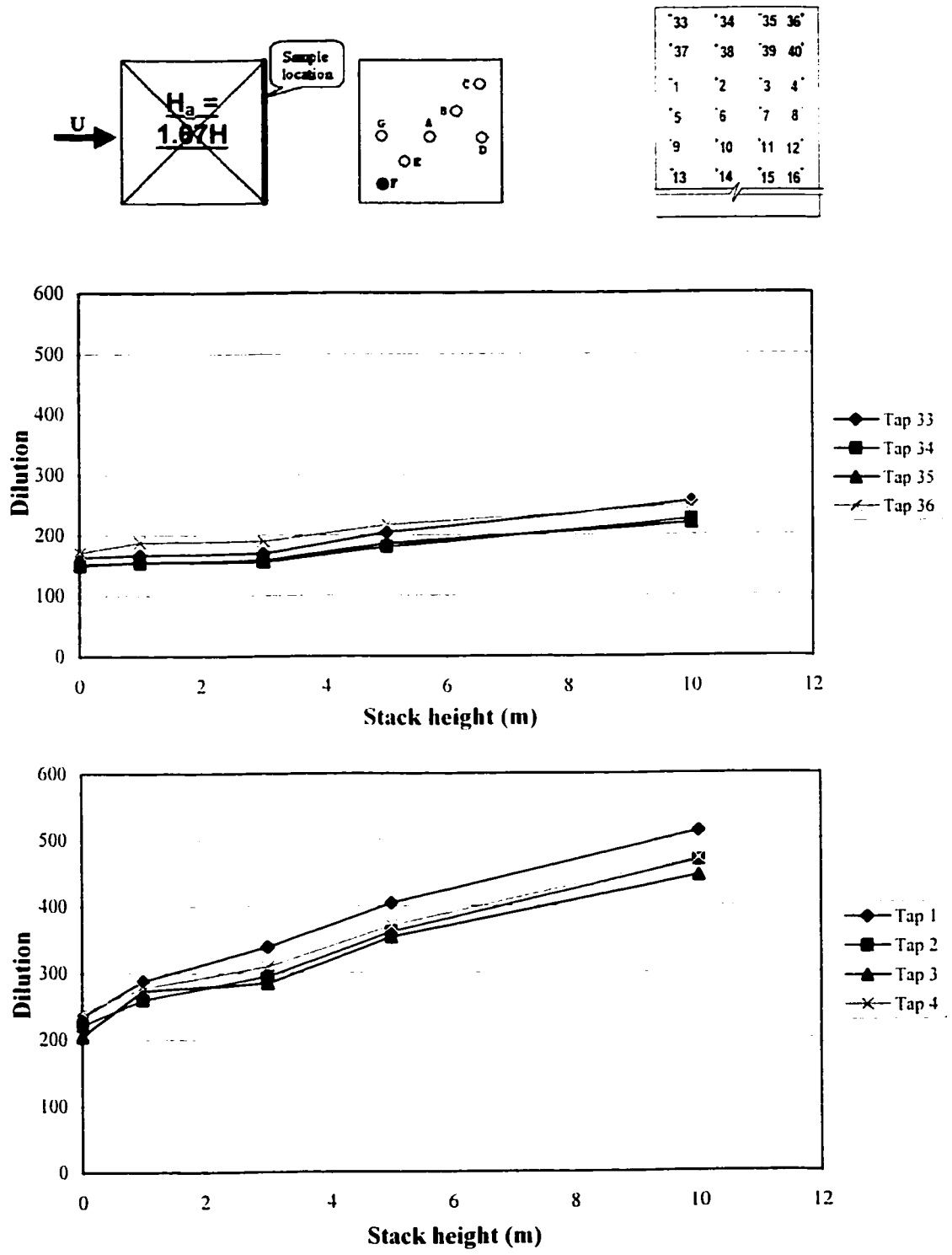

Figure 5.37 Dilutions variation with stack height for the case of H_a = 1.67H, W_a = W, S=0.75W, 0 = 0° (Stack F)

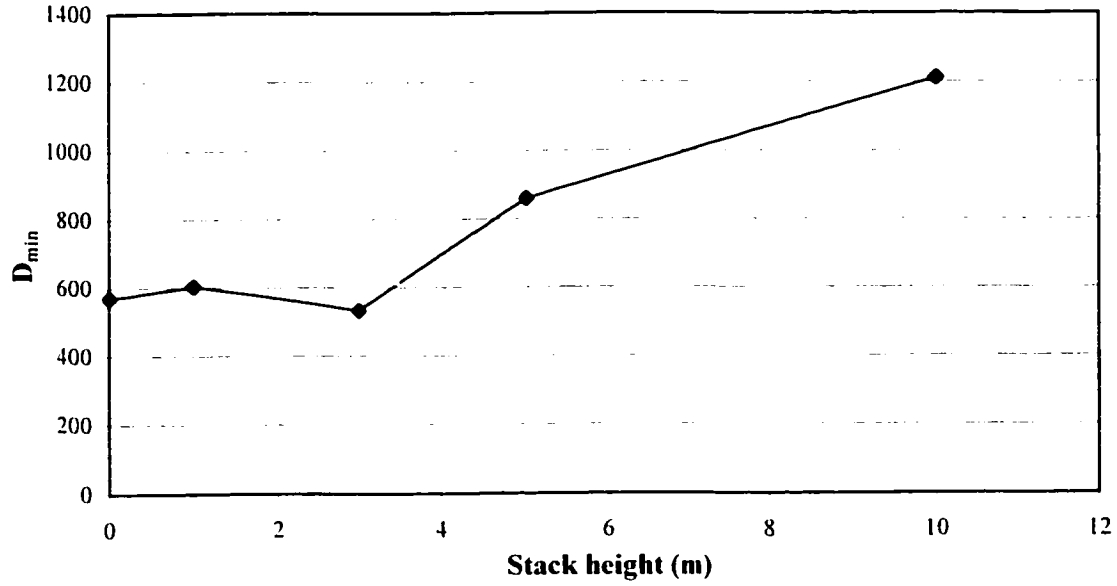

Figure 5.38 Minimum dilution variation with stack height for the case of $H_a = 1.67H$, $W_a = W$, $S=0.75W$, $0 = 0°$ (Stack A)

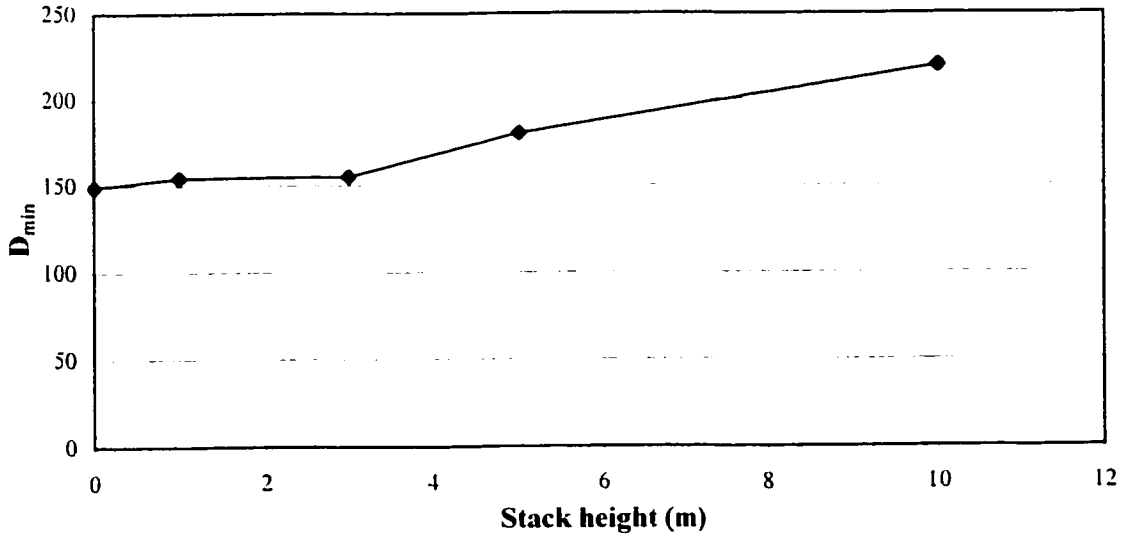

Figure 5.39 Minimum dilution variation with stack height for the case of $H_a = 1.67H$, $W_a = W$, $S=0.75W$, $0 = 0°$ (Stack F)

5.10 Effect of distance between emitting and adjacent building on dilution

Figure 5.40 shows the variation of D_{min} with distance from stack for buildings with or without gap for H_a = 1.33H, W_a =W, M=2, and θ = 0° for the centerline stacks. It was found that gap did not affect significantly the minimum dilution, as shown in Figure 5.40; however, the gap affected the dilution distribution on the upwind adjacent building leeward wall. As shown in Figures 5.41 and 5.42, two different distances between the stack and adjacent building, x_a = 0.5W (no gap, centerline stack) and x_a = 0.42W (with gap of 0.25W, centerline stack), were chosen to compare the effect of gap on dilution distribution. For the case of no gap, the dilution distribution is somewhat uniform, with values around 30 to 50. On the other hand, dilution exhibited quite a large variation from 30 to 490 that was not seen when there was no gap present.

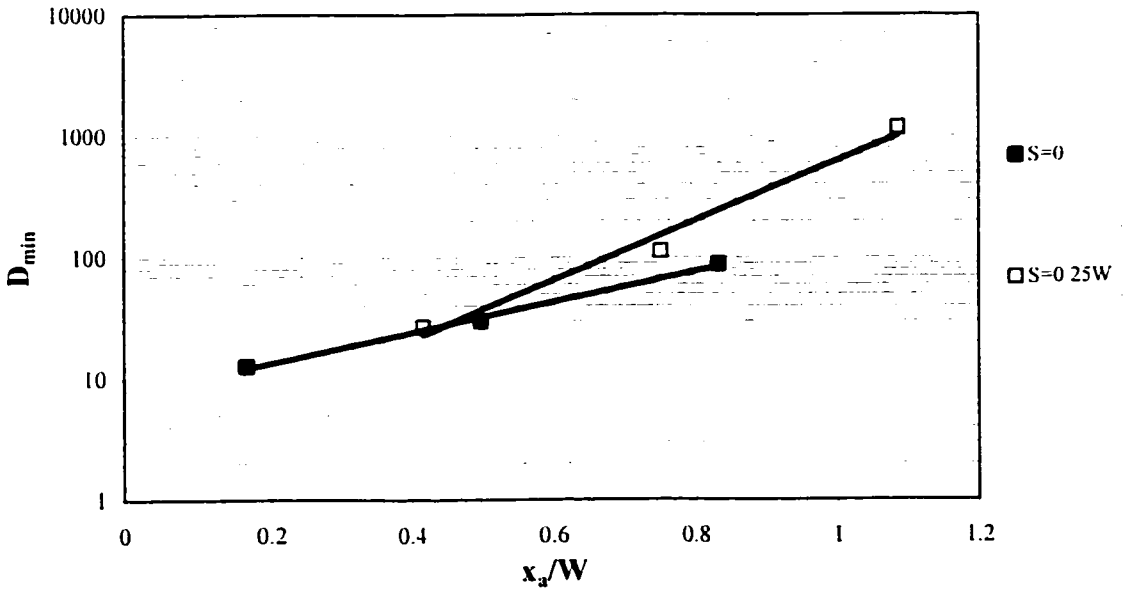

Figure 5.40 Effect of gap on the minimum dilution (for the case of H_a = 1.33H, W_a = W, M = 2, 0 = 0°)

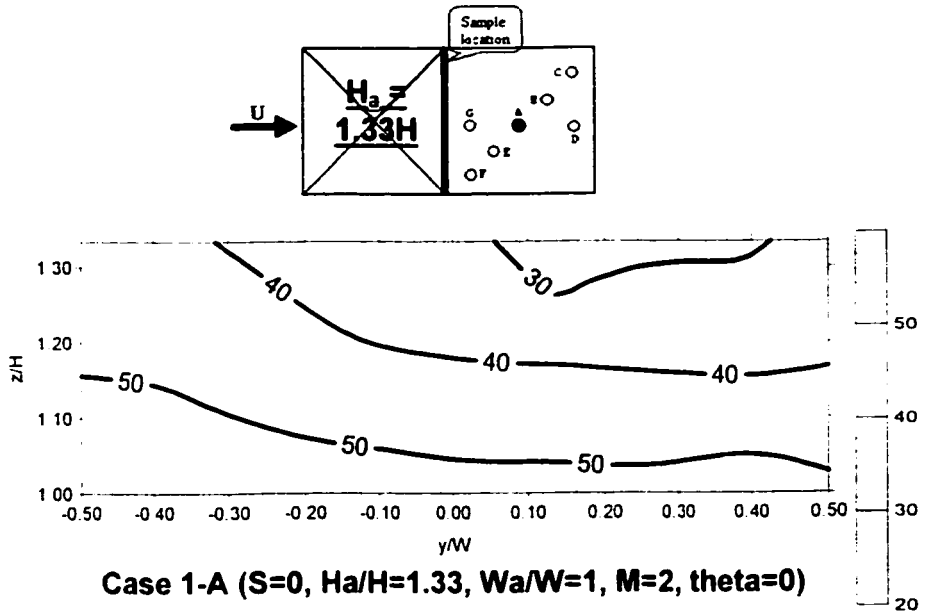

Case 1-A (S=0, Ha/H=1.33, Wa/W=1, M=2, theta=0)

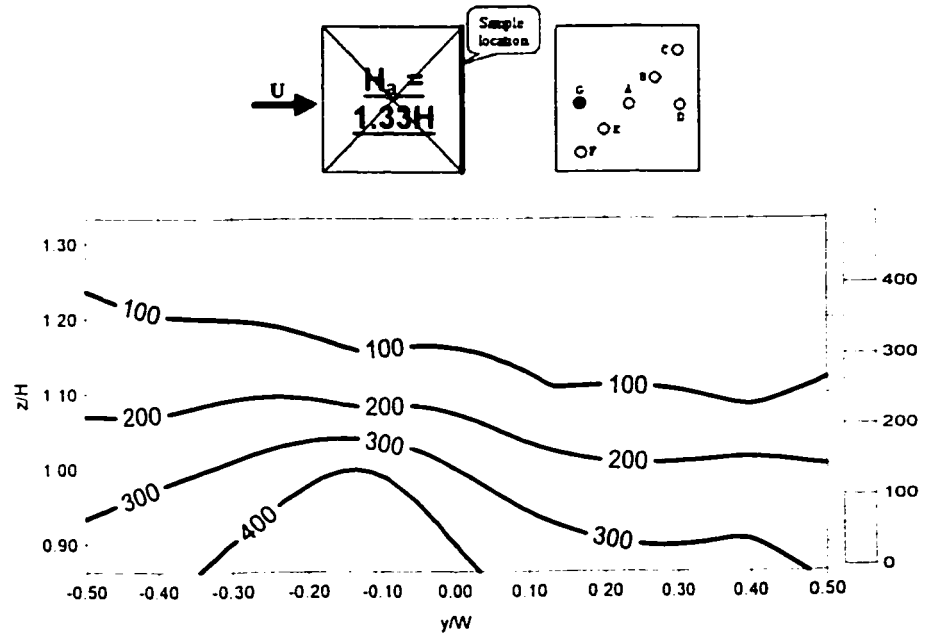

Case 6-G (S=0.25W, Ha/H=1.33, Wa/W=1, M=2, theta=0)

Figure 5.41 Dilution contours obtained by the cases of $x_a/W = 0.5$, S = 0 and $x_a/W = 0.42$, S = 0.25W

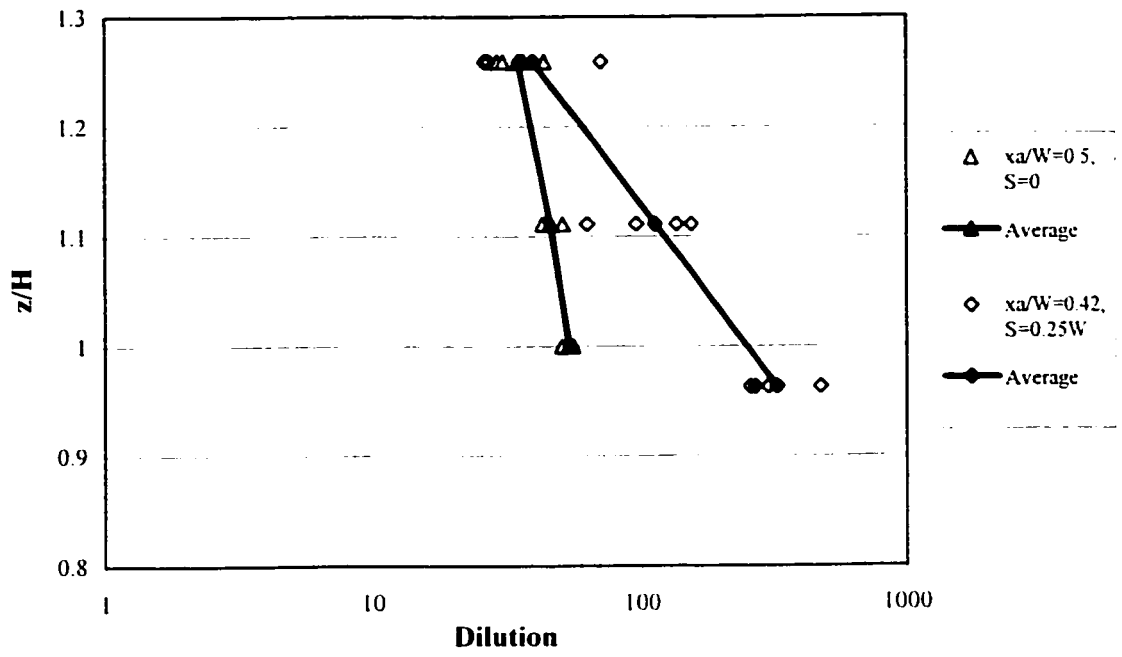

Figure 5.42 Effect of gap on dilution for the case of H_a = 1.33H, W_a = W, M = 2, 0 = 0°

Similar results can be found for the case of H_a = 2H, M = 2, θ = 0°. As shown in Figure 5.43, although minimum dilution obtained from the case with no gap is almost the same as that from the case with a gap of W/3, the dilution distribution presented a larger variation in the latter case.

It is interesting to find that for the case of H_a = 1.33H, W_a = W, M = 2, and θ = 45°, different results were obtained. As shown in Figure 5.44, in a semi-logarithm scale, minimum dilutions obtained were roughly proportional to the distance between the stack and adjacent building (x_a) for both cases with or without gap. And the dilution distribution did not appear quite difference in both cases, as shown in Figures 5.45 and 5.46 for centerline stack with x_a = 1.39W.

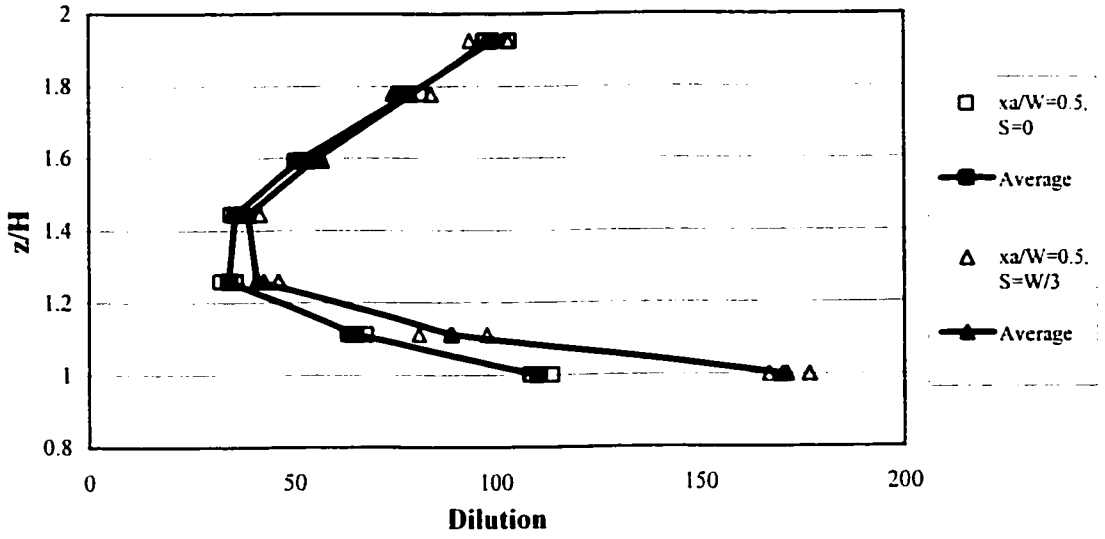

Figure 5.43 Effect of gap on dilution for the case of $H_a = 2H$, $W_a = W$, $M = 2$, $\theta = 0°$

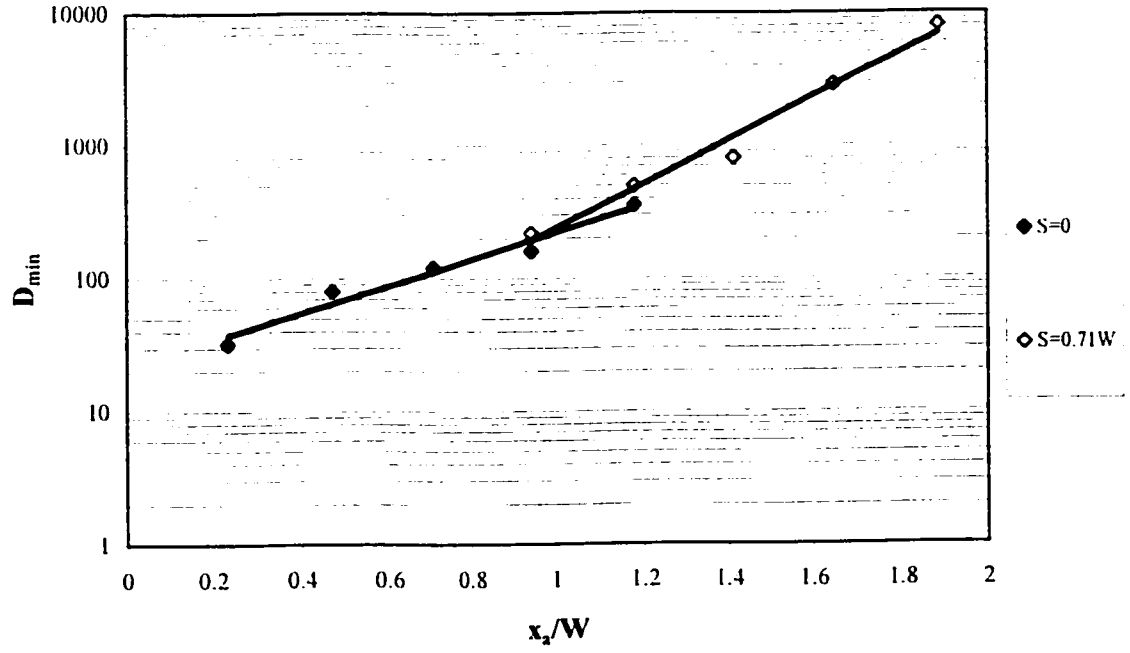

Figure 5.44 Effect of Gap on the minimum dilution for the case of $H_a = 1.33H$, $W_a = W$, $M = 2$, $\theta = 45°$

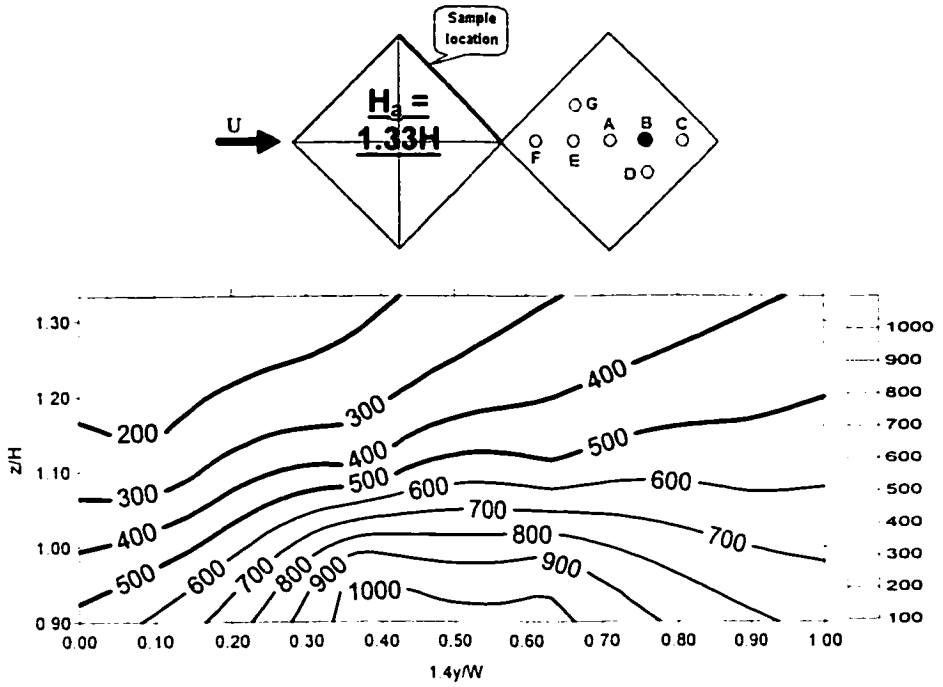

Case 21-B (S=0, Ha/H=1.33, Wa/W=1, M=2, theta=45)

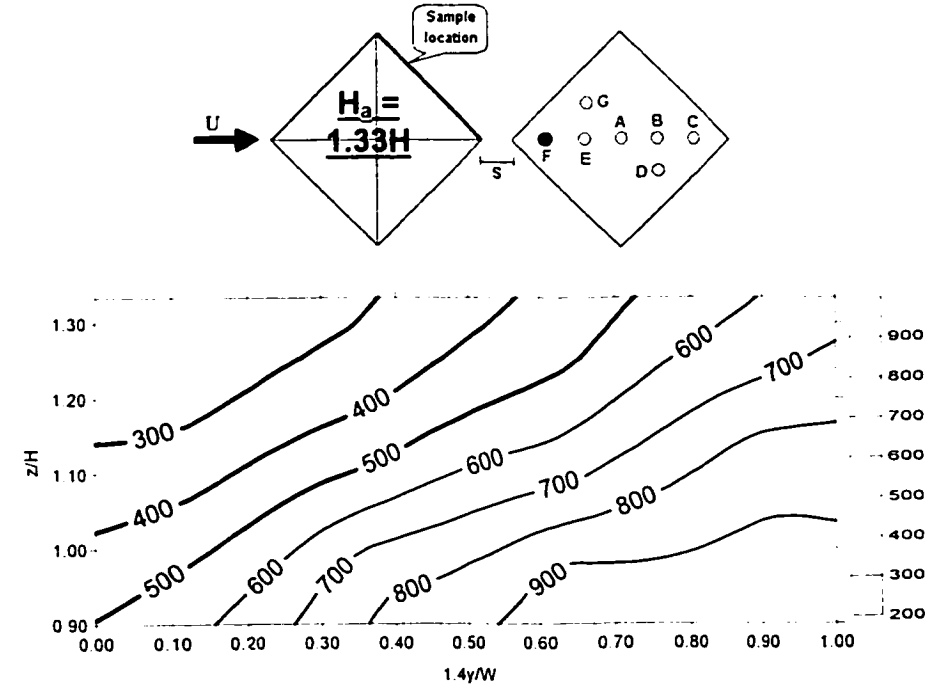

Case 22-F (S=0.7W, Ha/H=1.33, Wa/W=1, M=2, theta=45)

Figure 5.45 Dilution contours obtained by cases with and without gap, θ = 45°

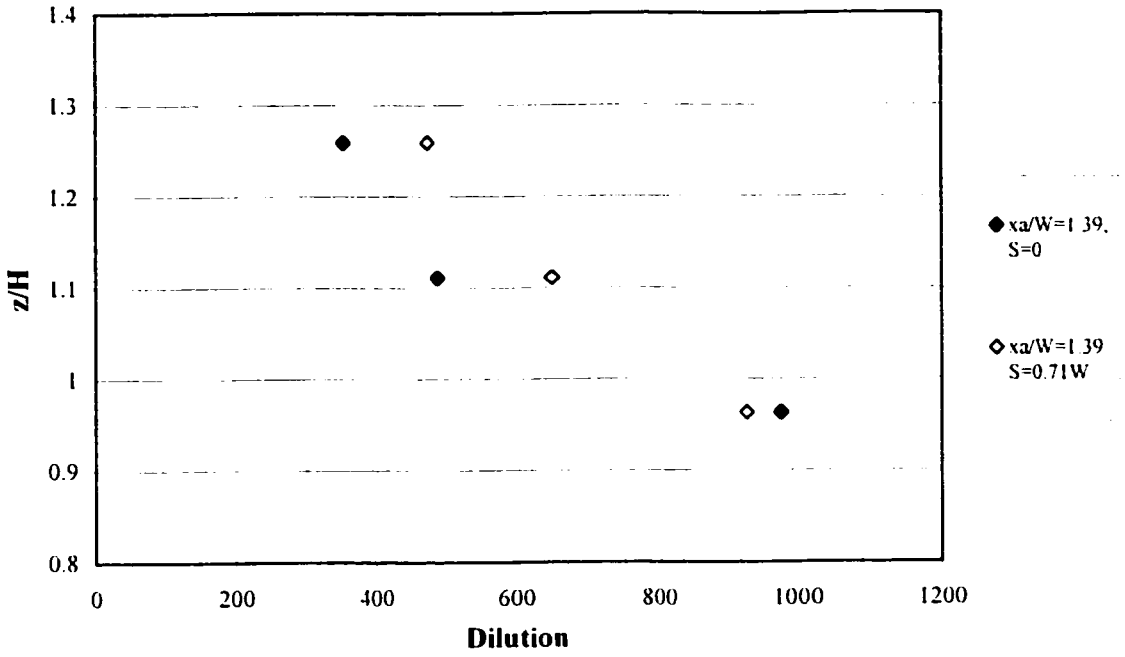

Figure 5.46 Effect of gap on dilution for the case of H_a = 1.33H, W_a = W, M = 2, 0 = 45°

5.11 Comparison with Wilson's (1998) study

Wilson et al. (1998) conducted a series water flume experiments to examine the effect of an adjacent building on dilution values. To compare with the Wilson's experimental data and Wilson model, normalized dilution, D_{nor}, is used. D_{nor} is defined by rearranging D = C_e/C to a normalized form using the building height (H) and wind speed (U_H) at roof height with no building present,

$$D_{nor} = \frac{DQ_e}{U_H H^2} \tag{5.14}$$

where D is measured dilution factor, Q_e is exhaust volume flow rate, U_H is the wind speed at the emitting building roof height H.

To compare with Wilson's (1998) experimental results, two building configurations were chosen with three different M-values (M = 1, 2, and 3). The configurations are:

- $H_a = 2H$, $W_a = W$, $\theta = 0°$, $S = 0$, $h_s = 0$, center stack (Stack A);
- $H_a = 2H$, $W_a = W$, $\theta = 0°$, $S = W/3$, $h_s = 0$, upstream center stack (Stack G).

Wilson's respective experimental data are given for the following configurations [Wilson et al. (1998)]:

- $H_a = 2H$, $W_a = W$, $\theta = 0°$, $S = 0$, $h_s = 0.175H$, center stack;
- $H_a = 2H$, $W_a = W$, $\theta = 0°$, $S = H = 0.2W$, $h_s = 0.175H$, upstream center stack.

Figures 5.47 and 5.48 show the data obtained by the two studies. The main differences between the two studies are as follows:

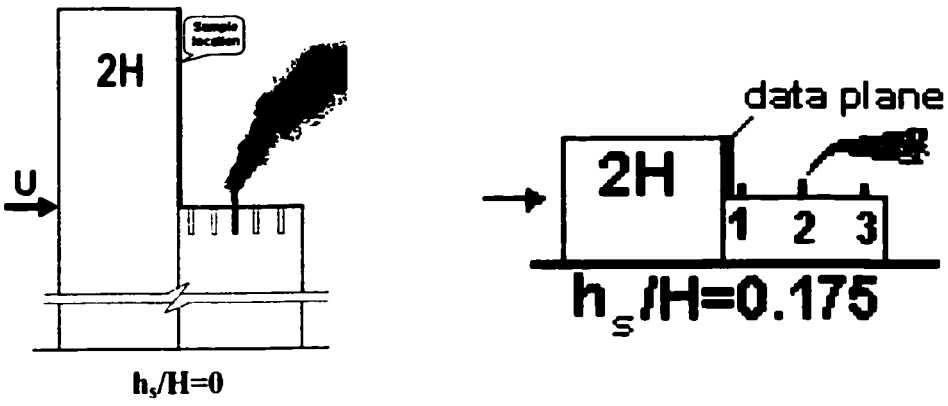

Present study **Wilson et al. (1998) study**

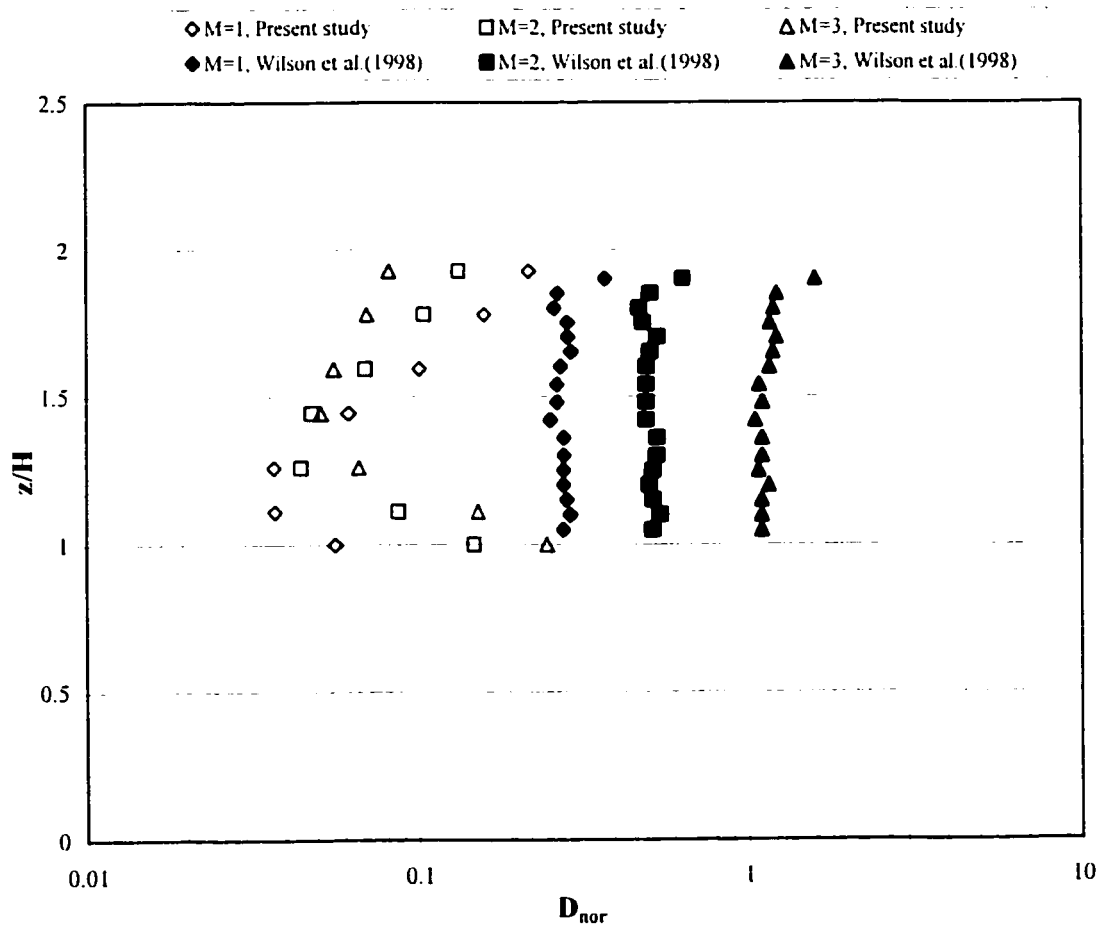

Figure 5.47 Comparison between the present study and Wilson's study, S = 0

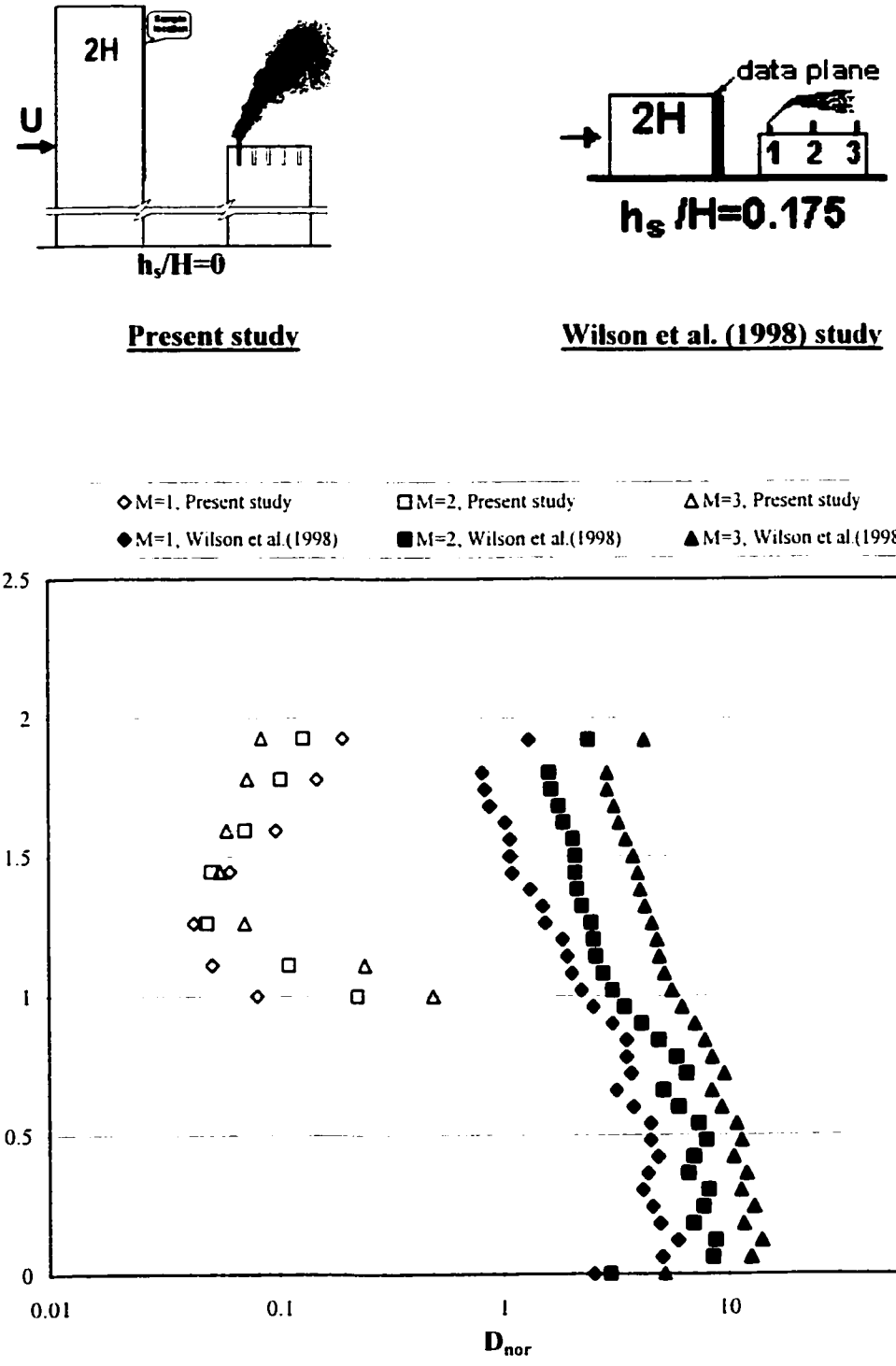

Figure 5.48 Comparison between the present study, S = 0.5W, and Wilson's study, S = 2.5W

- D_{nor} did not vary significantly with height in Wilson's study for a center stack and S = 0. However, D_{nor} varied with height in the present study;

- The magnitude and trends of D_{nor} distribution in Wilson's study depends on gap size. On the other hand, in the present study, the trends were almost the same, and the magnitudes were relatively the same, except at locations near the roof of the emitting building.

It should be noted that Wilson's case, H/W = 0.2, represented a low-rise building, whereas the present study, H/W = 1.8, represents a high-rise building. Another main difference is the stack height, which was 0.175H in Wilson's study and 0 in the present study. Distance from the stack to the upstream adjacent building, x_a, was 2.5W for Wilson's study, and 0.5W for present study. Finally, data obtained by Wilson was from a water channel while the present study used a wind tunnel. All of these factors may have an influence on the results.

Wilson et al. (1998) have developed a model to predict the effect of an adjacent building on dilution values based on their water flume study, as previously discussed in Chapter 2. Wilson et al. (1998) suggested that this model can be applied for building heights ranging from 3m to 49m. In the present study, the emitting building has a full-scale height of 54m, which is close but beyond the upper height limit of Wilson's model. However, the model does not provide results consistent with the findings of the present study.

For the case of a lower downstream emitting building, the normalized dilution on the

adjacent building leeward wall is [Wilson et al. (1998)]:

$$D_{min} = \frac{2D_{emit}D_{adj}}{D_{emit} + D_{adj}} \tag{5.15}$$

where D_{emit} and D_{adj} are the minimum dilutions obtained at the emitting and adjacent building roofs, which are given by,

$$\frac{D_{emit}Q_e}{U_H H^2} = \pi\left(\frac{\sigma_y}{H}\right)\left(\frac{\sigma_{z,wake}}{H}\right)\exp\left(\frac{h_{total}^2}{2\sigma_{z,wake}^2}\right) \tag{5.16}$$

$$\frac{D_{adj}Q_e}{U_H H^2} = \frac{2\pi\left(\frac{\sigma_y}{H}\right)\left(\frac{\sigma_{z,wake}}{H}\right)}{\exp\left[\frac{(\Delta H - h_{total})^2}{2\sigma_{z,wake}^2}\right] + \exp\left[\frac{(\Delta H + h_{total})^2}{2\sigma_{z,wake}^2}\right]} \tag{5.17}$$

where Q_e is exhaust volume flow rate, U_e is the effective plume convection windspeed and is equal to U_H for a rooftop stack which is 4.6m/s in the present study, σ_y is the plume spread in crosswind direction and $\sigma_{z,\,wake}$ is the total vertical plume spread, h_{total} is the effective plume height, z is the distance above the reflecting surface (i.e., emitting building roof), H is the emitting building height which is 0.135m in the present study and $\Delta H = (H_a - H)$ is the height difference between the emitting and adjacent building. See Appendix A for details.

The following three configurations were chosen to compare with the Wilson model for

five different M values (M = 0.5, 1, 2, 3, and 4):

- $H_a = 1.33H$, $W_a = W$, $S = 0$, $\theta = 0°$;
- $H_a = 2H$, $W_a = 2W$, $S = 2W$, $\theta = 0°$; and
- $H_a = 1.67H$, $W_a = W$, $S = 1.1W$, $\theta = 45°$.

Figure 5.49 shows the case for $H_a = 1.33H$, $W_a = W$, $S = 0$, $\theta = 0°$, Stack A (center stack) Generally the minimum normalized dilution at the upstream adjacent building leeward wall is much lower than the model predicted, except for a few cases with high M-values.

Significant change occurred when building configurations changed to $H_a = 2H$, $W_a = 2W$, $S = 2W$, $\theta = 0°$, as shown in Figure 5.50. Minimum normalized dilution at the adjacent building leeward wall is much higher than the model predicted. Similar results were obtained for the third case ($H_a = 1.67H$, $W_a = W$, $S = 1.1W$, $\theta = 45°$), as shown in Figure 5.51. It should be noted in Wilson et al. did not obtain data for $\theta = 45°$ in their study.

The Wilson (1998) model was developed from water flume results obtained with a relatively low-rise building. In Wilson's study, the emitting building has an aspect ratio (H/W) of 0.2 and stack height $h_s/H = 0.175$ to 0.5. In the present study, H/W = 1.8 with a flush stack. The flow structure is consequently very different for the wake cavity, since there is a significant difference in the flow around a high-rise building in comparison to that around a low-rise building. In addition, data obtained from a water flume may differ

from those coming from a wind tunnel. Therefore, this model cannot really be applied in the present study.

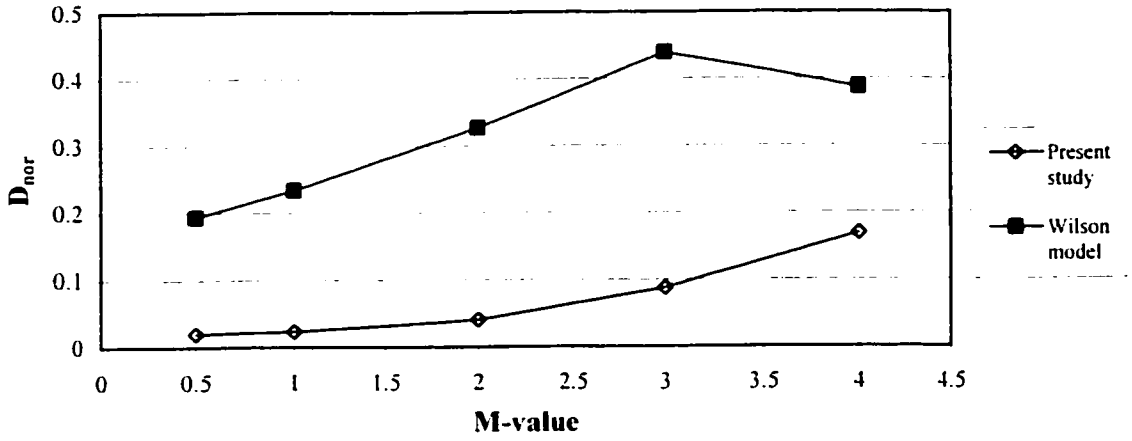

Figure 5.49 Comparison of experimental data to Wilson model for the case of $H_a = 1.33H$, $W_a = W$, $S = 0$, $\theta = 0^o$ (center stack)

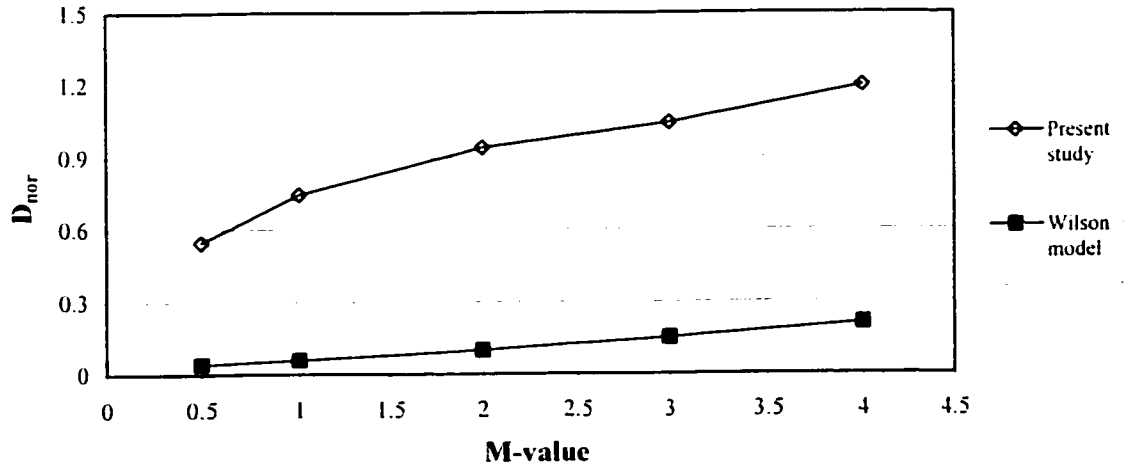

Figure 5.50 Comparison of experimental data to Wilson model for the case of $H_a = 2H$, $W_a = 2W$, $S = 2W$, $\theta = 0^o$ (center stack)

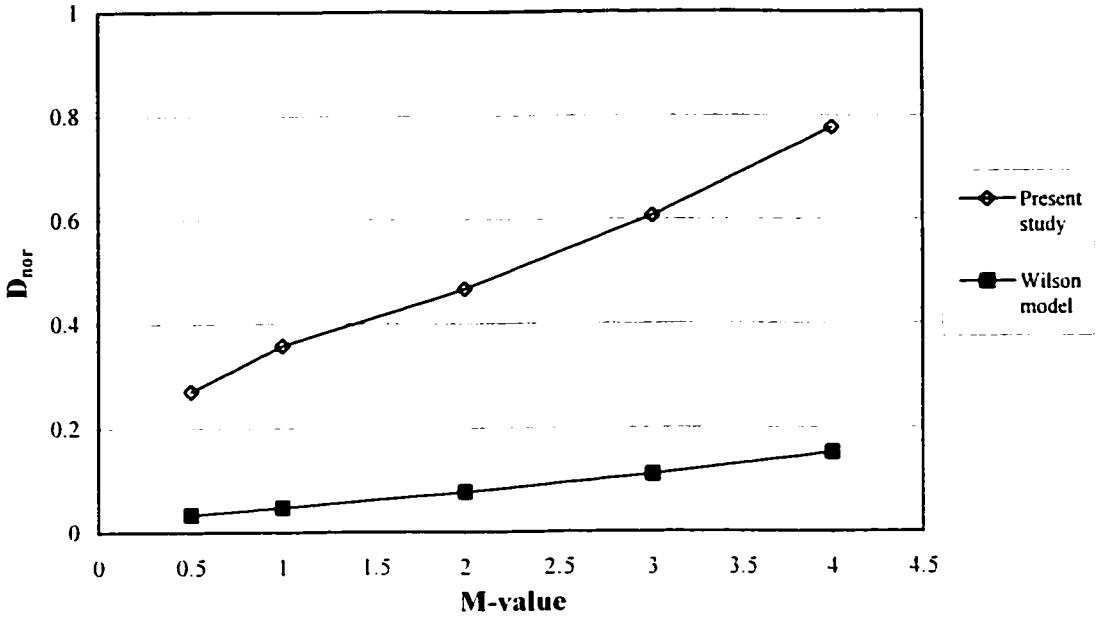

Figure 5.51 Comparison of experimental data to Wilson model for the case of $H_a = 1.67H$, $W_a = W$, $S = 1.1W$, $\theta = 45^{\circ}$

5.12 Comparison with Wilson-Lamb model and ASHRAE critical dilution estimation model

Dilution measurements were compared with predicted values of minimum dilution model developed by Wilson-Lamb (1994) and the ASHRAE (1999) recommended critical dilution estimation model. The minimum dilution model, which has been previously described in Chapter 2, is:

$$D_{min} = \left(D_a^{0.5} + D_d^{0.5}\right)^2 \tag{2.15}$$

where initial dilution D_o and distance dilution D_d can be obtained by

$$D_o = 1 + 13M \tag{2.18}$$

and

$$D_d = B_1 \frac{U_H s^2}{Q_e} \tag{2.17}$$

where M is the exhaust momentum ratio, U_H is the wind speed (4.6m) at emitting building roof, s is the exhaust-to-intake stretched-string distance, as shown in Figure 2.12, and $Q_e = \pi w_e R_s^2$ is the exhaust volume flux, where R_s is the radius of the exhaust stack (0.002m in the present study), and w_e is the exhaust velocity.

For the distance dilution parameter B_1 in Equation (2.17) ASHRAE (1999) recommends that the first term of Equation (2.20) be set at 0.027 for the roof intake and 0.10 for the wall intake. This recommendation applies to hidden wall intakes. In the present study, the receptors were not hidden. Therefore, the default value of B_1 = 0.059 was used. This value of B_1 simulated a moderate turbulence level (σ_0 = 15°) in the approaching flow (not at stack location).

As presented in Chapter 2, the ASHRAE critical dilution estimation model for a flush vent is by finding the absolute minimum dilution in Equations (2.14) to (2.18), the critical wind speed for a flush vent can be given by:

$$U_{crit,o} = \frac{3.6 w_e}{s}\left(\frac{A_e}{B_1}\right)^{0.5} \tag{2.21}$$

The critical dilution at this wind speed and distance, s, is given by: [ASHRAE (2001)]

$$D_{crit,o} = \frac{\left(1 + \frac{26 w_e}{U_{crit,o}}\right)^2}{1 + \frac{13 w_e}{U_{crit,o}}} \tag{2.22}$$

where A_e is the exhaust effective area ($12.57 * 10^{-6} m^2$ in the present study).

Table 5.7 presents the variables used in the present study.

Table 5.7 Variables used in the present study

M-value	D_o	w_e (m/s)	Q_e ($10^{-6} m^3/s$)
0.5	7.5	2.3	28.90
1	14	4.6	57.81
2	27	9.2	115.61
3	40	13.8	173.42
4	53	18.4	231.22

Figures 5.52 and 5.53 represent the comparison results with Wilson-Lamb D_{min} and critical dilution curves for M = 0.5 for different building configurations. As shown in Figure 5.52, neither the Wilson-Lamb minimum dilution model nor the ASHRAE $D_{crit.\,o}$ model provides conservative estimates of dilution on the leeward wall of the upstream adjacent building for the case of separation distance S = 0. However, for the case of S > 0, both models provide realistic predictions. In addition, Wilson-Lamb model provides better estimation. Similar results obtained for M = 1, as shown in Figures 5.54 and 5.55.

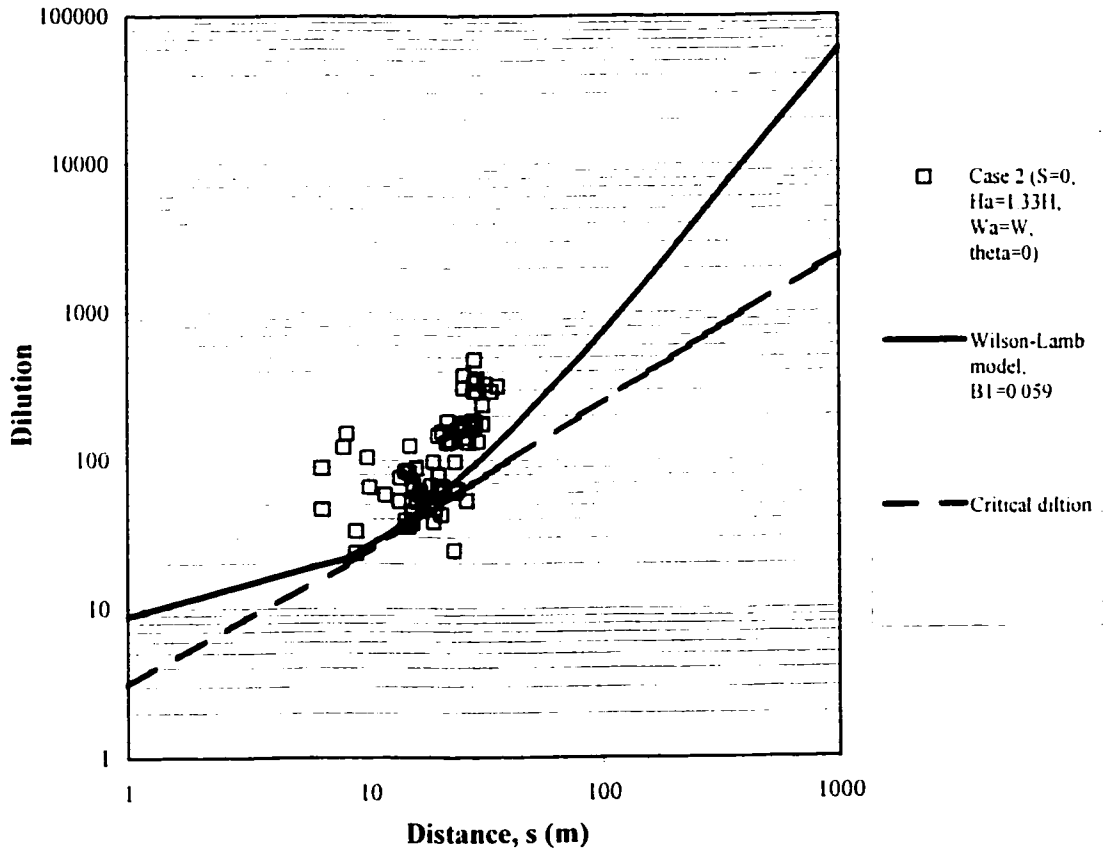

Figure 5.52 Dilution comparison with Wilson-Lamb Model and ASHRAE critical dilution model for M = 0.5, S = 0

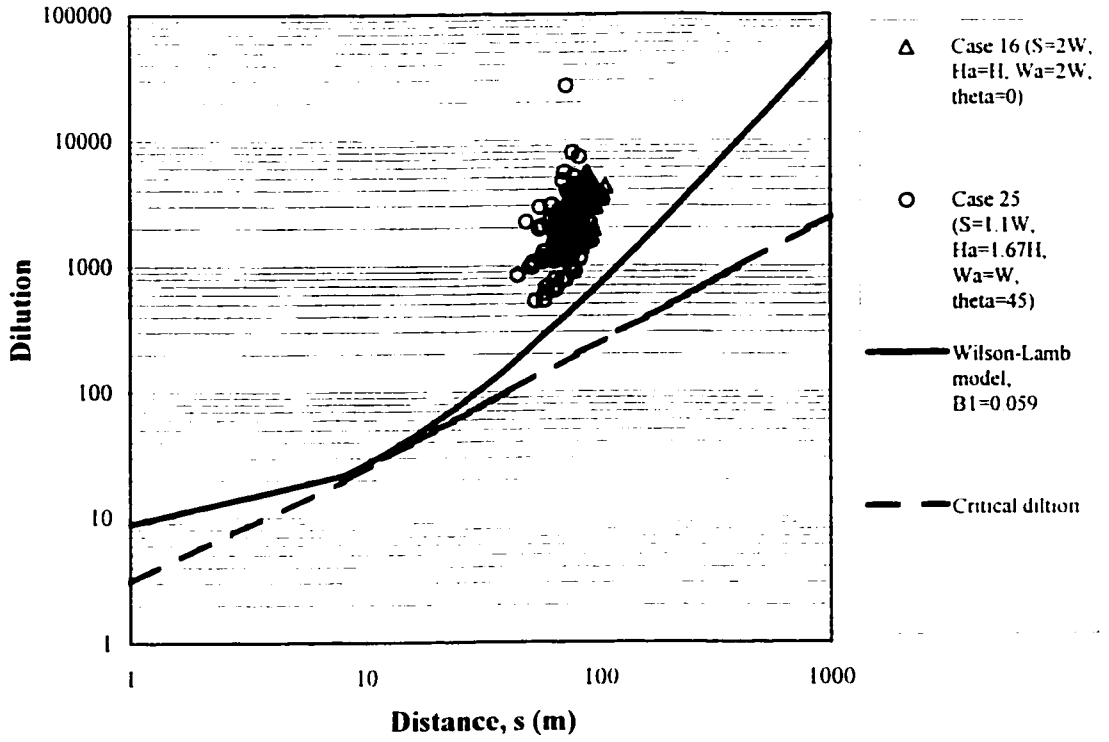

Figure 5.53 Dilution comparison with Wilson-Lamb Model and ASHRAE critical dilution model for M = 0.5, S > 0

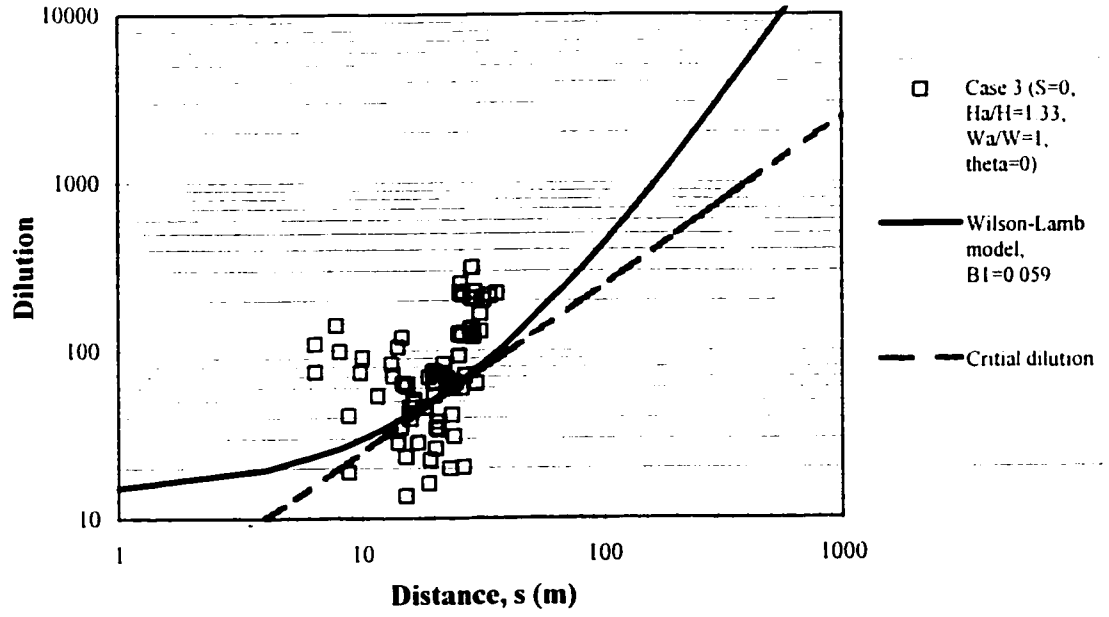

Figure 5.54 Dilution comparison with Wilson-Lamb Model and ASHRAE critical dilution model for M = 1, S = 0

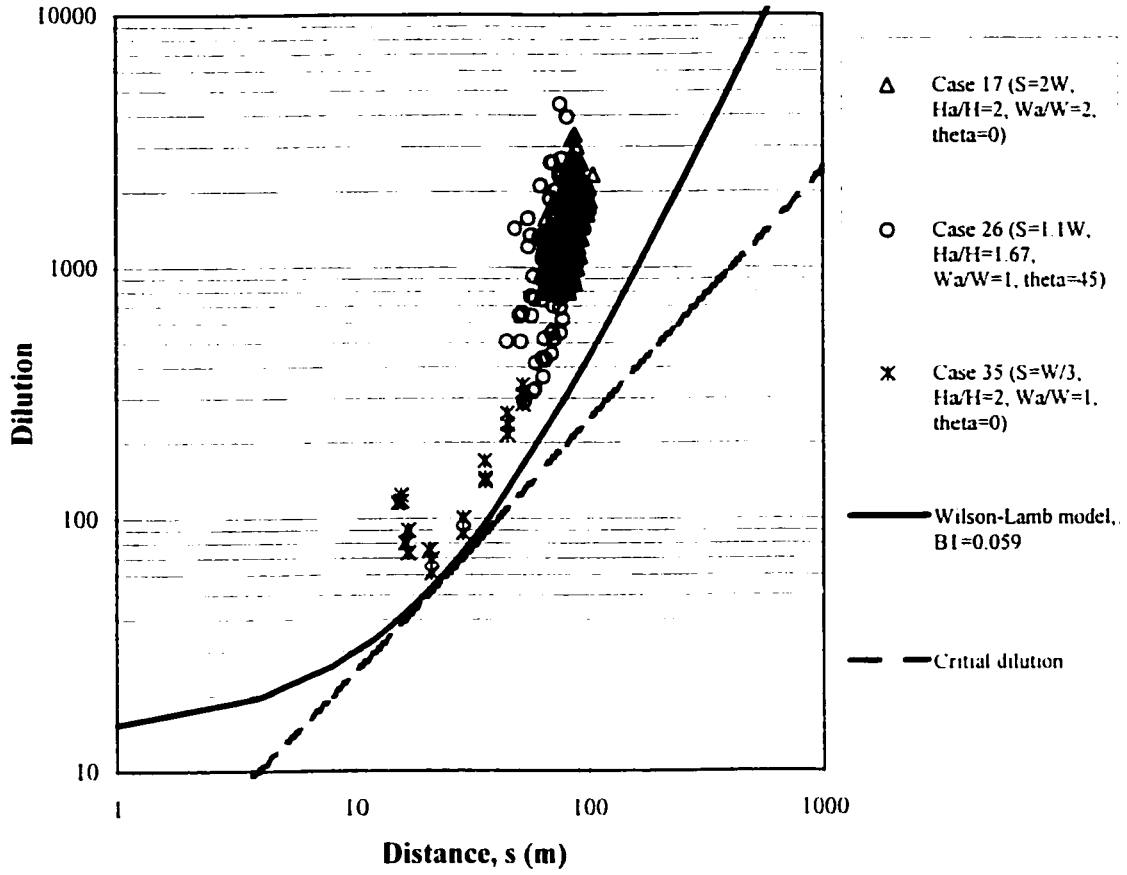

Figure 5.55 Dilution comparison with Wilson-Lamb Model and ASHRAE critical dilution model for M = 1, S > 0

For the case of M = 2, W_a = W, θ = 0°, as shown in Figures 5.56 and 5.57, neither the Wilson-Lamb minimum dilution model nor the ASHRAE $D_{crit,o}$ model provides conservative estimates of dilution on the leeward wall of the upstream adjacent building except for the case of S > 0.75W.

When wind direction changed to θ = 45°, the models provide realistic predictions for all the cases, except few points, as shown in Figures 5.58 and 5.59.

For the case of M = 2, W_a = 2W, S ≥ 0.75W, as shown in Figure 5.60, both the Wilson-Lamb minimum dilution model and the ASHRAE $D_{crit,\ o}$ model provide conservative prediction of dilution on the wall of the upstream taller building.

For high M-value (M = 3, 4), it was found that neither model could be expected to provide conservative estimations of dilution when the two buildings are attached, as presented in Figures 5.61 and 5.63. However, when the separation distance S is greater than 1.06W, the two models provide realistic prediction, as shown in Figures 5.62 and 5.64.

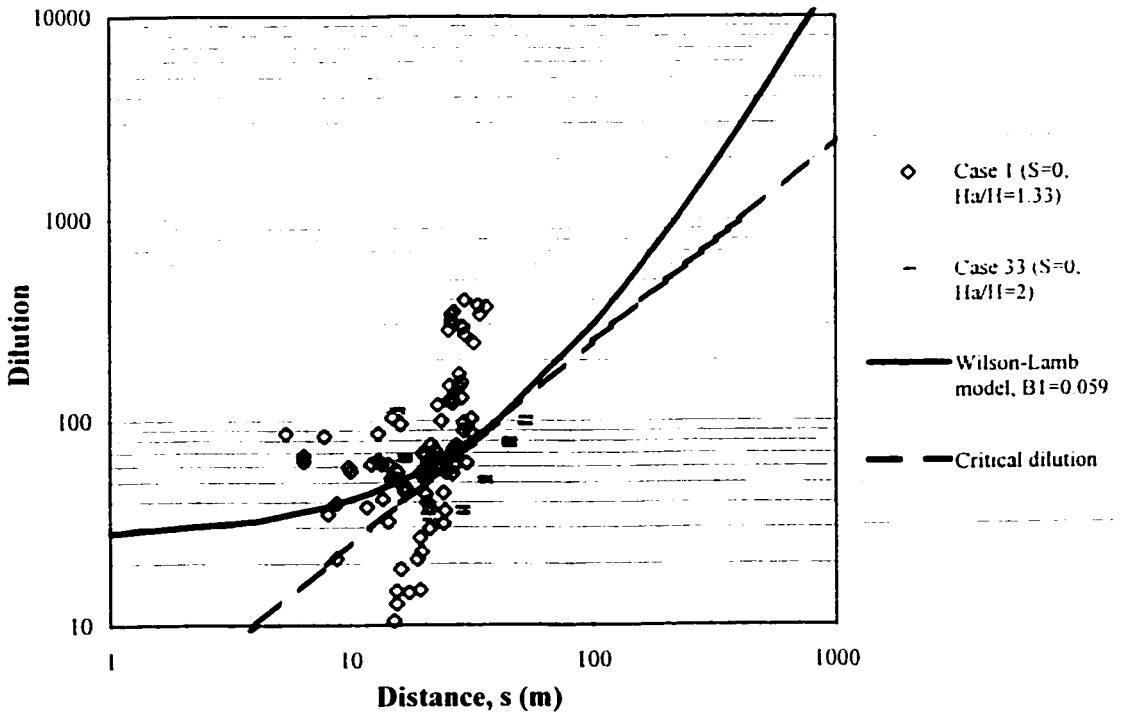

Figure 5.56 Dilution comparison with Wilson-Lamb Model and ASHRAE critical dilution model for W_a = W, M = 2, θ = 0°, S = 0

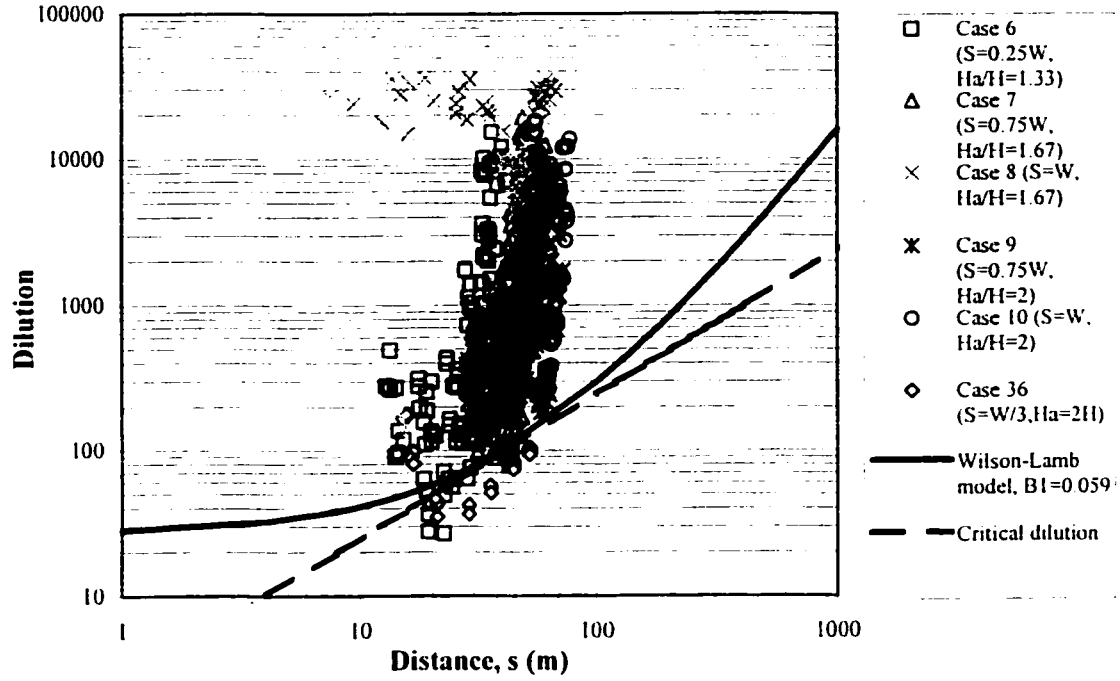

Figure 5.57 Dilution comparison with Wilson-Lamb Model and ASHRAE critical dilution model for $W_a = W$, $M = 2$, $0 = 0°$, $S > 0$

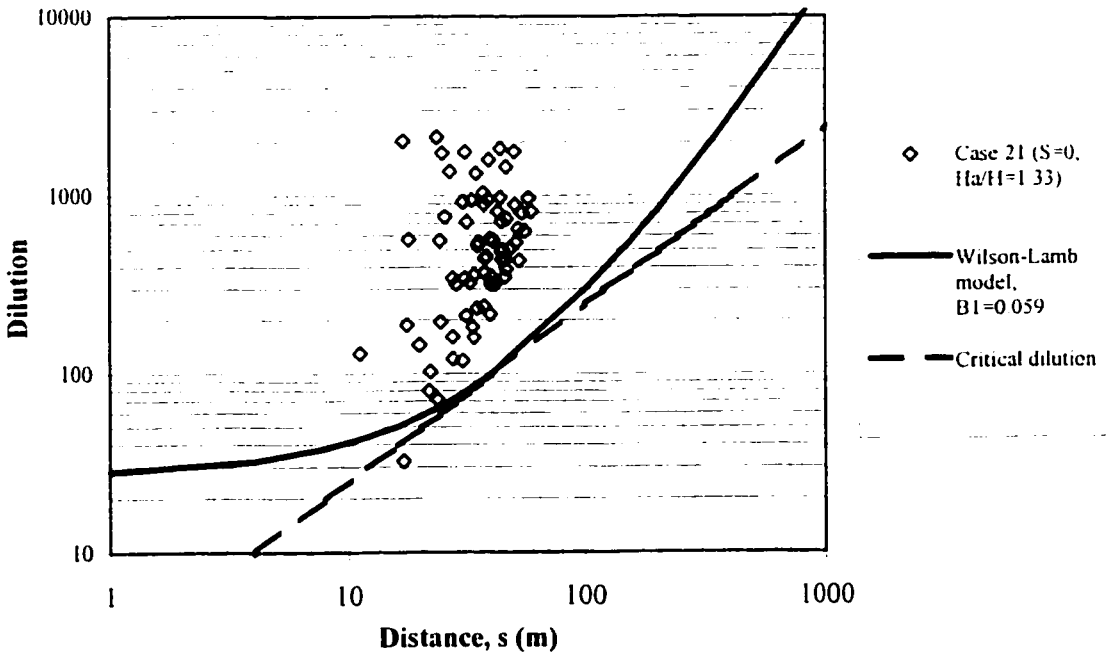

Figure 5.58 Dilution comparison with Wilson-Lamb Model and ASHRAE critical dilution model for $M = 2$, $0 = 45°$, $S = 0$

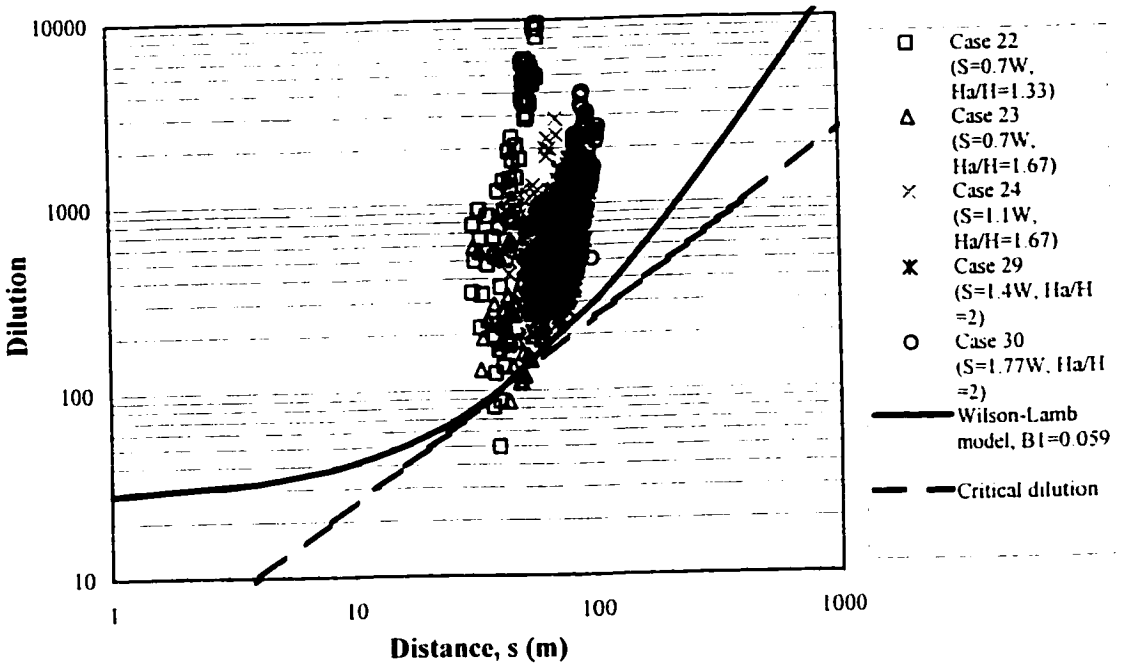

Figure 5.59 Dilution comparison with Wilson-Lamb Model and ASHRAE critical dilution model for M = 2, 0 = 45°, S > 0

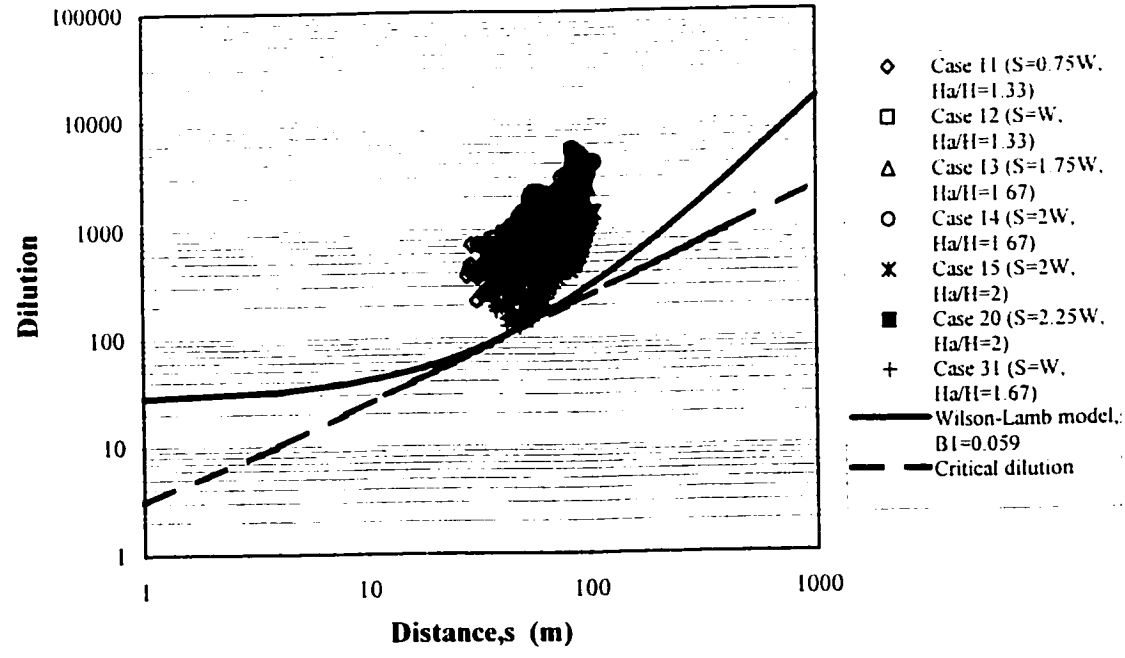

Figure 5.60 Dilution comparison with Wilson-Lamb Model and ASHRAE critical dilution model for W_a =2W, M = 2, 0 = 0° S >0

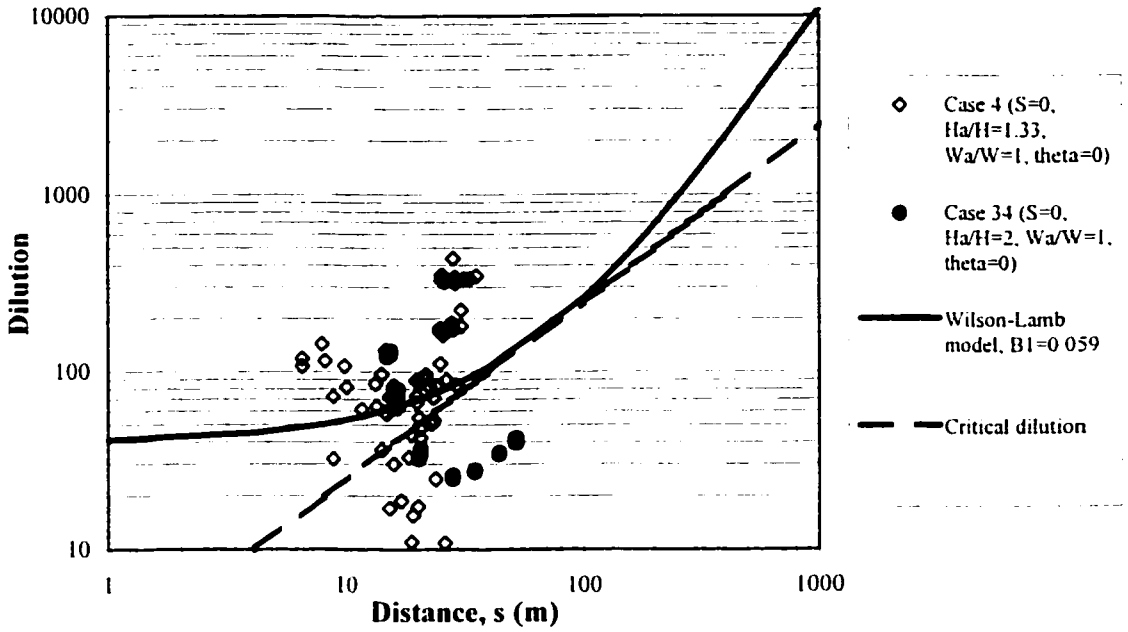

Figure 5.61 Dilution comparison with Wilson-Lamb Model and ASHRAE critical dilution model for M = 3, S = 0

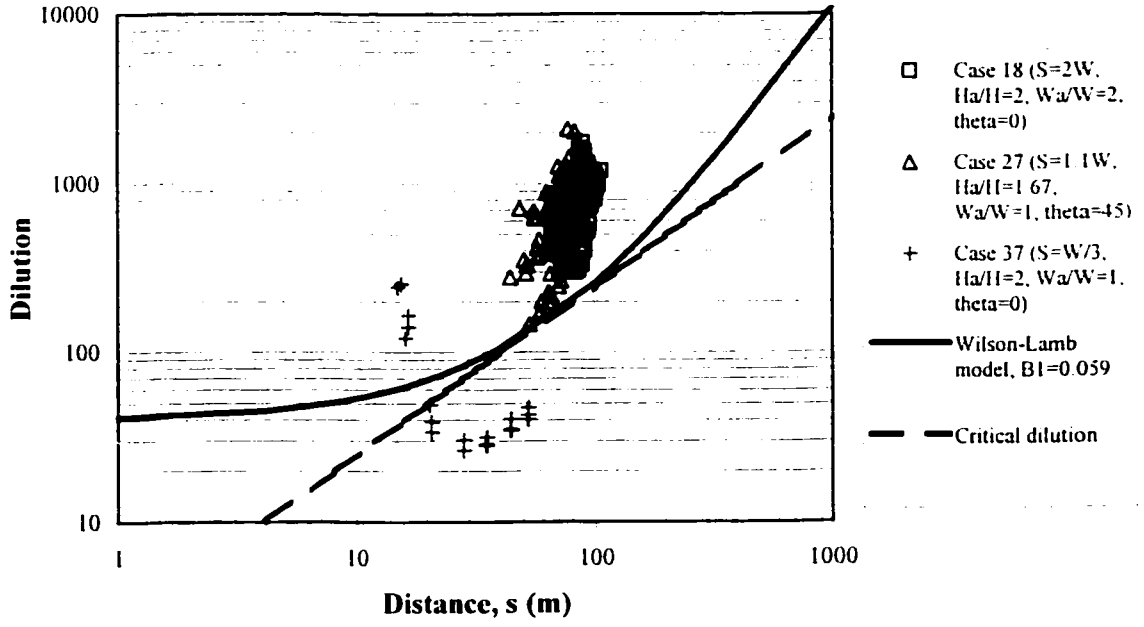

Figure 5.62 Dilution comparison with Wilson-Lamb Model and ASHRAE critical dilution model for M = 3, S > 0

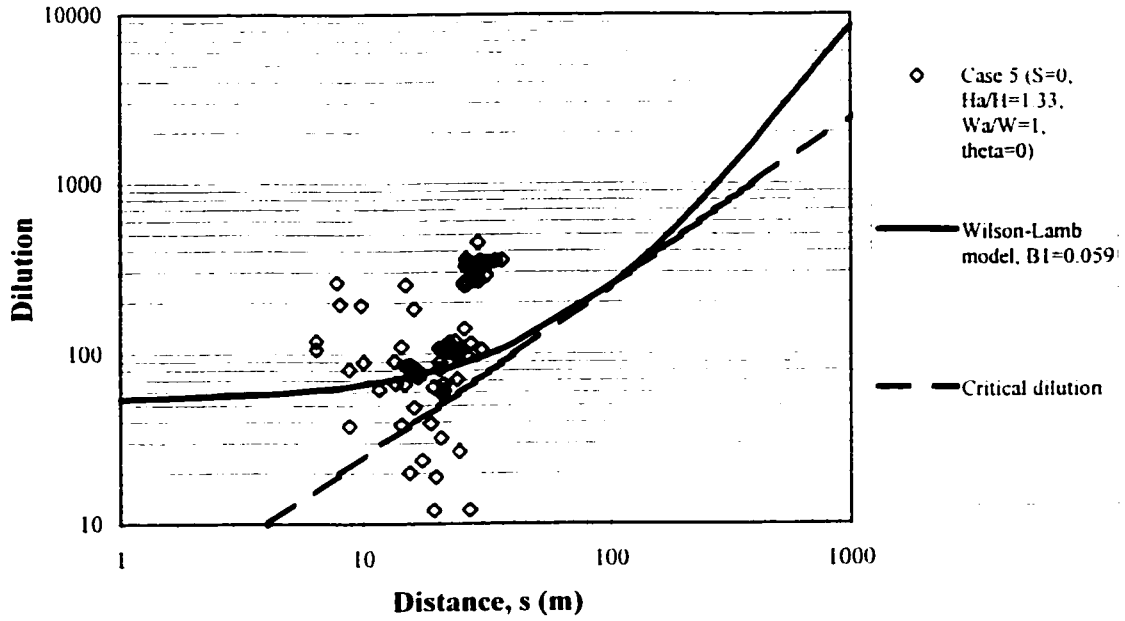

Figure 5.63 Dilution comparison with Wilson-Lamb Model and ASHRAE critical dilution model for M = 4, S = 0

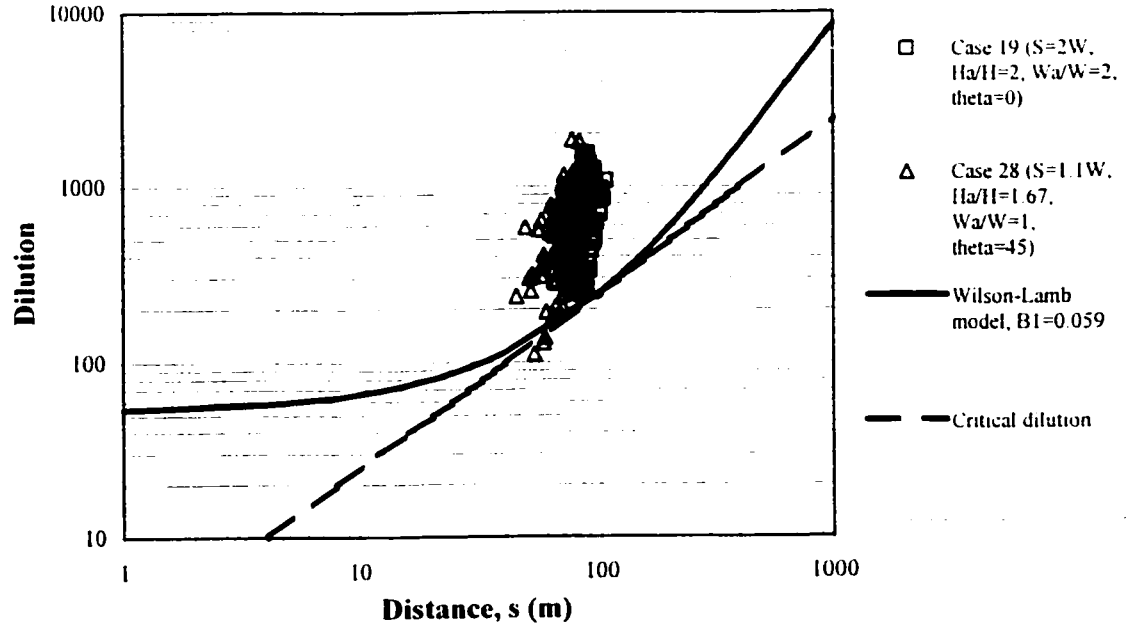

Figure 5.64 Dilution comparison with Wilson-Lamb Model and ASHRAE critical dilution model for M = 4, S > 0

Table 5.8 lists different cases examined in the present study which the ASHRAE models provide good estimations, regardless of adjacent building height.

Table 5.8 List of cases for which the minimum dilution can be estimated by ASHRAE models

M-value	Separation Distance (S)	Adjacent Building Width (W_a)	Wind Direction (0°)
0.5	$\geq$ 1.1W	W, 2W	0, 45
1	$\geq$ W/3	W, 2W	0, 45
2	$\geq$ 0.75W	W	0
2	$\geq$ 0	W	45
2	$\geq$ 0.75W	2W	0
3	$\geq$ 1.06W	W, 2W	0, 45
4	$\geq$ 1.06W	W, 2W	0, 45

CHAPTER 6

CONCLUSION AND SUGGESTIONS FOR FUTURE WORK

6.1 Summary and conclusions

Numerous visualization experiments have been carried out to investigate the critical building configurations consisting of a tall building close to a lower emitting building and the flow patterns in the wake region in a water flume. Results of thirty-seven tracer gas experiments performed in a boundary layer wind tunnel have been analyzed to investigate the dilution distribution on the wall, the effects of stack distance, exhaust momentum ratio, adjacent building height and width, wind direction, stack location and stack height, as well as distance between buildings. Thirteen empirical equations for different particular cases have been derived, based on the experimental data obtained. Dilution data were used to evaluate the accuracy of ASHRAE dilution dispersion models and other minimum dilution models appearing in the literature. The study led to the following conclusions:

1. The results generally showed a good qualitative agreement between water flume visualization experiments and wind tunnel tracer gas experiments. Plume behavior becomes complex and unpredictable in the presence of upstream buildings. Digital image analysis can provide detailed information regarding the behavior of plumes emitted from roof top stacks.

2. Minimum dilution normally occurred at the center top of the upstream building wall for wind direction $\theta = 0°$, and at the downwind corner top for $\theta = 45°$. However, when adjacent building height increases to 2H, D_{min} occurred at about 1.5H to 2/3H height, for either $\theta = 0°$ or $\theta = 45°$.

3. Snyder–Lawson model (1994) provides a good estimation of wake cavity size in most cases; however, Wilson's wake size model (1998) does not give a realistic wake cavity size for some particular cases;

4. The distance between stack and adjacent building played a very important role in dilution values obtained on the upstream taller adjacent building wall. Generally, minimum dilution obtained on the wall is proportional to the logarithm of distance between stack and adjacent building. This phenomenon is independent of wind direction, M-value, stack location, adjacent building height and width, buildings with or without gap.

5. Wind tunnel tests show that the plume behavior is dramatically affected by the exhaust momentum ratio. Dilution values decrease significantly when M changes from 0.5 to 2, but much more slowly for $M > 2$. This phenomenon which is independent of stack location, building separation distance and wind direction appeared in all the building configurations except the case of two buildings without gap for $\theta = 0°$.

6. A taller upstream building gives lower minimum dilution due to the larger

recirculation cavity formed.

7. A wider upstream adjacent building results in a large wake region. Minimum dilution values change by a factor from 3 to about 70 when adjacent building width changes from W to 2W for the case of $H_a = 1.67H$.

8. Wind direction affects dilution distribution significantly. Dilution for $\theta = 45°$ exhibits clearly a different behavior for $\theta = 0°$. However, the minimum dilution obtained for $\theta = 45°$ is lower than that for $\theta = 0°$ assuming the same building configuration.

9. Within the wake cavity formed by a taller adjacent building, different stack locations with the same distance along the wind direction for the adjacent building wall yield similar dilutions.

10. Increasing stack height produces higher wall dilution on the upstream building. Dilution values are generally proportional to the logarithm of distance from stack.

11. Although a gap between the buildings does not affect the minimum dilution, it affects the distribution of dilution on the building wall.

12. Wilson's model (1998) cannot apply since for the case of a building attached to the emitting building, the model provides relatively high D_{min}; and for the

case of building separated, the model provides a low prediction of D_{min}.

13. ASHRAE minimum dilution can be applied for wall dilution distribution within wake zone for wind direction $\theta = 45°$ and some cases for $\theta = 0°$ when the separation distances between the buildings are larger than 0. However, for the cases of M = 2, S < W/3; M = 3, S < W/3; and M = 4, S <W/3, the models do not provide a realistic prediction.

6.2 Suggestions for future work

Based on the work done by the study, some suggestions are made for future work. These can be summarized as follows:

Conduct more experiments to investigate the effect of M-value in more detail, since in the present study there are two kinds of dilution variation with M-value.

More experiments using a number of wind directions and building shapes should be conducted to investigate further the dilution distribution in the wake region.

Conduct a full-scale experiment to evaluate the accuracy of the wind tunnel study and develop a new model to be applied in the wake zone.

Numerical simulation may be developed based on the Computational Fluid Dynamics (CFD) to yield additional results for cases not investigated in the present study.

REFERENCES

Allwine, K., Meroney, R. and Peterka, J. (1980), "Rancho Seco building wake effects on atmospheric diffusion: simulation in a meteorological wind tunnel", NUREG/CR-1286

ASHRAE (2001) Chapter 16, "Airflow Around Buildings", *ASHRAE handbook--2001 fundamentals*, American Society of Heating, Refrigeration, and Air-Conditioning Engineering Inc., Atlanta

ASHRAE (1999) Chapter 43, "Building Air Intake and Exhaust Design", *ASHRAE handbook--1999 applications*, American Society of Heating, Refrigeration, and Air-Conditioning. Engineering Inc., Atlanta

ANSI/ASHRAE 1989 "ANSI/ASHRAE Standard 62-1989, Ventilation for Acceptable Indoor Air Quality," American Society of Heating, Refrigeration, and Air-Conditioning Engineering Inc., Atlanta

Bahnfleth, D. and Govan F. (1987) "Effect of Building Airflow on Reentry and IAQ," *Proceedings of IAQ'87*, ASHRAE, 185-194

Bachlin, W., Theurer, W. and Plate, E.J. (1991), "Wind field and dispersion in a built-up area - a comparison between field measurements and wind tunnel data", *Atmospheric*

Environment, Vol. 25A, No.7, 1135-1142

Biétry, J., Sacré, C., and Simiu, E. (1978), "Mean wind profiles and changes of terrain roughness", *J. Struct. Div.*, ASCE, 104 (Oct. 1978), 1585-1593

Castro, I.P. (1973), "An experimental investigation of the flow around a surface mounted cube in a uniform free stream", Central Electricity Generating Board, Report R/M/N687

Castro, I.P. and Robins, A.G. (1975), "The effect of a thick incident boundary layer on the flow around a small surface mounted cube", Central Electricity Generating Board, Report R/M/N687

Castro, I.P. and Robins, A.G. (1977), "The flow around a surface-mounted cube in uniform and turbulent streams", *Journal of Fluid Mechanics*, Vol. 79, 307-335

Cermak, J.E. (1976), "Nature of air flow around buildings", *ASHARE Transactions*, 82, Part 1, 1044-1060

Counihan, J. (1971), "An experimental investigation of the wake behind a two-dimensional block and behind a cube in a simulated boundary layer flow", Central Electricity research Laboratories, Note No. RD/L/N115/71,C.E.R.L., Leatherhead, Survey, England

Eskridge, R.E. and Thompson, R.S. (1982), "Experimental and theoretical study of the wake of a block-shaped vehicle in a shear-free boundary flow", *Atmospheric Environment* 16, No. 12, 2821-2836

Georgakis, K. et al. (1995) "Review and evaluation of models estimating the minimum atmospheric dilution of gases exhausted near buildings", *Journal of the Air & Waste Management Association*, Vol. 45, 722-729

Guenther, A. et al. (1990) "Three-dimensional numerical simulation of plume downwash with a k-ε turbulence model", *J. of Appl. Met.* 29, 633-643

Halitsky, J. (1961), "Diffusion of vented gas around buildings", New York University, Paper No. 61-35.25p

Halitsky, J. (1963), "Gas diffusion near buildings", *ASHRAE Transactions*, Vol. 69, 464-484

Halitsky, J. (1990), "Calculation of minimum available atmospheric dilution downwind of building exhausts", *ASHRAE Transactions*, Vol. 96, 46-52

Higson, H. L. et al. (1994), "Concentration measurements around an isolated building: a comparison between wind tunnel and field data", *Atmospheric Environment*, Vol. 28, No.11, 1827 –1836

Hosker, R. (1979), "Empirical estimation of wake cavity size behind block-type structures", *Fourth Symposium on Turbulence, Diffusion and Air Pollution*, Jan.15-18, 603-609

Hosker, R. (1980), "Dispersion in the vicinity of buildings", *Research paper*, Air Resources, Atmospheric Turbulence and Diffusion Laboratory, National Ocean and Atmospheric Administration, Oak Ridge, Tenn.

Huber, A.H. and Snyder, W.H. (1982), "Wind tunnel investigation of the effects of a rectangular-shaped building on dispersion of effluents from short adjacent stacks", *Atmospheric Environment*, Vol. 28, No. 12, 2837-2848

Huber, A.H. (1989), "The influnce of building width and orientation on plume dispersion in the wake of a building", *Atmospheric Environment*, 11, 2109-2116

Huber, A.H. et al. (1991), "Preliminary studies of video images of smoke dispersion in the near wake of a model building", *Atmospheric Environment*, 25A, No. 7, 1199-1209

Hunt, J. (1970), "Further aspects of the theory of wake behind buildings and a comparison of the theory with experimental results", *CEGB Lab. Report*, RD/L/R1665

Hunt, J.C.R. (1971), "The effect of single building and structures", *Transactions of the*

Royal Philosophical Society 269, 457-467

Hunt, J.C.R. et al. (1978), "Kinematical studies of the flows around free or surface-mounted obstacles", *Journal of Fluid Mechanics,* Vol. 86, Part 1, 179-200

Kot, S.C. (1989), "Numerical modelling of contaminant dispersion around buildings", *Building and Environment,* Vol. 24, No. 1, 33-37

Kukadia V. and Palmer J. (1996) "Optimum Ventilation and Air Flow Control in Buildings," *proceedings of the 17th AIVC conference*, Gothenburg Sweden, pp. 41-53

Lam, K.S. and Kot, S.C. (1993), "Field study of roof top dispersion in an urban area", *3rd Asia-Pacific Symposium on Wind Engineering*, Dec. 13-15, Hong Kong

Lamb, B. and Cronn, D. (1986), "Fume hood exhaust re-entry into a chemistry building", *Journal of the American Industrial Hygiene Association*, Vol. 47(2), 115-123

Lee, J.T. et al. (1988), "A video image analysis system for concentration measurements and flow visualization in building wakes", *Progress Report*, November, Los Alamos National Laboratory, Los Alamos, USA.

Li, W. and Meroney, R. (1983), "Gas dispersion near a cubical building model", *Journal of Wind Engineering and Industrial Aerodynamics,* 12, 15-23

Martin, J.E. (1965), "The correlation of wind tunnel and field measurements of gas

diffusion using Krypton-85 as a tracer", University of Michigan, Phoenix Project, 272, Ann Arbor

Meroney, R.N. (1982), "Turbulent diffusion near buildings", *Engineering Meteorology*, Elsevier, Amsterdam

Meroney, R.N. and Yang, B.T. (1982), "Gaseous plume diffusion about isolated structure of simple geometry", 2nd. *International Air Pollution Conf. Proceedings*, Dec. 6-11

Munn, R.E. and Cole, A.F. W. (1967), "Turbulence and diffusion in the wake of a building", *Atmospheric Environment*, Part 1, 33-43

Murakami, S. and Mochida, A. (1983), "3-D numerical simulation of airflow around a cubic model by means of the k-ε model", *Journal of Wind Engineering and Industry Aerodynamics*, 31, 283-303

Ogawa, Y. and Oikawa, S. (1982), "Afield investigation of the flow and diffusion around a model cube", *Atmospheric Environment*, 16, No. 2, 207-222

Ogawa, Y. et al. (1983), "Field and wind tunnel study of the flow and diffusion around a model cube, I: Flow measurements", *Atmospheric Environment*, 17, No.6, 1145-1159

Ogawa, Y. et al. (1983), "Field and wind tunnel study of the flow and diffusion around a model cube, --II: Near-field and cube surface flow and concentration patterns",

Atmospheric Environment, 17, No. 6, 1161-1171

Olivari, D. and Babuska, V. (1990), "Use of video camera recording and digital image processing for the analysis of pollutant dispersion in the near wake of a cube", *Journal of Wind Engineering and Industrial Aerodynamics,* 34 (1990) 291-301

Pasquill F. (1962), "Atmospheric Diffusion, The Dispersion of Windburn Material from Industrial and Other Sources", D. Van Nostrand Company, Ltd., London, England

Paterson, D. and Alpelt, C. (1986), "Computation of wind flows over three-dimensional buildings", *Journal of Wind Engineering and Industrial Aerodynamics,* 24, 192-213

Perera, M.D. et al. (1991), "Assessing Intake contamination from atmospheric dispersion of building exhaust", *Proceedings of the 12th AIVC Conference,* Ottawa, 347-357

Petersen, R.L. (1986), "Wind tunnel investigation on the effect of platform-type structures on dispersion of effluents from short stacks", *Journal of the Air Pollution Control Association,* 36, 1347-1352

Petersen, R.L. and Ratcliff, M.A. (1991), "An objective approach to laboratory stack design", *ASHRAE Transactions,* Vol. 97, No.2

Ramsdell Jr., J.V. and Fosmire, C.J. (1997), "Estimating concentrations in plumes released in the vicinity of buildings: model development", *Atmospheric Environment,*

32, 1663-1689

Robins, A.G. and Castro, I.P. (1977), "A wind tunnel investigation of plume dispersion in the vicinity of a surface mounted cube", *Atmospheric Environment,* 11, 291-311

Rock, B. and Moylan, K. (1999), "Placement of ventilation air intakes for improved IAQ", *ASHRAE Transactions,* 105(1), 71-79

Saathoff P. and Melbourne W. (1997), "Effects of free-stream turbulence on surface pressure fluctuations in a separation bubble", *Journal of Fluid Mechanics,* Vol. 337, 1-24

Saathoff, P. and Stathopoulos, T. (1997), "Dispersion of exhaust gases from roof level stacks and vents on a laboratory building—Discussion", *Atmospheric Environment,* 31, 1087-1089

Saathoff, P., Wu, H. and Stathopoulos, T. (1996), "Dilution of exhaust from rooftop stacks --Comparison of wind tunnel data with full-scale measurements", *Proceedings of 9th Joint Conference on Applications of Air Pollution Meteorology,* Amer. Meteorological Soc. -- Air & Waste Management Assoc., Atlanta 341-345

Seinfeld, J. (1975), "Air Pollution, Physical and Chemical Fundamentals", McGraw-Hill, Inc., New York, United States

Selvam, R. and Huber, A. (1995), "Computer modelling of pollutant dispersion around buildings: current status", *Proceedings of the 9th International Conference on Wind Engineering*, New Delhi, India, 594-605

Simu, E. and Scanlan, R.H. (1996), "Wind effects on structures – fundamentals and applications to design", third edition, John Wiley & Sons, Inc, (1996), New York

Slawson, P.R. and Hitchman, G.J. (1987), "Plant air quality following accidental radioactive releases: Literature survey and model tests on recirculation and interface for two in line cubes", *Supply and Service Canada Report*, DSS File No. 52ss-87035-6-4082

Snyder, W.H. and Lawson, R.E. (1994), "Wind-tunnel measurements of flow fields in the vicinity of buildings", *8th Joint Conference on Applications of Air Pollution Meteorology (AMS/AWMA)*, Nashville, TN, Jan. 23-28, 1994, pp.244-250

Start, G. et al. (1977), "Rancho Seco building wake effects on atmospheric diffusion", *NOAA Tech. Memo*. ERL ARL-69

Stathopoulos, T., Lazure, L. and Saathoff, P. (1999), "Tracer Gas Investigation of Reingestion of Building Exhaust in an Urban Environment," Institut de recherche en santé et en sécurité du travail du Québec, Montréal, Canada

Thompson, R. (1991), "Concentrations from above-roof releases of laboratory exhausts -

a wind tunnel study", *ASHRAE Transactions*, Vol. 97, Part 2

Turner, D. (1994), "Workbook of Atmospheric Dispersion Estimates", 2nd Ed., CRC Press

Vincent, J.H. (1977), "Model experiments on the nature of air pollution transport near buildings", *Atmospheric Environment*, 11, 765-774

Vincent, J.H. (1978), "Scalar transport in the near aerodynamic wakes of surface-mounted cubes", *Atmospheric Environment*, 12, 1319-1322

Wilson, D.J. (1976), "Contamination of air intakes from roof exhaust vents", *ASHRAE Transactions*, 82(1), 1024-1038

Wilson, D.J. (1979), "Flow patterns over flat-roofed buildings and application to exhaust stack design", *ASHRAE Transactions*, 85(2), 284-295

Wilson, D.J. (1983), "A design procedure for estimating air intake contamination from nearby exhaust vents", *ASHRAE Transactions*, Vol. 88, Part 2

Wilson, D.J. (1995), "Concentration Fluctuations and Averaging Time in Vapor Clouds", Center for Chemical Process Safety of the American Institute of Chemical Engineers, New York, United States

Wilson, D.J. (1997), "Dispersion of exhaust gases from roof level stacks and vents on a

laboratory building - Author's Reply", *Atmospheric Environment*, 31, 1091-1093

Wilson, D.J. et al. (1998), "Adjacent building effects on laboratory fume hood exhaust stack design", *Final Report of ASHRAE RP-897*, February

Wilson, D.J. and Britter, R.E. (1982), "Estimates of building surface concentrations from nearby sources", *Atmospheric Environment*, 16, No. 11, 2631-2646

Wilson, D.J. and Chui, E. (1985), "Influence of exhaust velocity and wind incidence angle on dilution from roof vents", *ASHRAE Transactions*, 91(2B) 1693-1706

Wilson, D.J. and Chui, E. (1987), "Effect of Turbulence from Upwind Buildings on Dilution of Exhaust Gases", *ASHRAE Transactions*, 93(2), 2186-2197

Wilson, D.J. and Chui, E. (1994), "Influence of building size on rooftop dispersion of exhaust gas", *Atmospheric Environment*, 28, 3099-3111

Wilson, D.J. and Lamb, B. (1994), "Dispersion of exhaust gases from roof level stacks and vents on a laboratory building", *Atmospheric Environment*, 28, 2325-2334

Wilson, D.J. and Winkel, G. (1982), "The effect of varying exhaust stack height on contaminant concentration at roof level", *ASHRAE Transactions*, Vol. 88, Part 1

Wu, G. et al. (1991), "Application of digital image processing in wind engineering", 8^{th} *International Conference on Wind Engineering*, London, Ontario.

APPENDIX A

DISPERSION MODEL FOR THE BACKWALL DILUTIONS WITH LOWER EMITTING BUILDING DOWNWIND

A.1 Normalized dilution functions

Considering a continuous source with exhaust volume concentration C_e and exhaust volume flow rate Q_e, the concentration C at any location (x, y, z) is given by,

$$C(x,y,z;h) = \frac{C_e Q_e}{2\pi U_c \sigma_y \sigma_z} \exp\left[-\frac{y^2}{2\sigma_y^2}\right]\left\{\exp\left[-\frac{(h-z)^2}{2\sigma_z^2}\right] + \exp\left[-\frac{(h+z)^2}{2\sigma_z^2}\right]\right\} \qquad (A.1)$$

where U_c is the effective plume convection wind speed, h is the effective plume height, and σ_y and σ_z are plume spreads in crosswind and vertical directions, respectively.

The maximum concentration C_r on the plume centerline (y = 0) at the level of the reflecting surface is the primary interest for exhaust stack design and environmental impact studies. ASHRAE (1997) noted that the mass reflecting surface z = 0 is the roof level of the emitting building.

The dilution factor D is defined as the ratio of pollutant concentration in the exhaust gas (C_e) to the pollutant concentration at any receptor (C), D = Ce/C. In order to use the

measurement results for stack design, the measured dilutions are normalized in a form that allows them be adjusted to a variety of full scale wind conditions, and varying ratios of exhaust velocity to wind speed. Considering roof level concentration for Gaussian concentration profile for a plume dispersing in homogeneous turbulence over a roof, with reflection at building roof level, this roof centerline concentration C_r at z = 0 is, [Panofsky and Dutton (1984)]

$$C_r = \frac{C_e Q_e}{\pi U_c \sigma_y \sigma_z} \exp\left(\frac{-(h_s + \Delta h)^2}{2\sigma_z^2}\right) \tag{A.2}$$

where h_s is the stack height above the reflecting surface, Δh is the plume rise.

For a building roof top stack, $U_c = U_H$, independent of stack height and plume rise. Defining the emitting building roof level minimum dilution as $D_{min} = C_e/C_r$, Equation (A.2) can be rearranged to a normalized form,

$$\frac{D_{min} Q_e}{U_H H^2} = \pi \frac{\sigma_y}{H} \frac{\sigma_z}{H} \left(\frac{U_c}{U_H}\right) \exp\left(\frac{h^2}{2\sigma_z^2}\right) \tag{A.3}$$

A.2 Recirculation cavity dimensions

The dimensions of the building roof level cavity are, from ASHRAE (2001),

$$L_c = 0.9\ R \tag{A.4}$$

$$X_c = 0.5R \tag{A.5}$$

$$H_c = 0.22R \tag{A.6}$$

The height-difference scaling length R based on increase or decrease in height ΔH of the roof level at the upwind edge where the cavity forms,

$$R = \Delta H^{2/3} Y^{1/3} \qquad \text{for } \Delta H \leq Y \tag{A.7}$$

$$R = \Delta H^{1/3} Y^{2/3} \qquad \text{for } \Delta H > Y \tag{A.8}$$

where Y is the crosswind width of the upwind wall of the building where the roof edge cavity forms. The height change ΔH for the upwind building is just the roof height above ground. For a downwind building,

$$\Delta H = | H_a - H | \tag{A.9}$$

Note that a roof edge recirculation cavity will only form on the edge of a downwind building is higher than the upwind one.

A.3 Effective plume height h

The effective plume height h above the reflecting surface (z = 0, i.e., roof) is

$$h = h_s + \Delta h \tag{A.10}$$

where h_s is the stack height above the roof, Δh is the plume rise by jet momentum Δh_m or exhaust gas buoyancy above the top of the stack Δh_b, and stack tip downwash Δh_d, which are given by [Briggs (1975)] ,

$$\Delta h = \left(\Delta h_m^3 + \Delta h_b^3\right)^{1/3} - \Delta h_d \qquad \text{(A.11)}$$

For case of no plume buoyancy, Equation (A.11) becomes

$$\Delta h = \Delta h_m - \Delta h_d \qquad \text{(A.12)}$$

where Δh_m is a function of the final momentum rise height, $\Delta h_{m,f}$, and plume final rise distance, $x_{m,f}$:

$$\Delta h_m = \Delta h_{m,f}\left(\frac{x}{x_{m,f}}\right)^{1/3} \qquad \text{for } x < x_{m,f} \qquad \text{(A.13)}$$

and

$$\Delta h_m = \Delta h_{m,f} \qquad \text{for } x \geq x_{m,f} \qquad \text{(A.14)}$$

From Briggs (1975), the final momentum rise height $\Delta h_{m,f}$ is,

$$\Delta h_{m,f} = B_3 M d_s \qquad \text{(A.15)}$$

where the final momentum rise constant of $B_3 = 3.0$ [Briggs (1975)] based on a survey of experimental data, d_s is the stack diameter, and M is defined as the density-weighted ratio of exhaust velocity w_e at density ρ_e to stack-height wind speed U_s at air density ρ_a,

$$M = \left(\frac{\rho_e}{\rho_a}\right)^{0.5} \frac{w_e}{U_s} \tag{A.16}$$

Assuming $\rho_e = \rho_a$, $U_s = U_H$, Equation (A.16) becomes,

$$M = \frac{w_e}{U_H} \tag{A.17}$$

Following Briggs (1975), the distance $x_{m.f}$ to the point of final momentum rise is,

$$x_{m.f} = \left(\frac{4\beta^2 B_3^3}{3}\right) M d_s \tag{A.18}$$

where $\beta = 0.6$ is the internal self-generated turbulent entrainment constant, which is independent of x, but may be dependent on M [ASHRAE (2001)].

The stack tip downwash is given by,

$$\Delta h_d = A_1 (3.0 - M) d_s \tag{A.19}$$

with $A_1 = 1.0$ for $M \leq 3.0$ and $A_1 = 0$ for $M > 3.0$.

A.4 Model adjustments

The plume model gradually undergoes a transition to the undisturbed roof level dispersion limit for a stack far downwind of the recirculation cavity. It was accomplished by making the following adjustments:

- Shifting the virtual origin of the plume trajectory back to the wall location of the upwind adjacent building if the plume lies inside the wake cavity trapping zone. Otherwise, the plume trajectory origin remains above the stack.

- Adding an initial source size $\Delta\sigma_{o,wake}$ at the trajectory origin (or virtual origin) to account for the extra initial dilution caused by the wake.

- Adding an increase in vertical plume spread $\Delta\sigma_{z,wake}$ to account for increased turbulence in the wake of the upwind building.

- Shifting the plume trajectory origin downward by a building wake downwash Δz_{wake} to account for the downward deflection of streamlines in the wake.

- Making $\Delta\sigma_{o,wake}$ $\Delta\sigma_{z,wake}$ and Δz_{wake} dependent on distance from the stack to the adjacent building wall, to account for the gradual decrease in cavity wake effect with downwind distance.

- No change in the product $\sigma_y U_c$ so that increased crosswind spread is cancelled

by a decrease in convection velocity when calculating plume centerline dilution, so σ_y and U_c for the undisturbed crosswind dispersion σ_y can be found to predict centerline dilution.

The proposed method treats the wake as continuous, with no specific boundary between the trapped recirculating flow and downwind diffusion with no recirculation. The recirculation cavity and the wake cavity trapping zone influence only the virtual origin, and not the increase in initial source size $\Delta\sigma_{o,wake}$ or the added vertical spread Δz_{wake}.

A.5 Conditions identification

There are two situations for the case with an emitting building downwind of a higher adjacent building, one is plumes fully trapped inside the wake recirculation cavity formed by the adjacent building, and the other is plumes that are able to fully escape the cavity. For dilutions on the back wall of the higher adjacent building, only case one is considered, because if most of the stack exhaust escape the recirculation cavity, there will be no significant concentration on the wall.

Thus, the first step is to determine if the plume can or cannot escape the cavity (i.e., is it necessary to shift the virtual origin to the position of the upwind adjacent building).

By examining dilution measurements, an upwind shift of the virtual origin should be made if the final rise height trajectory origin fell roughly within,

$$x_a < L_{cavity} \tag{A.20}$$

$$h < 0.75\, L_{cavity} \tag{A.21}$$

where the length of the recirculation cavity is

$$L_{cavity} = 2.0R \tag{A.22}$$

where R is height-difference scaling length given by Equations (A.7) and (A.8), and x_a is the distance from the stack to the wall of the adjacent building. Then, if the plume is moved back to the adjacent building, the distance x is measured from this virtual origin and not from the stack location.

A.6 Dilution on the adjacent building backwall

The dilution D at any distance z above the reflecting surface is given by

$$\frac{DQ_e}{U_H H^2} = 2\pi\left(\frac{\sigma_y}{H}\right)\left(\frac{\sigma_{z,wake}}{H}\right)\left[\exp\left(-\frac{(z-h_{total})^2}{2\sigma_{z,wake}^2}\right)+\exp\left(-\frac{(z+h_{total})^2}{2\sigma_{z,wake}^2}\right)\right]^{-1} \tag{A.23}$$

where Q_e is exhaust volume flow rate, U_H is wind speed at the emitting building height H, σ_y is plume spread in crosswind direction, $\sigma_{z,wake}$ is the total vertical spread, h_{total} is the effective plume height.

The model assumed constant dilution with height, so the minimum dilution over the

entire wall is,

$$D_{min} = \frac{2D_{emit}D_{adj}}{D_{emit} + D_{adj}} \tag{A.24}$$

where D_{emit} and D_{adj} are the dilutions obtained at the emitting and adjacent building roofs, which are given by, from Equation (A.23),

$$\frac{D_{emit}Q_c}{U_H H^2} = \pi\left(\frac{\sigma_y}{H}\right)\left(\frac{\sigma_{z,wake}}{H}\right)\exp\left(\frac{h_{total}^2}{2\sigma_{z,wake}^2}\right) \tag{A.25}$$

and

$$\frac{D_{adj}Q_c}{U_H H^2} = \frac{2\pi\left(\frac{\sigma_y}{H}\right)\left(\frac{\sigma_{z,wake}}{H}\right)}{\exp\left(\frac{(\Delta H - h_{total})^2}{2\sigma_{z,wake}^2}\right) + \exp\left(\frac{(\Delta H + h_{total})^2}{2\sigma_{z,wake}^2}\right)} \tag{A.26}$$

where ΔH is the height difference between the emitting and adjacent buildings.

Plume spread in crosswind direction σ_y is given by,

$$\sigma_y = Ay^*x + \sigma_o + \Delta\sigma_{o,wake} \tag{A.27}$$

where σ_o and $\Delta\sigma_{o,wake}$ are added initial dilution spreads.

The total vertical spread used in Equation (A.23) is defined as,

$$\sigma_{z,wake} = \sigma_o + \Delta\sigma_{o,wake} + \Delta\sigma_{z,wake} \tag{A.28}$$

Including an initial source size $B_o d_s$ in the limit of zero exhaust velocity (i.e., M = 0), the effective initial plume spread σ_o can be calculated as,

$$\sigma_o = \left[\frac{M}{8} + \frac{\beta_{eff}^2}{2}\left(\frac{\Delta h}{d_s}\right)^2 + B_o^2\right]^{0.5} d_s \tag{A.29}$$

where d_s is the stack diameter, $\beta_{eff} = 0.6$ is the effective entrainment constant, the same as β [Briggs (1975), ASHRAE (1997)].

The added initial dilution spreads $\Delta\sigma_{o,wake}$ and $\Delta\sigma_{z,wake}$ are functions of the x_a from the stack location to the upwind adjacent building,

$$\Delta\sigma_{o,wake} = \frac{B_8 R}{1 + 4.0\left(\frac{x_a}{L_{cavity}}\right)^3} \tag{A.30}$$

$$\Delta\sigma_{z,wake} = \frac{B_5 R}{\left(1 + B_6 \frac{|z_{impact}|}{R}\right)\left(1 + 4.0\left(\frac{x_a}{L_{cavity}}\right)^3\right)} \tag{A.31}$$

where the impact distance z_{impact} is the height of the plume trajectory above or below the

roof edge, before any adjustments for trajectory upwash or downwash,

$$z_{impact} = H + h - H_a \tag{A.32}$$

where H and H_a are the heights of the emitting and adjacent buildings, h is the height of the plume above the emitting building roof, see Equation (A.10). The empirical constants for all the $\Delta\sigma_z$, equations are, $B_5 = 0.4$, $B_6 = 1.0$, and $B_8 = 0.2$, respectively.

There is no distance dependence of plume spread $\Delta\sigma_{z,wake}$ since it is always evaluated at the virtual origin of the plume. With undisturbed plume rise h, the effective plume height is,

$$h_{total} = h - \Delta z_{wake} \tag{A.33}$$

The downwash of the plume trajectory can found as,

$$\Delta z_{wake} = \frac{0.2R\left(1 - \frac{|z_{impact}|}{\Delta H}\right)}{1 + 4.0\left(\frac{x_a}{L_{cavity}}\right)^3} \tag{A.34}$$

with $\Delta z_{wake} = 0$, for $|z_{impact}| > \Delta H$.

APPENDIX B

CALIBRATION OF THE GAS CHROMATOGRAPH (GC)

A calibration curve showing sulfur hexafluoride (SF_6) concentration as a function of the GC reading is shown in Figures B.1 to B4. A wide range of SF_6 concentration was obtained by mixing a flow of a certified SF_6-N_2 mixture with air. Since the volume of mixed air was controlled by a syringe, the concentration of the gas mixture could be calculated. A series of different concentration gases were measured.

During the study period, there were several technical problems including replacement of a valve in the GC. Different SF_6 concentration mixtures (from 1ppm to 100ppm) were used to meet the different dilution ranges. Re-calibration was carried several times and the GC readings were plotted with the corresponding actual concentration values for different dates, as shown in Figures B.1 to B.4.

The accuracy of the calibration curve was generally within 3%, although in some high concentration values the error reached 12.5%. Table B.1 shows the accuracy for the date of February 20, 2002.

The repeatability experiments were carried out for each calibration curve. Generally, the experiments are repeatable. Table B.2 shows the data obtained on April 1 and April 2, 2002, and their percentage difference.

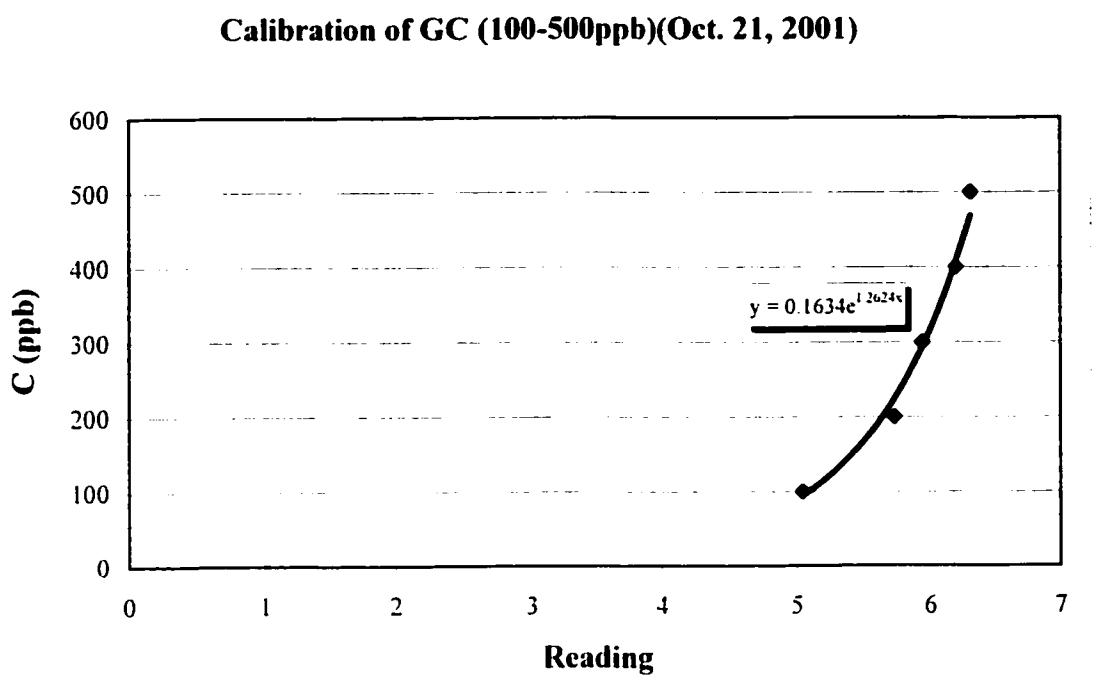

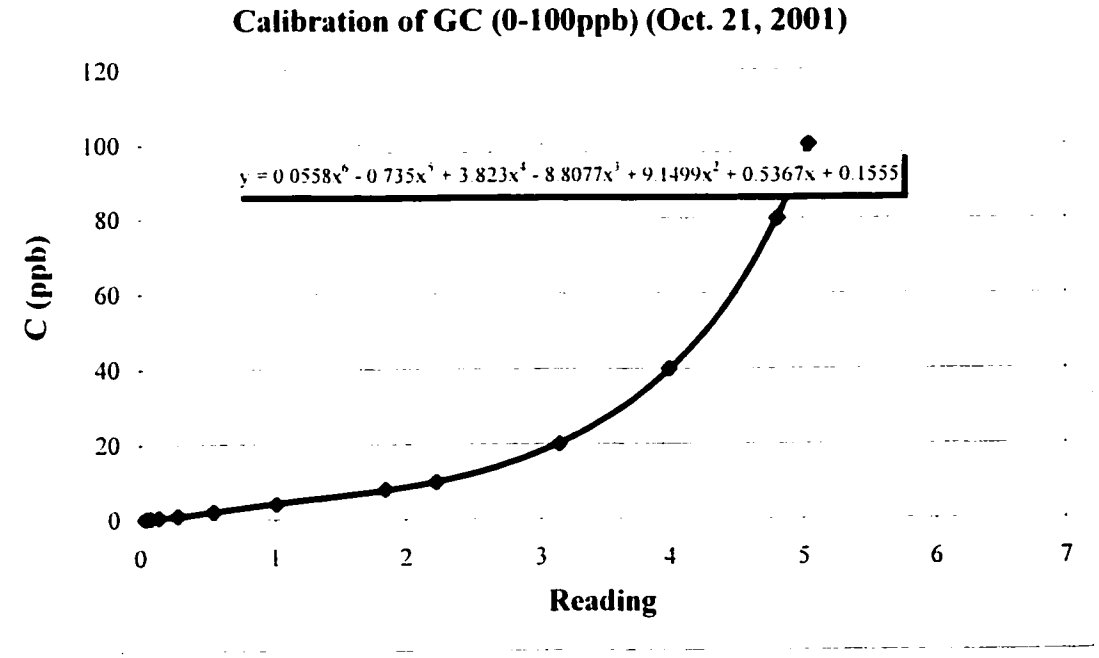

Figure B.1 GC Calibration curves of October, 21, 2001

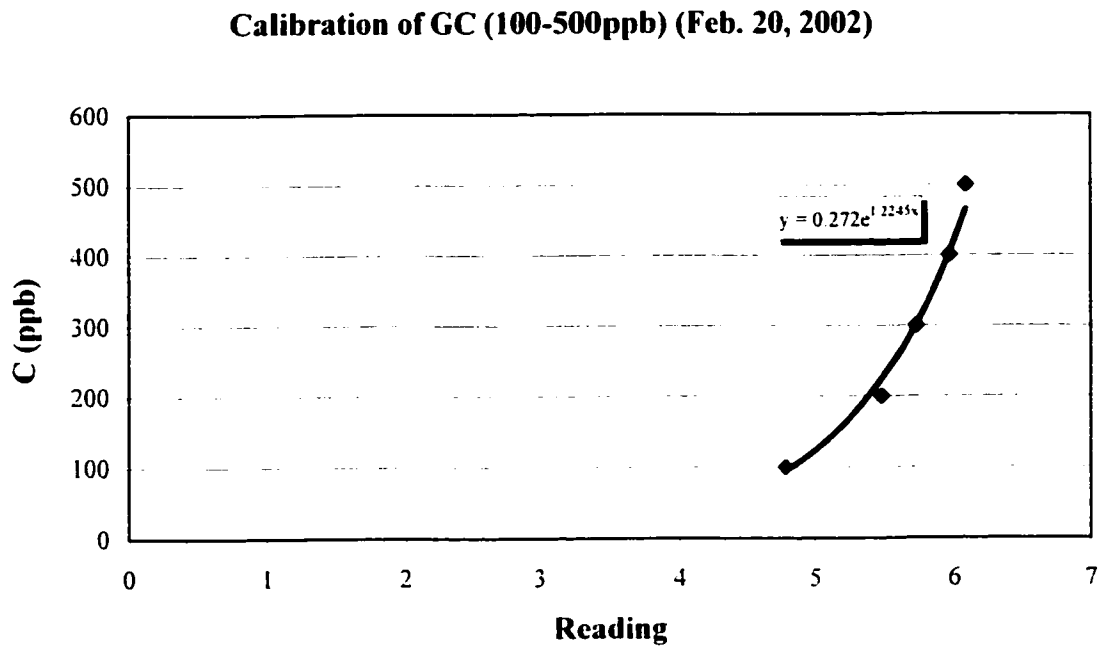

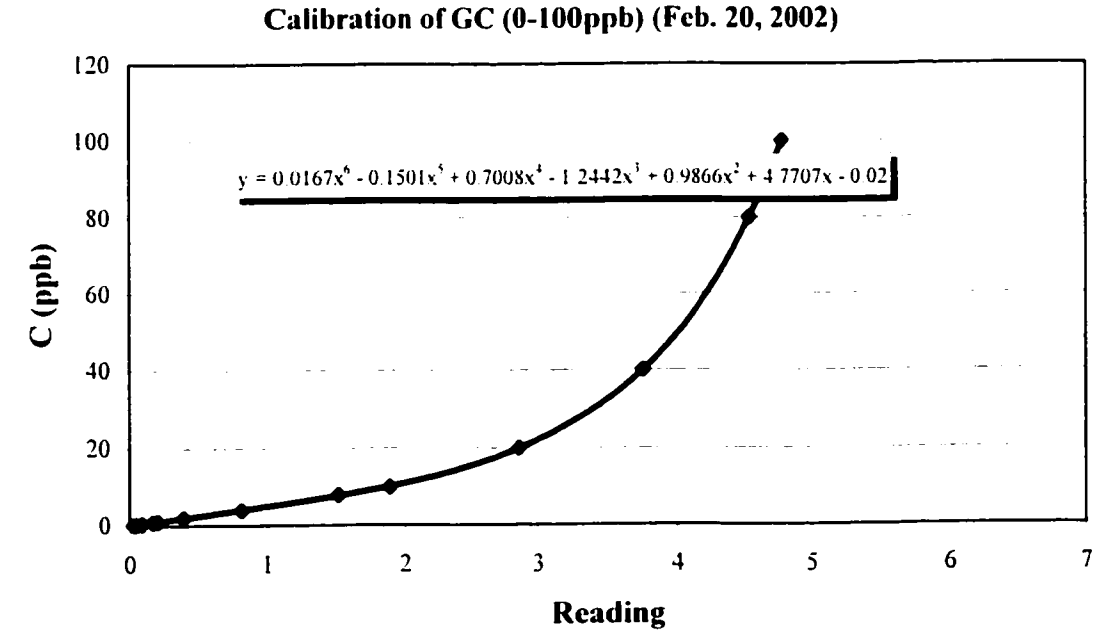

Figure B.2 GC Calibration curves of February 20, 2002

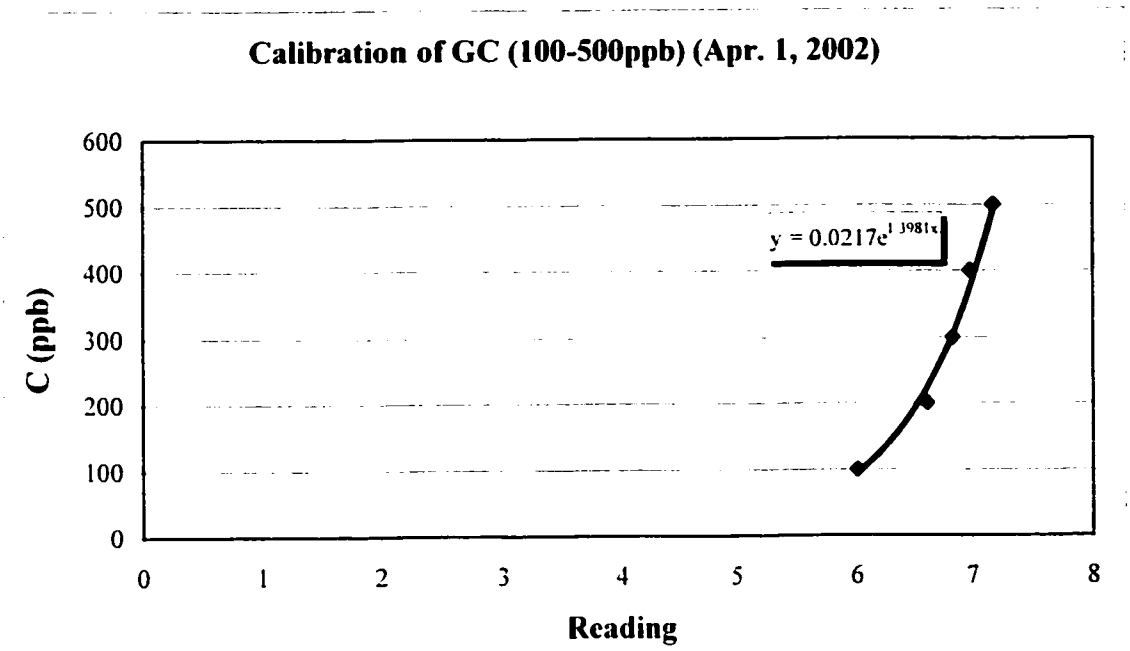

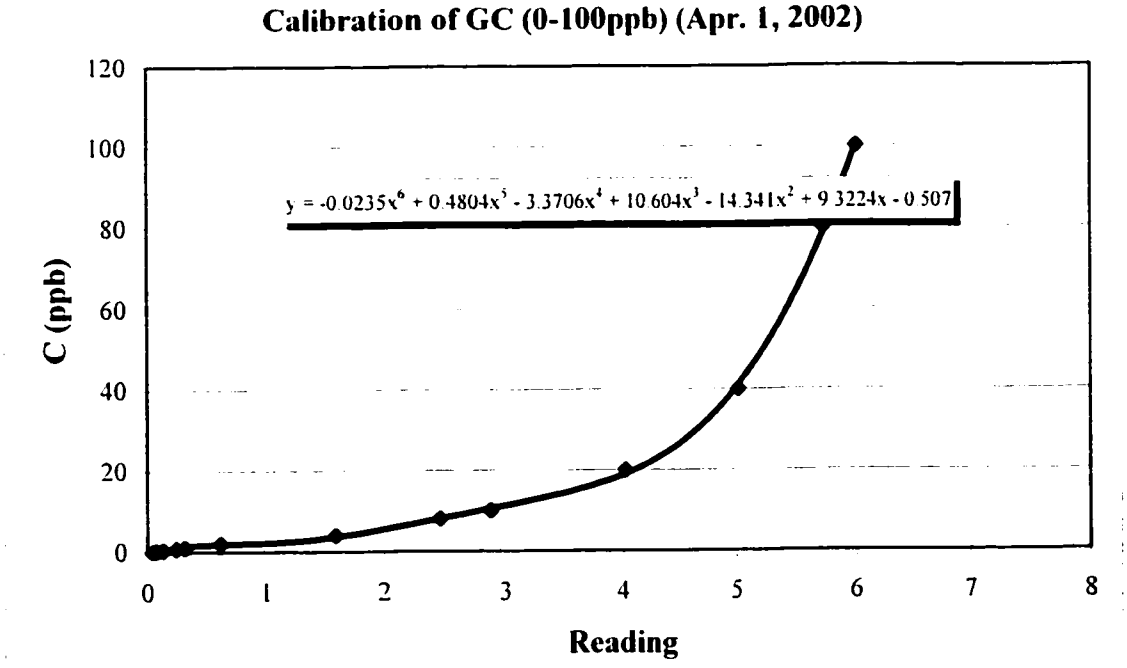

Figure B.3 GC Calibration curves of April 1, 2002

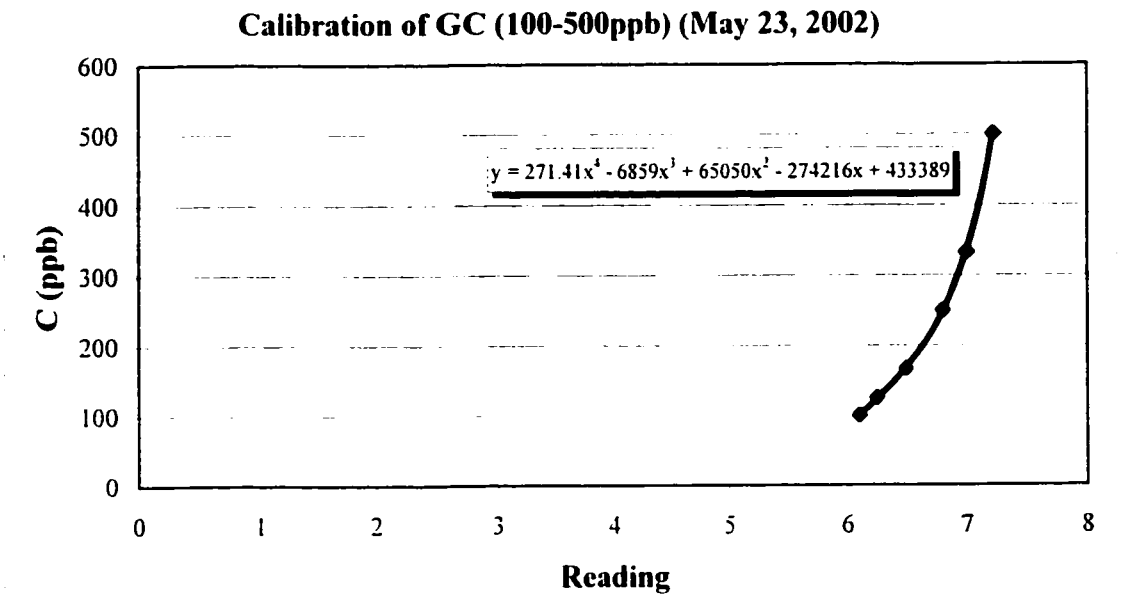

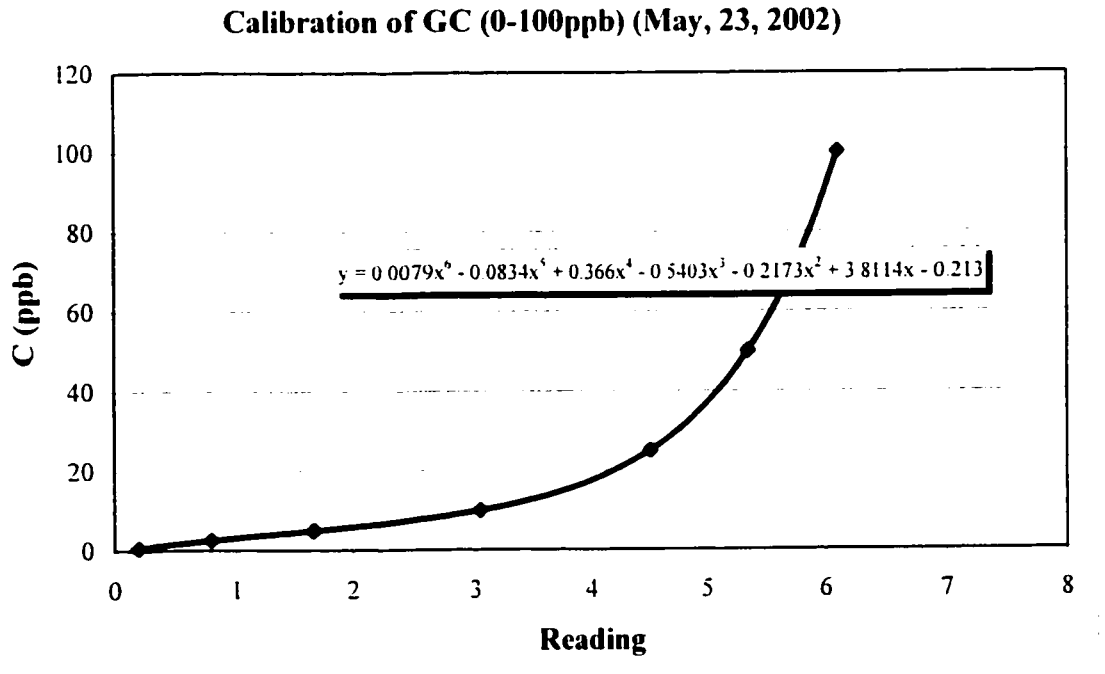

Figure B.4 GC Calibration curves of May 23, 2002

Table B.1 Accuracy of the calibration equation

Concentration (ppb)	Reading	Concentration retake by equation	Accuracy (%)
500	6.080	465.486	-6.90
400	5.963	403.495	0.874
300	5.723	300.457	0.152
200	5.483	224.151	12.08
100	4.780	99.934	-0.07
80	4.539	79.921	-0.10
40	3.755	40.010	0.03
20	2.863	19.935	-0.32
10	1.887	10.181	1.86
8	1.506	7.791	-2.62
4	0.815	4.109	2.73
2	0.395	1.958	-2.11
1	0.203	0.981	-1.97
0.8	0.165	0.789	-1.39
0.4	0.090	0.415	3.86
0.2	0.048	0.211	5.41
0.1	0.026	0.103	2.81

Table B.2 Repeatability of the calibration for the date of April 1st and 2nd, 2002

Date	Apr. 01, 02	Apr. 02, 02	
Concentration (ppb)	Reading	Reading	Difference (%)
500	7.175	7.185	0.14
400	6.980	7.047	0.95
300	6.832	6.970	1.98
200	6.613	6.870	3.75
100	6.001	5.992	-0.15
80	5.725	5.705	-0.36
40	5.018	4.973	-0.89
20	4.022	4.020	-0.05
10	2.877	2.962	2.88
8	2.454	2.362	-3.88
4	1.598	1.487	-7.44
2	0.616	0.584	-5.47
1	0.311	0.294	-5.52
0.8	0.237	0.218	-8.79
0.4	0.130	0.110	-18.10
0.2	0.073	0.070	-5.40
0.1	0.039	0.038	-4.00

APPENDIX C

DETAILED RESULTS OF THE WATER FLUME VISUALIZATION STUDY

Totally eighteen (18) building configurations with four (4) different exhaust momentum M-values, namely 0.5, 1, 2, 3, for two different models, square-shaped Model A and rectangular-shaped Model B, were tested in the water flume study to verify the general flow patterns for two wind directions ($\theta = 0°$ and $\theta = 45°$). Figures C.1 to C.18 present the detailed images acquired for the cases described in Figures 3.7 and 3.8.

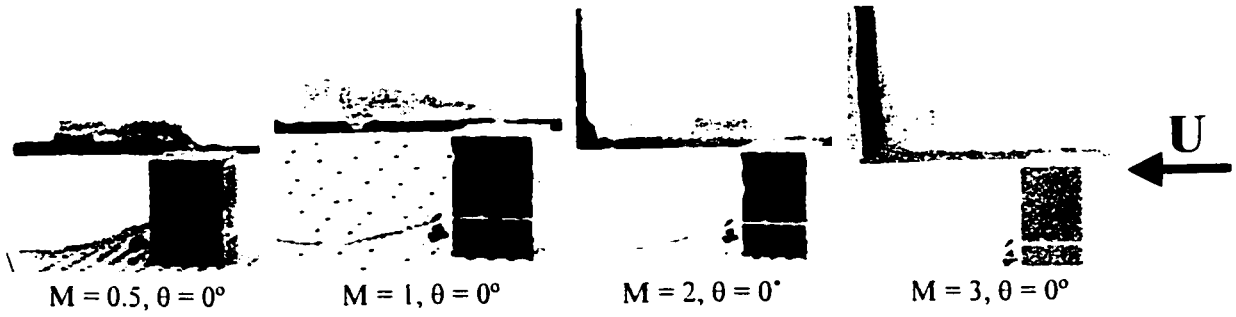

Figure C.1 Isolated building (Case I, Model A)

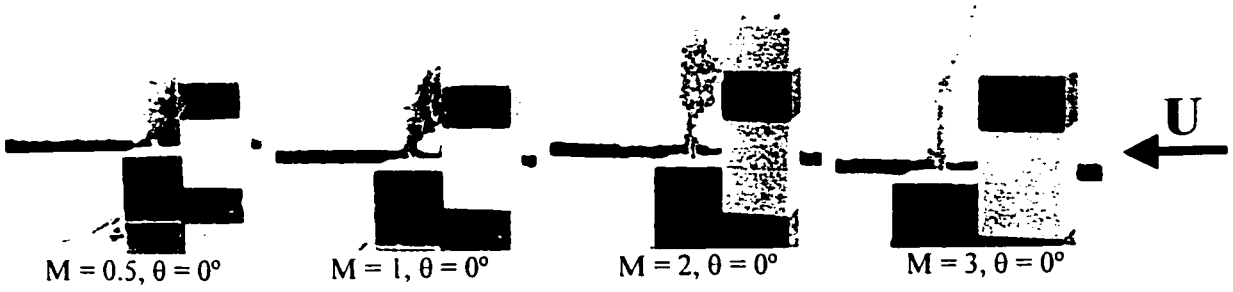

Figure C.2 With contacted tall building upwind (Case II, Model A)

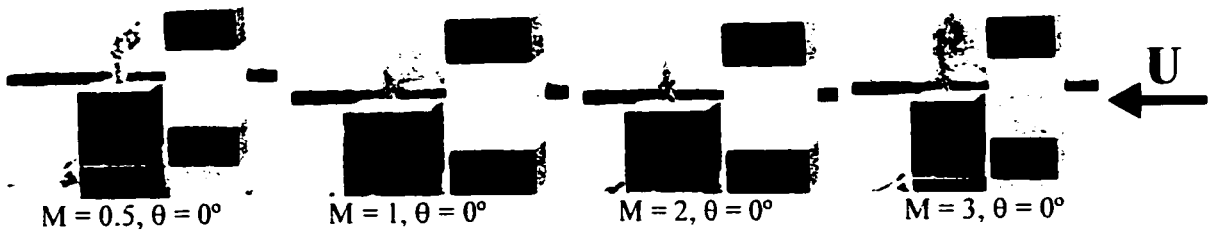

Figure C.3 With tall building upwind (Case III, Model A)

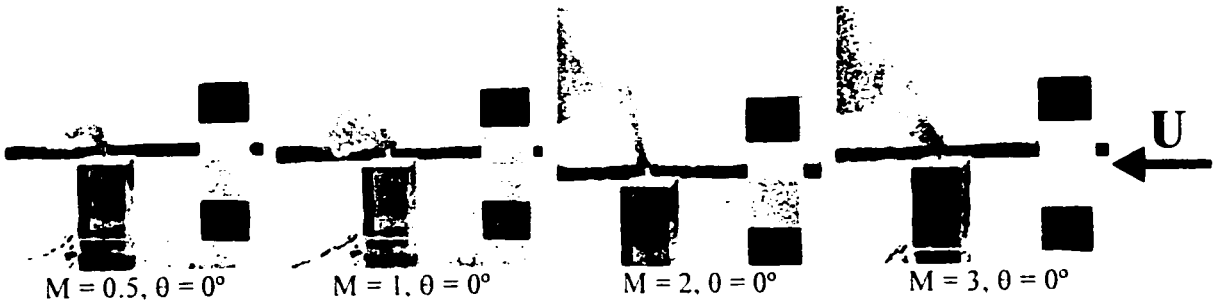

Figure C.4 With tall building upwind far from emitting building (Case IV, Model A)

Figure C.5 With same height building downwind (Case V, Model A)

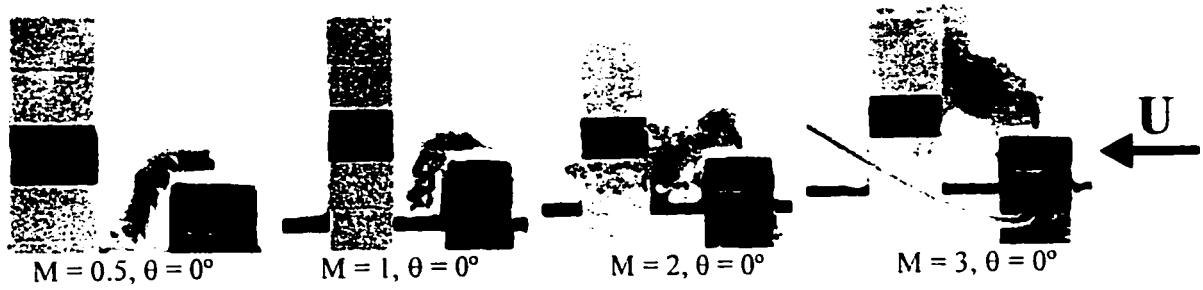

Figure C.6 With high building downwind (Case VI, Model A)

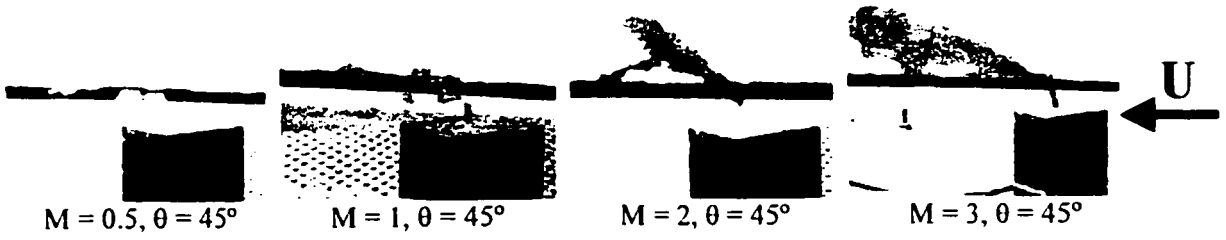

Figure C.7 Isolated building (Case VII, Model A)

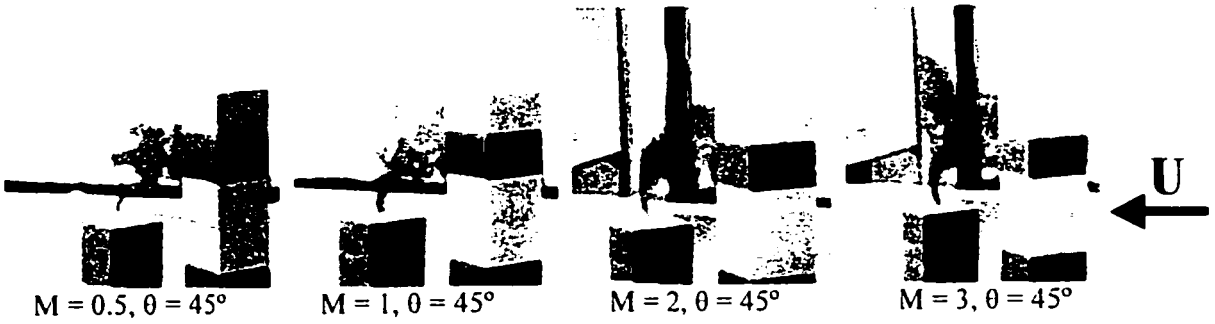

Figure C.8 With tall building upwind (Case VIII, Model A)

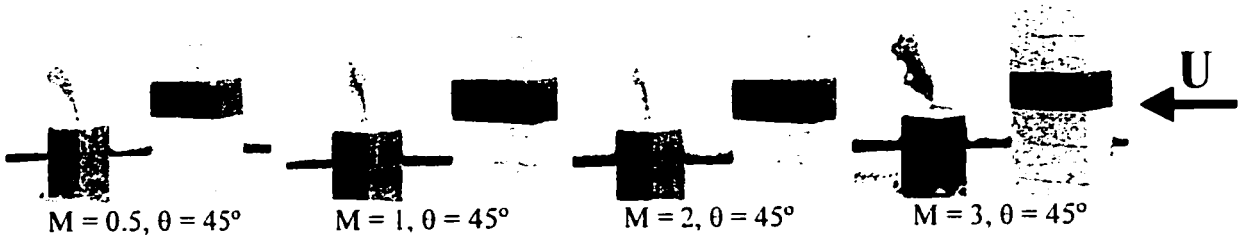

Figure C.9 With tall building upwind (Case IX, Model A)

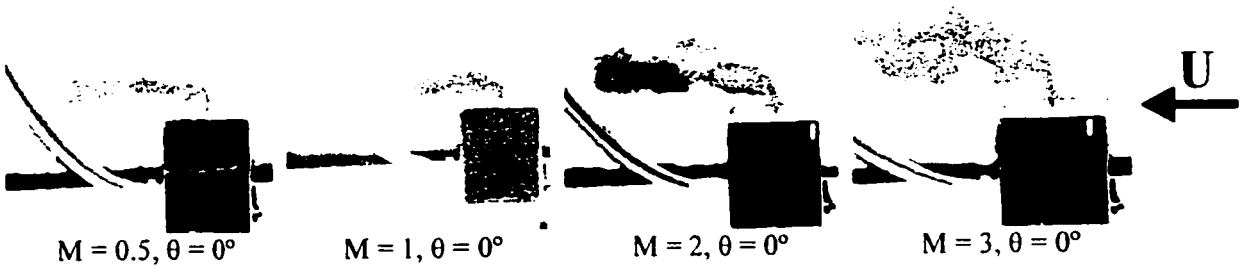

Figure C.10 Isolated building (Case I, Model B)

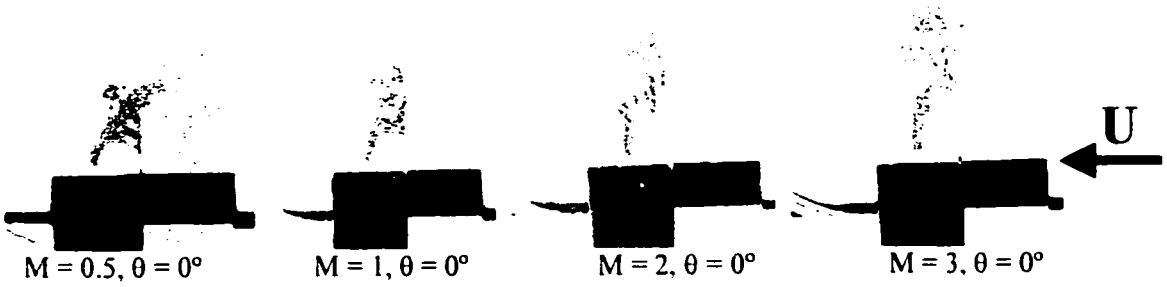

Figure C.11 With tall building upwind (Case II, Model B)

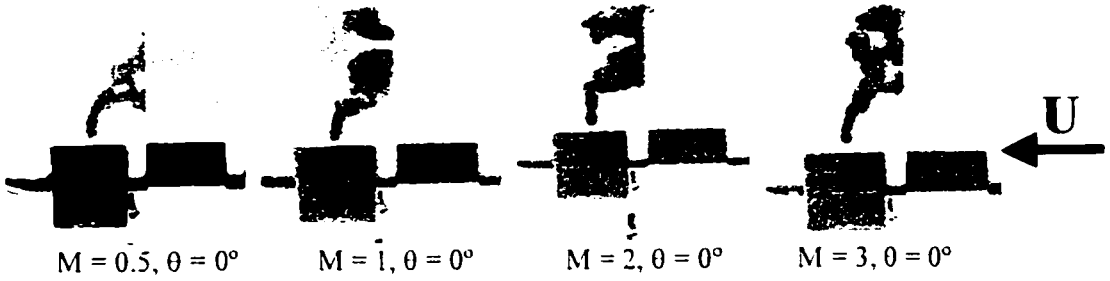

Figure C.12 With tall building upwind (Case III, Model B)

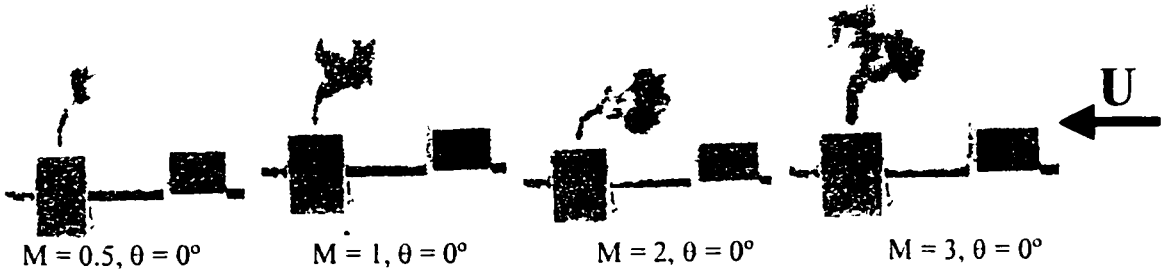

Figure C.13 With tall building upwind far from emitting building (Case IV, Model B)

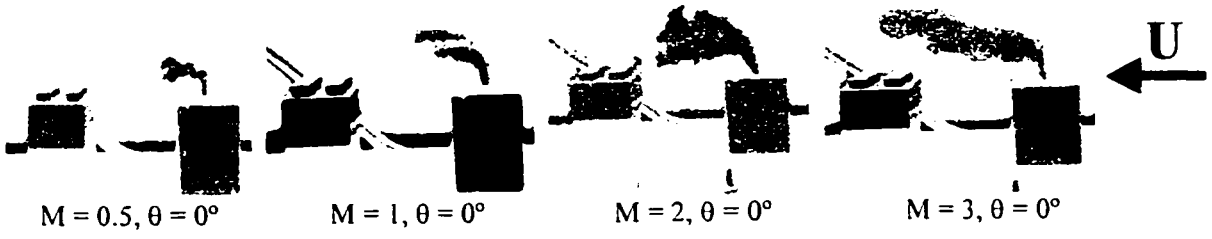

Figure C.14 With same height building downwind (Case V, Model B)

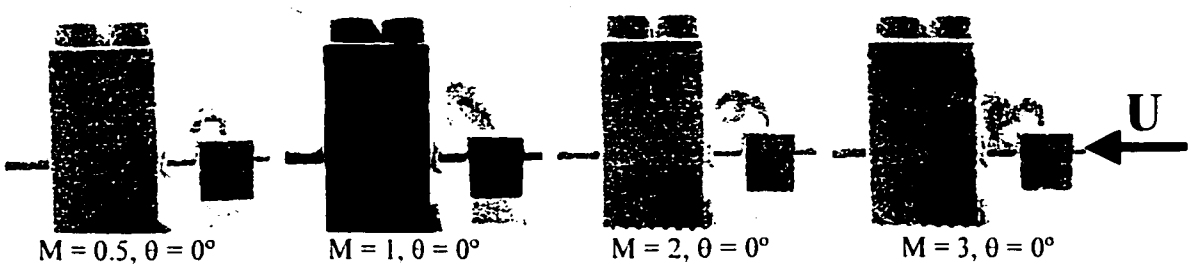

Figure C.15 Visualization of plume with high building downwind of emitting building (Case VI, Model B)

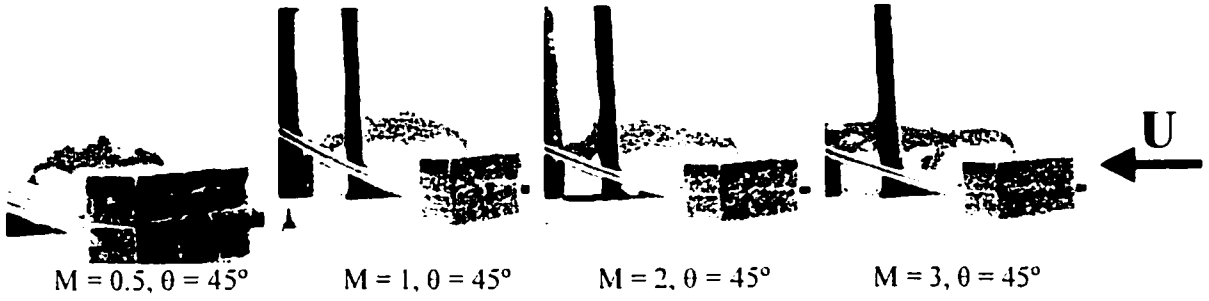

Figure C.16 Isolated building (Case VII, Model B)

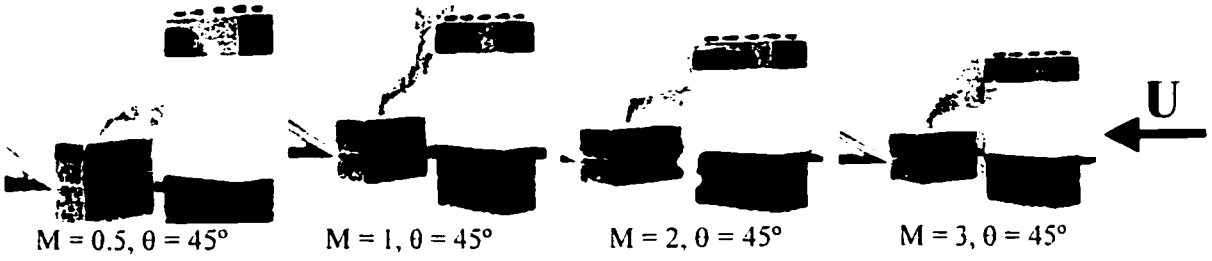

Figure C.17 With tall building upwind (Case VIII, Model B)

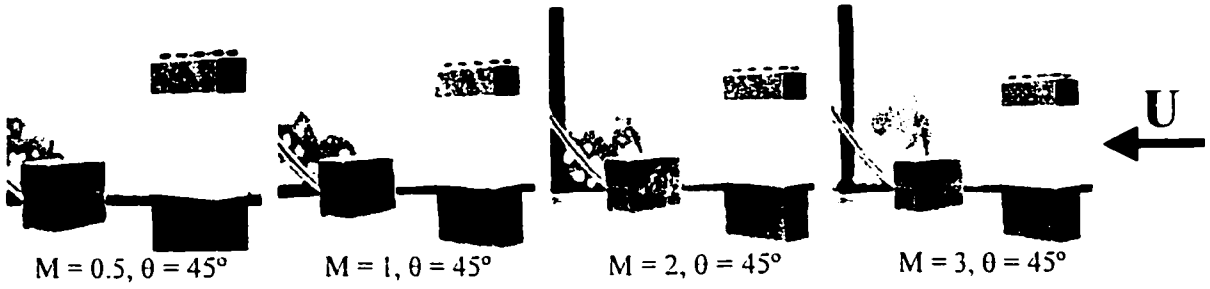

Figure C.18 With tall building upwind (Case IX, Model B)

APPENDIX D

DETAILED RESULTS OF THE WIND TUNNEL STUDY (DILUTION CONTOURS)

All the results obtained from the wind tunnel tracer gas experiments for thirty-one (31) configurations are presented in forms of the dilution ($D = C_e/C$, where C_e is the contaminate concentration in the exhaust and C is the contaminate concentration at receptor) contour plots by using the software "surfer".

Three (3) different relative adjacent building heights (H_a = 1.33H, 1.67H, and 2H), two (2) relative adjacent building widths (W_a = W and 2W), two (2) wind directions ($\theta = 0°$ and 45°), five (5) exhaust momentum ratios (M = 0.5, 1, 2, 3, 4), seven (7) stack locations (Stack A, B, C, D, E, F, and G), five (5) stack heights (0, 1m, 3m, 5m, and 10m) were examined in the present study for eleven (11) relative separation distances (S = 0, 0.25W, 0.71W, 0.75W, W, 1.06W, 1.41W, 1.75W, 1.77W, 2W and 2.25W), as described in Table 3.1.

The detailed results are arranged in the order of "case by case". The steps of the dilution contours depend on the dilution values.

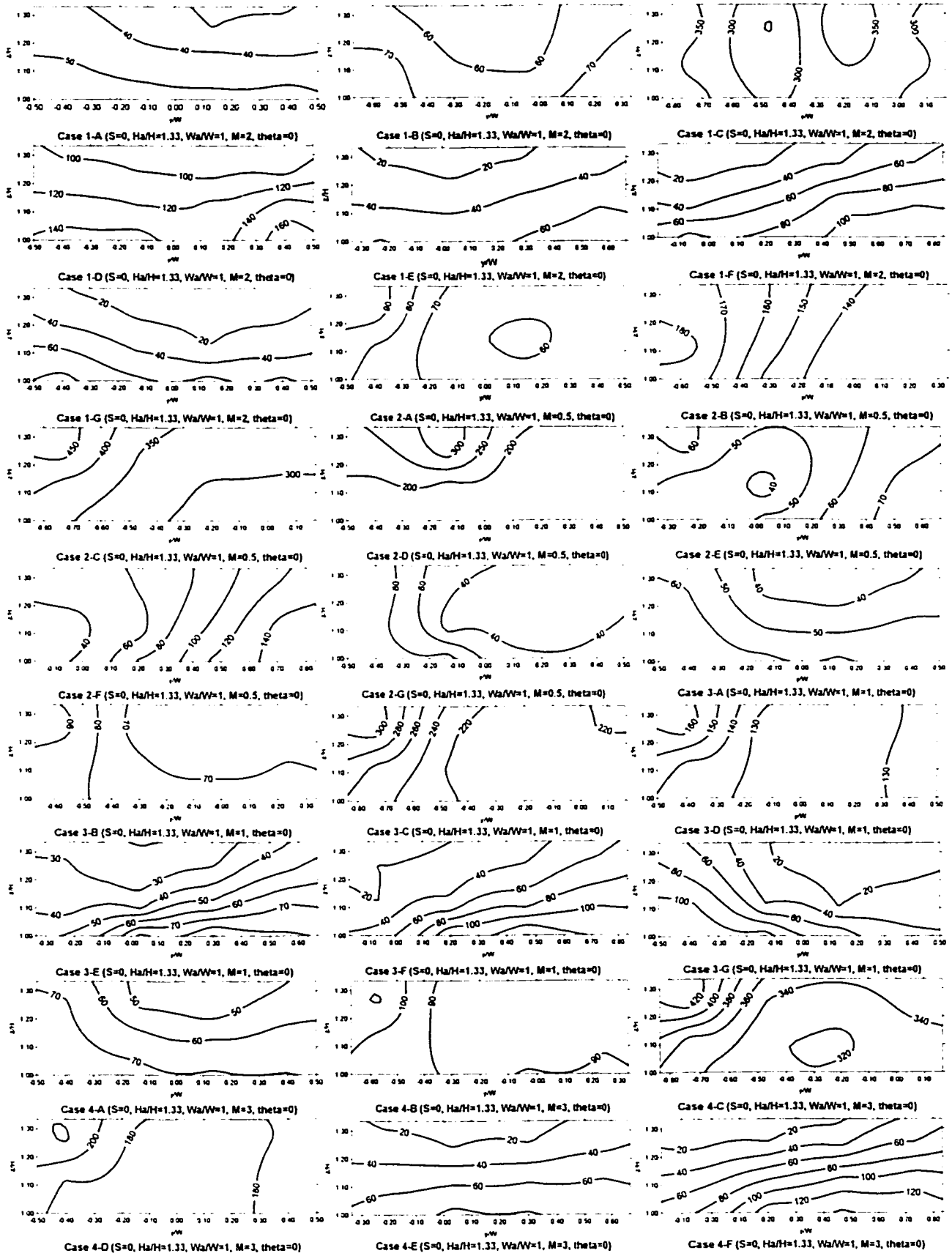
Case 1-A (S=0, Ha/H=1.33, Wa/W=1, M=2, theta=0)
Case 1-B (S=0, Ha/H=1.33, Wa/W=1, M=2, theta=0)
Case 1-C (S=0, Ha/H=1.33, Wa/W=1, M=2, theta=0)
Case 1-D (S=0, Ha/H=1.33, Wa/W=1, M=2, theta=0)
Case 1-E (S=0, Ha/H=1.33, Wa/W=1, M=2, theta=0)
Case 1-F (S=0, Ha/H=1.33, Wa/W=1, M=2, theta=0)
Case 1-G (S=0, Ha/H=1.33, Wa/W=1, M=2, theta=0)
Case 2-A (S=0, Ha/H=1.33, Wa/W=1, M=0.5, theta=0)
Case 2-B (S=0, Ha/H=1.33, Wa/W=1, M=0.5, theta=0)
Case 2-C (S=0, Ha/H=1.33, Wa/W=1, M=0.5, theta=0)
Case 2-D (S=0, Ha/H=1.33, Wa/W=1, M=0.5, theta=0)
Case 2-E (S=0, Ha/H=1.33, Wa/W=1, M=0.5, theta=0)
Case 2-F (S=0, Ha/H=1.33, Wa/W=1, M=0.5, theta=0)
Case 2-G (S=0, Ha/H=1.33, Wa/W=1, M=0.5, theta=0)
Case 3-A (S=0, Ha/H=1.33, Wa/W=1, M=1, theta=0)
Case 3-B (S=0, Ha/H=1.33, Wa/W=1, M=1, theta=0)
Case 3-C (S=0, Ha/H=1.33, Wa/W=1, M=1, theta=0)
Case 3-D (S=0, Ha/H=1.33, Wa/W=1, M=1, theta=0)
Case 3-E (S=0, Ha/H=1.33, Wa/W=1, M=1, theta=0)
Case 3-F (S=0, Ha/H=1.33, Wa/W=1, M=1, theta=0)
Case 3-G (S=0, Ha/H=1.33, Wa/W=1, M=1, theta=0)
Case 4-A (S=0, Ha/H=1.33, Wa/W=1, M=3, theta=0)
Case 4-B (S=0, Ha/H=1.33, Wa/W=1, M=3, theta=0)
Case 4-C (S=0, Ha/H=1.33, Wa/W=1, M=3, theta=0)
Case 4-D (S=0, Ha/H=1.33, Wa/W=1, M=3, theta=0)
Case 4-E (S=0, Ha/H=1.33, Wa/W=1, M=3, theta=0)
Case 4-F (S=0, Ha/H=1.33, Wa/W=1, M=3, theta=0)

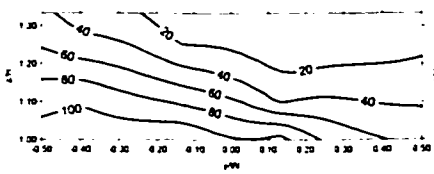

Case 4-G (S=0, Ha/H=1.33, Wa/W=1, M=3, theta=0)

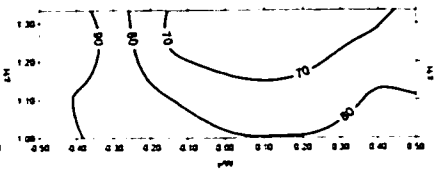

Case 5-A (S=0, Ha/H=1.33, Wa/W=1, M=4, theta=0)

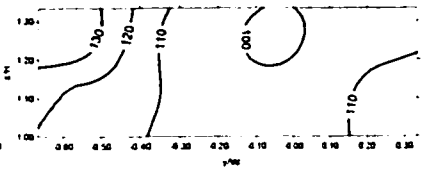

Case 5-B (S=0, Ha/H=1.33, Wa/W=1, M=4, theta=0)

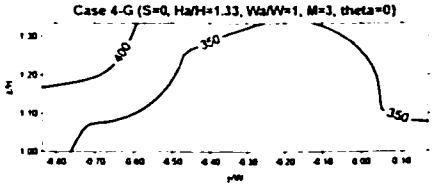

Case 5-C (S=0, Ha/H=1.33, Wa/W=1, M=4, theta=0)

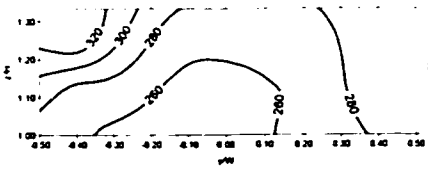

Case 5-D (S=0, Ha/H=1.33, Wa/W=1, M=4, theta=0)

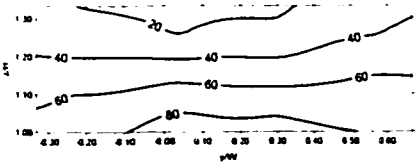

Case 5-E (S=0, Ha/H=1.33, Wa/W=1, M=4, theta=0)

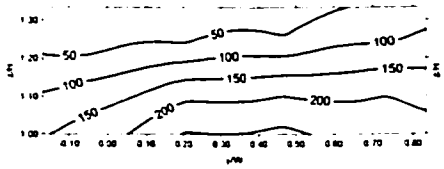

Case 5-F (S=0, Ha/H=1.33, Wa/W=1, M=4, theta=0)

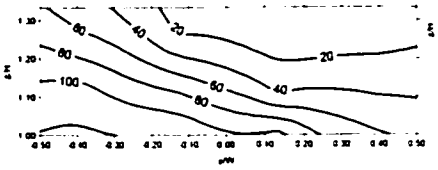

Case 5-G (S=0, Ha/H=1.33, Wa/W=1, M=4, theta=0)

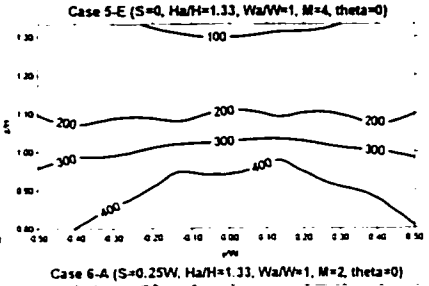

Case 6-A (S=0.25W, Ha/H=1.33, Wa/W=1, M=2, theta=0)

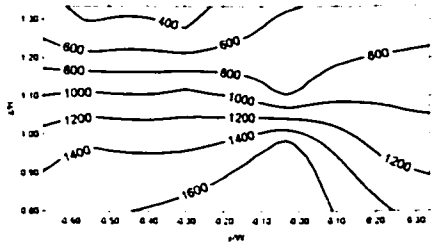

Case 6-B (S=0.25W, Ha/H=1.33, Wa/W=1, M=2, theta=0)

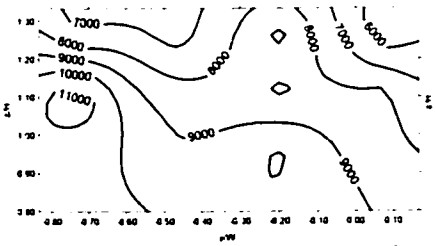

Case 6-C (S=0.25W, Ha/H=1.33, Wa/W=1, M=2, theta=0)

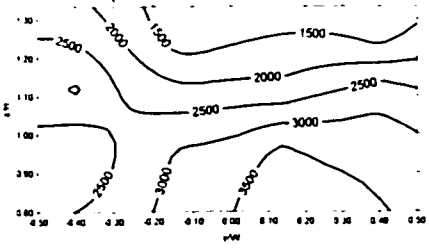

Case 6-D (S=0.25W, Ha/H=1.33, Wa/W=1, M=2, theta=0)

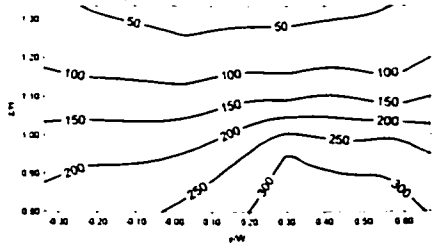

Case 6-E (S=0.25W, Ha/H=1.33, Wa/W=1, M=2, theta=0)

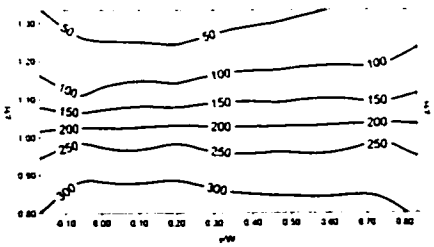

Case 6-F (S=0.25W, Ha/H=1.33, Wa/W=1, M=2, theta=0)

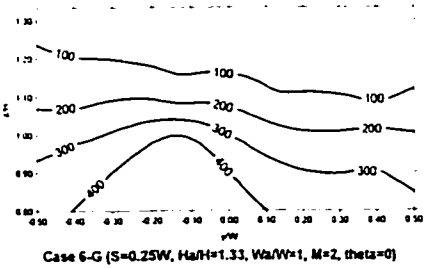

Case 6-G (S=0.25W, Ha/H=1.33, Wa/W=1, M=2, theta=0)

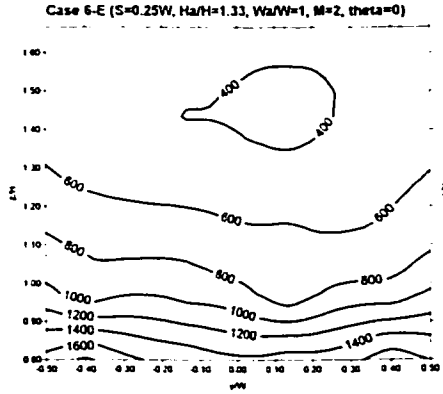

Case 7-A (S=0.75W, Ha/H=1.67, Wa/W=1, M=2, theta=0)

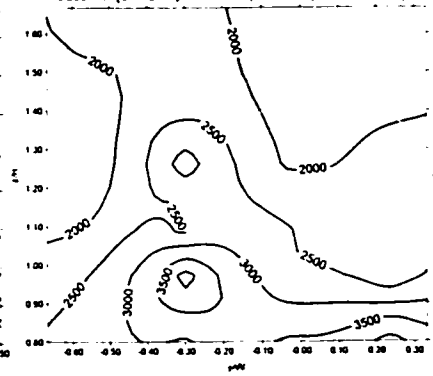

Case 7-B (S=0.75W, Ha/H=1.67, Wa/W=1, M=2, theta=0)

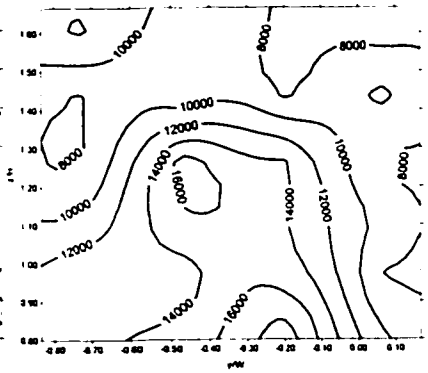

Case 7-C (S=0.75W, Ha/H=1.67, Wa/W=1, M=2, theta=0)

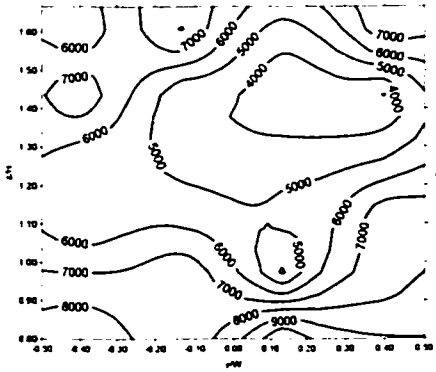

Case 7-D (S=0.75W, Ha/H=1.67, Wa/W=1, M=2, theta=0)

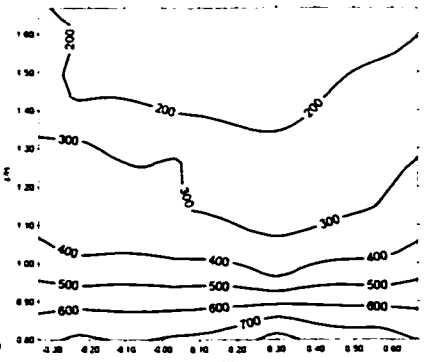

Case 7-E (S=0.75W, Ha/H=1.67, Wa/W=1, M=2, theta=0)

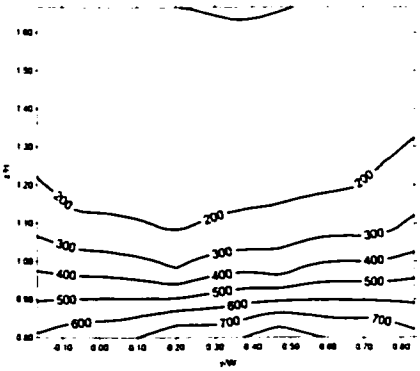

Case 7-F (S=0.75W, Ha/H=1.67, Wa/W=1, M=2, theta=0)

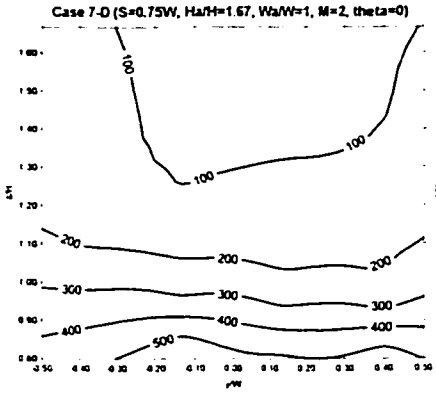

Case 7-G (S=0.75W, Ha/H=1.67, Wa/W=1, M=2, theta=0)

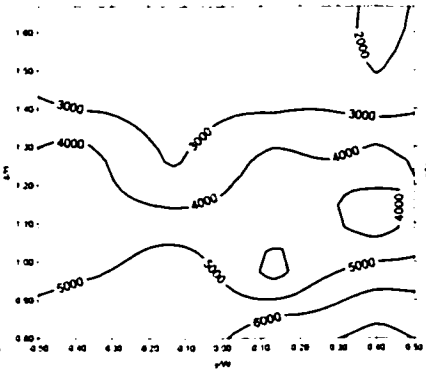

Case 8-A (S=W, Ha/H=1.67, Wa/W=1, M=2, theta=0)

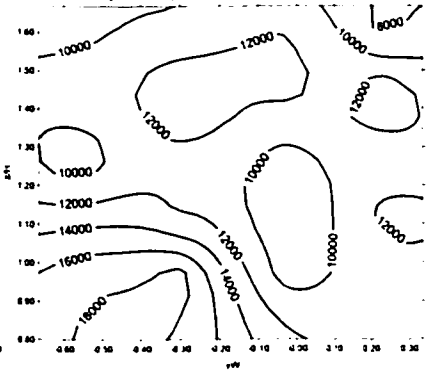

Case 8-B (S=W, Ha/H=1.67, Wa/W=1, M=2, theta=0)

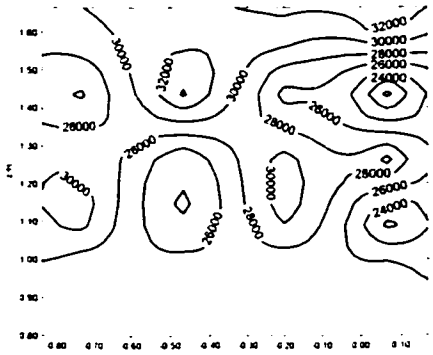

Case 8-C (S=W, Ha/H=1.67, Wa/W=1, M=2, theta=0)

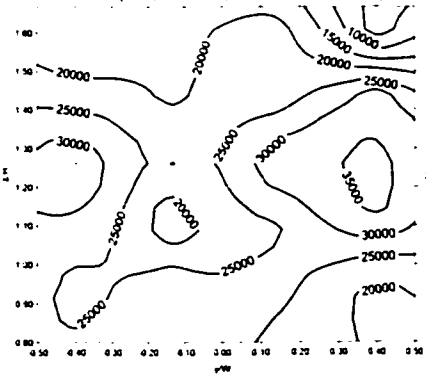

Case 8-D (S=W, Ha/H=1.67, Wa/W=1, M=2, theta=0)

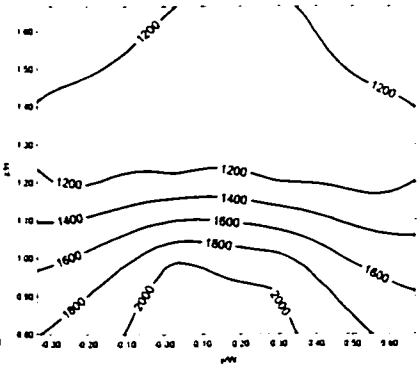

Case 8-E (S=W, Ha/H=1.67, Wa/W=1, M=2, theta=0)

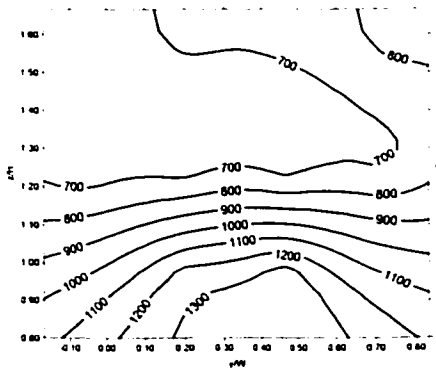

Case 8-F (S=W, Ha/H=1.67, Wa/W=1, M=2, theta=0)

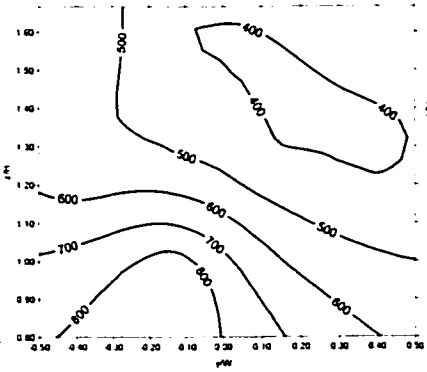

Case 8-G (S=W, Ha/H=1.67, Wa/W=1, M=2, theta=0)

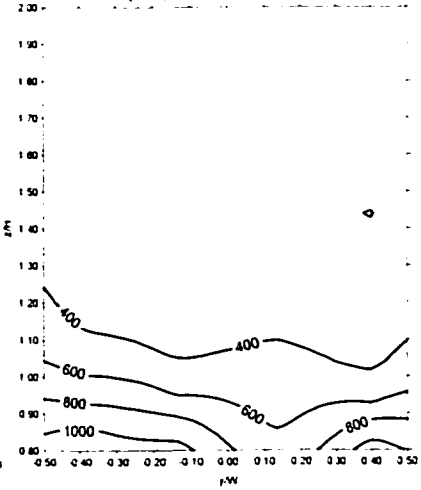

Case 9-A (S=0.75W, Ha/H=2, Wa/W=1, M=2, theta=0)

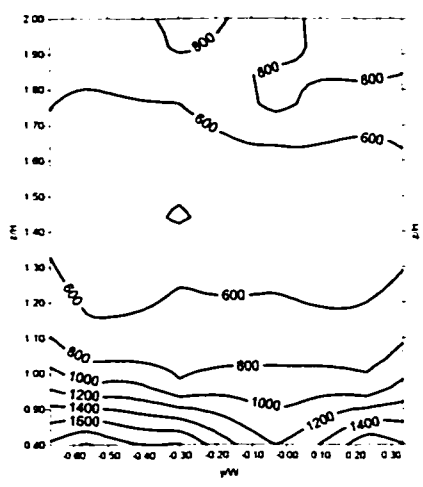

Case 9-B (S=0.75W, Ha/H=2, Wa/W=1, M=2, theta=0)

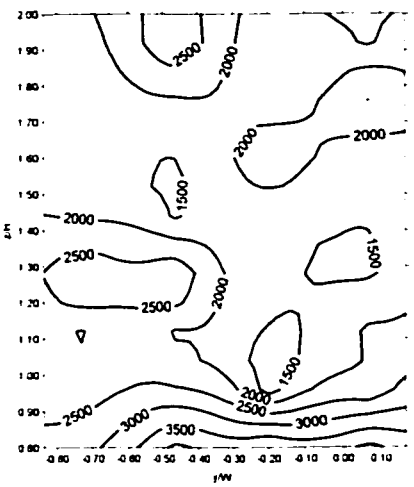

Case 9-C (S=0.75W, Ha/H=2, Wa/W=1, M=2, theta=0)

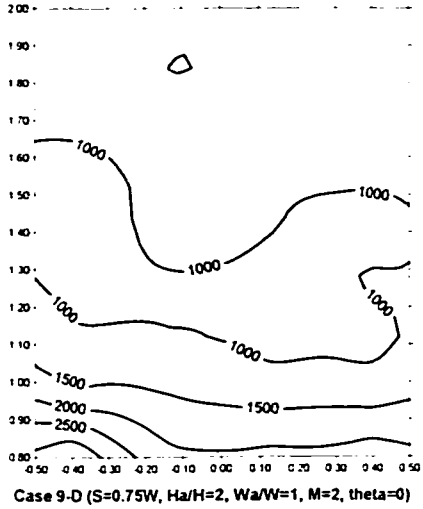

Case 9-D (S=0.75W, Ha/H=2, Wa/W=1, M=2, theta=0)

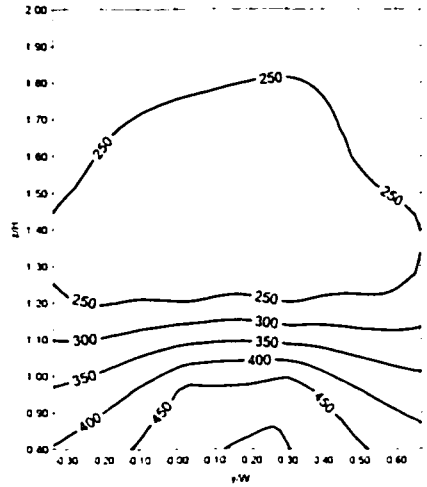

Case 9-E (S=0.75W, Ha/H=2, Wa/W=1, M=2, theta=0)

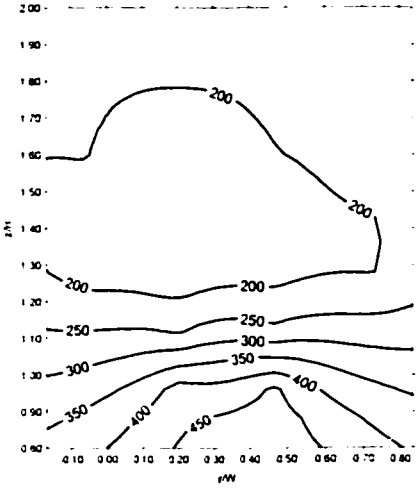

Case 9-F (S=0.75W, Ha/H=2, Wa/W=1, M=2, theta=0)

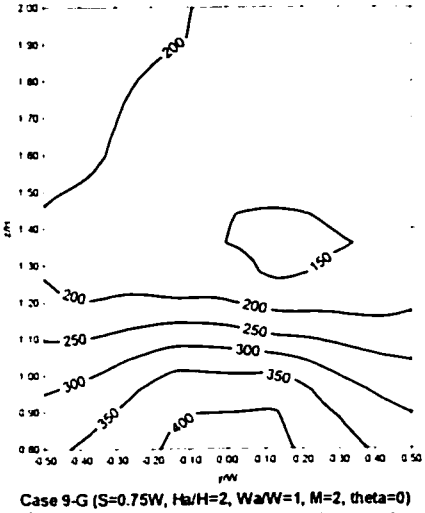

Case 9-G (S=0.75W, Ha/H=2, Wa/W=1, M=2, theta=0)

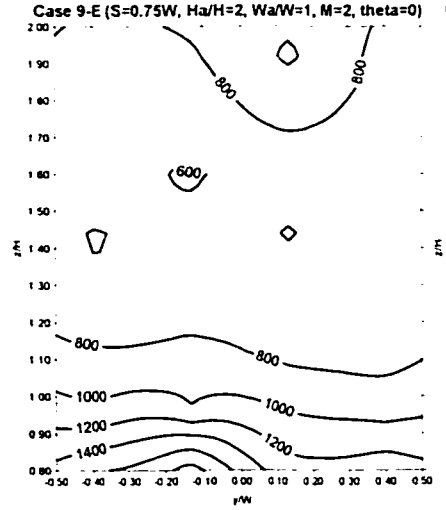

Case 10-A (S=W, Ha/H=2, Wa/W=1, M=2, theta=0)

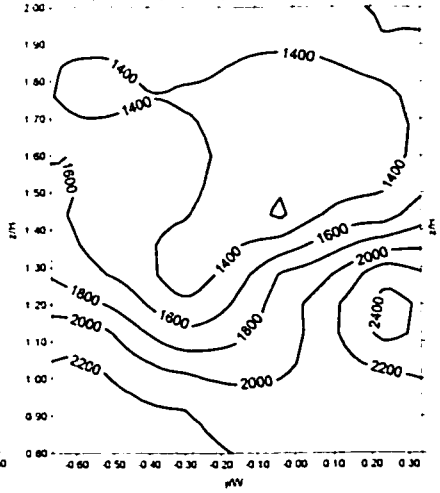

Case 10-B (S=W, Ha/H=2, Wa/W=1, M=2, theta=0)

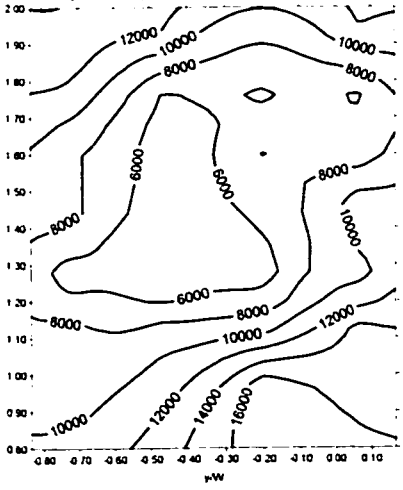

Case 10-C (S=W, Ha/H=2, Wa/W=1, M=2, theta=0)

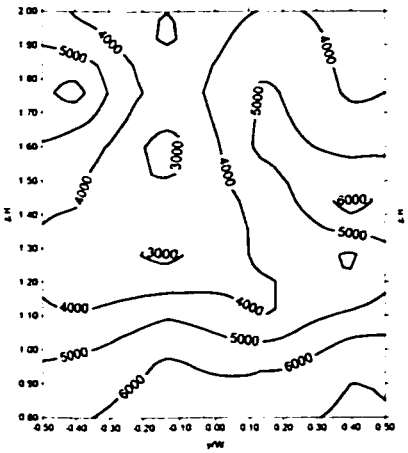

Case 10-D (S=W, Ha/H=2, Wa/W=1, M=2, theta=0)

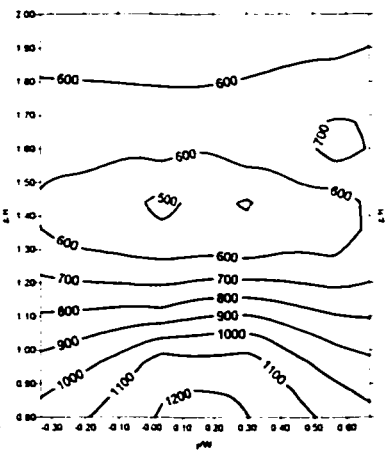

Case 10-E (S=W, Ha/H=2, Wa/W=1, M=2, theta=0)

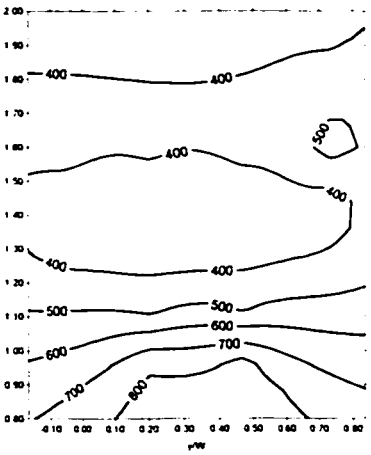

Case 10-F (S=W, Ha/H=2, Wa/W=1, M=2, theta=0)

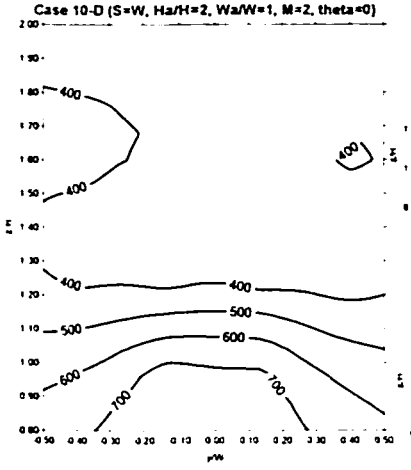

Case 10-G (S=W, Ha/H=2, Wa/W=1, M=2, theta=0)

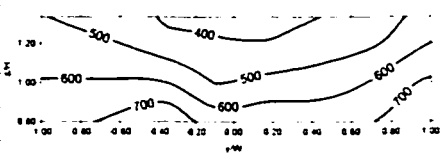

Case 11-A (S=0.75W, Ha/H=1.33, Wa/W=2, M=2, theta=0)

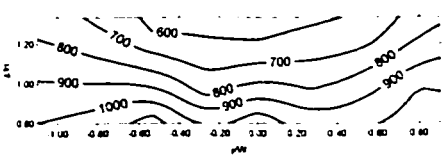

Case 11-B (S=0.75W, Ha/H=1.33, Wa/W=2, M=2, theta=0)

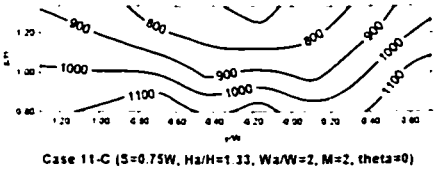

Case 11-C (S=0.75W, Ha/H=1.33, Wa/W=2, M=2, theta=0)

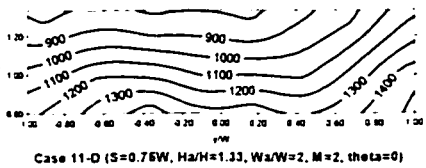

Case 11-D (S=0.75W, Ha/H=1.33, Wa/W=2, M=2, theta=0)

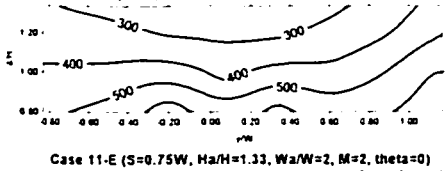

Case 11-E (S=0.75W, Ha/H=1.33, Wa/W=2, M=2, theta=0)

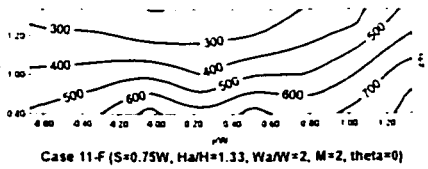

Case 11-F (S=0.75W, Ha/H=1.33, Wa/W=2, M=2, theta=0)

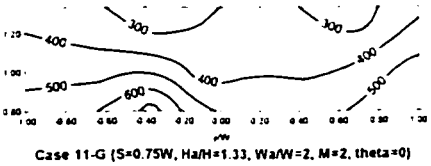

Case 11-G (S=0.75W, Ha/H=1.33, Wa/W=2, M=2, theta=0)

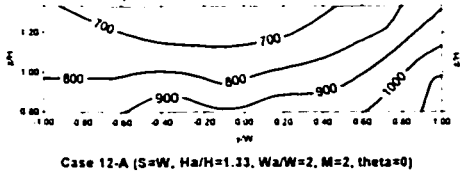

Case 12-A (S=W, Ha/H=1.33, Wa/W=2, M=2, theta=0)

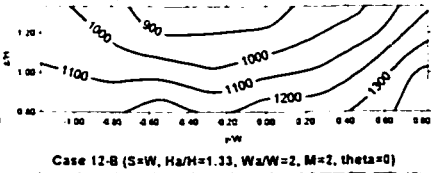

Case 12-B (S=W, Ha/H=1.33, Wa/W=2, M=2, theta=0)

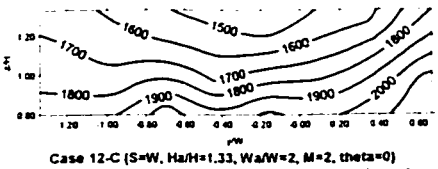

Case 12-C (S=W, Ha/H=1.33, Wa/W=2, M=2, theta=0)

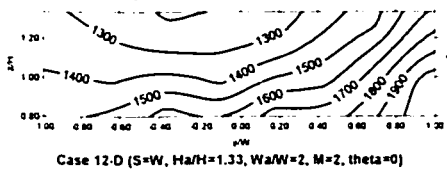

Case 12-D (S=W, Ha/H=1.33, Wa/W=2, M=2, theta=0)

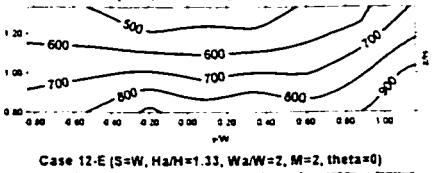

Case 12-E (S=W, Ha/H=1.33, Wa/W=2, M=2, theta=0)

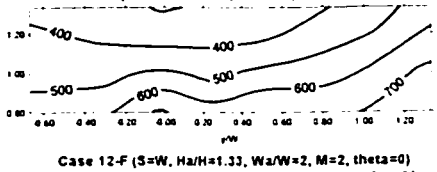

Case 12-F (S=W, Ha/H=1.33, Wa/W=2, M=2, theta=0)

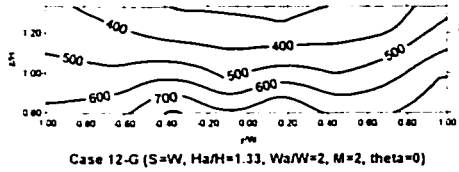

Case 12-G (S=W, Ha/H=1.33, Wa/W=2, M=2, theta=0)

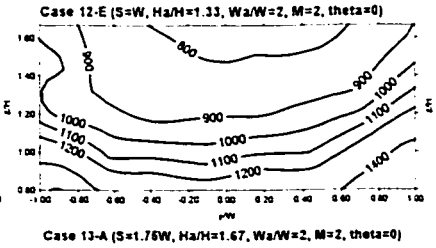

Case 13-A (S=1.75W, Ha/H=1.67, Wa/W=2, M=2, theta=0)

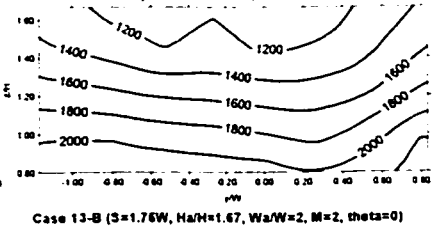

Case 13-B (S=1.75W, Ha/H=1.67, Wa/W=2, M=2, theta=0)

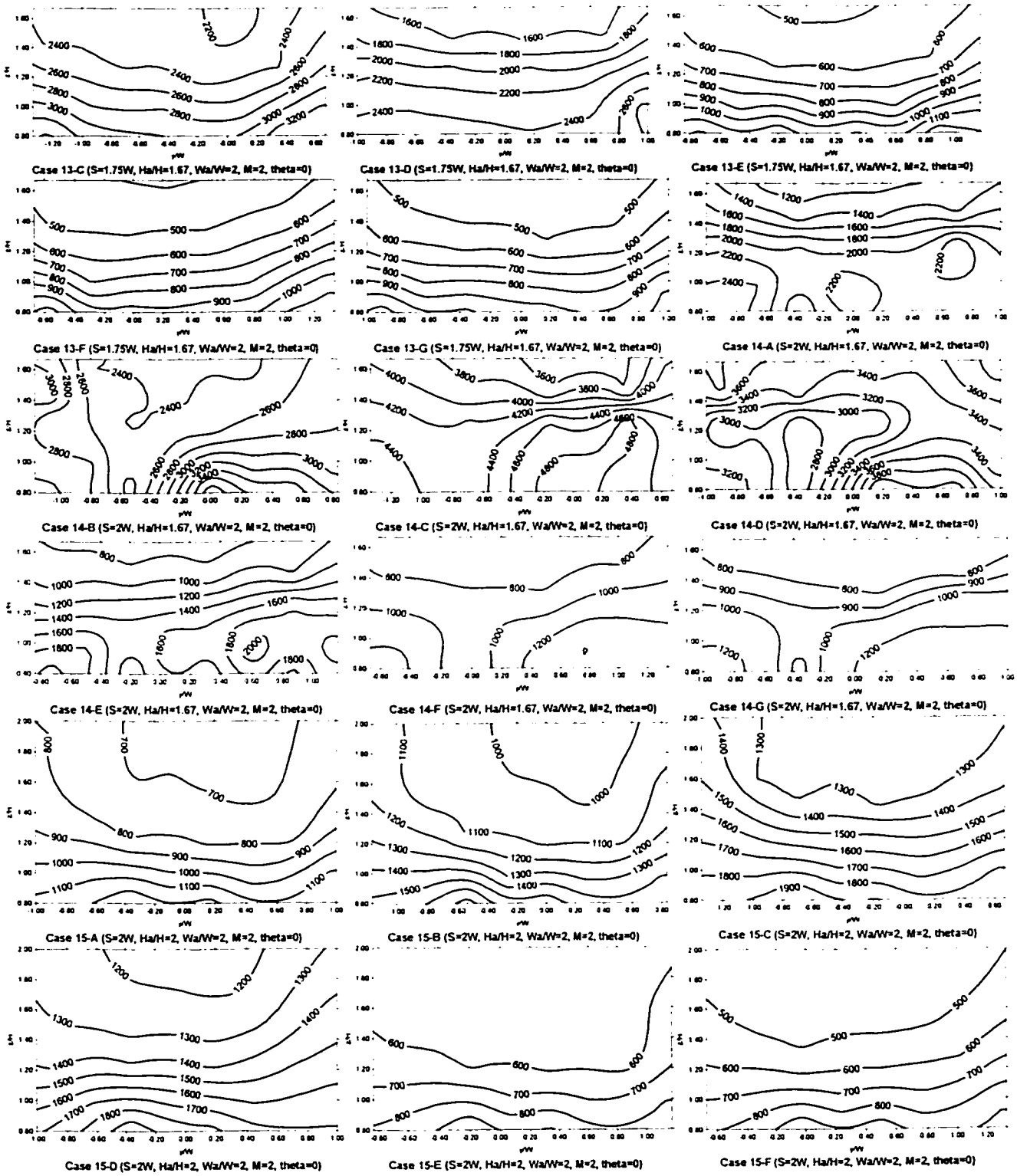
Case 13-C (S=1.75W, Ha/H=1.67, Wa/W=2, M=2, theta=0)
Case 13-D (S=1.75W, Ha/H=1.67, Wa/W=2, M=2, theta=0)
Case 13-E (S=1.75W, Ha/H=1.67, Wa/W=2, M=2, theta=0)
Case 13-F (S=1.75W, Ha/H=1.67, Wa/W=2, M=2, theta=0)
Case 13-G (S=1.75W, Ha/H=1.67, Wa/W=2, M=2, theta=0)
Case 14-A (S=2W, Ha/H=1.67, Wa/W=2, M=2, theta=0)
Case 14-B (S=2W, Ha/H=1.67, Wa/W=2, M=2, theta=0)
Case 14-C (S=2W, Ha/H=1.67, Wa/W=2, M=2, theta=0)
Case 14-D (S=2W, Ha/H=1.67, Wa/W=2, M=2, theta=0)
Case 14-E (S=2W, Ha/H=1.67, Wa/W=2, M=2, theta=0)
Case 14-F (S=2W, Ha/H=1.67, Wa/W=2, M=2, theta=0)
Case 14-G (S=2W, Ha/H=1.67, Wa/W=2, M=2, theta=0)
Case 15-A (S=2W, Ha/H=2, Wa/W=2, M=2, theta=0)
Case 15-B (S=2W, Ha/H=2, Wa/W=2, M=2, theta=0)
Case 15-C (S=2W, Ha/H=2, Wa/W=2, M=2, theta=0)
Case 15-D (S=2W, Ha/H=2, Wa/W=2, M=2, theta=0)
Case 15-E (S=2W, Ha/H=2, Wa/W=2, M=2, theta=0)
Case 15-F (S=2W, Ha/H=2, Wa/W=2, M=2, theta=0)

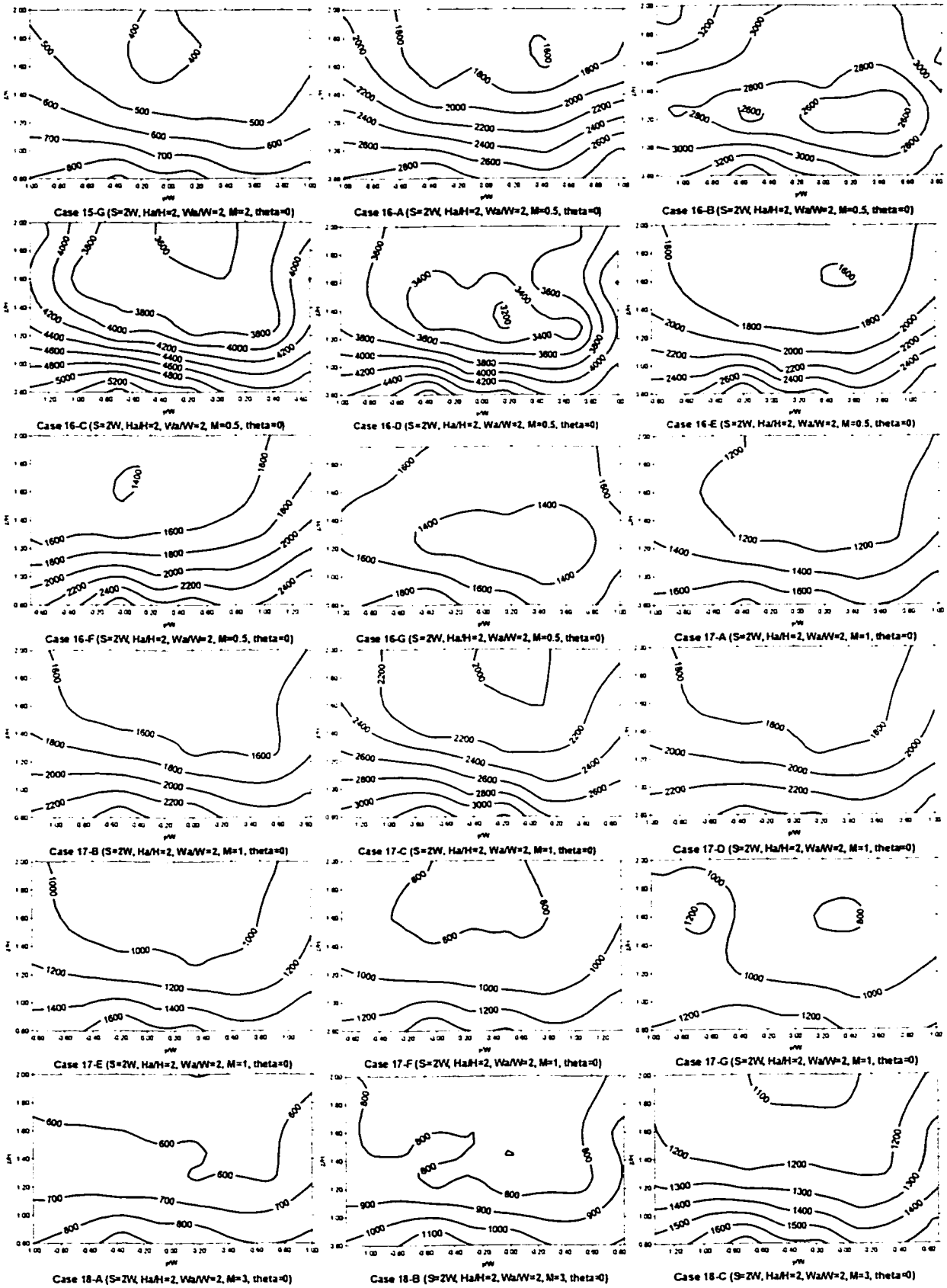
Case 15-G (S=2W, Ha/H=2, Wa/W=2, M=2, theta=0)
Case 16-A (S=2W, Ha/H=2, Wa/W=2, M=0.5, theta=0)
Case 16-B (S=2W, Ha/H=2, Wa/W=2, M=0.5, theta=0)
Case 16-C (S=2W, Ha/H=2, Wa/W=2, M=0.5, theta=0)
Case 16-D (S=2W, Ha/H=2, Wa/W=2, M=0.5, theta=0)
Case 16-E (S=2W, Ha/H=2, Wa/W=2, M=0.5, theta=0)
Case 16-F (S=2W, Ha/H=2, Wa/W=2, M=0.5, theta=0)
Case 16-G (S=2W, Ha/H=2, Wa/W=2, M=0.5, theta=0)
Case 17-A (S=2W, Ha/H=2, Wa/W=2, M=1, theta=0)
Case 17-B (S=2W, Ha/H=2, Wa/W=2, M=1, theta=0)
Case 17-C (S=2W, Ha/H=2, Wa/W=2, M=1, theta=0)
Case 17-D (S=2W, Ha/H=2, Wa/W=2, M=1, theta=0)
Case 17-E (S=2W, Ha/H=2, Wa/W=2, M=1, theta=0)
Case 17-F (S=2W, Ha/H=2, Wa/W=2, M=1, theta=0)
Case 17-G (S=2W, Ha/H=2, Wa/W=2, M=1, theta=0)
Case 18-A (S=2W, Ha/H=2, Wa/W=2, M=3, theta=0)
Case 18-B (S=2W, Ha/H=2, Wa/W=2, M=3, theta=0)
Case 18-C (S=2W, Ha/H=2, Wa/W=2, M=3, theta=0)

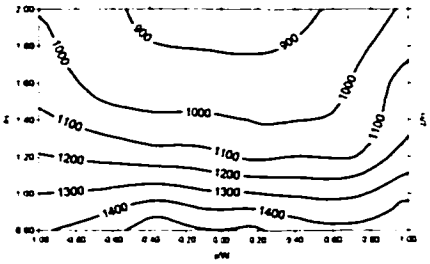

Case 18-D (S=2W, Ha/H=2, Wa/W=2, M=3, theta=0)

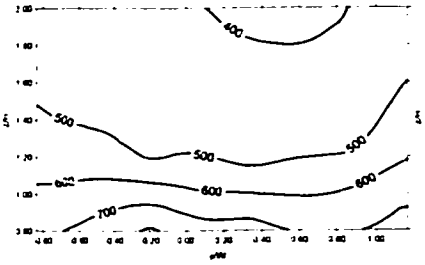

Case 18-E (S=2W, Ha/H=2, Wa/W=2, M=3, theta=0)

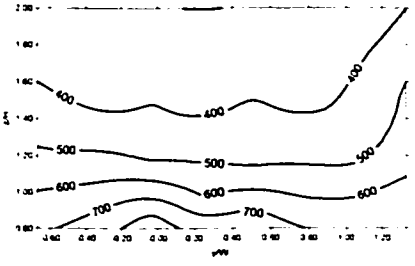

Case 18-F (S=2W, Ha/H=2, Wa/W=2, M=3, theta=0)

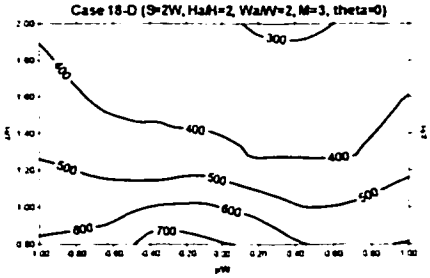

Case 18-G (S=2W, Ha/H=2, Wa/W=2, M=3, theta=0)

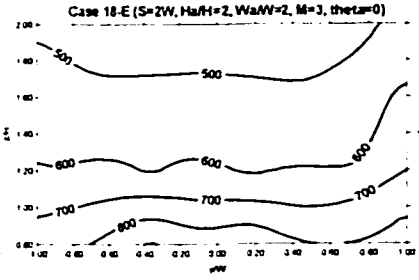

Case 19-A (S=2W, Ha/H=2, Wa/W=2, M=4, theta=0)

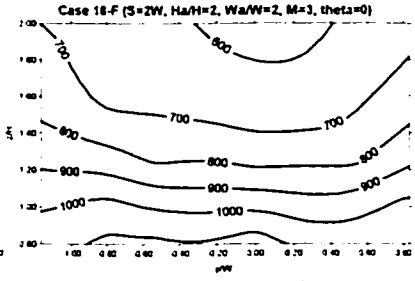

Case 19-B (S=2W, Ha/H=2, Wa/W=2, M=4, theta=0)

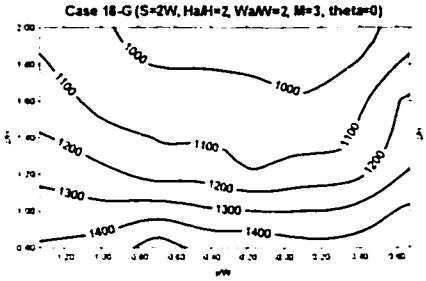

Case 19-C (S=2W, Ha/H=2, Wa/W=2, M=4, theta=0)

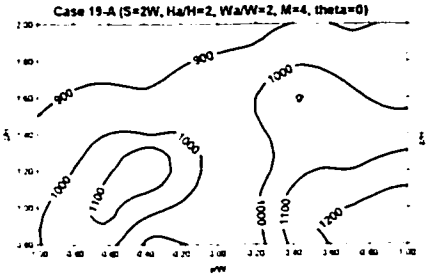

Case 19-D (S=2W, Ha/H=2, Wa/W=2, M=4, theta=0)

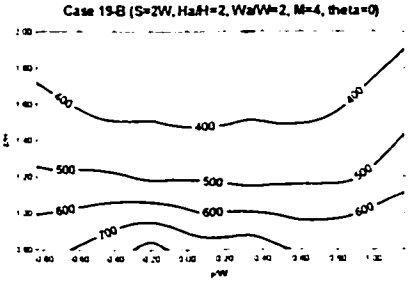

Case 19-E (S=2W, Ha/H=2, Wa/W=2, M=4, theta=0)

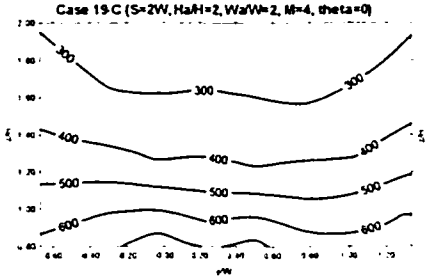

Case 19-F (S=2W, Ha/H=2, Wa/W=2, M=4, theta=0)

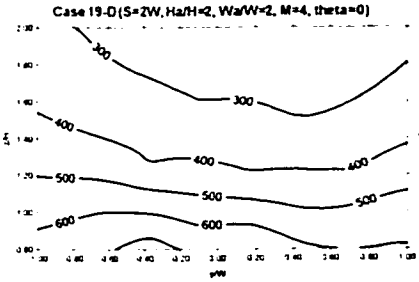

Case 19-G (S=2W, Ha/H=2, Wa/W=2, M=4, theta=0)

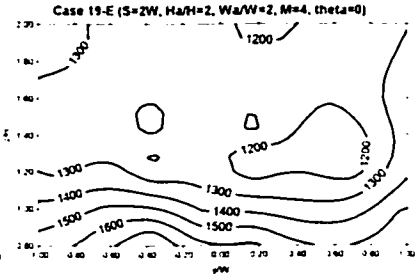

Case 20-A (S=2.25W, Ha/H=2, Wa/W=2, M=2, theta=0)

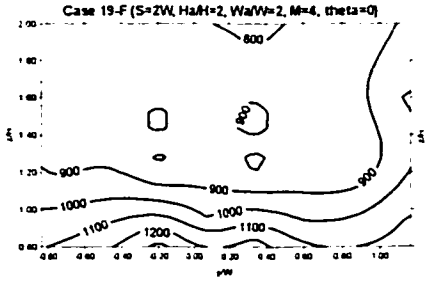

Case 20-E (S=2.25W, Ha/H=2, Wa/W=2, M=2, theta=0)

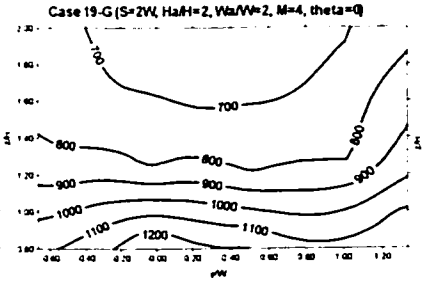

Case 20-F (S=2.25W, Ha/H=2, Wa/W=2, M=2, theta=0)

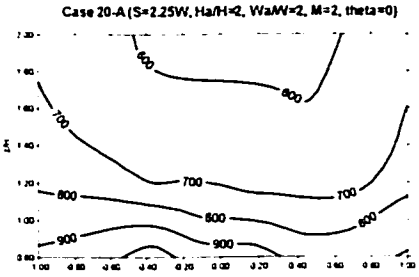

Case 20-G (S=2.25W, Ha/H=2, Wa/W=2, M=2, theta=0)

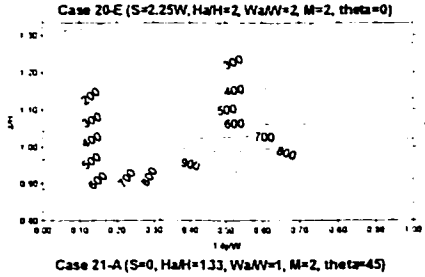

Case 21-A (S=0, Ha/H=1.33, Wa/W=1, M=2, theta=45)

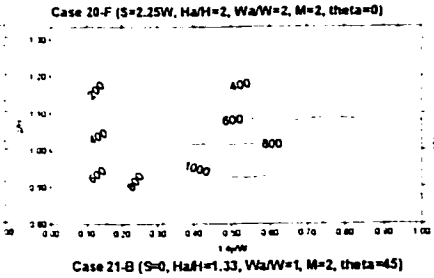

Case 21-B (S=0, Ha/H=1.33, Wa/W=1, M=2, theta=45)

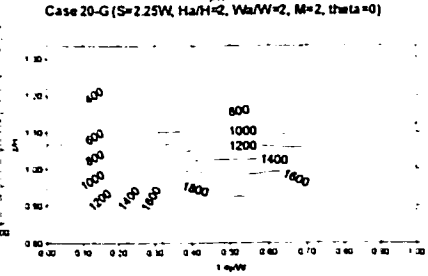

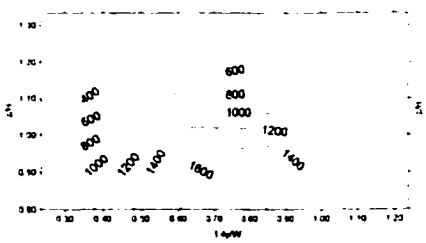

Case 21-D (S=0, Ha/H=1.33, Wa/W=1, M=2, theta=45)

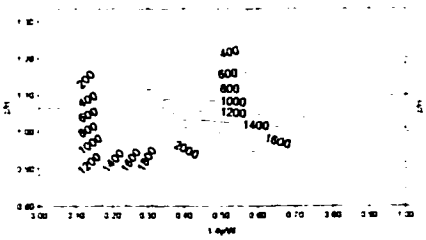

Case 21-E (S=0, Ha/H=1.33, Wa/W=1, M=2, theta=45)

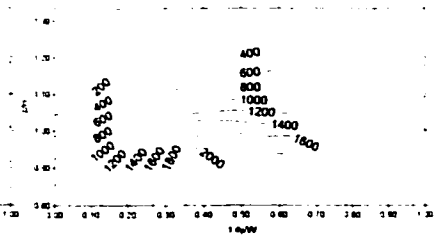

Case 21-F (S=0, Ha/H=1.33, Wa/W=1, M=2, theta=45)

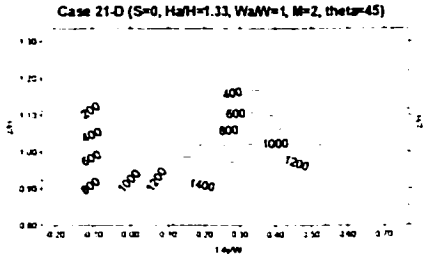

Case 21-G (S=0, Ha/H=1.33, Wa/W=1, M=2, theta=45)

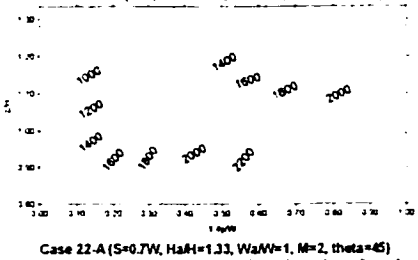

Case 22-A (S=0.7W, Ha/H=1.33, Wa/W=1, M=2, theta=45)

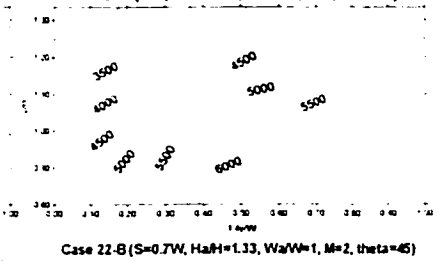

Case 22-B (S=0.7W, Ha/H=1.33, Wa/W=1, M=2, theta=45)

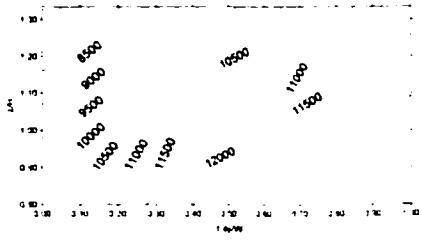

Case 22-C (S=0.7W, Ha/H=1.33, Wa/W=1, M=2, theta=45)

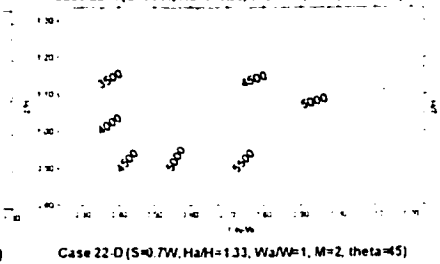

Case 22-D (S=0.7W, Ha/H=1.33, Wa/W=1, M=2, theta=45)

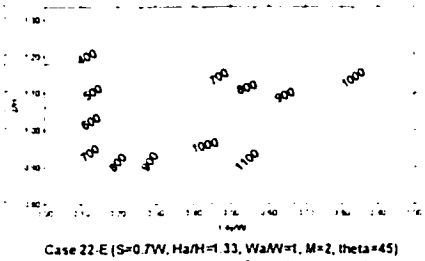

Case 22-E (S=0.7W, Ha/H=1.33, Wa/W=1, M=2, theta=45)

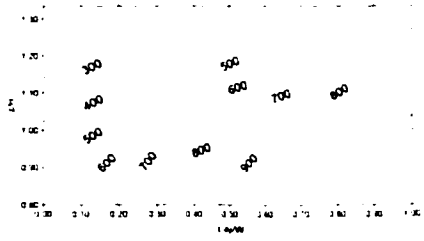

Case 22-F (S=0.7W, Ha/H=1.33, Wa/W=1, M=2, theta=45)

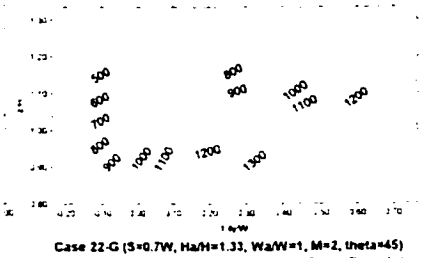

Case 22-G (S=0.7W, Ha/H=1.33, Wa/W=1, M=2, theta=45)

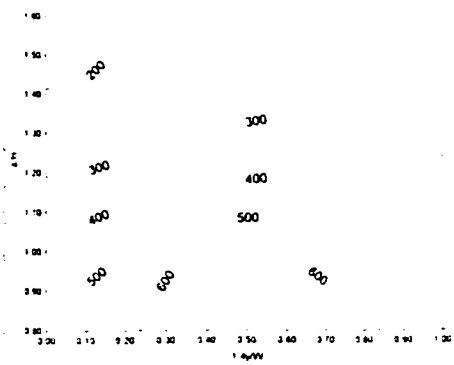

Case 23-A (S=0.7W, Ha/H=1.67, Wa/W=1, M=2, theta=45)

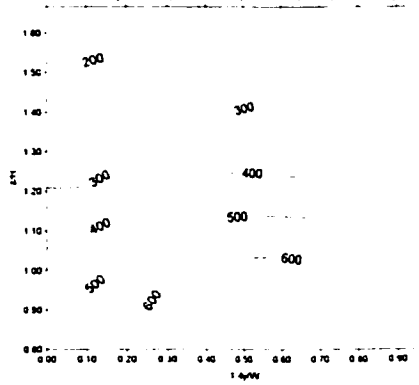

Case 23-B (S=0.7W, Ha/H=1.67, Wa/W=1, M=2, theta=45)

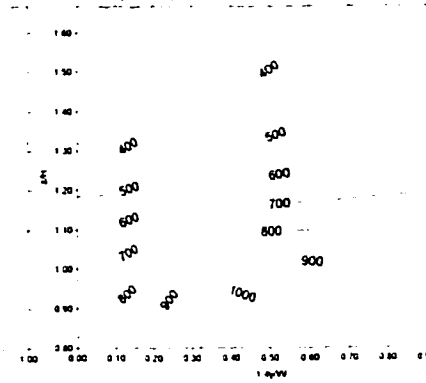

Case 23-C (S=0.7W, Ha/H=1.67, Wa/W=1, M=2, theta=45)

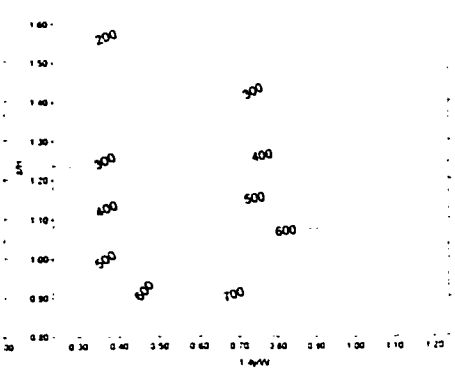

Case 23-D (S=0.7W, Ha/H=1.67, Wa/W=1, M=2, theta=45)

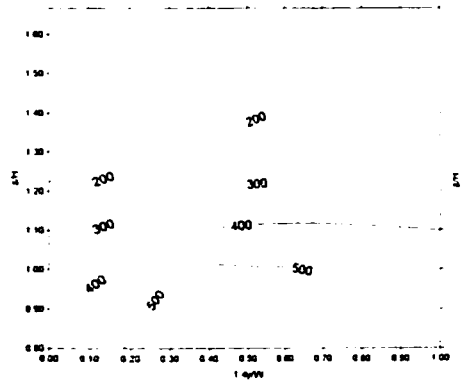

Case 23-E (S=0.7W, Ha/H=1.67, Wa/W=1, M=2, theta=45)

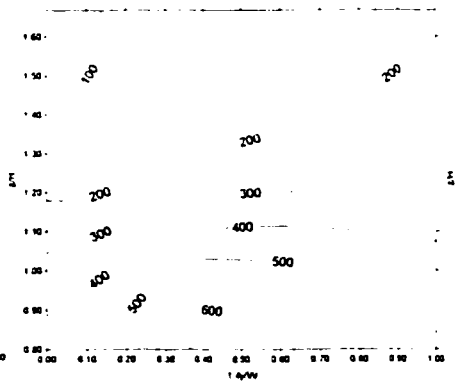

Case 23-F (S=0.7W, Ha/H=1.67, Wa/W=1, M=2, theta=45)

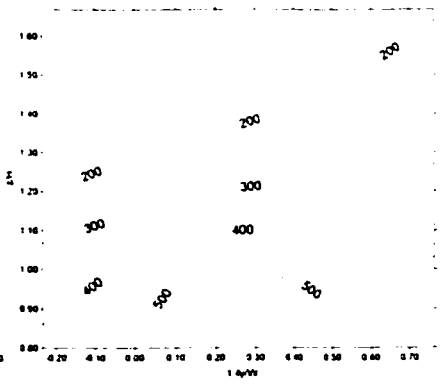

Case 23-G (S=0.7W, Ha/H=1.67, Wa/W=1, M=2, theta=45)

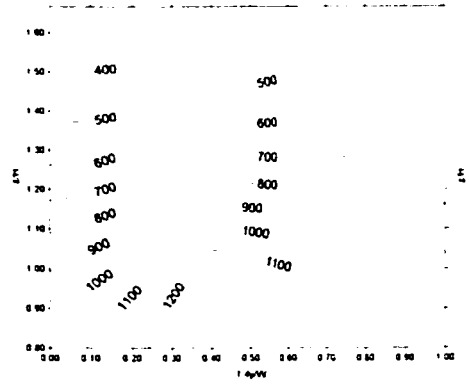

Case 24-A (S=1.1W, Ha/H=1.67, Wa/W=1, M=2, theta=45)

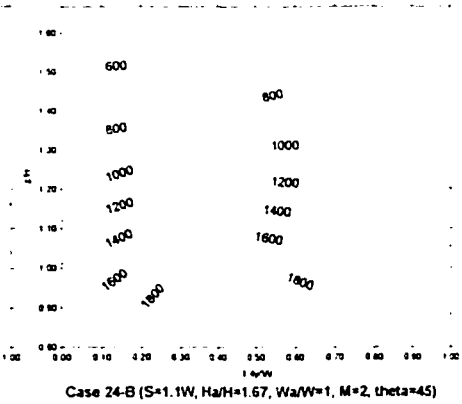

Case 24-B (S=1.1W, Ha/H=1.67, Wa/W=1, M=2, theta=45)

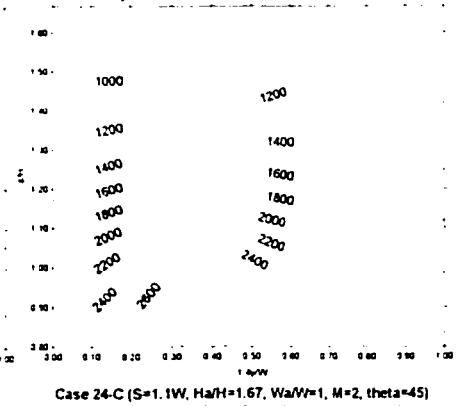

Case 24-C (S=1.1W, Ha/H=1.67, Wa/W=1, M=2, theta=45)

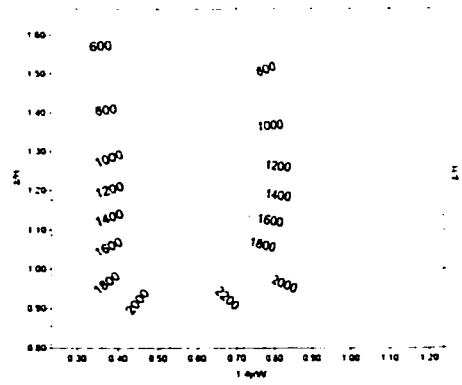

Case 24-D (S=1.1W, Ha/H=1.67, Wa/W=1, M=2, theta=45)

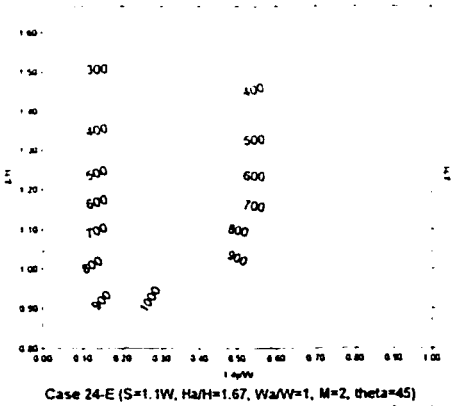

Case 24-E (S=1.1W, Ha/H=1.67, Wa/W=1, M=2, theta=45)

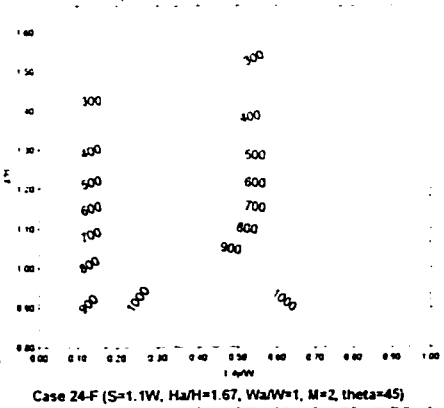

Case 24-F (S=1.1W, Ha/H=1.67, Wa/W=1, M=2, theta=45)

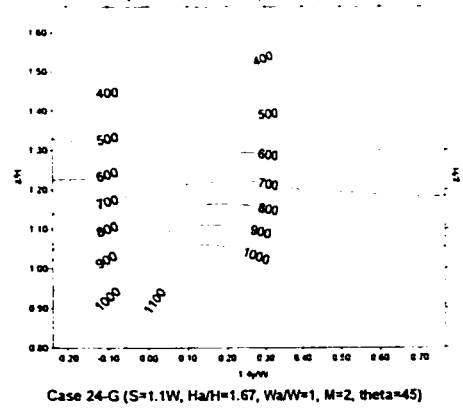

Case 24-G (S=1.1W, Ha/H=1.67, Wa/W=1, M=2, theta=45)

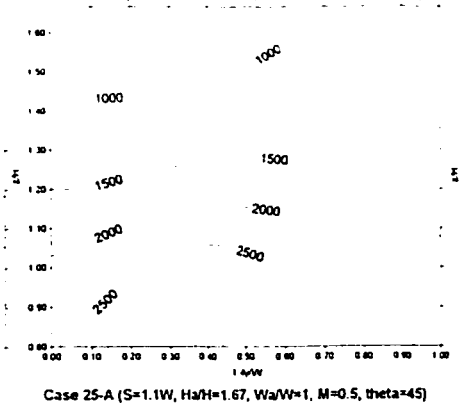

Case 25-A (S=1.1W, Ha/H=1.67, Wa/W=1, M=0.5, theta=45)

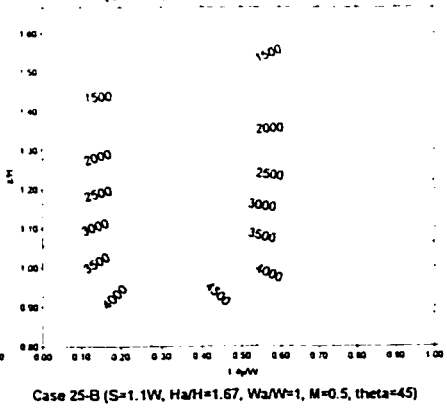

Case 25-B (S=1.1W, Ha/H=1.67, Wa/W=1, M=0.5, theta=45)

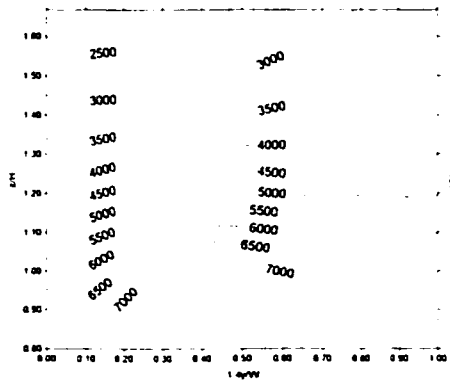

Case 25-C (S=1.1W, Ha/H=1.67, Wa/W=1, M=0.5, theta=45)

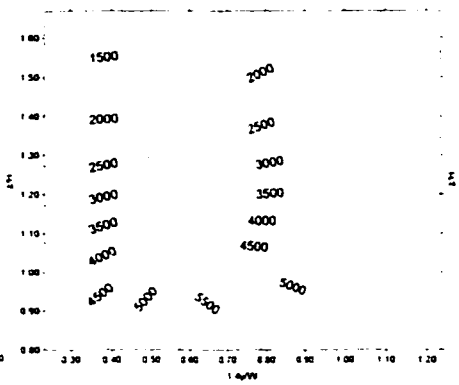

Case 25-D (S=1.1W, Ha/H=1.67, Wa/W=1, M=0.5, theta=45)

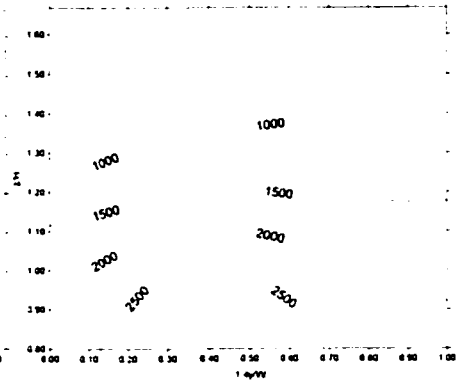

Case 25-E (S=1.1W, Ha/H=1.67, Wa/W=1, M=0.5, theta=45)

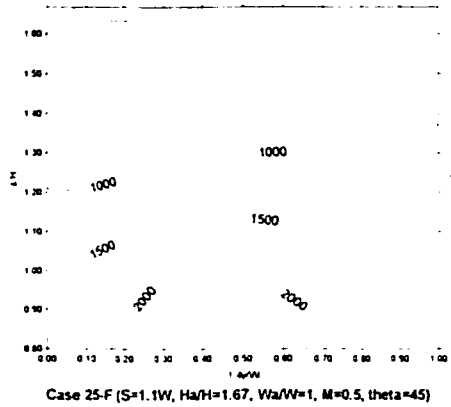

Case 25-F (S=1.1W, Ha/H=1.67, Wa/W=1, M=0.5, theta=45)

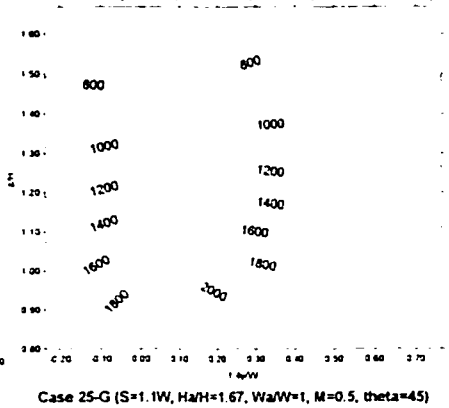

Case 25-G (S=1.1W, Ha/H=1.67, Wa/W=1, M=0.5, theta=45)

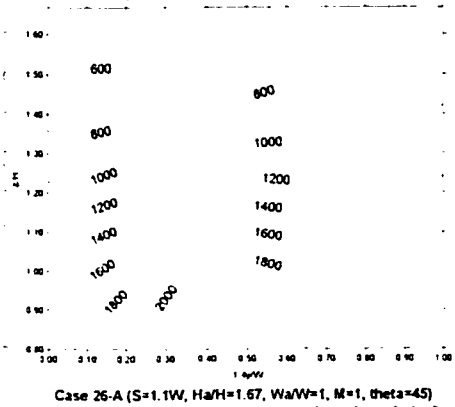

Case 26-A (S=1.1W, Ha/H=1.67, Wa/W=1, M=1, theta=45)

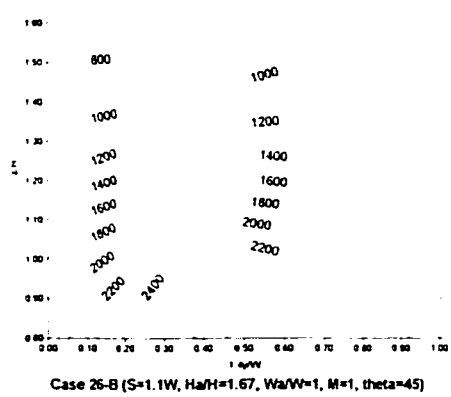

Case 26-B (S=1.1W, Ha/H=1.67, Wa/W=1, M=1, theta=45)

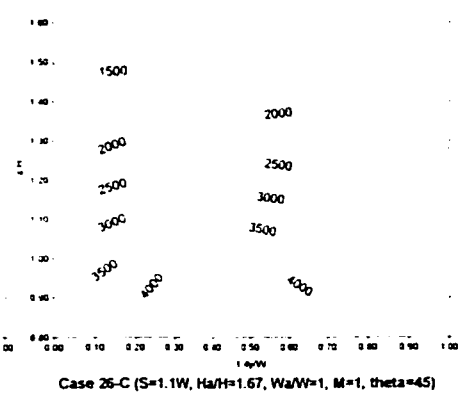

Case 26-C (S=1.1W, Ha/H=1.67, Wa/W=1, M=1, theta=45)

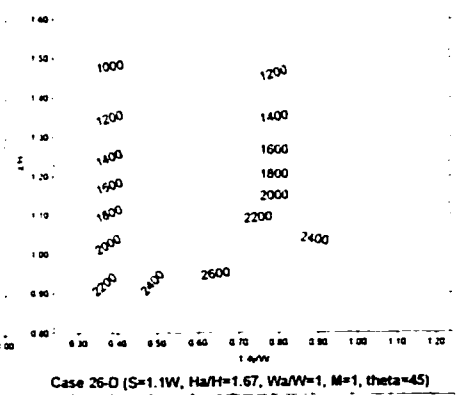

Case 26-D (S=1.1W, Ha/H=1.67, Wa/W=1, M=1, theta=45)

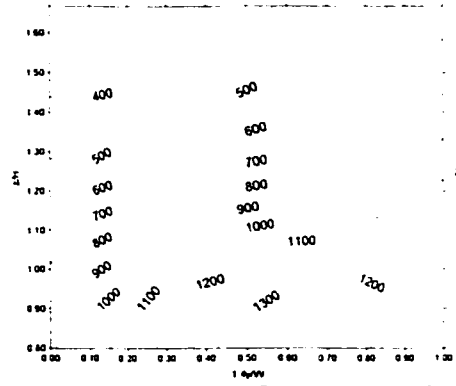

Case 26-E (S=1.1W, Ha/H=1.67, Wa/W=1, M=1, theta=45)

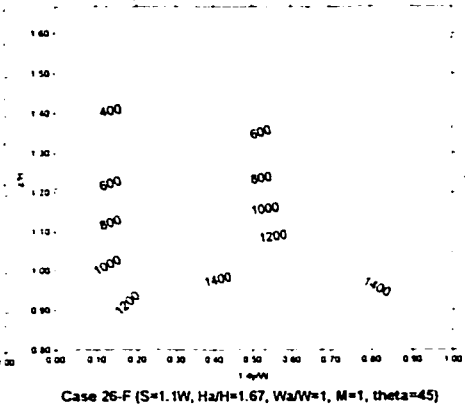

Case 26-F (S=1.1W, Ha/H=1.67, Wa/W=1, M=1, theta=45)

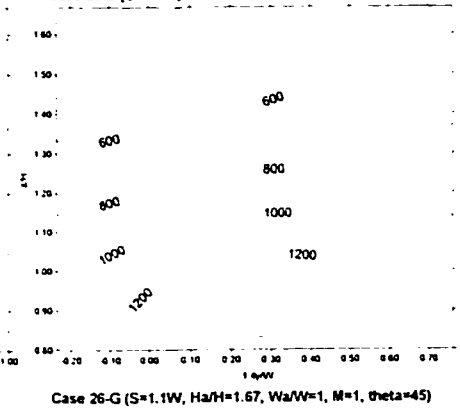

Case 26-G (S=1.1W, Ha/H=1.67, Wa/W=1, M=1, theta=45)

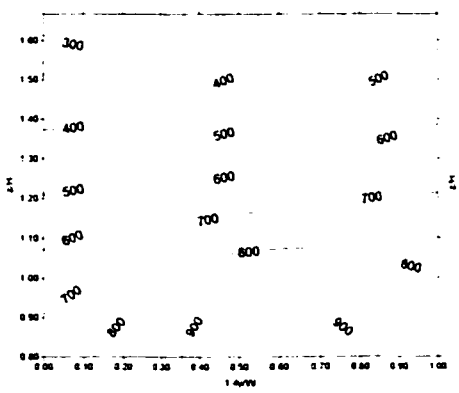

Case 27-A (S=1.1W, Ha/H=1.67, Wa/W=1, M=3, theta=45)

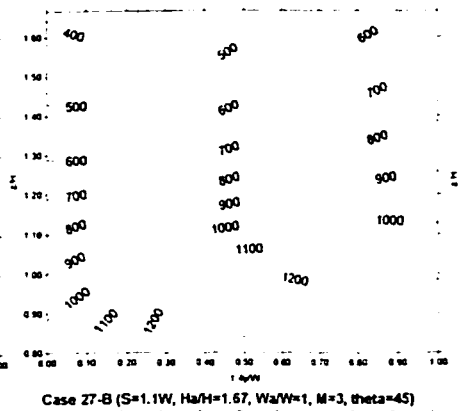

Case 27-B (S=1.1W, Ha/H=1.67, Wa/W=1, M=3, theta=45)

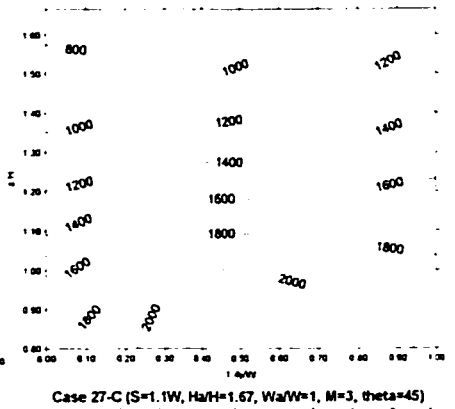

Case 27-C (S=1.1W, Ha/H=1.67, Wa/W=1, M=3, theta=45)

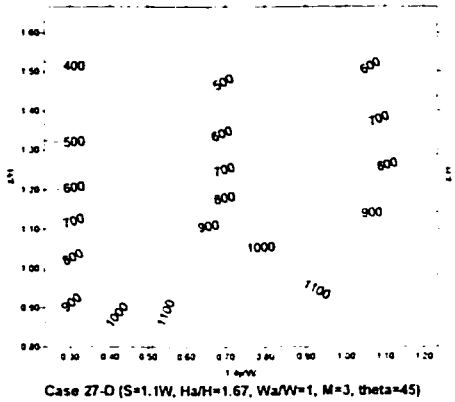

Case 27-D (S=1.1W, Ha/H=1.67, Wa/W=1, M=3, theta=45)

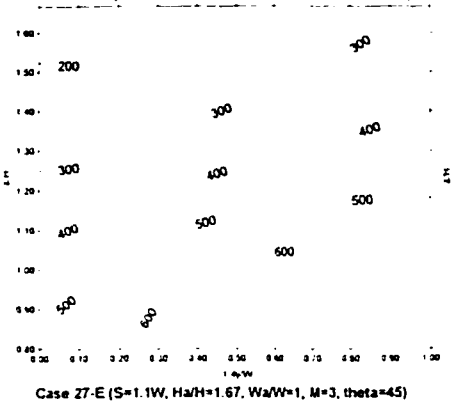

Case 27-E (S=1.1W, Ha/H=1.67, Wa/W=1, M=3, theta=45)

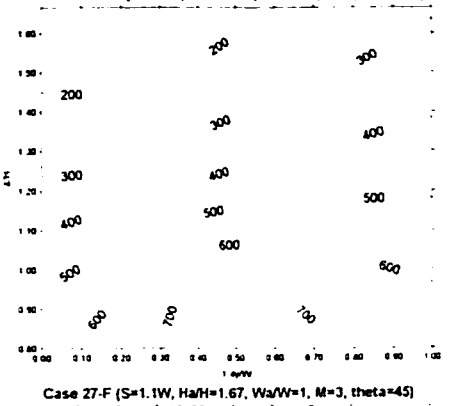

Case 27-F (S=1.1W, Ha/H=1.67, Wa/W=1, M=3, theta=45)

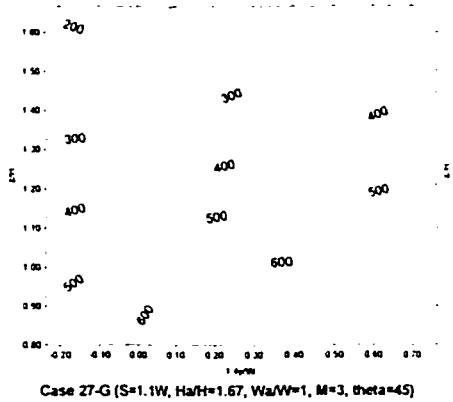

Case 27-G (S=1.1W, Ha/H=1.67, Wa/W=1, M=3, theta=45)

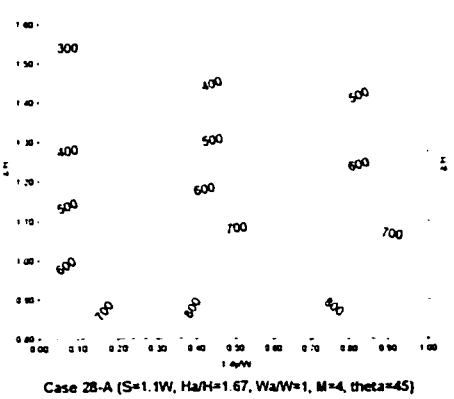

Case 28-A (S=1.1W, Ha/H=1.67, Wa/W=1, M=4, theta=45)

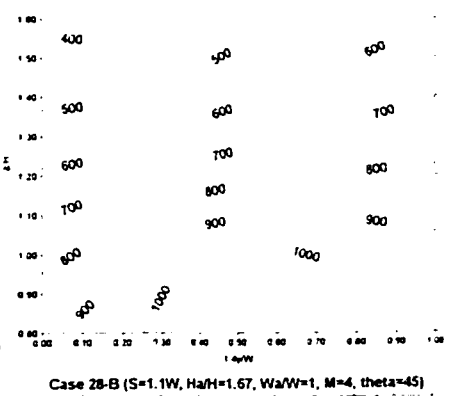

Case 28-B (S=1.1W, Ha/H=1.67, Wa/W=1, M=4, theta=45)

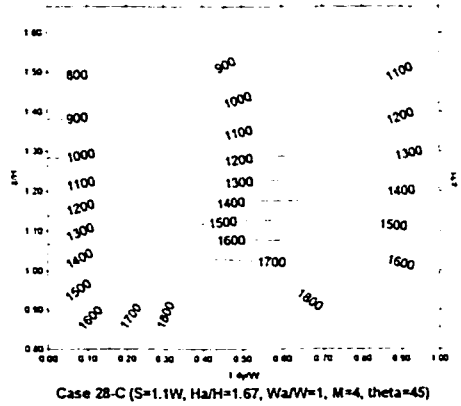

Case 28-C (S=1.1W, Ha/H=1.67, Wa/W=1, M=4, theta=45)

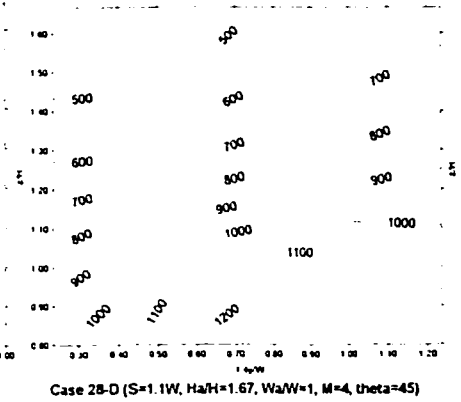

Case 28-D (S=1.1W, Ha/H=1.67, Wa/W=1, M=4, theta=45)

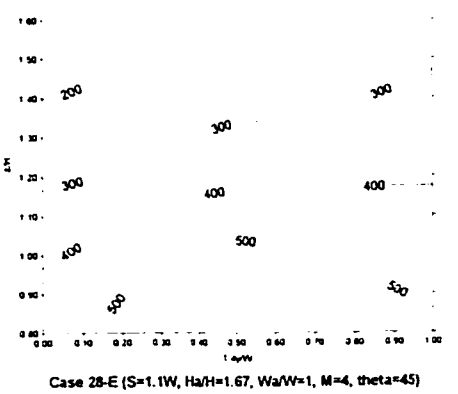

Case 28-E (S=1.1W, Ha/H=1.67, Wa/W=1, M=4, theta=45)

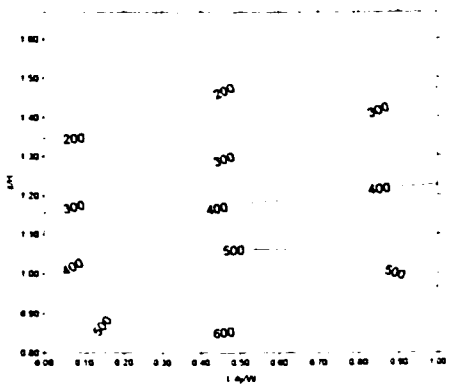

Case 28-F (S=1.1W, Ha/H=1.67, Wa/W=1, M=4, theta=45)

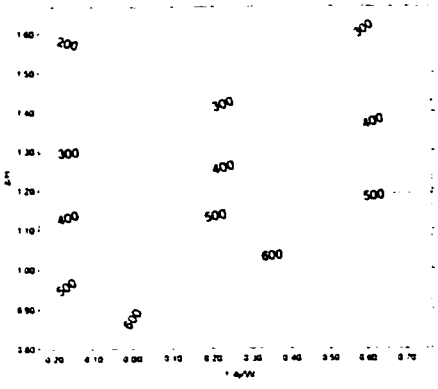

Case 28-G (S=1.1W, Ha/H=1.67, Wa/W=1, M=4, theta=45)

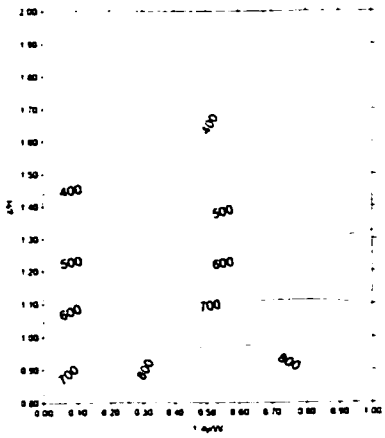

Case 29-A (S=1.4W, Ha/H=2, Wa/W=1, M=2, theta=45)

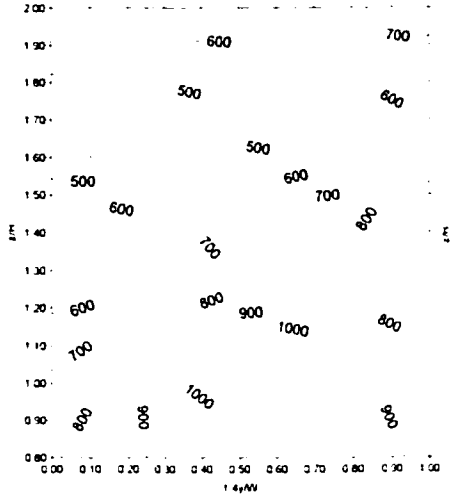

Case 29-B (S=1.4W, Ha/H=2, Wa/W=1, M=2, theta=45)

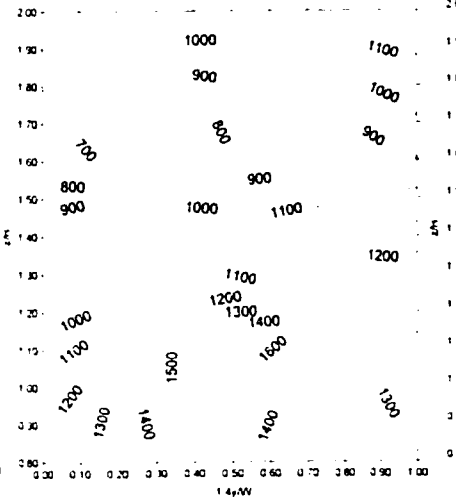

Case 29-C (S=1.4W, Ha/H=2, Wa/W=1, M=2, theta=45)

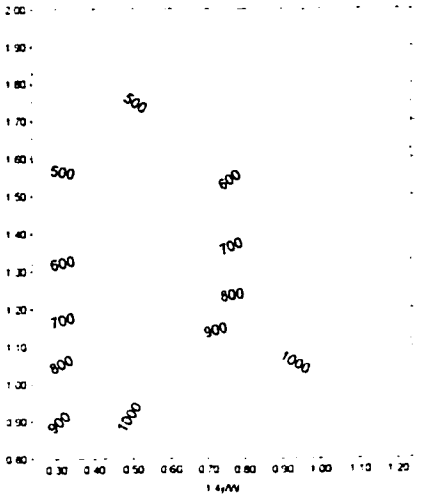

Case 29-D (S=1.4W, Ha/H=2, Wa/W=1, M=2, theta=45)

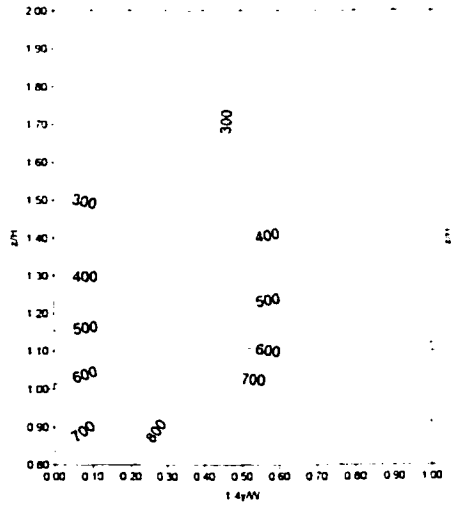

Case 29-E (S=1.4W, Ha/H=2, Wa/W=1, M=2, theta=45)

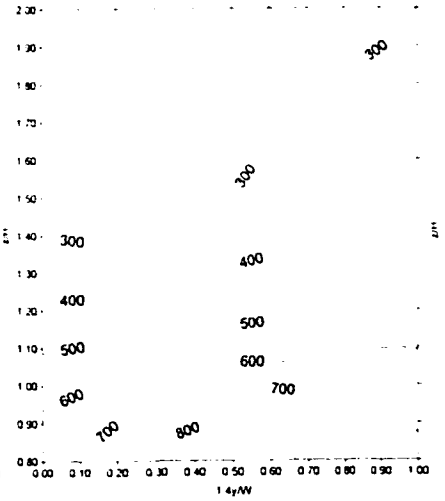

Case 29-F (S=1.4W, Ha/H=2, Wa/W=1, M=2, theta=45)

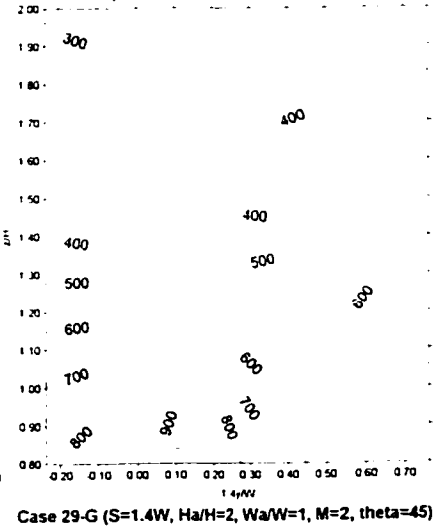

Case 29-G (S=1.4W, Ha/H=2, Wa/W=1, M=2, theta=45)

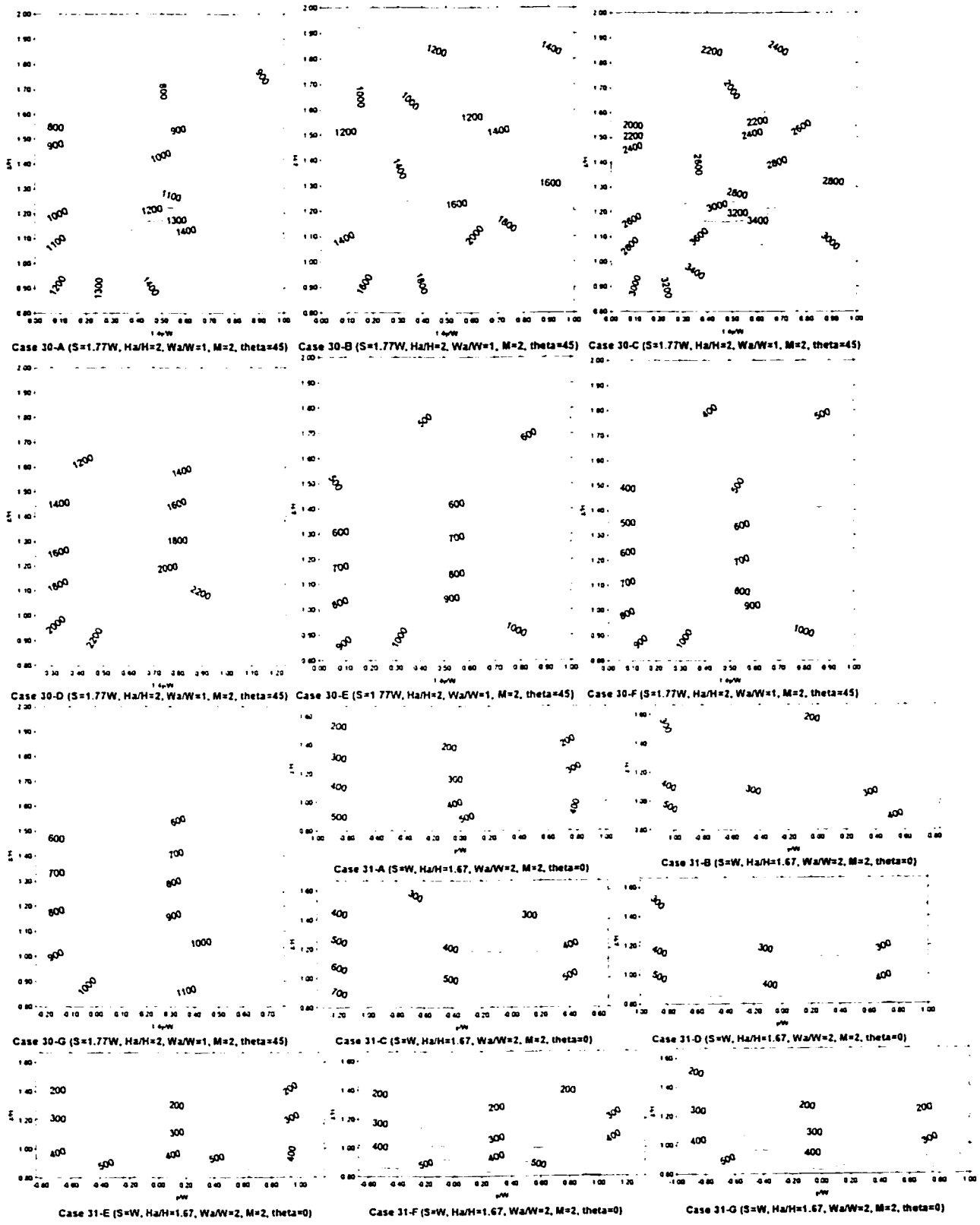

Case 30-A (S=1.77W, Ha/H=2, Wa/W=1, M=2, theta=45)

Case 30-B (S=1.77W, Ha/H=2, Wa/W=1, M=2, theta=45)

Case 30-C (S=1.77W, Ha/H=2, Wa/W=1, M=2, theta=45)

Case 30-D (S=1.77W, Ha/H=2, Wa/W=1, M=2, theta=45)

Case 30-E (S=1.77W, Ha/H=2, Wa/W=1, M=2, theta=45)

Case 30-F (S=1.77W, Ha/H=2, Wa/W=1, M=2, theta=45)

Case 30-G (S=1.77W, Ha/H=2, Wa/W=1, M=2, theta=45)

Case 31-A (S=W, Ha/H=1.67, Wa/W=2, M=2, theta=0)

Case 31-B (S=W, Ha/H=1.67, Wa/W=2, M=2, theta=0)

Case 31-C (S=W, Ha/H=1.67, Wa/W=2, M=2, theta=0)

Case 31-D (S=W, Ha/H=1.67, Wa/W=2, M=2, theta=0)

Case 31-E (S=W, Ha/H=1.67, Wa/W=2, M=2, theta=0)

Case 31-F (S=W, Ha/H=1.67, Wa/W=2, M=2, theta=0)

Case 31-G (S=W, Ha/H=1.67, Wa/W=2, M=2, theta=0)

APPENDIX E

DILUTION VARIATIONS WITH M-VALUE

The effect of M-value on dilution was investigated in detail by using five (5) different exhaust momentum ratios, namely 0.5, 1, 2, 3 and 4, in three (3) different building configurations for seven (7) stack locations. The three configurations are:

1. S=0, H_a=1.33H, W_a=W, θ=0°

2. S=2W, H_a=2H, W_a=2W, θ=0°, and

3. S=1.1W, H_a=1.67H, W_a=W, θ=45°.

The results are presented hereafter for all 21 cases in the order of "case by case" and "stack by stack".

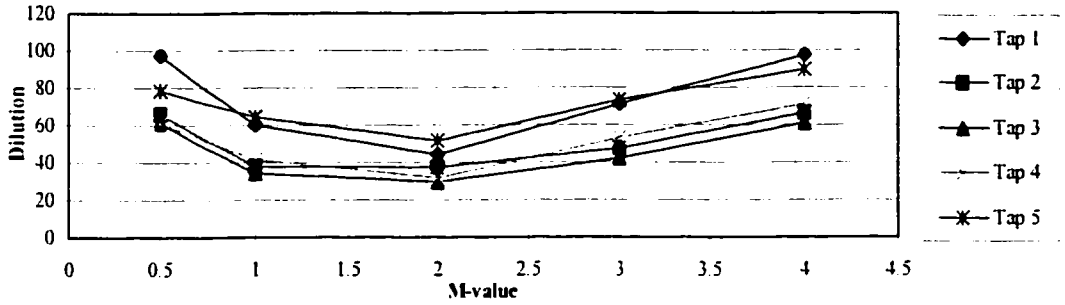

Stack A, S=0, H_a=1.33H, W_a=W, θ=0°, Taps 1-5

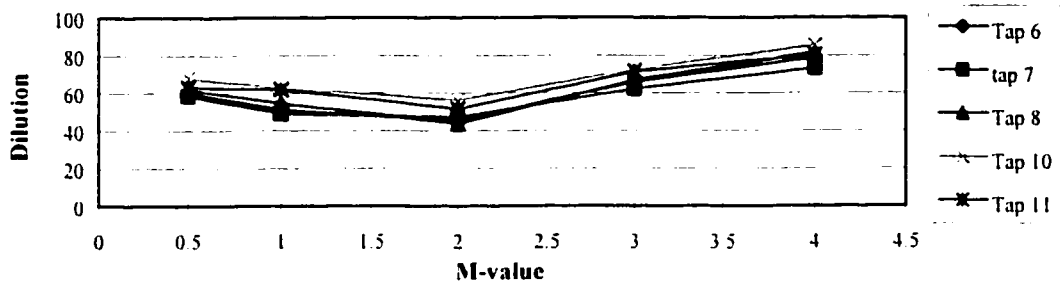

Stack A, S=0, H_a=1.33H, W_a=W, θ=0°, Taps 6-8, 10, 11

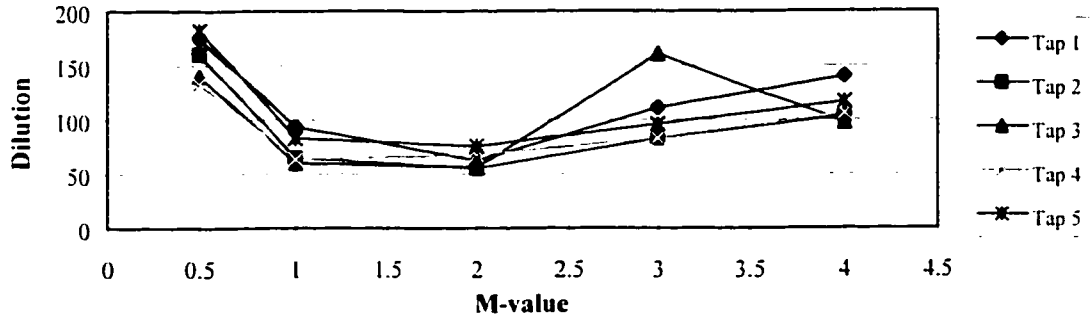

Stack B, S=0, H_a=1.33H, W_a=W, θ=0°, Taps 1-5

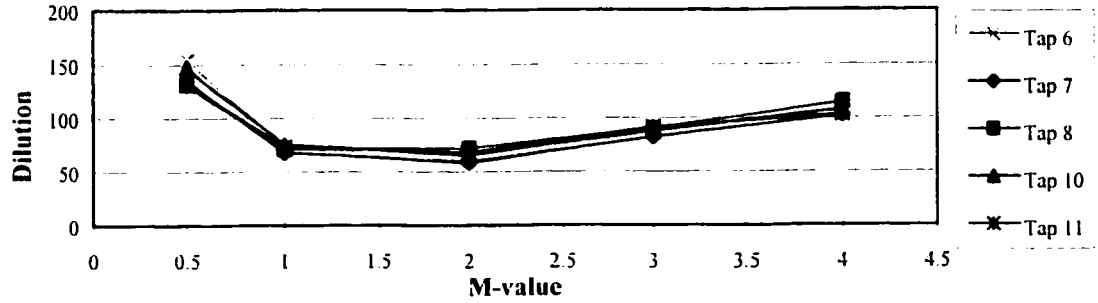

Stack B, S=0, H_a=1.33H, W_a=W, θ=0°, Taps 6-8, 10, 11

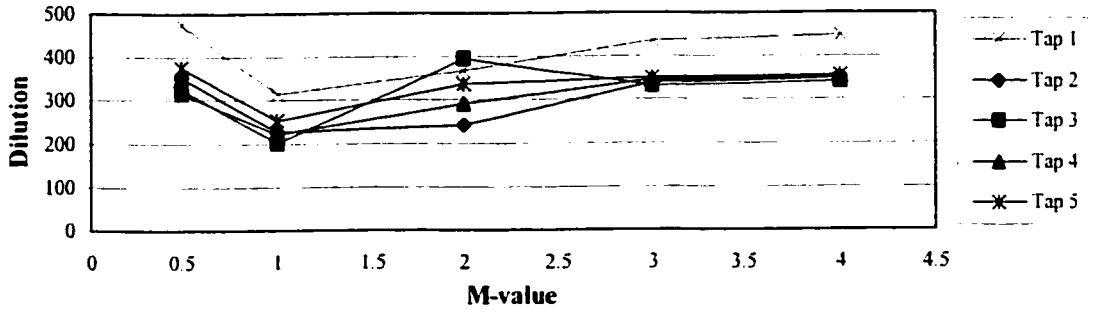

Stack C, S=0, H_a=1.33H, W_a=W, θ=0°, Taps 1-5

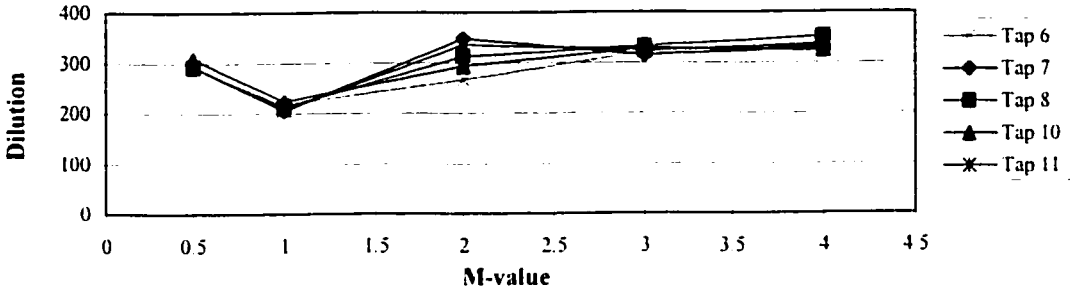

Stack C, S=0, H_a=1.33H, W_a=W, θ=0°, Taps 6-8, 10, 11

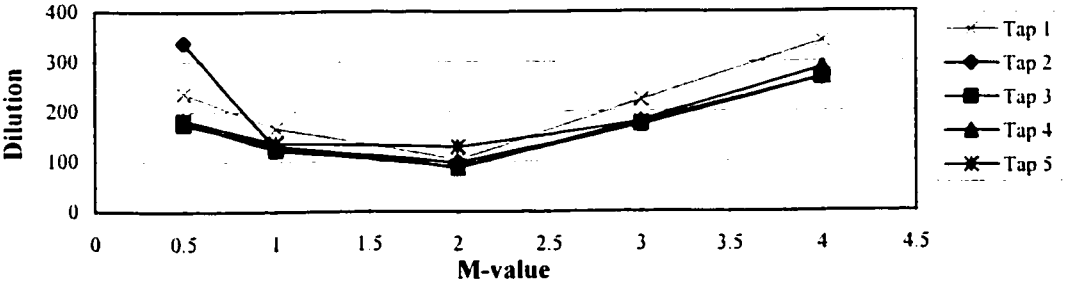

Stack D, S=0, H_a=1.33H, W_a=W, θ=0°Taps 1-5

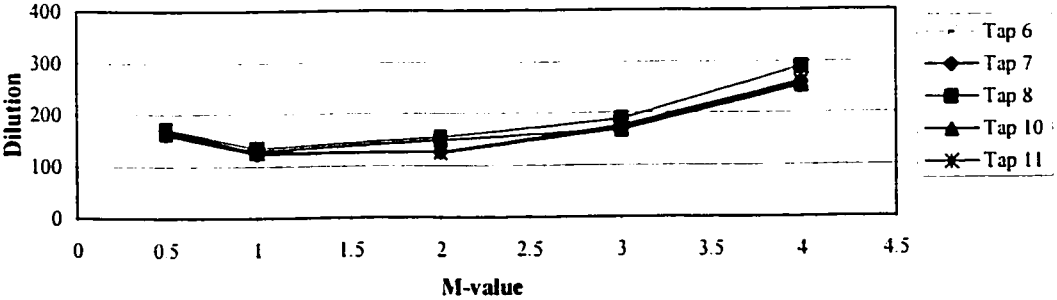

Stack D, S=0, H_a=1.33H, W_a=W, θ=0°, Taps 6-8, 10, 11

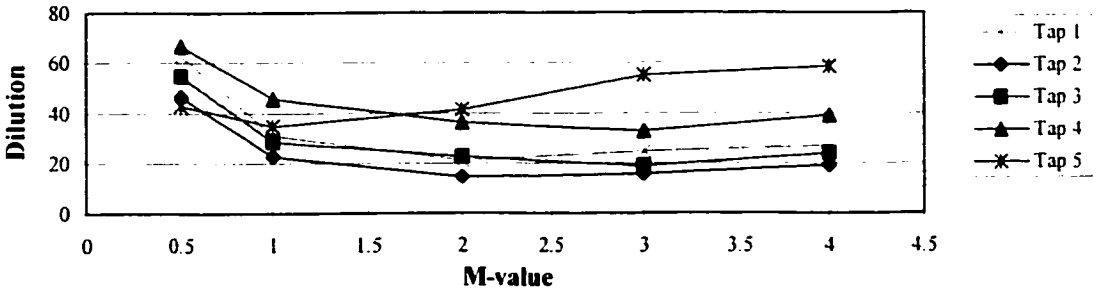

Stack E, S=0, H_a=1.33H, W_a=W, θ=0°, Taps 1-5

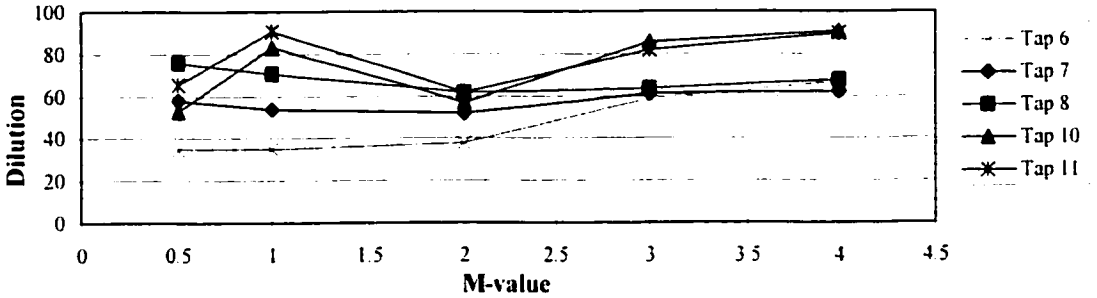

Stack E, S=0, H_a=1.33H, W_a=W, θ=0°, Taps 6-8, 10, 11

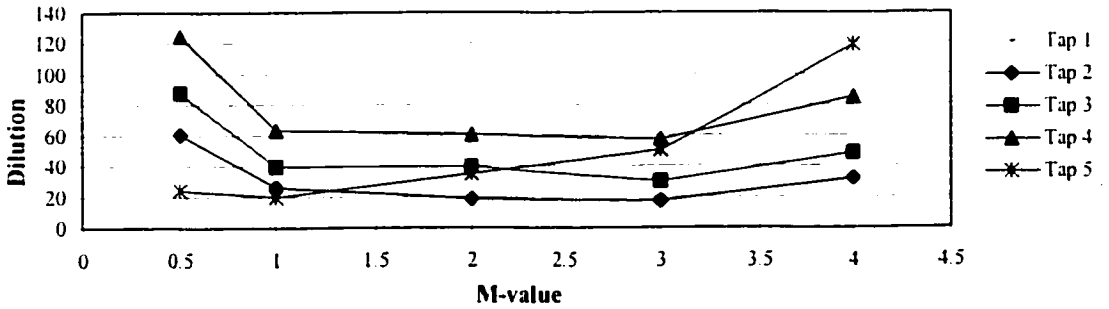

Stack F, S=0, H_a=1.33H, W_a=W, θ=0°, Taps 1-5

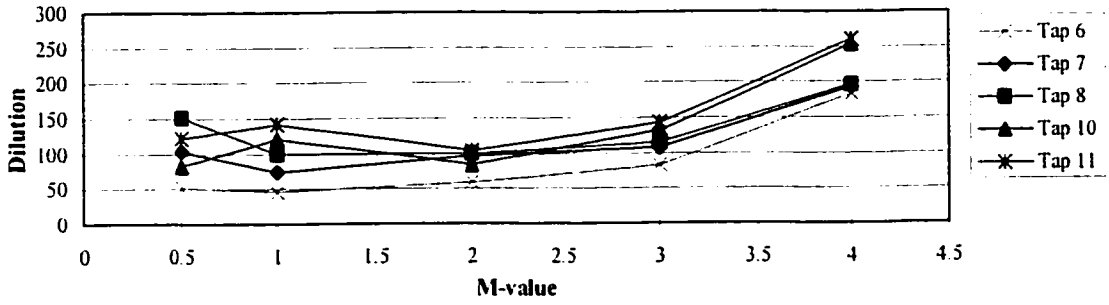

Stack F, S=0, H_a=1.33H, W_a=W, θ=0°, Taps 6-8, 10, 11

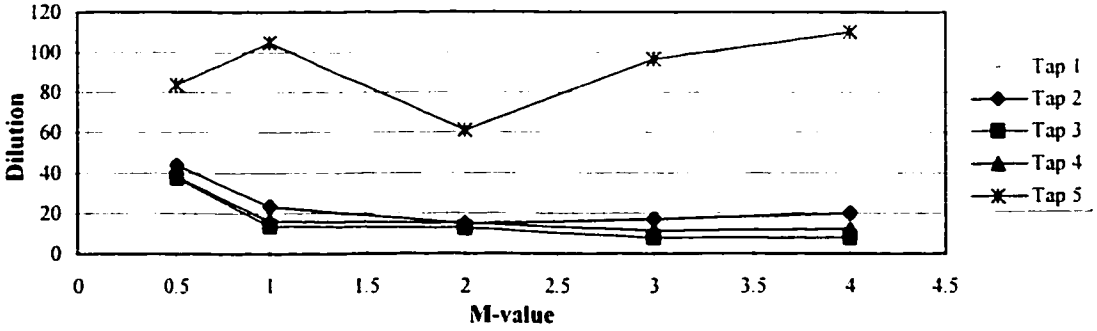

Stack G, S=0, H_a=1.33H, W_a=W, θ=0°, Taps 1-5

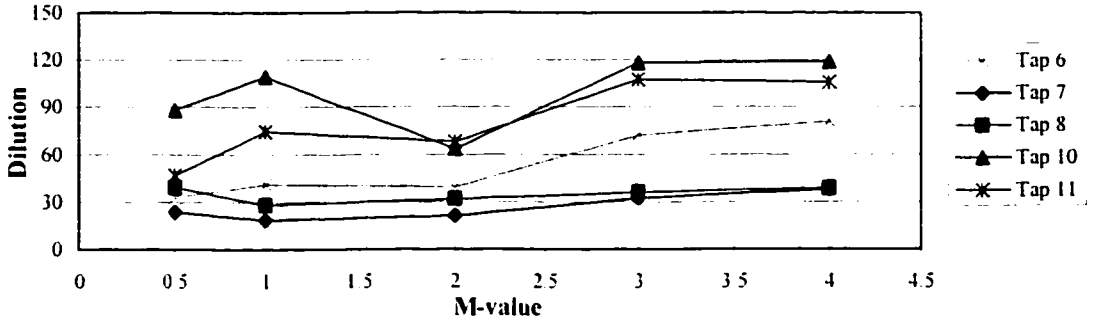

Stack G, S=0, H_a=1.33H, W_a=W, θ=0°, Taps 6-8, 10, 11

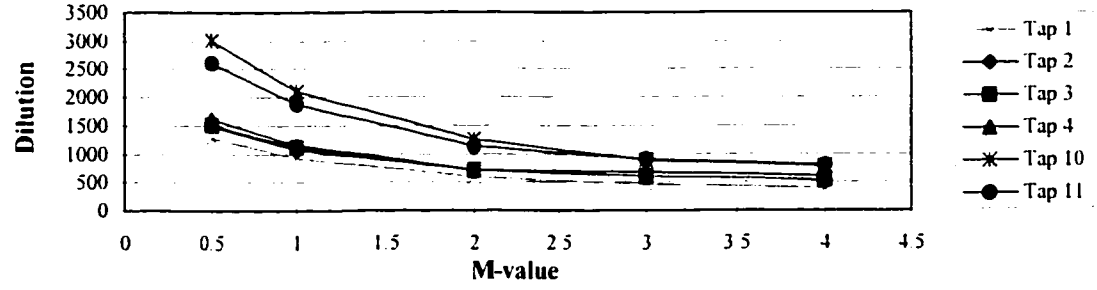

Stack A, S=1.1W, H_a=1.67H, W_a=W, θ=45°, Taps 1-4, 10, 11

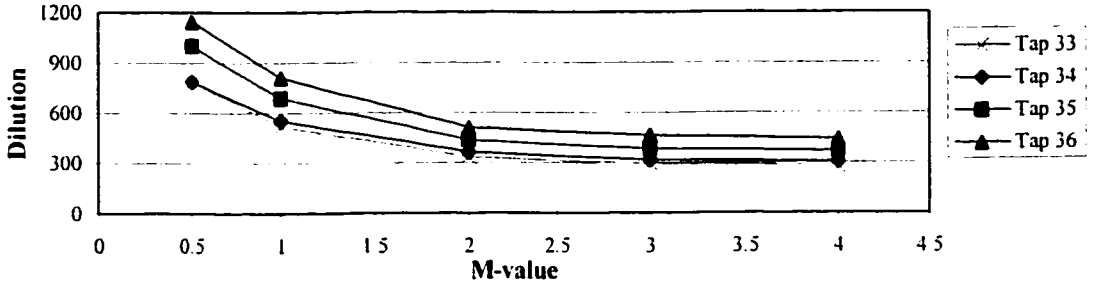

Stack A, S=1.1W, H_a=1.67H, W_a=W, θ=45°, Taps 33-36

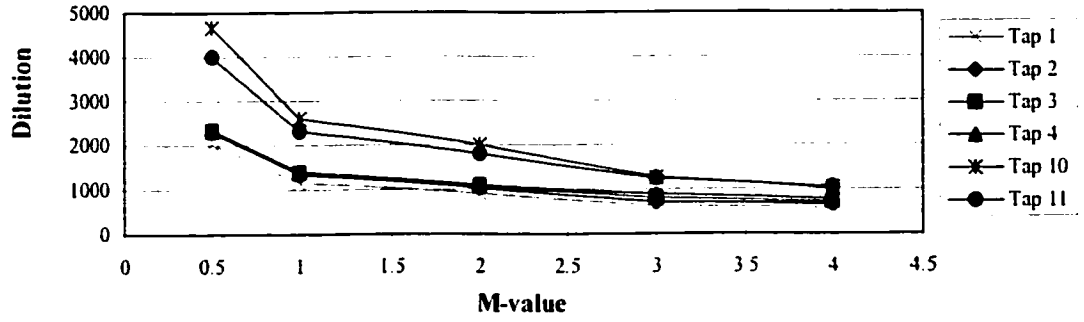

Stack B, S=1.1W, H_a=1.67H, W_a=W, θ=45°, Taps 1-4, 10, 11

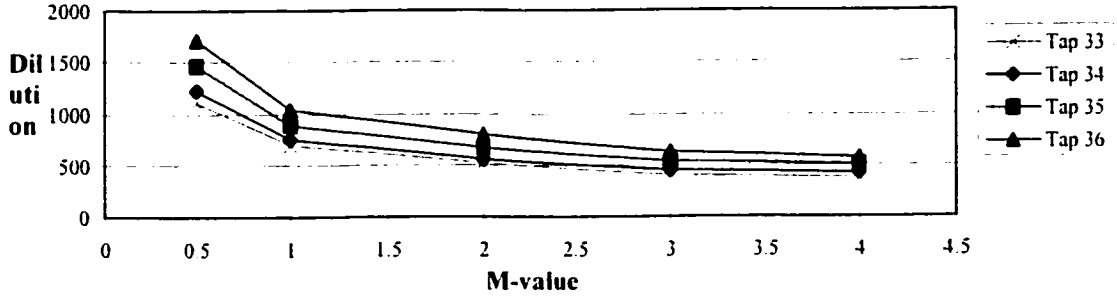

Stack B, S=1.1W, H_a=1.67H, W_a=W, θ=45°, Taps 33-36

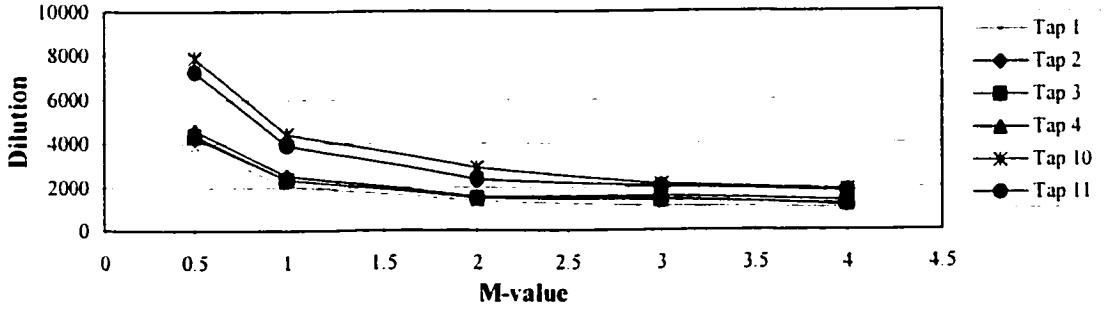

Stack C, S=1.1W, H_a=1.67H, W_a=W, θ=45°, Taps 1-4, 10, 11

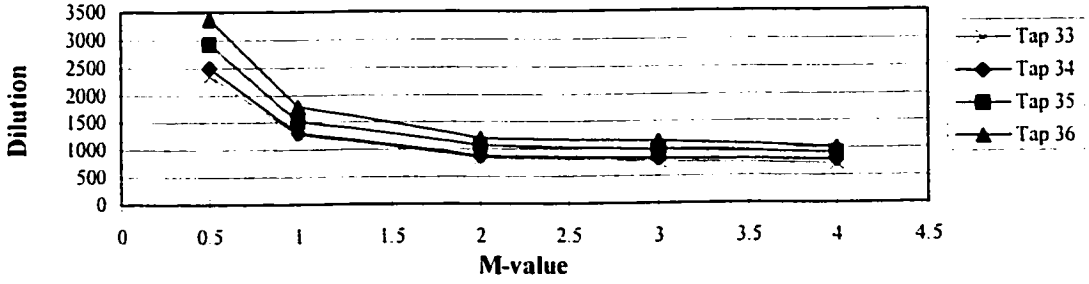

Stack C, S=1.1W, H_a=1.67H, W_a=W, θ=45°, Taps 33-36

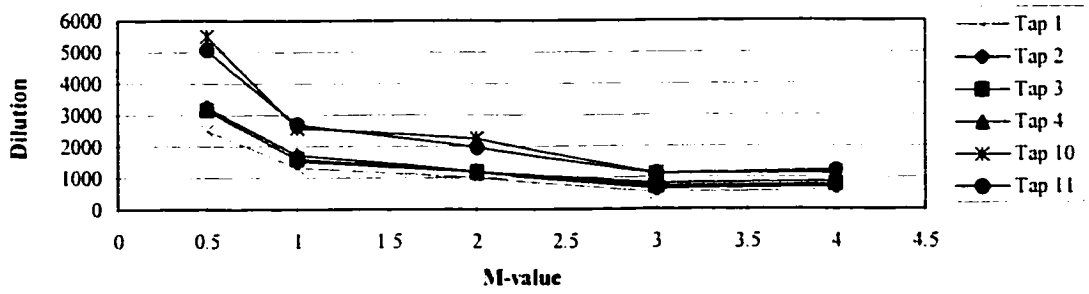

Stack D, S=1.1W, H_a=1.67H, W_a=W, θ=45°, Taps 1-4, 10, 11

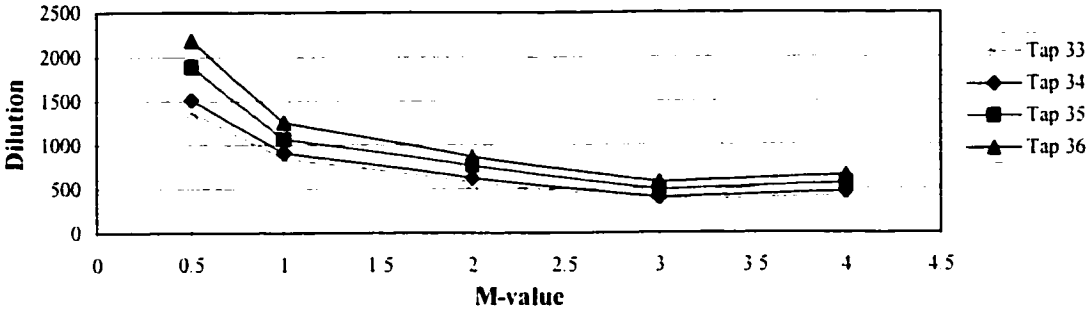

Stack D, S=1.1W, H_a=1.67H, W_a=W, θ=45°, Taps 33-36

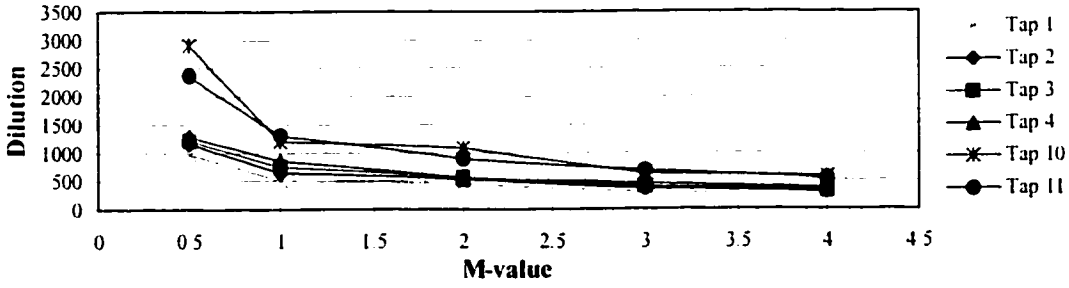

Stack E, S=1.1W, H_a=1.67H, W_a=W, θ=45°, Taps 1-4, 10, 11

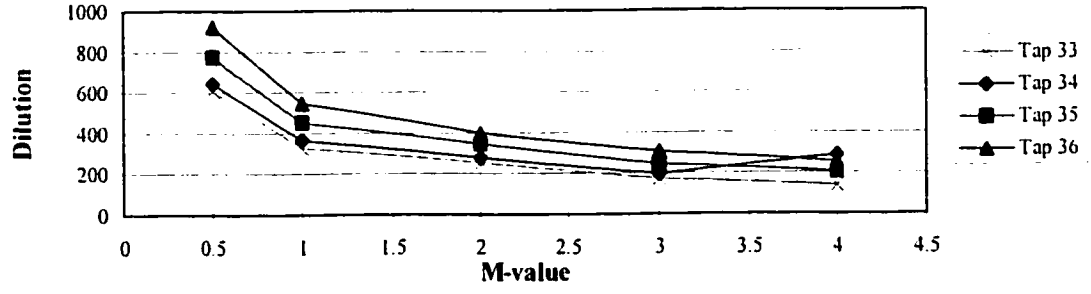

Stack E, S=1.1W, H_a=1.67H, W_a=W, θ=45°, Taps 33-36

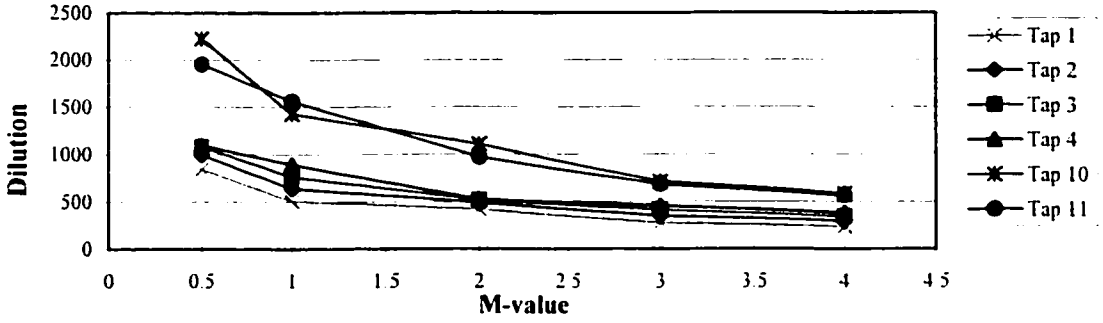

Stack F, S=1.1W, H_a=1.67H, W_a=W, 0=45°, Taps 1,2,3,4,10,11

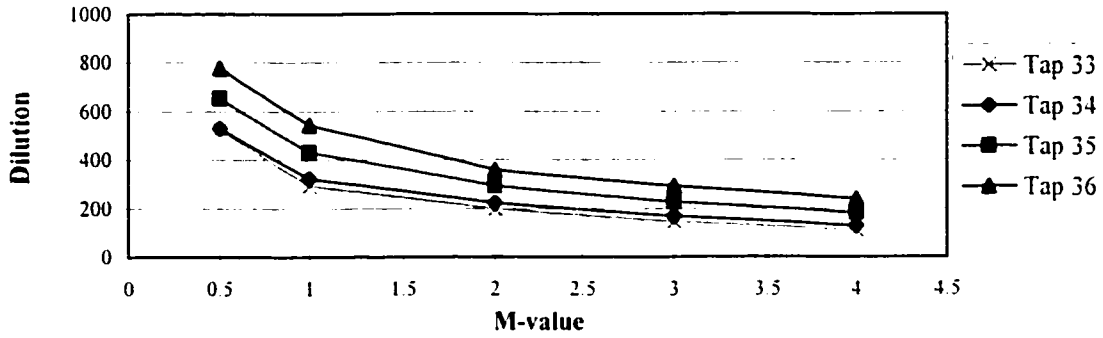

Stack F, S=1.1W, H_a=1.67H, W_a=W, 0=45°, Taps 33,34,35,36

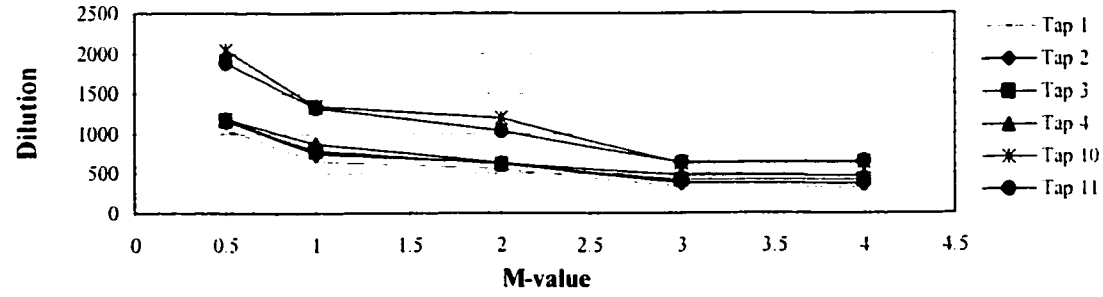

Stack G, S=1.1W, H_a=1.67H, W_a=W, 0=45°, Taps 1-4, 10, 11

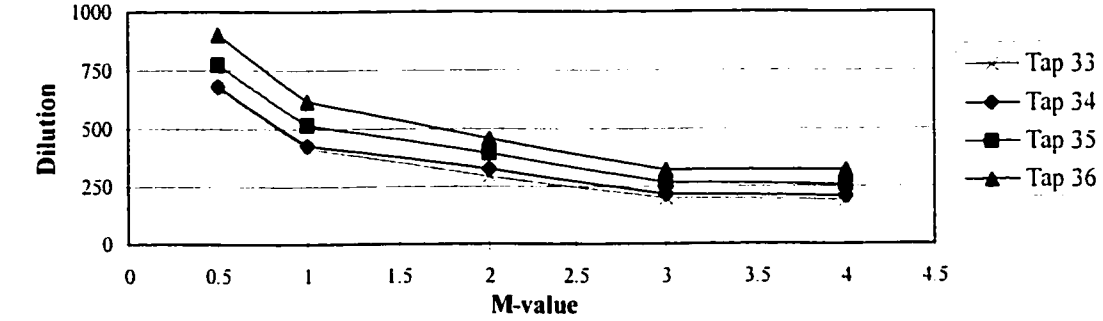

Stack G, S=1.1W, H_a=1.67H, W_a=W, 0=45°, Taps 33-36

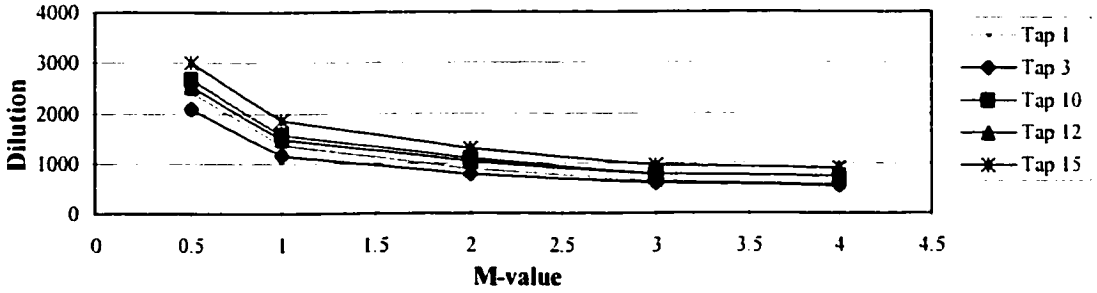

Stack A, S=2W, H_a=2H, W_a=2W, 0=0°, Taps 1, 3, 10, 12, 15

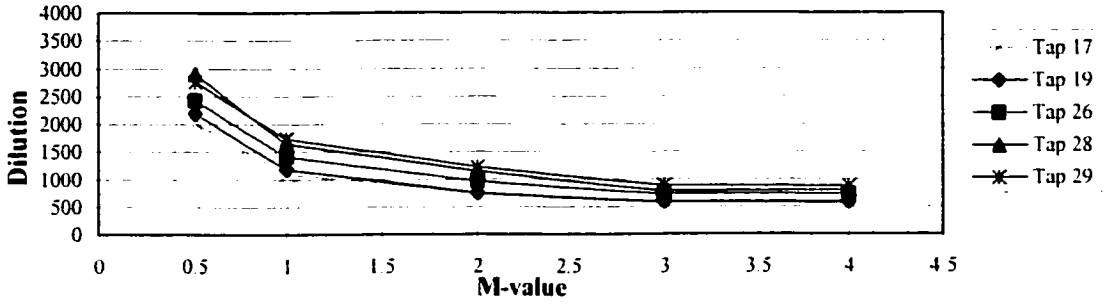

Stack A, S=2W, H_a=2H, W_a=2W, 0=0°, Taps 17, 19, 26, 28, 29

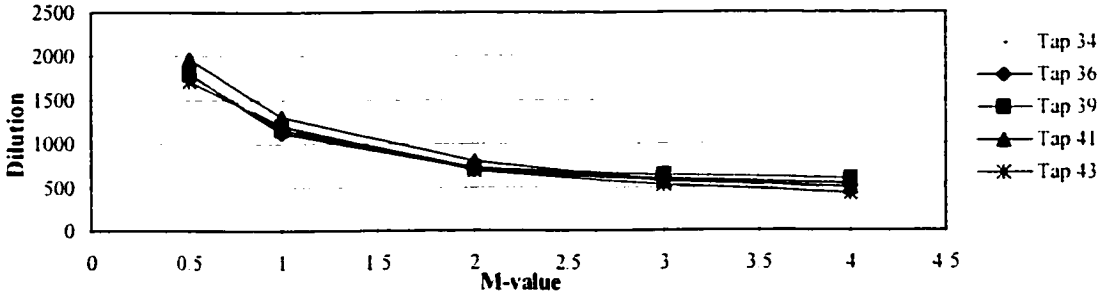

Stack A, S=2W, H_a=2H, W_a=2W, 0=0°, Taps 34, 36, 39, 41, 43

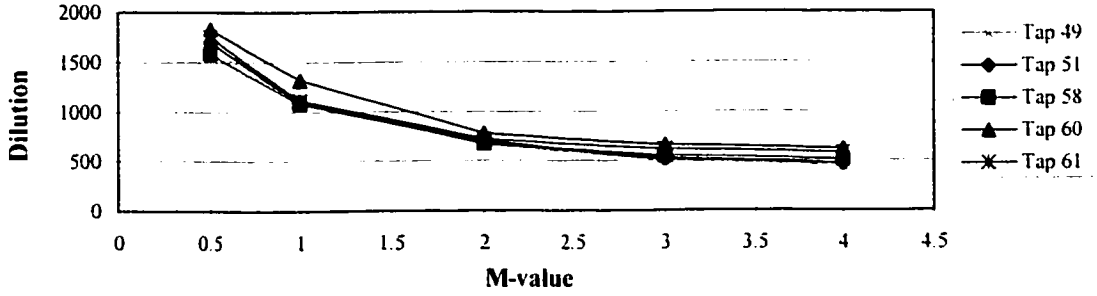

Stack A, S=2W, H_a=2H, W_a=2W, 0=0°, Taps 49, 51, 58, 60, 61

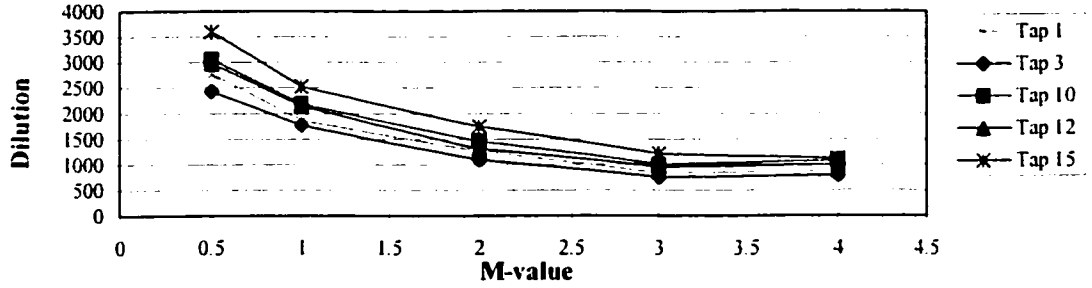

Stack B, S=2W, H_a=2H, W_a=2W, 0=0°, Taps 1, 3, 10, 12, 15

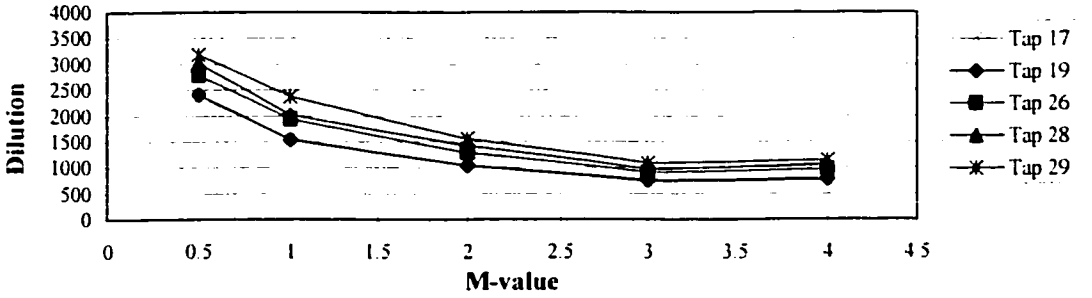

Stack B, S=2W, H_a=2H, W_a=2W, 0=0°, Taps 17, 19, 26, 28, 29

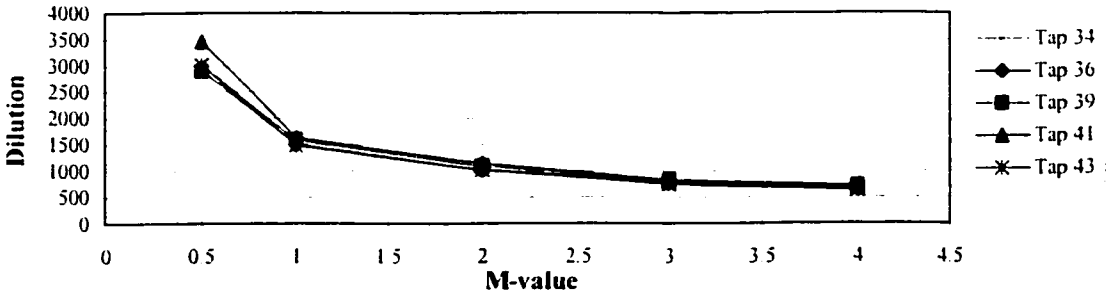

Stack B, S=2W, H_a=2H, W_a=2W, 0=0°, Taps 34,36,39,41,43

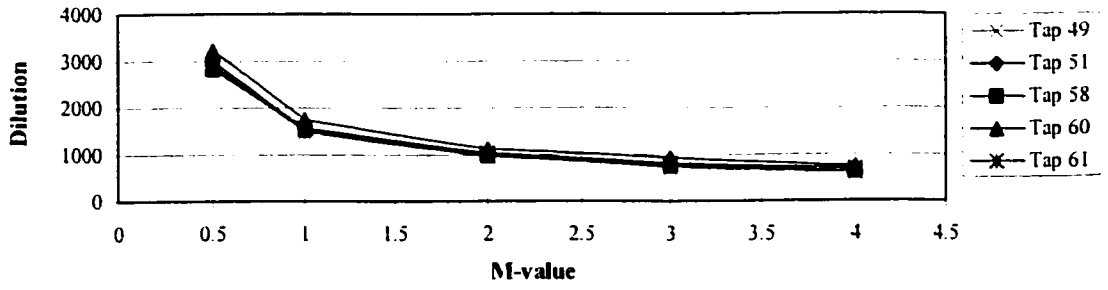

Stack B, S=2W, H_a=2H, W_a=2W, 0=0°, Taps 49,51,58,60,61

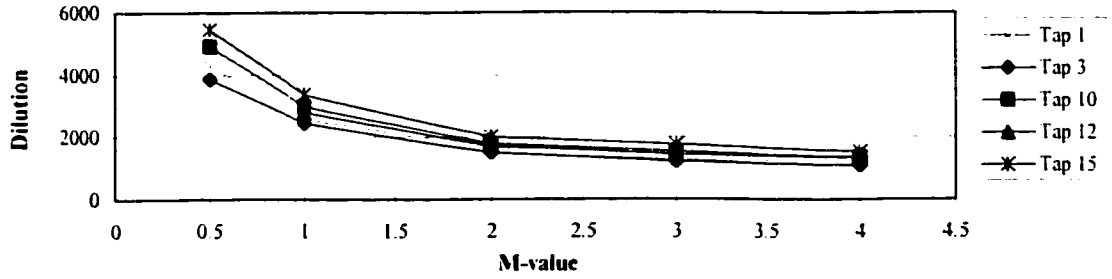

Stack C, S=2W, H_a=2H, W_a=2W, 0=0°, Taps 1,3,10,12,15

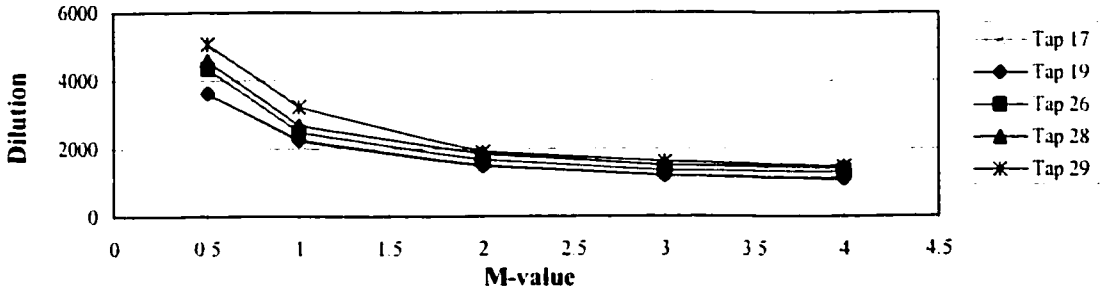

Stack C, S=2W, H_a=2H, W_a=2W, 0=0°, Taps 17,19,26,28,29

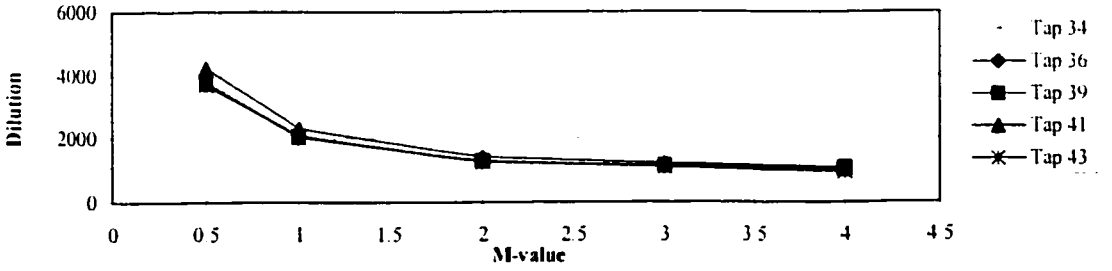

Stack C, S=2W, H_a=2H, W_a=2W, 0=0°, Taps 34,36,39,41,43

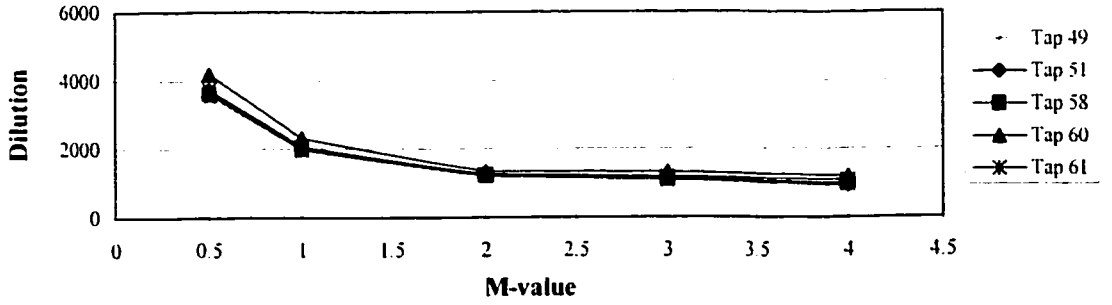

Stack C, S=2W, H_a=2H, W_a=2W, 0=0°, Taps 49,51,58,60,61

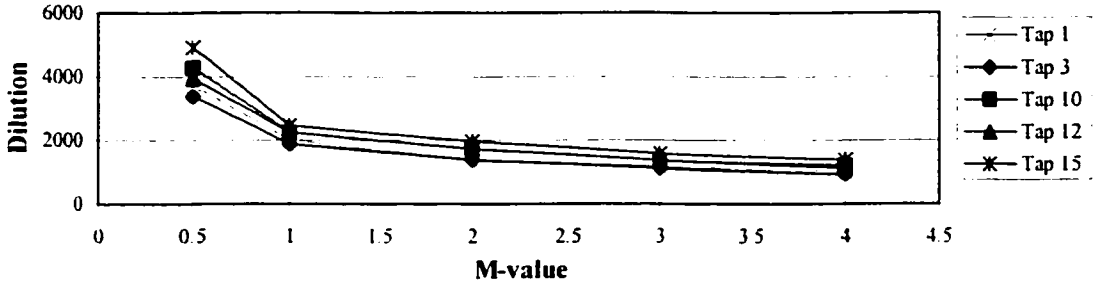

Stack D, S=2W, H_a=2H, W_a=2W, θ=0°, Taps 1,3,10,12,15

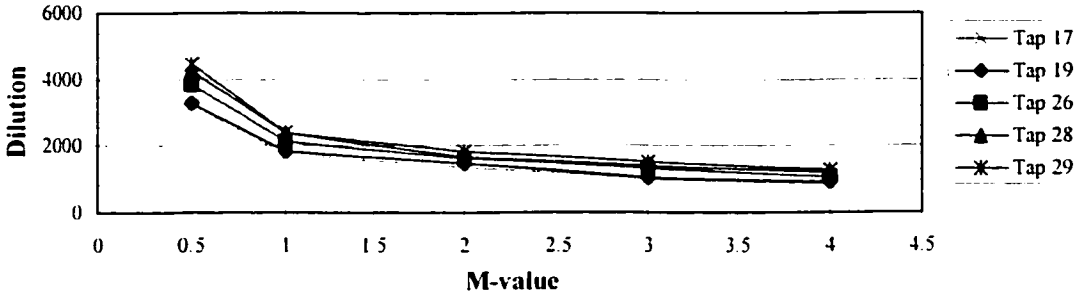

Stack D, S=2W, H_a=2H, W_a=2W, θ=0°, Taps 17,19,26,28,29

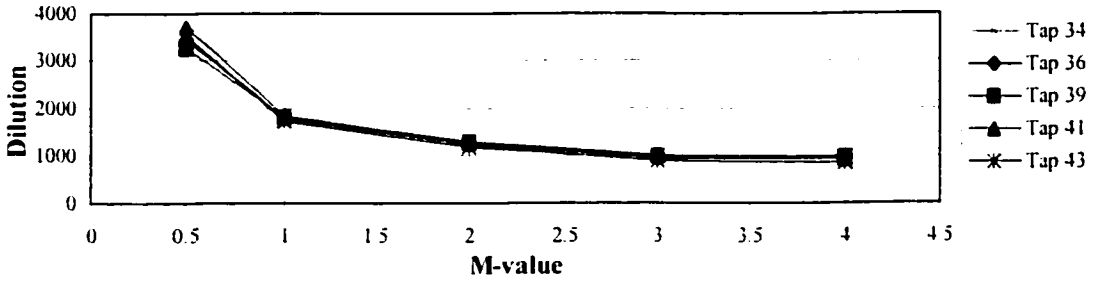

Stack D, S=2W, H_a=2H, W_a=2W, θ=0°, Taps 34,36,39,41,43

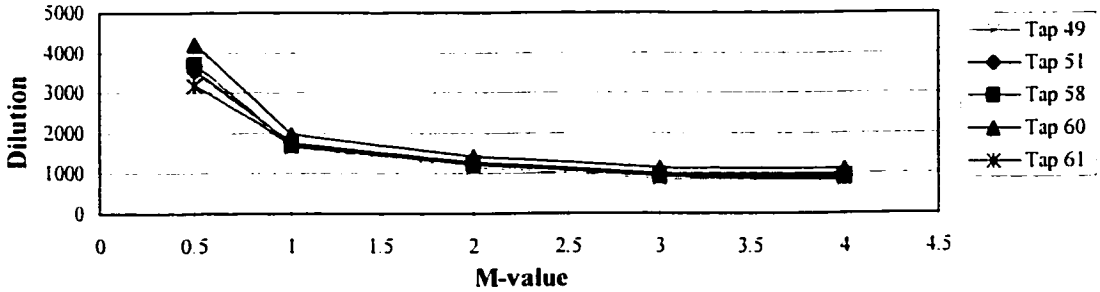

Stack D, S=2W, H_a=2H, W_a=2W, θ=0°, Taps 49,51,58,60,61

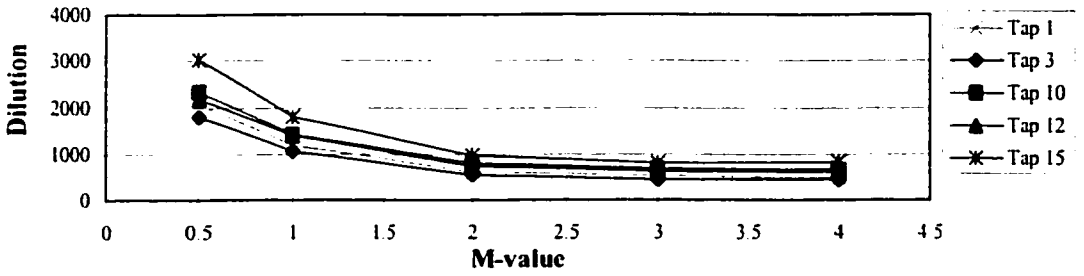

Stack E, S=2W, H_a=2H, W_a=2W, θ=0°, Taps 1,3,10,12,15

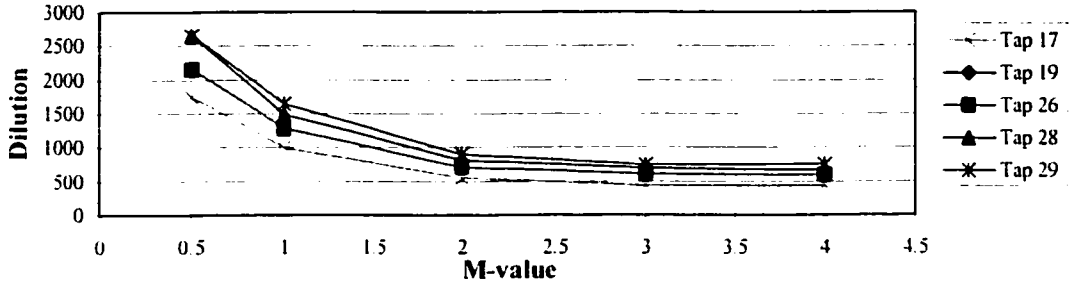

Stack E, S=2W, H_a=2H, W_a=2W, θ=0°, Taps 17,19,26,28,29

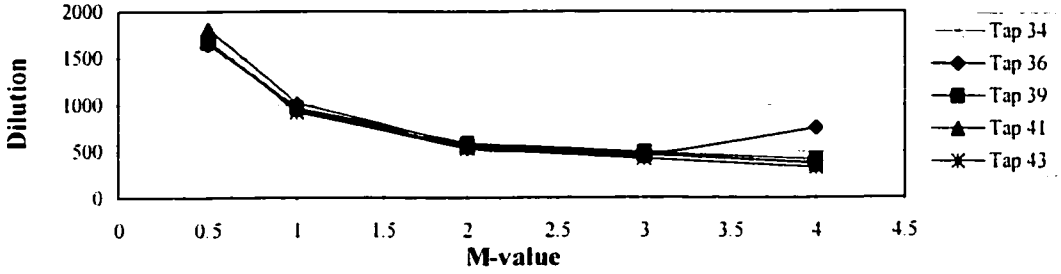

Stack E, S=2W, H_a=2H, W_a=2W, θ=0°, Taps 34,36,39,41,43

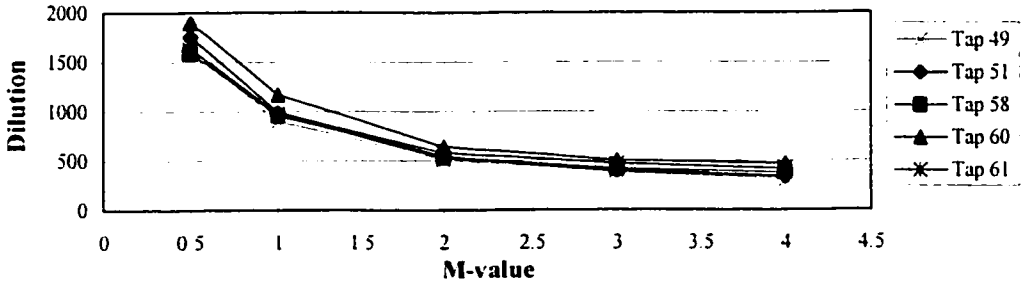

Stack E, S=2W, H_a=2H, W_a=2W, θ=0°, Taps 49, 51, 58, 60, 61

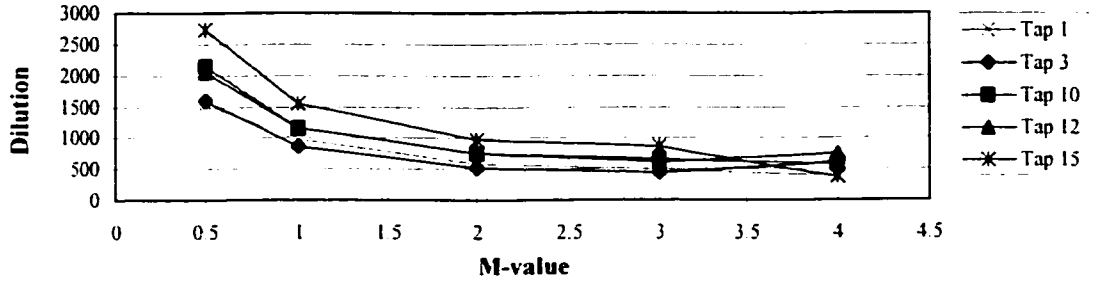

Stack F, S=2W, H_a=2H, W_a=2W, Taps 1, 3, 10, 12, 15

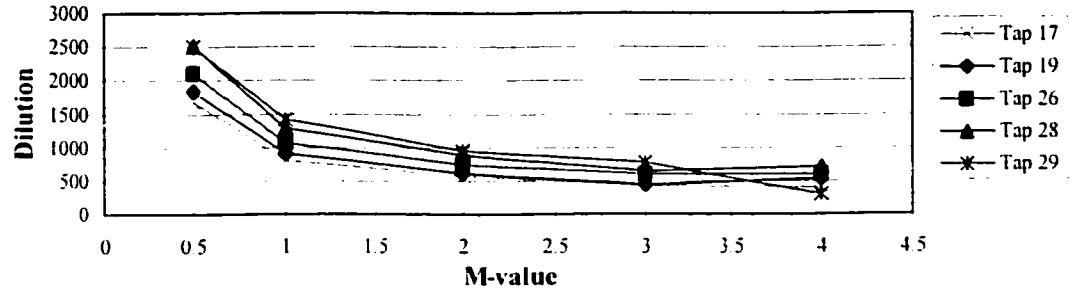

Stack F, S=2W, H_a=2H, W_a=2W, Taps 17,19,26,28,29

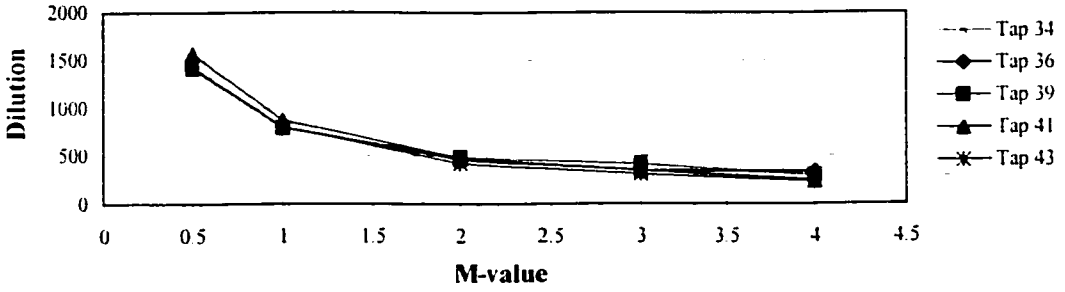

Stack F, S=2W, H_a=2H, W_a=2W, Taps 34,36,39,41,43

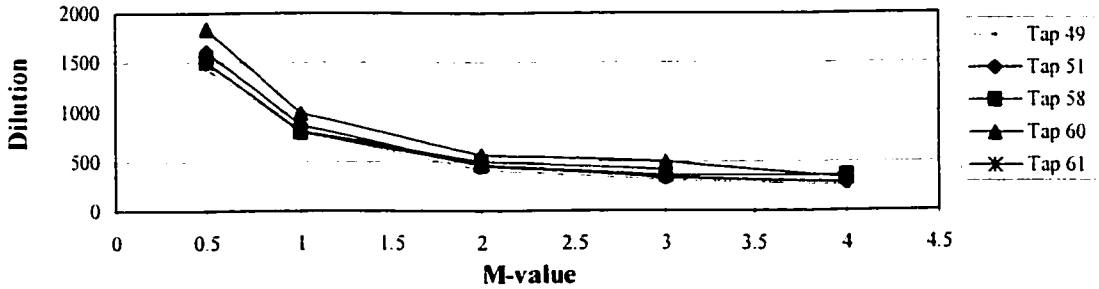

Stack F, S=2W, H_a=2H, W_a=2W, 0=0°, Taps 49, 51, 58, 60, 61

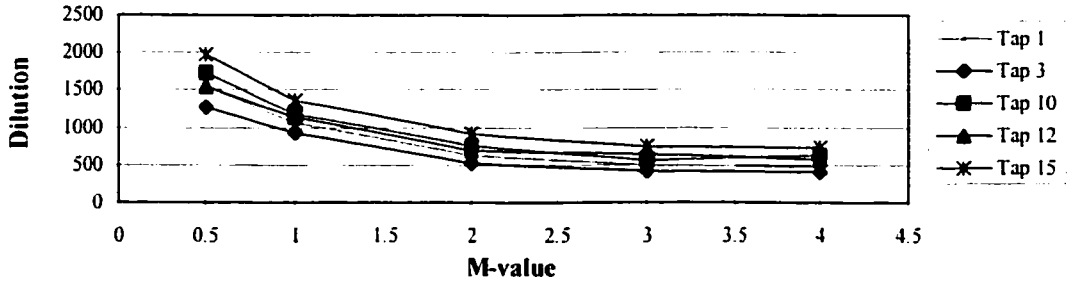

Stack G, S=2W, H_a=2H, W_a=2W, θ=0°, Taps 1, 3, 10, 12, 15

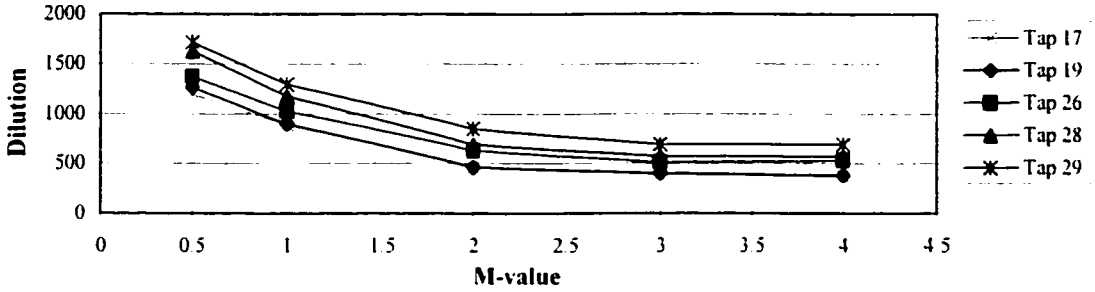

Stack G, S=2W, H_a=2H, W_a=2W, θ=0°, Taps 17, 19, 26, 28, 29

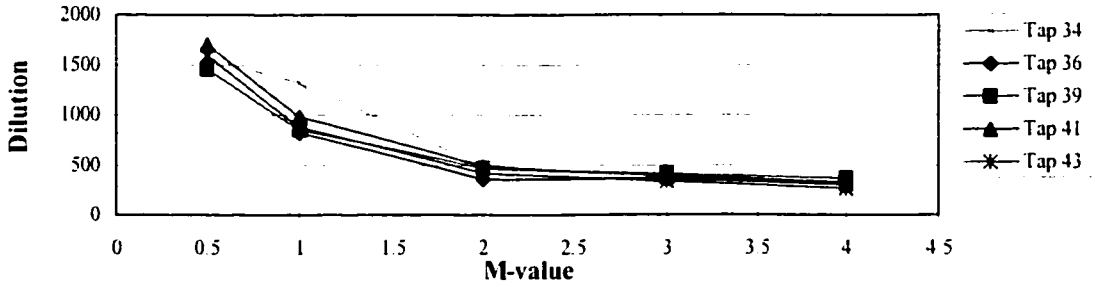

Stack G, S=2W, H_a=2H, W_a=2W, θ=0°, Taps 34, 36, 39, 41, 43

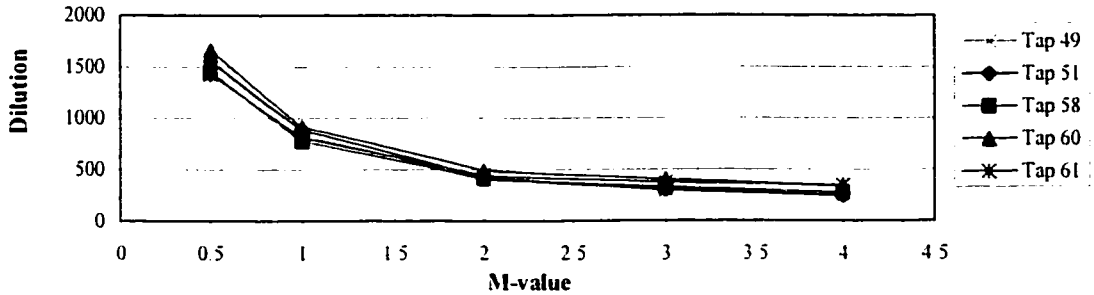

Stack G, S=2W, H_a=2H, W_a=2W, θ=0°, Taps 49, 51, 58, 60, 61